Therapeutic Potential of HP-β-CD in Ameliorating a poly(GA) Mouse Model of ALS

Ali Rezaei

Graduate School of Systemic Neurosciences

LMU Munich

Dissertation at the

Graduate School of Systemic Neurosciences

Ludwig-Maximilians-Universität München

February 2024

Supervisor
Prof. Dr. Dieter Edbauer
Deutsches Zentrum für Neurodegenerative Erkrankungen (DZNE)
Cell Biology of Neurodegeneration

First Reviewer: Prof. Dr. Dieter Edbauer
Second Reviewer: Prof. Dr. Irina Dudanova
External Reviewer: Prof. Dr. Karin Danzer

Date of Submission: 14.02.2024
Date of Defense: 10.06.2024

LMU | LUDWIG-MAXIMILIANS-UNIVERSITÄT MÜNCHEN | LMU excellent Graduate School of Systemic Neurosciences

v18/11/2024

Bekanntgabe von geringfügigen Änderungen der Dissertation nach der Verteidigung, unabhängig von den offiziellen Begutachtungen der Dissertation

Announcement for marginal Changes of the Dissertation after the defense, independent of the official evaluations of the dissertation

Name des/der Studierenden
Name of the student: *Ali Rezaei*

Name des 1. Supervisors + Lab/Location
Name of 1st supervisor + lab/location: *Prof.Dr. Dieter Edbauer – DZNE München, Feodor-Lynen-Straße 17, 81377 München*

Liste der Änderungen
List of changes:

Only change is in Figure 21 part b: p-value should be changed to 0.019; in figure legend the n should be changed to n = 7 vehicle vs 10 CD. The figure would then look as below (note the change in p-value):

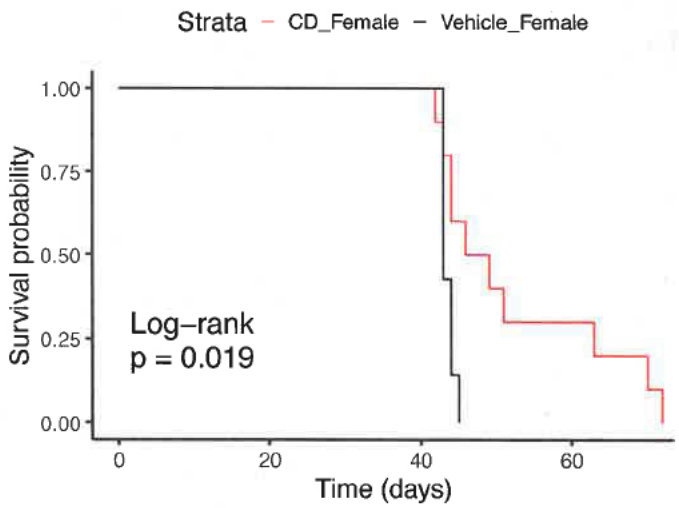

Note that the conclusion remains the same and no other change should be necessary as p-value is still significant.

Table of Contents

List of Abbreviations

ABCA1	ATP binding cassette subfamily A member 1
ACAT2	acetyl-coenzyme A acetyltransferase 2
AD	Alzheimer's disease
ADARB2	adenosine deaminase RNA specific B2
ALS	amyotrophic lateral sclerosis
ApoD / E	Apolipoprotein D / E
APP	amyloid precursor protein
ASO	antisense oligonucleotide
ADP	adenosine triphosphate
AMP	adenosine monophosphate
ATP	adenosine diphosphate
Aβ	amyloid-β peptide
BBB	blood-brain barrier
BCA assay	bicinchoninic acid assay
BSA	bovine serum albumin
BMI	body mass index
C4B	complement component 4B
CA2 (gene)	carbonic anhydrase 2
CA2 (Hipp region)	Cornu Ammonis 2
C9ORF72	chromosome 9 open reading frame 72
CD/HPβCD/HPbCD	2-hydroxypropyl-β-cyclodextrin
CE	cholesteryl ester
CHCHD10	coiled-coil-helix-coiled-coil-helix domain containing 10
CHO cells	Chinese hamster ovary cells
CLDN11	Claudin 11
CNP	2',3'-cyclic nucleotide 3' phosphodiesterase
CNS	central nervous system
CSF	cerebrospinal fluid
DAB IHC	3, 3'-diaminobenzidine immunohistochemistry
DAM	disease-associated microglia
DAMP	damage-associated molecular pattern

DAO / DOL	disease-associated oligodendrocyte
DAPI	4',6-Diamidino-2-Phenylindole, Dihydrochloride
DEGs	differentially expressed genes
DIV3	3 days *in vitro*
DNA	deoxyribonucleic acid
DPR	dipeptide Repeat Protein
DS	degree of substitution
E18	embryonic day 18
EAE	autoimmune encephalitis
EDTA	ethylenediaminetetraacetic acid
ER	endoplasmic reticulum
fALS	familial ALS
FANS	fluorescent-activated nuclei sorting
FAO	fatty acid oxidation
FBS	fetal bovine serum
FC	free cholesterol
FDA	food and drug administration
FTD	frontotemporal dementia
FUS	fused in sarcoma
GA (a DPR)	glycine-alanine
GA (a fixative)	glutaraldehyde
GEM	Gel bead-in-EMulsion
GM1	monosialotetrahexosylganglioside
GM3	monosialodihexosylganglioside
GO	gene ontology
GP	glycine-proline
GR	glycine-arginine
GABA	gamma-aminobutyric acid
GFAP	glial fibrillary acidic protein
GFP	green fluorescent protein
GRN	progranulin
HADHA	hydroxyacyl-coenzyme A dehydrogenase trifunctional multienzyme complex subunit alpha

HBSS	Hanks' Balanced Salt Solution
HD	Huntington’s disease
HDL	high-density lipoprotein
HEK-293 cells	human embryonic kidney 293 cells
HEPES	4-(2-hydroxyethyl)-1-piperazineethanesulfonic acid
HRP	horseradish peroxidase
HIER	heat-induced epitope retrieval
HSC70	Heat shock cognate 71 kDa protein
IFNγ	interferon-gamma
IL33	interleukin 33
iPSC	induced pluripotent stem cell
JAK	janus kinase
Jakinib	janus kinase inhibitor
LDL-C	low-density lipoprotein cholesterol
LFC	log fold change
LR (pair)	ligand-receptor (pair)
MEM	minimum essential medium
MPZ	myelin protein zero
MRI	magnetic resonance imaging
MS	multiple sclerosis
MSD	meso scale discovery
NAD(P)(H)	nicotinamide adenine dinucleotide (phosphate) (hydrogen)
NK cell	natural killer cell
NMJ	neuromuscular junction
NF-κB	nuclear factor kappa B subunit
NfL	neurofilament light chain
NPC	Niemann-Pick disease type C
P40	postnatal day 40
PA	proline-alanine
PBA	pseudobulbar effect
PBS	phosphate-buffered saline
PCA	principal component analysis

(q)PCR	(quantitative) polymerase chain reaction
PD	Parkinson's disease
PDL	poly-D-lysine
PES	polyethersulfone
PFA	paraformaldehyde
PKA	protein kinase A
PLIN4 / 2	perilipin 4 / 2
PR	proline-arginine
PVDF	polyvinylidene fluoride
QC	quality control
RAN	repeat associated non-ATG
RIPA buffer	radioimmunoprecipitation assay buffer
(m)RNA	(messenger) ribonucleic acid
sALS	sporadic ALS
SDS	sodium dodecyl sulfate
SEM	scanning electron microscopy
Sema4	Semaphorin-4A
Serpina3n	serine (or cysteine) peptidase inhibitor, clade A, member 3N
scRNAseq	single-cell RNA sequencing
snRNAseq	single-nucleus RNA sequencing
SOD1	superoxide dismutase 1
SQSTM1	sequestosome-1
SPTLC1	serine palmitoyltransferase, long chain base subunit 1
(p)STAT3	(phosphorylated) signal transducer and activator of transcription 3
TARDBP/TDP43	transactive response DNA binding protein 43 kDa
TBS	tris-buffered saline
TC	total cholesterol
Tg	transgenic
UMAP	uniform manifold approximation and projection
VCP	valosin containing protein
WB	western blot
WT	wildtype

Abstract

Amyotrophic lateral sclerosis (ALS) is a fatal and debilitating disease with very limited treatment options. Familial ALS (fALS), comprising 5-10% of cases, is genetically inherited, while the remainder of cases are sporadic (sALS). Approximately half of fALS cases and 5% of sALS cases are caused by a hexanucleotide expansion in C9ORF72. This expansion is translated in every reading frame of both the sense and antisense transcripts into five unique dipeptide repeat (DPR) proteins via repeat-associated non-ATG (RAN) translation. Notably, glycine-alanine repeats (poly(GA)) are the most abundant DPR species in the patient brain and spinal cord. In this study, we aimed to evaluate various therapeutic strategies for *C9orf72* ALS in a poly(GA) mouse model of ALS.

This mouse model expresses poly(GA) throughout the CNS by crossing with a Nes-Cre driver line, which results in neurodegeneration primarily in the hippocampus. Neurodegeneration is preceded by strong neuroinflammation, marked by proliferation of microglia, increased expression of interferon-gamma (IFNγ), and phosphorylation of STAT3. Mice expressing poly(GA) fail to gain weight at the rate observed in wildtype mice. Subsequently, weight loss becomes pronounced around 6-7 weeks of age, necessitating euthanasia due to the severity of the condition.

Given that neuroinflammation clearly precedes neurodegeneration in this model, we hypothesized that treatment with baricitinib, a JAK1/2 inhibitor, might alleviate the symptoms and prolong survival. Unfortunately, treatment with 10 mg/kg of baricitinib subcutaneously (s.c.) once daily (q.d.) from postnatal day 28 (P28) failed to extend survival, with minimal target engagement observed in the CNS as measured by STAT phosphorylation.

Given the notable weight loss in poly(GA)-expressing mice often necessitating euthanasia, we explored whether dietary interventions could ameliorate this symptom and thereby extend survival. Despite attempts to counteract this phenotype through dietary adjustments, including supplementation of normal chow with carbohydrate-rich DietGel Recovery and protein-rich DietGel 76A, no improvement in weight loss and

survival rates were observed. In light of the disrupted metabolism noted in both poly(GA)-expressing mice and ALS patients, we hypothesized that protein aggregation could cause hypermetabolism or other metabolic disturbances even on the cellular level. However, monitoring of energy carriers in primary cortical or hippocampal neurons from rats expressing a poly(GA) construct did not reveal any differences arguing against our hypothesis.

Investigation into gene expression changes in the bulk transcriptomic data of poly(GA) mouse model and ALS patients from previous data unveiled significant disturbances in cholesterol metabolism. This included the upregulation of genes linked to cholesterol storage and the downregulation of those involved in its biosynthesis. Thus, we hypothesized that ameliorating the cholesterol phenotype might have therapeutic potential for the GA-Nes mouse model. Treatment with 2-hydroxypropyl-β-cyclodextrin (CD) at 2000 mg/kg s.c. q.d. from P21 on female mice significantly improved survival and reduced levels of neurofilament light chain (NfL) at P40, indicating decreased neurodegeneration.

Single-nucleus RNA sequencing (snRNAseq) pinpointed disease-associated oligodendrocytes (DAO) characterized by expression of several markers, chiefly Serpina3n, as the primary targets of CD administration. We confirmed disturbances in cholesterol metabolism, aligning with findings in ALS patients. Scanning Electron Microscopy (SEM) and Luxol Fast Blue staining confirmed CD's partial rescue of white matter and myelinated axon shrinkage. Mass spectrometry revealed enhanced levels of cholesteryl esters in GA-Nes mice, consistent with the accumulation of cholesterol-rich myelin debris, which CD administration effectively ameliorated. Upregulation of cholesterol-associated genes, ApoD and Plin4, in oligodendrocytes of vehicle-treated transgenic animals, were rescued by CD administration. Furthermore, Plin4 staining in patient spinal cords highlighted its upregulation, underscoring its potential as a therapeutic marker or direct target in ALS. The findings highlight the necessity for further research aimed at effectively targeting the cholesterol phenotype in ALS to develop viable therapies for patients.

1. Introduction

1.1 Amyotrophic Lateral Sclerosis (ALS)

Amyotrophic lateral sclerosis (ALS), also known as Lou Gehrig's disease, is a progressive and fatal neurodegenerative disease characterized by the loss of upper and lower motor neurons (Peters & Brown, 2023). Approximately 10% of cases are familial (fALS), autosomal dominant mutations in over 20 genes discovered that cause ALS with high penetrance and several variants that increase the risk of developing ALS. Nevertheless, the majority of ALS cases are sporadic (sALS) with unknown etiology (Peters & Brown, 2023). The prognosis for ALS patients is dire, with most surviving only 3-5 years from the onset of symptoms (Lynch, 2023). Median survival time from symptom onset ranges between 20 to 48 months, and merely 10-20% of patients live longer than 10 years (Chio et al., 2009). Data from the national ALS registry of the United States, collected from 2014 to 2016, revealed an age-adjusted yearly incidence rate of ALS is about 1.6 to 1.8 per 100,000 U.S. residents (Mehta et al., 2022).

Frontotemporal dementia (FTD) shares clinical presentations, pathological features, and genetic underpinnings with ALS, placing them on a continuum of a disease spectrum commonly referred to as ALS/FTD (Weishaupt et al., 2016). This thesis is focused on the ALS end of the spectrum, but many conclusions likely also apply to FTD.

ALS was first described by French neurologist Jean-Martin Charcot in mid 19th century. A decade later Kahler and Pick documented the atrophy of motor convolutions (Davison, 1941). Typically manifesting around the age of 55, the disease often begins focally, usually in a distal limb, and progressively involves more motor neurons (Peters & Brown, 2023). However, there is considerable variability in its early presentation, with some cases initially manifesting as painful muscle cramps (Kuzel et al., 2017). In its advanced stages, the disease leads to widespread muscle atrophy due to denervation of the neuromuscular junctions, with a noted preferential denervation of extensor muscles over flexor muscles (Peters & Brown, 2023). Ultimately, most patients succumb to respiratory failure (Niedermeyer et al., 2019).

1.1.1 Genetic Causes of ALS

Recent advancements have substantially enhanced our understanding of the genetic foundations of ALS. fALS cases provide a unique form of opportunity to study the molecular mechanisms of ALS because it is generally postulated that similar pathways are also affected in the more heterogenous sALS population. The landmark discovery by Rosen et al. in 1993, identifying mutations in the superoxide dismutase 1 (SOD1) gene as a causative factor for ALS, marked a pivotal moment in ALS research (Rosen et al., 1993). Subsequent investigations identified over 150 different mutations in the SOD1 gene that are associated with ALS, underscoring complexity of the disease (Renton et al., 2014). SOD1 mutations are responsible for approximately 20% of fALS cases and 2% of sALS cases (Andersen & Al-Chalabi, 2011).

Since the discovery of the first ALS-associated gene in 1993, research has unveiled several other genes that play crucial roles in the disease's pathophysiology. Chief among these genes, TARDBP coding for TAR DNA-binding protein 43 (TDP-43), Fused in Sarcoma (FUS), and Chromosome 9 open reading frame 72 (C9ORF72) are some of the most noteworthy genes due to their prevalence and the insights they provide into the mechanism of the disease. However, it's important to acknowledge that numerous other genes have also been associated with ALS (Ghasemi & Brown, 2018).

Cytoplasmic accumulation of ubiquitinated TDP-43 is a hallmark of most ALS/FTD cases (Neumann et al., 2006). Remarkably, even in the absence of TARDBP mutations, TDP-43-positive inclusions are present in approximately 97% of all ALS cases, underscoring the protein's central role in the disease (Mackenzie et al., 2007). TDP-43 aggregates contain C-terminal fragments of TDP-25 and TDP-35 (Cicardi et al., 2018). Because TDP-43 has a critical role in RNA splicing, its accumulation in the cytoplasm can result in loss of function. Concurrently, toxic gain of function has also been shown, making TDP-43 a key protein in ALS etiology (Kabashi et al., 2010).

FUS plays an important role in RNA splicing and transport. Mutations in FUS have been shown to cause cytoplasmic mislocalization of its encoded protein, leading

to neurodegeneration (Kwiatkowski et al., 2009; Vance et al., 2009). Similar to TDP-43 pathology, the mislocalization of FUS results in a loss of its nuclear function and additionally induces a toxic gain of function through its accumulation in the cytoplasm of motor neurons, ultimately leading to cell death (Scekic-Zahirovic et al., 2016).

The identification of Chromosome 9 open reading frame 72 (C9ORF72) and its role in ALS marked a breakthrough in the field. In 2011, it was determined that this hexanucleotide repeat expansion in the first intron of *C9ORF72* is the most frequent cause of fALS, accounting for approximately half of all fALS cases (DeJesus-Hernandez et al., 2011; Renton et al., 2011). Presumably due to increased DNA-methylation, the heterozygous repeat expansion leads to a 40% reduction of function of the normal *C9ORF72* protein levels (Farg et al., 2014). Additionally, the $(G_4C_2)_n$ expansion causes gain of function toxicity from its transcribed mRNA products (Donnelly et al., 2013; Mizielinska et al., 2013) and the five repeat-associated non-ATG-translated dipeptide repeat proteins (DPRs) from both sense and antisense transcripts (Ash et al., 2013; Mori, Arzberger, et al., 2013; Mori, Weng, et al., 2013). Given that the mouse model used in this dissertation focuses on one of these DPRs, specifically poly(GA), a detailed examination of C9ORF72's role in ALS/FTD is warranted in the subsequent section.

Several additional genes play significant roles in the pathogenesis of ALS. Optineurin, involved in vesicular trafficking and regulation of NF-kB signaling pathway, VCP, implicated in autophagy, Profilin1, involved in ATP-mediated actin polymerization, Ataxin2, implicated in RNA processing as well as receptor tyrosine kinase endocytosis, and Angiogenin, involved in vascularization, RNA processing, and neurite outgrowth, are some of the among the genes that account for more than 1% of fALS cases (Ghasemi & Brown, 2018).

Mutations in various other genes, such as *ERBB4*, *CHCHD10*, *SQSTM1*, and *UBQLN2* have been shown to be the main cause of some fALS cases, although they reportedly account for less than 1% of cases (Ghasemi & Brown, 2018). Figure 1 summarizes the main genes that are responsible for more than 1% of reported fALS cases.

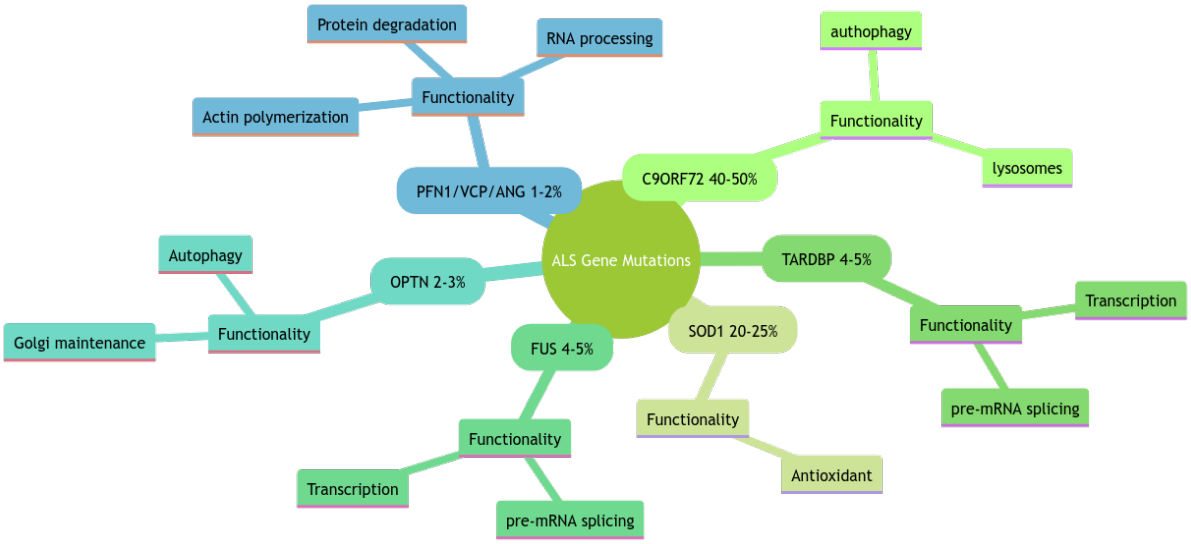

Figure 1: Diagram of common fALS genes, with the fraction of fALS cases caused by these genes given as percentages. The figure is adapted from Table 1 of Ghasemi & Brown, 2018 (Ghasemi & Brown, 2018) and made with diagrams.helpful.dev and Mermaid v10.7.0 Live Editor (helpful.dev, 2024).

1.1.1.1 C9ORF72 nucleotide repeat expansion

C9ORF72 repeat expansion mutation in ALS arises from a hexanucleotide GGGGCC expansion in the intron between alternative exons 1a and 1b and thus overlaps with the promoter region of the dominant transcript initiated at exon 1b. While healthy individuals typically possess less than 30 repeats of this hexanucleotide, individuals affected with ALS harbor hundreds or thousands of base pairs corresponding to this repeat (DeJesus-Hernandez et al., 2011; Renton et al., 2011). Although C9ORF72 is the most common cause of fALS (Ghasemi & Brown, 2018), the exact repeat length is not inherited consistently, as repeat length becomes unstable after approximately 20 repeats, leading to potential shrinkage and expansion (Beck et al., 2013).

Patients carrying the C9ORF72 expanded repeat mutation typically experience a more aggressive disease course compared to other ALS cases, characterized by an earlier age of onset, reduced survival, and a more rapid decline in behavioral and cognitive functions (Byrne et al., 2012). Almost all carriers of this mutation show cytoplasmic TDP-43 inclusion in key regions of neurodegeneration such as the spinal cord, frontal cortex, and temporal or motor cortex (Stewart et al., 2012).

As previously discussed, this repeat expansion not only leads to a loss of function of the normal *C9ORF72* protein levels (Farg et al., 2014), but also induces gain of function toxicity from its transcribed mRNA products (Mizielinska et al., 2013) and the production of the five non-ATG-translated dipeptide repeat proteins (DPRs) from both sense and antisense strand (Ash et al., 2013; Mizielinska et al., 2013; Zhang et al., 2014).

C9ORF72 protein is implicated in a variety of cellular functions, with recent research uncovering roles in immune system regulation in the CNS (Lai & Ichida, 2019), autophagy and endosomal trafficking (Zhu et al., 2020), and axonal trafficking (Abo-Rady et al., 2020). The hexanucleotide repeat expansion may reduce the mRNA expression of the C9ORF72 gene, resulting in the haploinsufficiency of the gene product. This disruption can impair its various functions, leading to a loss of function phenotype (Zhu et al., 2020).

On the toxic gain of function side of the hexanucleotide repeat expansion, both RNA and dipeptide repeat proteins (DPRs) play pivotal roles. One of the two original discoveries of the C9ORF72 repeat expansion showed that RNA foci accumulate in the nuclei of cortex and spinal cord of ALS patients (DeJesus-Hernandez et al., 2011). Subsequent studies identified RNA foci in the cytoplasm as well, although they predominantly reside in the nucleus (Donnelly et al., 2013). C9ORF72 RNA and its resulting foci have been shown to sequester RNA binding proteins (RBPs), such as ADARB2, resulting in impaired RNA processing and inflammatory responses (Donnelly et al., 2013; Kumar et al., 2017), thereby disturbing the neuronal homeostasis.

The repeat-containing C9ORF72 RNA can be translated into 5 unique DPRs along all 6 reading frames of sense and antisense strand through Repeat-Associated Non-ATG (RAN) translation (Mori, Arzberger, et al., 2013; Mori, Weng, et al., 2013). Coincidentally, this non-canonical translation pathway was discovered for CAG repeats just a few months before the discovery of C9ORF72 as an ALS gene (Zu et al., 2011). Moreover, these DPR proteins are prone to aggregate, which are part of

p62-positive TDP-43-negative inclusions that are found in C9ORF72 ALS patients (Mori, Arzberger, et al., 2013).

Translation of the sense strand forms poly(glycine-alanine) (poly(GA)), poly(glycine-proline) (poly(GP)), and poly(glycine-arginine) (poly(GR)). Translation of the antisense strand forms poly(glycine-proline) (poly(GP)), poly(proline-arginine) (poly(PR)), and poly(proline-alanine) (poly(PA)) (Balendra & Isaacs, 2018). Figure 2 summarizes the DPR formations from each strand. Each DPR has been shown to have a varying degree of toxicity, solubility, and aggregation. Studies have also uncovered that they can be transmitted between cells via exosomes (Westergard et al., 2016). Further, DPR inclusions have been detected in in skeletal muscle of 40% of patients (Cykowski et al., 2019), suggesting a potential systemic involvement of DPR pathology beyond the central nervous system.

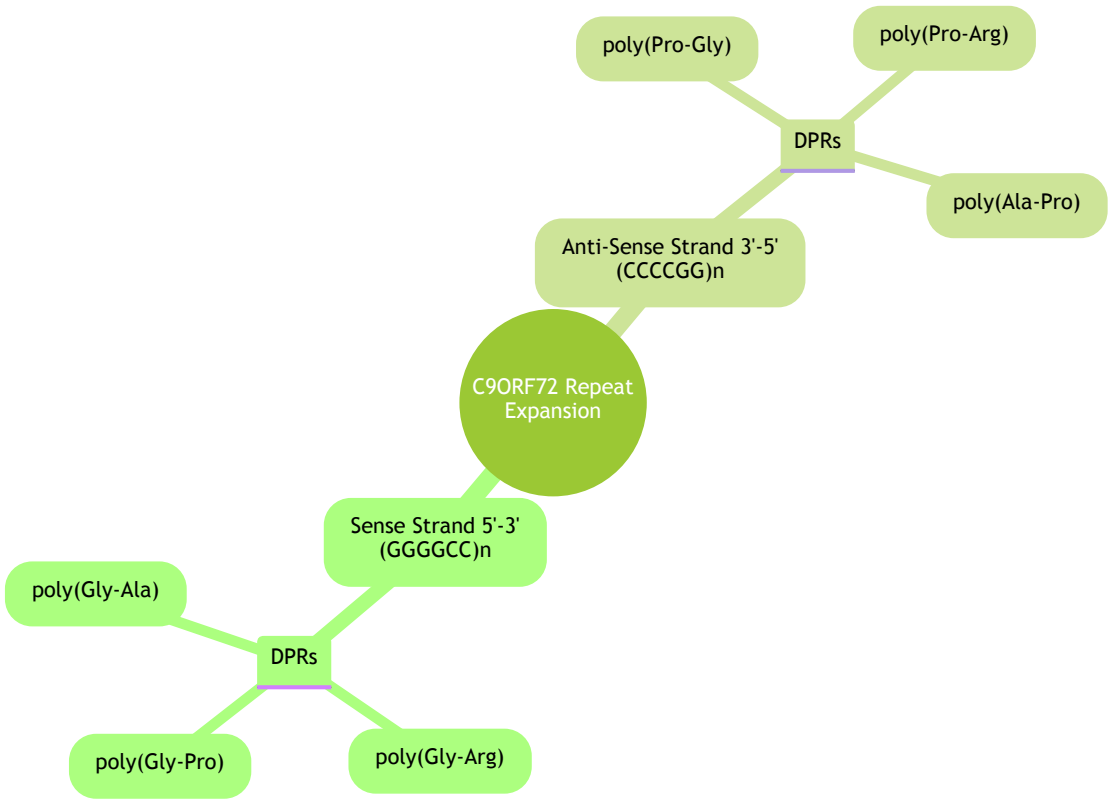

Figure 2: Diagram of DPR formation from sense and antisense strands. The figure is made with diagrams.helpful.dev and Mermaid v10.7.0 Live Editor (helpful.dev, 2024).

1.1.1.2 Poly(GA) Mouse Model of ALS

Among the five DPRs, poly(GA) is clearly the most abundant DPR species (Mori, Weng, et al., 2013), while poly(PR) and poly(GR) induce pronounced toxicity in cellular models (Kwon et al., 2014), with recent studies suggesting that the least abundant DPR species, poly(PR), may exhibit the highest toxicity (Jafarinia et al., 2020). In efforts to elucidate the pathogenic mechanisms underlying DPR toxicity, the Edbauer lab engineered a mouse model that solely expresses 175 repeats of poly(GA) but no other DPRs, and another mouse model with 175 repeats of poly(PR) but no other DPRs. This is achieved by using alternate codon sequences to avoid RAN translation products (LaClair et al., 2020). The poly(GA) or poly(PR) mice were then crossed with a Nes-Cre mouse to induce DPR expression (hence also called GA-Nes).

The GA-Nes mouse model with widespread poly(GA) inclusions showed the most similarity to ALS pathology. It requires euthanasia at around 6-7 weeks of age, primarily due to attributed to notable weight loss (LaClair et al., 2020). The GA-Nes mice display uncommon nuclear TDP-43 aggregates in approximately 1% of neuronal nuclei. These aggregates are primarily observed in the lateral frontal cortex and the CA regions of the hippocampus (LaClair et al., 2020). Additionally, the GA-Nes mice demonstrated substantial early infiltration of microglia into hippocampus, elevated levels of pStat3 and IFNγ, as well as near complete degeneration of neurons in the CA2 region of hippocampus at end stage (LaClair et al., 2020). Importantly, these findings underscore the role of neuroinflammation as a precursor to neurodegeneration, with inflammation subsiding following the advancement of neurodegenerative processes. Figure 3, taken from (LaClair et al., 2020), depicts the key characteristics of the GA-Nes mouse model.

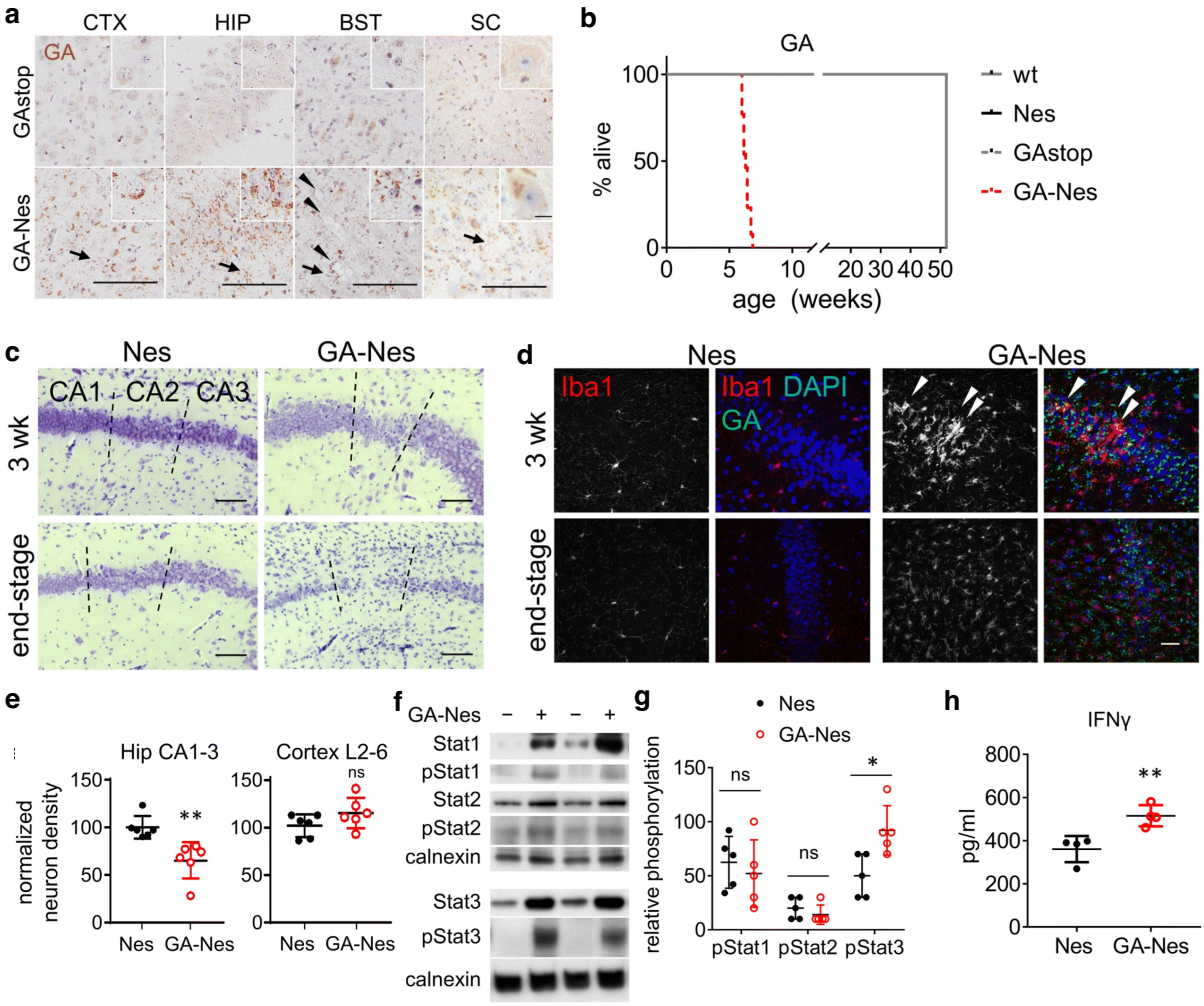

Figure 3: GA-Nes mice experience early neuroinflammation, rapid neurodegeneration, and early mortality. a) The poly(GA) mice express poly(GA) only when crossed with a Cre mouse model, where they show poly(GA) inclusions in all CNS tissue. b) GA-Nes mice show early mortality, around 6-7 weeks of age. c) GA-Nes mice show widespread neurodegeneration, with near total ablation of hippocampal CA2 neurons at end stage. d) GA-Nes mice show massive neuroinflammation, which subdues to a certain extent once neurodegeneration is complete, demonstrating that neuroinflammation precedes neurodegeneration. e) Quantification of neuron density indicates the degeneration is more apparent in hippocampus, and not cortex. f,g) Stat3, but not Stat1 and Stat2, is relatively more phosphorylated, indicating specific immune modulation. h) IFNγ production is increased in GA-Nes, further supporting the Stat3 phosphorylation. Please note that this figure was assembled from material in (LaClair et al., 2020), distributed under the terms of the Creative Commons CC BY license.

1.2 Inflammation in ALS

Most neurodegenerative diseases are characterized by prominent neuroinflammation (Kwon & Koh, 2020). In ALS pathology, microglial and astrocytic activation, peripheral immune cell infiltration (particularly T-cells), and the release of both pro-inflammatory and anti-inflammatory cytokines are observed. These inflammatory signs are common in neurodegeneration (Appel et al., 2021; Beers &

Appel, 2019). The precise role of neuroinflammation in ALS remains elusive, with hypotheses suggesting potential dual effects. In early disease stages, inflammation may confer a protective role, wherein glial cells release neurotrophic factors and anti-inflammatory cytokines to support neuronal survival, promote repair, and mitigate further damage (Beland et al., 2020). However, as the disease progresses, chronic neuroinflammation may ensue, characterized by sustained activation of astrocytes and microglia, leading to prolonged release of pro-inflammatory cytokines and exacerbating disease outcomes (Beers & Appel, 2019; McCauley & Baloh, 2019).

One such cytokine implicated in the inflammatory response in ALS is IFNγ, which is mainly secreted by T-cells and natural killer cells. IFNγ production can drive microglia and macrophages toward a proinflammatory state while suppressing T-regulatory cells (De Marchi et al., 2021). Moreover, IFNγ can activate the JAK-STAT pathway, which can in turn have profound effects on the cell by modulating gene expression (Horvath, 2004). IFNγ has also been shown to induce apoptosis in neurons, thereby contributing to neurodegeneration (Guzel et al., 2021). Importantly, blocking the entry of immune cells with Natalizumab in two ALS mouse models, namely hSOD1^{G93A} and TDP43^{A315T} mice, reduced IFNγ, increased motoneuron number, and extended the survival of the mice (Garofalo et al., 2022).

As previously discussed, GA-Nes mice exhibit elevated levels of IFNγ, which can activate the JAK-STAT signaling pathway, as evidenced by the detection of phosphorylated Stat3 and Stat1 in these mice (LaClair et al., 2020). The JAK-STAT signaling pathway is typically activated by cytokines, such as interferons, which upon binding to their respective receptor sites, lead to the activation of the Janus kinase (JAK) family of tyrosine kinases (Bousoik & Montazeri Aliabadi, 2018). Activated JAKs phosphorylate specific tyrosine residues on the receptor itself, thereby facilitating the recruitment of STAT proteins. JAKs phosphorylate STATs, which leads to their dimerization, enabling their translocation to the nucleus (Villarino et al., 2015). Inside the nucleus, the dimerized STATs bind to specific regions of the DNA, and drive the transcription of interferon-stimulated genes (ISGs). ISGs are crucial to the cell's antiviral defense mechanism (Schoggins & Rice, 2011). Figure 4 visualizes this signaling pathway.

In ALS, aberrant activation of the JAK-STAT pathway may occur, potentially contributing to disease pathogenesis. Targeting this pathway could offer therapeutic benefits, akin to its efficacy in various inflammatory diseases, including COVID-19 (Hoang et al., 2021) and certain myopathies (Ll Wilkinson et al., 2021). To explore the therapeutic value of reducing inflammatory processes, I inhibited JAK1/2 with baricitinib, results of which are shown in the respective section of this dissertation.

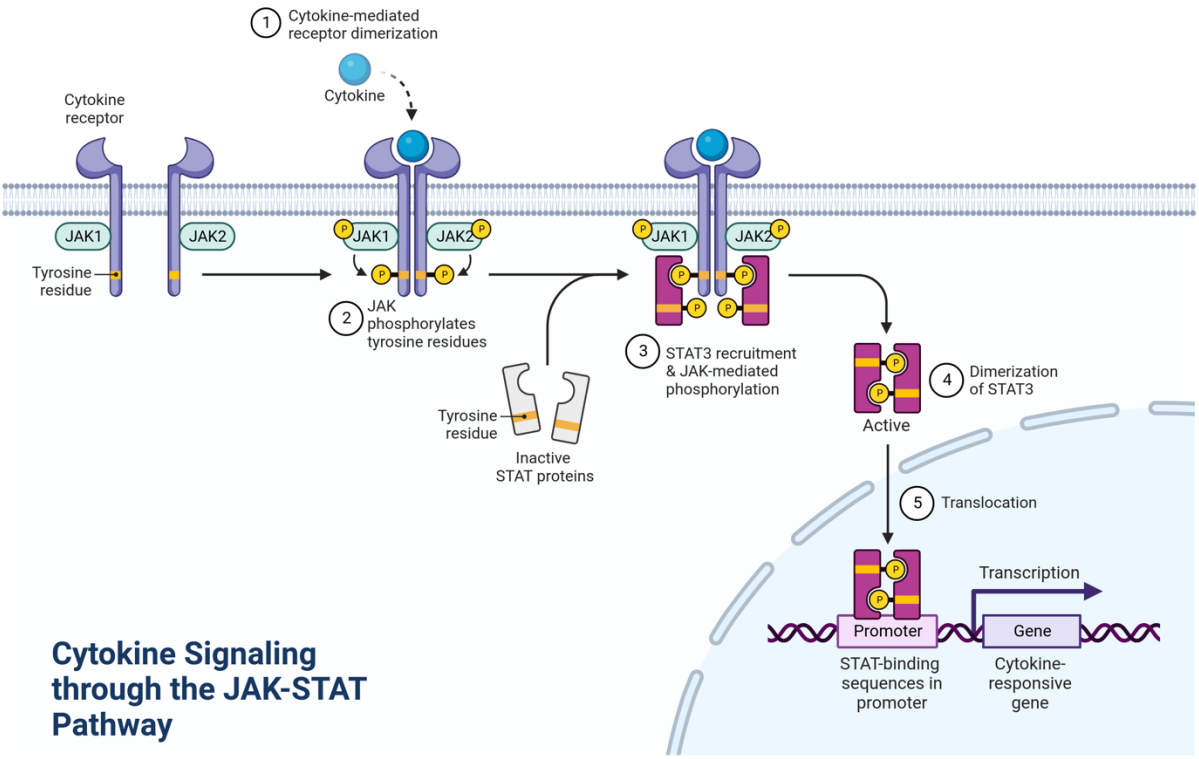

Figure 4: JAK/STAT signaling pathway. The figure was supplied by BioRender.com, and a publication license was obtained from BioRender for the purpose of this dissertation.

1.3 Metabolic Dysfunction in ALS

Energy homeostasis is crucial for life (Langhans et al., 2016). However, ALS patients show consistent metabolic alterations (Dupuis et al., 2011). Patients often exhibit hypermetabolism, while energy intake may be lowered (Vandoorne et al., 2018). The exact prevalence of hypermetabolism among ALS patients remains unclear, with reports indicating that 25-68% of all ALS patients exhibit this condition (Tefera et al., 2021). Interestingly, obesity (to a certain degree) is associated with a 30–40% reduced risk of developing ALS (O'Reilly et al., 2012), and a lower body mass

index (BMI) results in poor survival outcomes. Specifically, the optimal BMI range for ALS patients is reported to be between 30-35, with every 5% decrease in weight linked to a 30% increase in mortality risk (Marin et al., 2011). Furthermore, hypercholesterolemia is linked to the incidence of ALS, while dysfunctions in the metabolism of glucose and lipids are associated with the progression of the disease (D'Amico et al., 2021). Additionally, ALS occurs more in males compared to females, with a ratio of 1.6:1 (Chio et al., 2013), further suggesting a potential link between metabolic factors and disease susceptibility.

There is mounting evidence for the role of mitochondrial dysfunction in ALS. There is evidence of structural damage to mitochondria, defective mitochondrial respiration and ATP production, oxidative stress, calcium mishandling, pro-apoptotic signaling, impaired dynamics (aberrant fissure and fusion, disrupted quality control), impaired axonal transport of mitochondria, and interaction of ALS-associated proteins with mitochondria (Smith et al., 2019). Further, dysfunctional mitochondria could release damage-associated molecular patterns (DAMPs) that can activate microglia and increase neuroinflammation (Mehta et al., 2019).

Glucose metabolism is notably affected in ALS. There are various metabolic impairments in glucose uptake and transport, TCA cycle, oxidative phosphorylation, and glycolysis (Tefera et al., 2021). Furthermore, elevated glycogen levels have been observed in the lumbar spinal cord of $SOD1^{G93A}$ mice, both at disease onset and at end stage (Li et al., 2019). Additionally, research on induced astrocytes of C9ORF72 fALS patients revealed that glycogen phosphorylase and phosphoglucomutase (glycogen mobilization enzymes) were decreased at RNA and protein levels (Allen et al., 2019), which translates to less available glycogen, despite its accumulation.

Metabolic changes have also been documented in various ALS mouse models. For instance, heterozygous $hTDP\text{-}43^{A315T}$ knock-in mice exhibit mitochondrial dysfunction, reduced body weight, and altered blood levels of HDL cholesterol, fatty acids, and glucose (Stribl et al., 2014). It has been further shown that the primary cultures from $SOD1^{G93A}$ presymptomatic motor neurons demonstrate upregulation of fatty acid oxidation (FAO) and the ketogenic components HADHA and ACAT2,

respectively (Szelechowski et al., 2018b). The GA-Nes mice, central to this dissertation, demonstrate significant metabolic disturbances, with weight loss being a primary reason for euthanasia (LaClair et al., 2020). As a high-caloric diet improves survival significantly in ALS patients (Ludolph et al., 2020), we devised an experiment that aimed to explore dietary modifications in the GA-Nes mice, the results of which are shown in the respective section of this dissertation.

1.3.1 Lipids in ALS

Metabolism of lipids is evidently altered in ALS (Tracey et al., 2021). Disruptions in lipid metabolism, encompassing alterations in lipid biosynthesis, overall lipid profiles, and the metabolism of fatty acids and cholesterol, have been extensively documented in ALS (Tracey et al., 2021). The significance of lipids in ALS has escalated to the point where various lipid molecules are being identified as potential disease biomarkers (González De Aguilar, 2019).

Despite ALS primarily affecting the central nervous system, the altered lipid profiles in patients can be detected in the serum, illustrating the systemic nature of metabolic dysregulation in ALS. For instance, a Mendelian randomization study demonstrated a causal relation between elevated low-density lipoprotein (LDL) levels in the blood and a higher risk of ALS (Zeng & Zhou, 2019). Conversely, a study by Dupuis et al. suggested that hyperlipidemia, characterized by high cholesterol and triglyceride levels, may confer a protective effect in ALS, with notably high ratios of LDL to high-density lipoprotein (HDL) associated with an increase in survival time by more than 12 months (Dupuis et al., 2008). Nevertheless, subsequent studies, presented arguments for the causal link between ALS and low-density lipoprotein cholesterol (LDL-C) and total cholesterol (TC), indicating the complex relationship between lipid metabolism and disease risk and progression (Chen et al., 2018).

Irregularities in lipid synthesis and degradation are evident in ALS, potentially interacting with other known protein pathologies or directly causing ALS. Simpson et al. in 2004 found that sera from sporadic ALS (sALS) patients contain significantly elevated levels of lipid peroxides, contributing to oxidative stress and immune activation (Simpson et al., 2004). Research conducted in Sanofi revealed increased

levels of ceramide, glucosylceramide, galactocerebroside, lactosylceramide, globotriaosylceramide, and the gangliosides GM3 and GM1, in the spinal cord of ALS patients (Dodge et al., 2015). Their study in $SOD1^{G93A}$ mice demonstrated increased levels of ceramide, glucosylceramide, GM3, and hexosaminidase activity (Dodge et al., 2015). In another study, research showed that variants in *SPTLC1*, which is critical for sphingolipid synthesis, have been linked to a monogenic form of ALS in childhood (Mohassel et al., 2021). The results indicated that these variants shift serine palmitoyltransferase (SPT) amino acid usage from serine to alanine, resulting in higher levels of deoxysphingolipids, eventually leading to neuropathy (Mohassel et al., 2021), underscoring the critical role of sphingolipid biosynthesis in ALS.

The metabolism of cholesterol is also closely associated with ALS. The ratio of low-density lipoprotein (LDL) to high-density lipoprotein (HDL) has been identified as a prognostic factor. (Dupuis et al., 2008). Cholesterol metabolism is broadly recognized as being disrupted in ALS. Highlighting this, one study specifically identified that the bioactivity of CYP27A1, a key enzyme primarily responsible for the biosynthesis of (an acidic branch of) bile acids and active within the CNS, is impaired in ALS. This dysfunction leads to a reduced capacity of the CNS to eliminate excess cholesterol where excess cholesterol was found in CSF of patients (Abdel-Khalik et al., 2017), highlighting issues with lipid clearance in the disease. For a comprehensive understanding of cholesterol metabolism, Figure 5 outlines the homeostasis of cellular cholesterol, while Figure 6 depicts the brain-specific aspects of cholesterol metabolism; both figures are taken from (Martin et al., 2014).

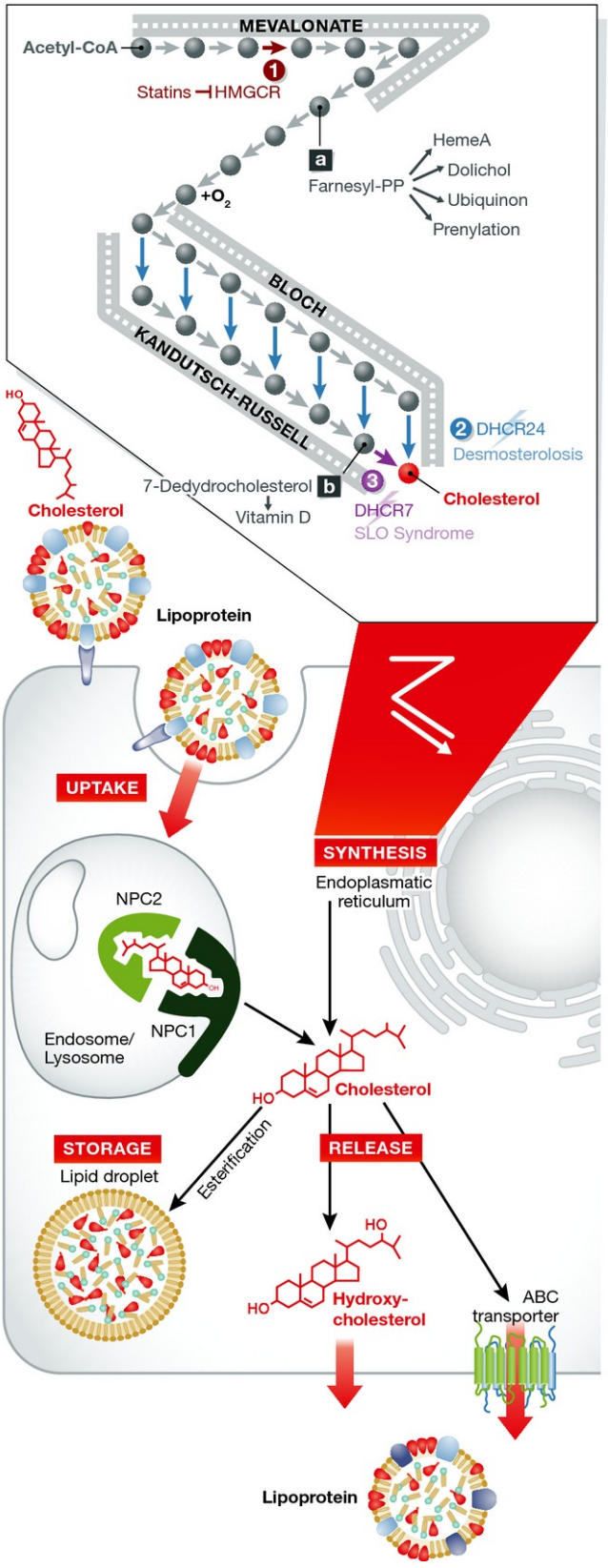

Figure 5: Cellular homeostasis of cholesterol. Storage of cholesteryl esters in lipid droplets involves phospholipids and one or more of the perilipin family members that surround the lipid droplet. Several molecules, such as ApoE, are involved in the uptake and release of cholesterol and its metabolites. This figure is taken from (Martin et al., 2014) with permission to reuse in this dissertation under license ID 1446584-1.

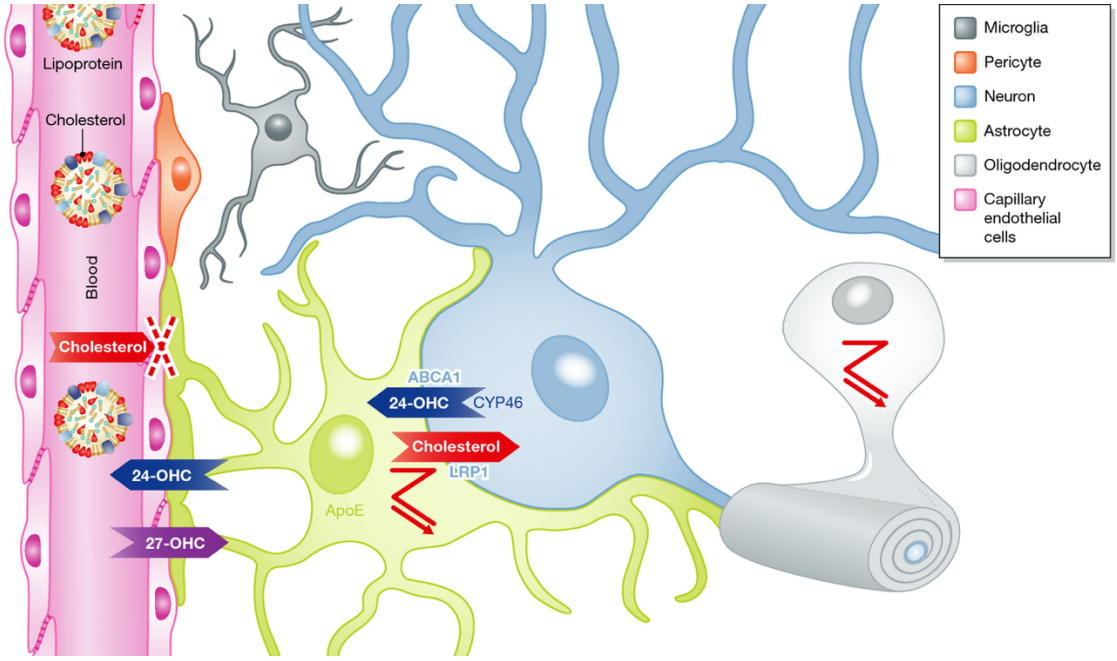

Figure 6: Brain-specific aspects of cholesterol metabolism. Cholesterol cannot cross the blood brain barrier (BBB), while oxysterols such as 24-OHC and 27-OHC can do so. 24-OHC levels in plasma can therefore be used by the periphery as a measure of CNS cholesterol. Zagged lines indicate glia that can synthesize cholesterol, which neurons can import by LRP1. The figure is taken from (Martin et al., 2014) with permission to reuse in this dissertation under license ID 1446588-1.

Moreover, cholesterol esters (CEs) have been implicated in disease pathogenesis. One study showed that triacylglycerols and CEs are elevated in the grey matter spinal cord of sporadic ALS patients (Dodge et al., 2020). Along with triglycerides, CEs are the major constituents of lipid droplets (LDs) that form in neurons as well as glia, which have been linked to ALS pathology (Pennetta & Welte, 2018). A study in yeast showed that lipid droplets are essential in the clearance of cytosolic inclusion bodies (Moldavski et al., 2015), linking aggregate clearance with lipid droplets. *C9ORF72* haploinsufficiency exacerbates these effects, leading to increased LDs and dysregulated lipid metabolism (Liu et al., 2018). Furthermore, a study identified the accumulation of 25-hydroxycholesterol, a toxic oxysterol derivative, in the serum of ALS patients, correlating with accelerated disease progression—a finding also replicated in $SOD1^{G93A}$ mice (Kim et al., 2017).

The involvement of lipids in other neurodegenerative diseases, such as Alzheimer's disease (AD) and Parkinson's disease (PD), highlights the broader significance of lipid clearance and metabolism in neurodegeneration (Estes et al., 2021). For example, ApoE, mainly responsible for lipid transport, is heavily linked to

AD. This link was established by the discovery of APOE type 4 allele as the “strongest genetic risk factor for AD” (Corder et al., 1993). In light of this, our study employed 2-hydroxypropyl-β-cyclodextrin (HP-β-CD, “CD”), a cholesterol-sequestering agent, to investigate its therapeutic potential in ALS. The methodology and outcomes of this investigation are detailed in a subsequent section of this dissertation.

1.4 Lipid Droplets and PLIN4

Lipid droplets (LDs) are dynamic intracellular organelles whose synthesis begins in the endoplasmic reticulum (Walther & Farese, 2012). The formation of LDs involves the accumulation of neutral lipids like sterol esters and triacylglycerols (TAGs) between the leaflets of the ER membrane, constituting LD precursors. Additional lipids and proteins are recruited to further mature the lipid droplets (Walther & Farese, 2012). Therefore, LDs have a core comprised of neutral lipids such as sterol esters and TAGs, which are surrounded by a monolayer of phospholipids. This monolayer is itself coated with a sundry of proteins, especially perilipins, which are crucial for the dynamics of LDs (Martin & Parton, 2006).

LDs are not just energy storage containers that consist of fatty acids and cholesterols. They also play an active role in cell signaling and metabolism by interacting with other organelles such as peroxisomes and mitochondria to coordinate lipid signaling and metabolism (Greenberg et al., 2011). Recent advancements in research have shed light on the role of LDs beyond metabolism. For example, lipid droplets have been shown to protect against ER stress and mitochondrial damage (Olzmann & Carvalho, 2019).

Perilipins (PLINs) are the most prevalent family of proteins that inhabit the LD surface. PLINs influence all aspects of LD biology (Najt et al., 2022). PLIN1, predominantly expressed in adipose tissue, regulates lipolysis by modulating the access of lipases to the lipid core; *PLIN1* undergoes phosphorylation in response to lipolytic stimuli, playing a key role in hormonal regulation of lipolysis (Greenberg et al., 1991). PLIN2 (ADRP/adipophilin) and PLIN3 (TIP47), involved in the formation and stabilization of LDs, are expressed across a broad range of tissues and cell types

(Brasaemle et al., 1997; Wolins et al., 2006). Specifically, PLIN2 is ubiquitously expressed and is suggested to protect LDs against lipolysis (Brasaemle et al., 1997) while PLIN3 is implicated in the trafficking of LDs and is considered essential for the efficient storage of lipids (Wolins et al., 2006). The most recently identified member, PLIN5 (OXPAT/LSDP5), is predominantly expressed in tissues characterized by high oxidative metabolism, such as the heart and skeletal muscles. It regulates lipolysis and fatty acid oxidation, displaying anti-lipolytic properties under basal conditions but facilitating lipolysis under “PKA-stimulated conditions” (Najt et al., 2022).

PLIN4 (S3-12), while less studied than other perilipin family members, is known to be expressed in adipose tissue and skeletal muscle. It is believed to influence LD formation and size regulation, though its functions require further elucidation (Wolins et al., 2003). One study discovered that PLIN4-dependent LDs hamper neuronal mitophagy in a mouse model of Parkinson’s Disease (PD) (Han et al., 2018). It was shown that inhibition of LD storage by downregulating PLIN4 promoted the survival of cells by alleviating mitochondrial damage through restoration of autophagy. Therefore, the authors proposed PLIN4 as a potential biomarker in PD (Han et al., 2018). Further research has indicated that neuronal SH2B1 may attenuate apoptosis by facilitating PLIN4 degradation, underlining PLIN4's involvement in neurodegenerative pathology through the SH2B1-HSC70-PLIN4 axis (X. Han et al., 2022).

In the context of ALS, one study using $SOD1^{G93A}$ mouse model of ALS reported that PLIN4 is extensively distributed in neurons, with its expression increasing from pre-onset to onset to progression stages while significantly correlating with neuronal death (Zhu et al., 2021). Our investigation also delves into the gene expression profile of PLIN4, particularly in oligodendrocytes, as recently reported in an MS model (Falcão et al., 2018), with findings presented in the results and discussion sections.

1.5 Available Therapies in ALS

Drugs

As with many neurodegenerative diseases, the therapeutic options for amyotrophic lateral sclerosis (ALS) are limited, yet the landscape is evolving rapidly

due to a deeper understanding of the disease. Until 2018, the only available therapy for ALS was riluzole, which is an anti-glutaminergic drug that extends survival by two to three months (Miller et al., 2012). The ALS landscape began to change in 2019 with the approval of Edaravone, and subsequently, AMX0035—a combination of sodium phenylbutyrate and taurursodiol—in 2022 in the United States (withdrawn later). Most recently, in 2023, the U.S. Food and Drug Administration (FDA) approved Tofersen, bringing the total number of available drugs for ALS to four (Ilieva et al., 2023), marking a significant period of accelerated therapeutic discoveries for the disease.

Edaravone targets a subset of ALS patients by mitigating oxidative stress through its action as a free radical scavenger (Writing-Group-Edaravone, 2017). The combination of sodium phenylbutyrate and taurursodiol is believed to alleviate cell death, reduce ER distress, and improve mitochondrial function. Administration of this compound has resulted in slower functional decline compared to a placebo over a period of 24 weeks (Paganoni et al., 2020). In April 2023, Tofersen, an antisense oligonucleotide (ASO) leading to non-selective degradation of wildtype and mutant SOD1 mRNA, was approved, offering the first causal treatment option for ALS (Ilieva et al., 2023) and confirming a dominant gain-of-function toxicity of these mutations.

While not technically an ALS medication, the combination of dextromethorphan hydrobromide and quinidine sulfate (Nuedexta) is used as a treatment for pseudobulbar affect (PBA), which is a relatively common non-motor symptom of ALS (Johnson et al., 2022). This underscores the importance of addressing the broader spectrum of ALS symptoms beyond direct disease modification.

Research into ASO therapies targeting C9ORF72 and FUS mutations is actively underway (Ilieva et al., 2023), although some trials have been terminated. One of the more promising therapies is ION363 (Jacifusen). ION363 is an ASO drug against FUS and has had a miraculous result on a patient with FUS^{P525L} mutation where a paralyzed patient is able to walk again (Fossgreen, 2023; Thadeusz, 2022), although it's important to note that the initial patient in the study passed away despite reduced *FUS* levels, highlighting the complex nature of ASO therapy outcomes (Korobeynikov et al., 2022). Therefore, despite various failures of ASO therapies,

there is a lot of potential ahead. Additionally, potential therapies focusing on neuroinflammation, excitotoxicity, and oxidative stress are being explored for their therapeutic value in ALS (Tzeplaeff et al., 2023).

Supportive Therapy

There are various forms of palliative and supportive care provided to ALS patients. Non-motor symptoms affect an estimated 5-80% of all patients (Fang et al., 2017). Such symptoms can range from vascular irregularities to neuropsychiatric issues, underscoring the need for comprehensive care (Fang et al., 2017). The main avenues of supportive therapy are symptomatic medical treatment, mobility, speech and swallowing, ventilation, counseling and palliative care (Tzeplaeff et al., 2023).

Symptomatic medical treatments primarily involve pharmacotherapy, while counseling and palliative care focus on psychotherapy and end-of-life decisions, respecting legal frameworks where applicable (Tzeplaeff et al., 2023). Mobility support includes the utilization of assistive technologies such as robotics and wheelchairs, alongside physical and occupational therapy to maximize independence (Tzeplaeff et al., 2023). For speech and swallowing difficulties, interventions range from communication devices, such as brain-computer interfaces, to nutritional support (for example high caloric supplements to avoid weight loss when BMI < 35) and speech therapy (Tzeplaeff et al., 2023). As the disease progresses and swallowing becomes difficult, alternate routes of nutrition via nasogastric tube (NGT), radiologically inserted gastronomy (RIG), or percutaneous gastrostomy (PEG) could become necessary (Diagnosis et al., 2012). Ventilation support is provided through both invasive and non-invasive ventilation options, along with cough-assisting devices, to aid respiratory function (Tzeplaeff et al., 2023).

1.6 HP-β-CD (CD) and Its Therapeutic Application

Cyclodextrins, the main focus of this dissertation, are cyclic oligomers derived from amylose that consist of a variable number of glucose units linked by α-1-4 bonds (Gould & Scott, 2005). These oligomers create a cone-shaped cavity that allows substances to enter and form a water-soluble complex, thereby altering the physical

and chemical properties of the cargo (Gould & Scott, 2005). Given these characteristics, cyclodextrins are often utilized as pharmaceutical vehicles for poorly soluble drugs.

Common cyclodextrins used as vehicles are α-, β-, and γ-cyclodextrins, which differ in the number of glucose molecules they contain, with each containing 6, 7, and 8 glucose molecules, respectively (Gould & Scott, 2005). α- and β-cyclodextrins are primarily degraded by intestinal flora, whereas γ- cyclodextrin is also subject to degradation by pancreatic enzymes, making the toxicity of γ- cyclodextrin the least of the three (Antlsperger & Schmid, 1996). Among these, α-cyclodextrin is thought to have the slowest metabolism, while γ-cyclodextrin has the fastest metabolism rate (Frömming & Szejtli, 1994).

2-hydroxylpropyl-β-cyclodextrin (HP-β-CD, also referred to simply as CD in this dissertation) possesses enhanced water solubility and is possibly less toxic, thus a superior alternative to either α-, β-, or γ-cyclodextrins (Yoshida et al., 1988). This advantageous profile makes CD a valuable tool in the formulation of pharmaceuticals, offering improved delivery and efficacy of therapeutic agents.

Toxicological evaluations of CD have yielded a wide range of outcomes, underscoring the influence of slight variations in formulation and dosing on toxicity and efficacy (Antlsperger & Schmid, 1996; Frömming & Szejtli, 1994; Gould & Scott, 2005; Liu et al., 2020; Thackaberry et al., 2010; Walenbergh et al., 2015). This variability suggests the need for establishing specific toxicity profiles in each study, particularly at doses at or above 1000 mg/kg, where some literature reports potential toxicity. Notable concerns include kidney damage and iatrogenic hearing loss from chronic exposure, as well as respiratory and body temperature regulation issues in acute settings (Antlsperger & Schmid, 1996; Frömming & Szejtli, 1994; Gould & Scott, 2005; Liu et al., 2020; Thackaberry et al., 2010; Walenbergh et al., 2015). While the majority of studies report minimal toxicity below 1000 mg/kg, one study detected bone loss in a chronic treatment at only 200 mg/kg CD (Kantner & Erben, 2012). Thus, customizing clear toxicological parameters to monitor each study is crucial to facilitate the development of effective and safe pharmaceutical formulations.

CD is recognized not only as a versatile excipient but also for its notable pharmacological property of sequestering lipids, especially cholesterol (Kilsdonk et al., 1995; Walenbergh et al., 2015). This property has facilitated its use in the treatment of various conditions, including Niemann-Pick disease type C (NPC) (Liu et al., 2008), atherosclerosis (Wang et al., 2019; Zimmer et al., 2016), and to a lesser extent, stroke (Becktel et al., 2022) and Alzheimer's disease (Yao et al., 2012). In NPC, the loss of function of *NPC1* protein results in impaired lipid trafficking and accumulation of cholesterol within lysosomes, resulting in cellular dysfunction and death (Vanier, 2010). HP-β-cyclodextrin (CD) and HP-γ-cyclodextrin, but not HP-α-cyclodextrin, attenuate the accumulation of sphingolipids, mainly sphingomyelins, and free cholesterol, as well as lysosomal expansion in *Npc1*-null CHO cells (Hoque et al., 2020). Although initially thought to not cross the blood-brain barrier (BBB), subsequent research demonstrated that high-dose subcutaneous or intraperitoneal administration of CD can indeed have central nervous system (CNS) effects (Calias, 2017). Thus, CD acts by solubilizing lipids and aids their clearance.

A formulation of CD known as adrabetadex, approved for compassionate use in NPC1 patients, did not show a reduction in NfL levels in patients (Agrawal et al., 2023). Nevertheless, a new formulation of CD called Trappsol Cyclo is in trial for NPC1 and AD, with promising initial results (Sharma et al., 2023). An alternative, less explored mechanism of cyclodextrins may involve their anti-inflammatory properties, particularly relevant in the context of neurodegenerative diseases (Lucia Appleton et al., 2021).

In the ALS field, the application of CD has been tested in a SOD1 model. A study involving $SOD1^{G93A}$ mice, where CD was administered weekly at a dose of 4000 mg/kg subcutaneously, did not yield improvements in body mass, grip-strength, muscle force, contractile properties or motor unit number estimates (Greensmith & Bryson, 2023). However, as discussed in this section, dosing, formulation, and route of administration play a pivotal role in the toxicity and effectivity of CD, and as I will demonstrate later, this compound shows remarkable results in extending the survival of GA-Nes mice.

1.7 Single Cell RNA Sequencing

The advent of 'omics' technologies has revolutionized biology, enabling the simultaneous and precise analysis of molecular processes at a level of detail previously unimaginable. The integration of various 'omics' data sets allows researchers to achieve an unprecedented resolution of cellular processes, though such integration can be challenging (Joyce & Palsson, 2006). Transcriptomics, in particular, focuses on analyzing the transcriptome—the complete set of RNA transcripts produced by the genome. The introduction of next-generation sequencing (NGS) and RNA sequencing (RNAseq) has transformed not just transcriptomics but the entire field of biology (Wang et al., 2009).

Single-cell transcriptomics advances this transformation further by enabling gene expression analysis at the individual cell level. A pivotal study in 2009 by Tang et al. introduced the concept of single-cell RNA sequencing (scRNAseq), showcasing its potential and superiority over previous techniques. Even with what would now be considered rudimentary technology, their approach detected the expression of 75% more genes than could be identified using microarray techniques (Tang et al., 2009).

Since 2009, single-cell technology has developed at a fast pace and has become a mainstay in unraveling various mechanisms underlying biological mechanisms. For example, scRNAseq has been used to define cell types and states in a diverse set of tissues, which has contributed immensely to our understanding of the disease (Svensson et al., 2018). For instance, scRNAseq enabled the identification of a disease-associated microglia (DAM) subtype in the context of Alzheimer's disease, which has been shown to have consequential implications in the disease (Hadas Keren-Shaul et al., 2017).

The array of single-cell technologies has significantly expanded, introducing a variety of methods to analyze individual cells at unprecedented scales (Baysoy et al., 2023). Drop-seq represents a pioneering advancement, offering a high-throughput, microfluidic-based approach for analyzing thousands of cells through parallel processing in a single run (Macosko et al., 2015). Smart-seq and Smart-seq2 offer

another approach to snRNAseq where they cover the full-length transcripts, but are generally less high-throughput and more expensive than comparable techniques (Picelli et al., 2014). The 10x Genomics platform, employed in the research presented here, leverages a unique barcoding system that allows for the analysis of tens of thousands of cells in a single run. The 10x platform has become the most widely used single cell platform, given its scalability and high-throughput capabilities (Zheng et al., 2017).

The foundation of 10x platform lies in its unique barcoding strategy. It utilizes a microfluidic chip to partition thousands of cells into nanoliter-scale Gel Bead-In-Emulsions (GEMs) (Zheng et al., 2017). Cell lysis occurs within each GEM, where a unique barcode is attached to each mRNA molecule that effectively tags transcripts from each cell with a distinct identifier (Zheng et al., 2017). This process allows for parallel processing of numerous cells. Following barcoding, the mRNA is reverse-transcribed into cDNA, which is then pooled, amplified, and subsequently sequenced (Zheng et al., 2017). The resulting data undergoes analysis to demultiplex the barcodes, assigning transcripts back to their originating cells and integrating the data for comprehensive analysis (Stuart et al., 2019; Stuart & Satija, 2019). Figure 7 showcases the workflow of a GemCode single-cell technology (such as that of 10x Genomics platform).

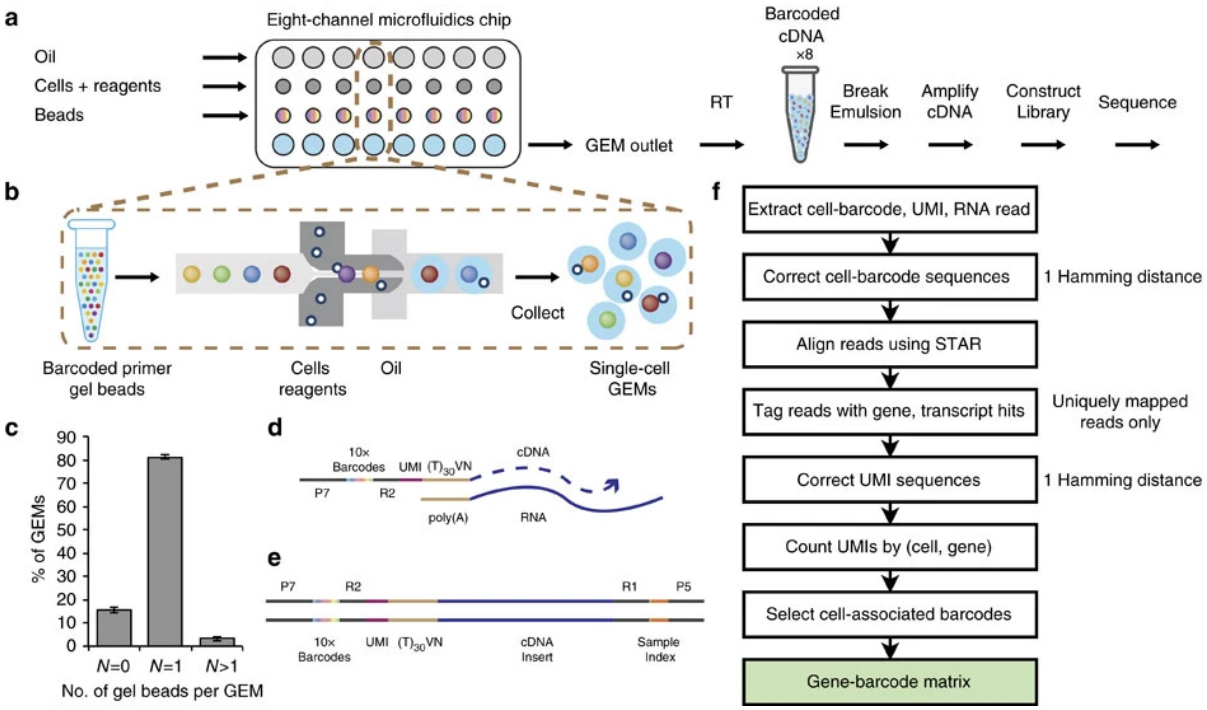

Figure 7: GemCode single-cell technology of 10x platform. a) scRNAseq workflow inside each GEM, where cDNA synthesis takes place, and the transcripts are pooled and amplified to construct a library. b) Primers are loaded into gel beads. c) Bar graph showing the big majority of GEMs contain 1 gel bead. d) Gel beads contain the cDNA along with oligo dTs, unique molecular identifiers (UMIs), 10x barcodes, and Illumina adapters (for sequencing with Illumina pipeline). e) Molecules in the finished library contain illumine adapters and sample indices, which allows pooling. f) Workflow with the 10x CellRanger software. This figure is taken from (Zheng et al., 2017), licensed under a Creative Commons Attribution 4.0 International License.

10x Genomics' single-cell transcriptomics platform has been widely adopted not only due to its high-throughput capabilities, but also because of its ability to handle diverse sample types, from blood to brain to tumor tissue, and even nuclei (Stuart & Satija, 2019). In this study, we indeed used nuclei, which grant the ability to sequence from frozen tissue, allowing direct comparability to frozen human tissue.

1.8 Disease Associated Oligodendrocyte (DAO)

Oligodendrocytes, the myelinating cells of the CNS, are crucial for neuronal survival, offering both myelination and metabolic support (S. Han et al., 2022). In the context of neurodegenerative diseases, myelin damage is a recurring feature. While earlier views focused on neuronal apoptosis leading to myelin damage, it is now understood that myelin impairment can also directly cause neuronal death, although the main disease mechanism is neuronal. This is exemplified in multiple sclerosis (MS), where disease-specific oligodendrocyte lineages have been characterized

(Falcão et al., 2018). Similarly, in Alzheimer's disease (AD), oligodendrocytes contribute to disease progression through myelin breakdown and association with neurofibrillary tangles (Blanchard et al., 2022; Cai & Xiao, 2016).

With the advent of scRNAseq, more evidence has emerged from various neurodegenerative diseases and their respective models for a shared gene signature in oligodendrocytes, termed disease-associated oligodendrocytes (DAOs). Several key markers such as Serpina3n, C4b, and Il33 have been identified as markers of DAOs in an array of neurodegenerative diseases (Kenigsbuch et al., 2022; Pandey et al., 2022). The DAO signature displayed more differences between AD mouse models and patients than between MS mice and patients (Pandey et al., 2022). In ALS, the DAO signature is not well-characterized, however, there are many reports on the dysfunction of oligodendrocytes. Such oligodendrocyte dysfunctions range from impaired differentiation of OPCs (mediated by oxidative stress), insufficient local energy supply to axons, myelin damage, and inflammatory injury (Gong et al., 2022).

The precise role of DAOs in disease progression is still unclear. They may represent either a disease-driving factor or a protective response, with both adaptive and maladaptive changes reported (Kenigsbuch et al., 2022). The gene expression profile in DAOs indicates a compromised capacity for myelin regeneration or repair, particularly notable in MS, a primary demyelinating disease (Kenigsbuch et al., 2022). Furthermore, DAOs' reduced ability to support neuronal metabolism may exacerbate neuronal death and dysfunction (Clayton & Tesar, 2021). It has also been proposed that DAOs produce more pro-inflammatory cytokines, exacerbating the inflammatory milieu in neurodegenerative diseases (Chen et al., 2023), while oxidative stress and neuronal ferroptosis have been linked with DAOs as well (Zhou et al., 2023).

Using snRNAseq, I detected DAOs in poly(GA) mice. Utilizing 2-hydroxypropyl-β-cyclodextrin (CD), we partially rescued the DAO signature, with detailed findings presented in the results section.

2. Aims of This Work

The objective of this dissertation is to deepen our understanding of the poly(GA) model of *C9ORF72* ALS and to test potential novel treatment strategies for this condition. This dissertation consists of three main parts: anti-inflammatory therapy, dietary adjustment in mice coupled with metabolic monitoring in cells, and cholesterol-sequestering therapy.

Hypotheses and Objectives

1. **Neuroinflammation and Neurodegeneration**: Based on findings that microglia infiltration precedes neurodegeneration in GA-Nes mice (LaClair et al., 2020), I aim to test the hypothesis that anti-inflammatory therapy with the JAK inhibitor baricitinib might decelerate disease progression and enhance survival rates.
2. **Metabolic Intervention and Monitoring:**
   A) Given hypermetabolism in ALS (Bouteloup et al., 2009), and observed weight loss of GA-Nes mice requiring euthanasia (LaClair et al., 2020), I aim to test whether carbohydrate or protein-rich dietary supplementation can extend survival.
   B) Given the documented metabolic disturbances in ALS (Dupuis et al., 2011), we aim to assess ATP/ADP and NADH/NAD^+ ratios using imaging techniques and mass spectrometry in primary hippocampal and cortical neurons expressing poly(GA) to elucidate whether protein aggregation itself causes metabolic stress.
3. **Cholesterol-Sequestering Therapy with HP-β-CD (CD):**
   A) Given the evidence for cholesterol dysmetabolism in poly(GA) mice and ALS patients, we hypothesized that a cholesterol-sequestering compound, such as CD can extend survival.
   B) The cellular targets of CD administration should be dissected using single nucleus transcriptomic snRNAseq.
   C) Given the high cholesterol content in myelin, we hypothesize that disturbances in myelination or myelin degradation could contribute to the observed cholesterol phenotype, which we further hypothesized to be potentially rescued by CD administration.

3. Materials and Methods

Important Notice: Please be advised that parts of this section will appear in a peer-reviewed publication. At the time of final submission of this dissertation, the manuscript is under revision at Nature Communications, titled "Correction of dysregulated lipid metabolism normalizes gene expression in oligodendrocytes and prolongs lifespan of a poly-GA C9orf72 mouse model". The sole first author of this work is myself, and the corresponding author is Prof. Dr. Dieter Edbauer. This notice serves to obviate any allegations of plagiarism.

All citations in this work were made with EndNote 20 (The-EndNote-Team, 2013). The entire text was written by me (Ali Rezaei) in Microsoft Word for Mac version 16.63.1. Text generation was entirely done by me, with insights used from the literature, which are cited. The entire text was proofread paragraph by paragraph by open-AI's GPT-4 for mistakes in spelling, grammar, and style, using a self-made custom GPT for this purpose in the ChatGPT interface. AI was not used for any original text generation in this work; its use was limited to paraphrasing in order to preserve tenses and professionalism in scientific writing. The text was then proofread by my supervisor and further changes were made to increase scientific quality and readability. Exact methods for outsourced experiments (mass spectrometry at Sanofi and at Creative Proteomics) are not available. In all figures, where p-values are not explicitly indicated, the following keys for p-values apply:
ns: => 0.05, * : < 0.05, ** : < 0.01, and *** : < 0.001.

3.1 Animal Experiments

All animal experiments were implemented following our approved animal experiment license protocol, which complies with the German government's regulations and is approved by ethics committees. All animal experiments followed German animal welfare law and were approved by the government of upper Bavaria. All mice were housed in our pathogen-free animal facility, in standard cages with 12-h light/dark cycle with ad libitum access to water and food. In total, I performed 3 separate animal experiments: baricitinib study, DietGel study, and cyclodextrin study.

All animals were identified by ear biopsies, which were performed on P21 upon weaning. This ear biopsy was also used for genotyping.

Breeding and Genotyping

Breeding and genotyping schemes follow the previously published protocol in which Katherine LaClair and others from the Edbauer lab generated the GA-Nes mice (LaClair et al., 2020). Essentially, GAstop homozygous animals (genotyped for the presence of GFP and absence of the wildtype Rosa26 band) were crossed with Nes-Cre heterozygous mice (genotyped for the presence of Cre). The resulting offspring were the experimental animals, half of which would be wildtype controls, and the other half would be the transgenic mice. The transgenic animals were identified by genotyping for the presence of Cre.

To perform genotyping, an ear biopsy was selected to isolate DNA from using the HotSHOT method (Truett et al., 2000). 20 μL of a 25mM NaOH / 0.2 mM EDTA solution was added to the ear biopsy, and incubated at 95 ˚C for 30 minutes in a thermal cycler. Subsequently, 20 μL of a 40 mM Tris HCl (pH 5.5) solution was added to the mixture. Next, the mixture was briefly centrifuged to precipitate the debris from the biopsy. 1 μL of this mixture would suffice for a 25 μL PCR reaction for genotyping. Table 1 details the GoTaq® PCR mix (Promega, M7845) for 1 reaction, while Table 2 details the primers used for this purpose. Table 3 details the thermal cycler settings used for genotyping.

Component	µL Amount
DNA	1
5x GoTaq buffer	5
Fwd. Primer (20µM)	0.25
Rev. Primer (20µM)	0.25
dNTPs (10mM)	0.5
GoTaq Enzyme	0.125
H_2O	Fill up to 25

Table 1: PCR master mix for GANes-related genotypings

Primer	Sequence
Cre Fwd.	5’ - ATGCCCAAGAAGAAGAGGAAGGT
Cre Rev.	5' - GAAATCAGTGCGTTCGAACGCTA
Rosa26_wt Fwd.	5’ - GCTCAGTTGGGCTGTTTTGG
Rosa26_wt Rev.	5' - TGGAAAATACTCCGAGGCGG
eGFP Fwd.	5' - AAGTTCATCTGCACCACCG
eGFP Rev.	5’ - TCCTTGAAGAAGATGGTGCG

Table 2: Primers used for genotyping GANes breeder and experimental mice

Step	Temperature (°C)	Time (s)	
Initial Denaturation	95	120	
Denaturation	95	20	**Repeat for 35 Cycles**
Annealing	58	30	
Elongation	72	45	
Final Elongation	72	300	

Table 3: Thermal cycler settings for GANes-related genotyping

The PCR reactions were run on a 1% agarose gel. Agarose gels were made in 1x sodium borate buffer (5 mM $Na_2[B_4O_5(OH)_4]$, adjusted to pH 8.0 with H_3BO_3) and mixed with appropriate amounts of GelRed (Millipore, SCT123). Gels were run at a constant voltage of 100 volts. A 1Kb plus DNA ladder (Invitrogen, 10787018) was used to aid in size determination. The gels were placed under UV light to visualize the DNA.

Baricitinib Study

For this study, determining the frequency of treatment was an integral part of the experimental process. The treatment schedule is detailed in the Results section and illustrated in Figure 10. Experimental animals were administered daily subcutaneous injections of baricitinib (AmBeed, A102707) from P28 until they reached the humane endpoint. The vehicle for the drug consisted of 5% DMSO, 50% PEG-300, 5% Tween-80. Initially, 50 mg/Kg doses were prepared. Just prior to injection, both the drug and the vehicle were diluted 1:5 with PBS, resulting in a final dose of 10 mg/Kg. The reason for the lowered dose was that the mice could not withstand the 50 mg/Kg dose at this age.

The mice were monitored daily for any sign of distress, and detailed scoresheets were kept for each animal, detailing their weight and a score for their general well-being. Once the mice reached the upper threshold of “medium” burden according to our government-approved score sheet, they were euthanized. In almost all cases, this threshold was reached due to mice losing weight, either 5% of the maximum weight lost in 2 consecutive days or reaching below 20% of their maximum weight. Analysis of survival results was implemented in R version 4.3 (R-Core-Team, 2023) and survminer package version 0.4.9 (Alboukadel Kassambara, 2021).

Throughout the study, wet food was provided to the mice in the following way: dry food pellets were soaked in water, mashed to make a purée, and served on alternate days on a petri dish placed on the cage floor. As wet food could contribute further to the squalor in the cages, the cages were changed twice a week. The mice also had access to normal dry pellets as usual. A new water bottle with an extended nuzzle (to reach the small transgenic animals) was provided to the mice on a weekly basis.

At postnatal day 40 (P40), blood was collected from the retro-orbital vein. Upon reaching their humane endpoint, mice were euthanized via intraperitoneal injection of a ketamine solution (20% Xylazine, 20% NaCl, 60% Ketamine). The volume of ketamine injection was determined based on the weight of the animals, at 10 μL per gram of body weight (but never more than 200 μL in one injection site). After confirming the absence of pain reflexes, mice were perfused with 20 mL of cold PBS. Subsequently, the brain was carefully dissected out of the skull and further divided into two hemispheres. One hemisphere was fixed overnight in a 4% PFA solution and then embedded in paraffin to facilitate immunohistochemistry studies after being sectioned on microtome at 5 μm and mounted directly on Superfrost™ Plus Microscope Slides (Thermo Scientific, J1800AMNZ). The other hemisphere was further dissected into the following regions: cortex, hippocampus, midbrain, and hindbrain (including pons, medulla oblongata, and cerebellum). The dissected brain regions were frozen on dry ice and transferred to a -80˚C freezer for further biochemical investigations.

To stain neuromuscular junction (NMJ), quadriceps muscles were dissected and fixed in 4% PFA dissolved in phosphate buffer (1x PB: 0.0754 M Na2HPO4.2H2O and 0.0246M NaH2PO4.H2O; pH adjusted to 7.3) for 1-2 hours on ice. The tissue was then transferred to cold PB. Promptly after, the tissue was embedded in 3% agarose and sectioned (100 μm) on vibratome. Free-floating sections were then immediately stained for neuromuscular junction (NMJ), details of which are provided in the immunostaining section.

DietGel Study

In this experiment, the diet of the GA-Nes mice was supplemented to assess the role of diet on survival of the transgenic mice. DietGel® Recovery (ClearH_2O, 72-06-5022), DietGel® 76A (ClearH_2O, 72-07-5022), and HydroGel® (ClearH_2O, 70-01-1082) were provided to the animals, served on a petri dish and placed on the cage floor. The gels were provided starting at P2, with a fresh one replaced every second day. From P35 onwards, fresh gels were provided daily, given the increased consumption. Prior to P21, the animals were identified by paw tattooing. Table 4 outlines the components of each gel. The formulation of each gel has undergone slight modifications by the manufacturer since 2020; Table 4 presents the nutritional composition as it was at the time of the experiment (July 2020). DietGel® 76A, closely resembles the new DietGel® 76A with animal protein.

Nutritional Facts/100g DietGel® 76A

Nutritional Component	Amount
Calories	99.8 kcal
Protein	4.8 g
Carbohydrates	17.8 g
Sugars	14.7 g
Dietary Fiber	1.5 g
Fat	1.5 g
Saturated Fat	0.1 g
Moisture	72-74%
Calcium	227.7 mg
Potassium	280.8 mg
Sodium	42.7 mg
Phosphorus	262 mg

Nutritional Facts/100g DietGel® Recovery

Nutritional Component	Amount
Calories	120 kcal
Protein	0.6 g
Carbohydrates	25.2 g
Sugars	23.0 g
Dietary Fiber	0.8 g
Fat	1.9 g
Saturated Fat	0.2 g
Moisture	70-75%
Calcium	6.0 mg
Potassium	101.3 mg
Sodium	51.8 mg
Chloride	105.2 mg

Nutritional Facts/100g HydroGel®

Nutritional Component	Amount
Calories	3.5 kcal
Protein	0.07 g
Carbohydrates	0.9 g
Dietary Fiber	0.9 g
Moisture	97-99%
Calcium	20.4 mg
Potassium	25.1 mg
Sodium	23.6 mg
Phosphorus	23.9 mg

Table 4: nutritional value of each of the three gels per 100g.

The general wellbeing and weight of animals were monitored on P2, P4, P7, P14, P21, P28, P30, P32, P35 and then daily until the mice reached the humane endpoint. This endpoint was defined as reaching the upper threshold of "medium" burden according to our government-approved score sheet. In all cases, this threshold was reached due to mice losing weight, either 5% of the maximum weight lost in 2 consecutive days or reaching below 20% of their maximum weight. Upon reaching the endpoint, animals were euthanized by CO_2 followed by decapitation, in accordance with the instructions of the animal care facility.

Cyclodextrin Study

In this experiment, there were two major cohorts: survival, and fixed time point (P40). In both cohorts, (2-Hydroxypropyl)-β-cyclodextrin (CAS #128446-35-5; Sigma-Aldrich, H107-100G, batch Degree of Substitution (DS) = 5), hereafter referred to as CD or cyclodextrin for simplicity, was used. The vehicle in this experiment was 30 mM citric buffer at pH 5.0 in normal saline. CD was dissolved at 20% in this vehicle. The ensuing steps were taken to prepare the solution: 1) A 30 mM pH 5.0 citrate buffer was prepared by weighing 0.509 g of sodium citrate dihydrate, and 0.244 g of citric acid and 80 mL normal saline (0.9% NaCL in water). 2) pH was verified by a meter and adjusted with HCl or NaOH if needed to pH 5.0. 3) 20 g of CD was added and the solution was filled up to 100 mL with saline.

From P21 onwards, all mice were administered daily subcutaneous injections of 2000 mg/Kg CD solution (as previously described) or an equivalent volume of the vehicle. Survival cohort mice were kept until they reached the humane endpoint, while fixed cohort mice were harvested at P40. Analysis of survival results was implemented in R version 4.3 (R-Core-Team, 2023) and survminer package version 0.4.9 (Alboukadel Kassambara, 2021).

Throughout this study, wet food was provided to the mice in the following way: dry food pellets were soaked in water, mashed to make a purée, and served daily on a petri dish placed on the cage floor. As wet food could contribute further to the squalor in the cages, the cages were changed twice a week. The mice also had access to dry

pellets as usual. New water bottles with extended nuzzle (to reach the small transgenic animals) were provided to the mice on a weekly basis.

Once the mice reached the upper threshold of “medium” burden according to our government-approved score sheet, they were euthanized. In almost all cases, this threshold was reached due to mice losing weight, either 5% of the maximum weight lost in 2 consecutive days or reaching below 20% of their maximum weight. When euthanasia was required, a ketamine solution (20% Xylazine, 20% NaCl, 60% Ketamine) was administered via an intraperitoneal injection. Ketamine injection volume was determined by the weight of the animals, specifically, 10 μL per gram of weight (maximum volume of 200 μL). After confirming the absence of pain reflexes, intracardiac blood was collected in kaolin tubes (Kabe Labortechnik 078031) for serum isolation. The animal was then perfused with 20 mL of ice-cold PBS. Subsequently, the brain was carefully dissected out of the skull and further divided into two hemispheres.

One hemisphere was fixed overnight in a 4% PFA solution and then embedded in paraffin to facilitate immunohistochemistry studies after being sectioned on microtome at 5 μm and mounted on the Superfrost™ Plus Microscope Slides (Thermo Scientific, J1800AMNZ). As some antibodies and dyes only work with frozen tissue and paraffinization interferes with their binding, a smaller number of these hemispheres were freeze-protected in successive 15% and 30% sucrose solutions. They were then embedded with M-1 Embedding Matrix (Epredia™ 1310) in Peel-A-Way® Embedding Molds (Polysciences, 18646A-1) and stored at -80 ˚C. The frozen blocks were later attached to the chuck of the cryostat with Tissue-Tek® O.C.T. Compound (Sakura® Finetek 4583). They were sectioned at 30 μm and mounted on the Superfrost™ Plus Microscope Slides (Thermo Scientific, J1800AMNZ). The inner chamber of the cryostat was maintained at -20 ˚C, and all materials were incubated inside the chamber for 30 minutes before any sectioning commenced.

The other hemisphere was further dissected into the following regions: cortex, hippocampus, midbrain, and hindbrain (including pons, medulla oblongata, and

cerebellum). The dissected brain regions were directly snap-frozen in liquid nitrogen and were subsequently stored at -80 ˚C to allow further biochemical investigations.

3.2 Neurofilament Light Chain Assay

As mentioned in the section on animal experiments, intracardiac blood was collected from animals in kaolin tubes (Kabe Labortechnik 078031), which have a gel layer on the bottom. After 30 minutes of incubation at room temperature to promote coagulation, the sample tubes were centrifuged at 2500g for 10 minutes at 4 ˚C. Thus, serum was separated on top of the gel layer, and the cellular layer was on the bottom of the gel later, allowing for easy pipetting of serum for storage. The isolated serum was stored at -80 ˚C in protein LoBind® Tubes (Eppendorf, Catalog No. 022431064).

Due to the high amount of NfL in these mice, the serum was diluted 1:40 and assayed with NF-light Advantage Assay Kit (Quanterix, Cat. No. 103186). The assay was performed according to the manufacturer's instructions by Brigitte Nuscher. Results were analyzed by R version 4.3 (R-Core-Team, 2023) and plotted with ggplot2 (Wickham, 2016).

3.3 Immunostaining

For NMJ staining, the free-floating sections were immediately transferred to 100 μL of NMJ blocking buffer in a 96-well plate. To make 100 mL of NMJ blocking buffer, 0.5 mL Triton-X-100, 1 g of bovine serum albumin (Sigma-Aldrich, A7030), and 10 mL of normal goat serum were added to 90 mL of phosphate buffer (described under baricitinib study materials and methods). Immediately, Alexa Fluor 555 Mouse anti-β-Tubulin III (BD Pharmingen, 560339; 1:100) and Bungarotoxin Alexa Fluor 647 (Thermo Fisher, B35450; 1:250) were prepared in blocking buffer. 100μL of the antibody solution was added to each well that already contained blocking buffer (1:1). The plate was then shaken at 4 ˚C for 48-72 hours while covered with aluminum foil. After incubation, the sections were washed with 1x PB at room temperature for 30 minutes. Subsequently, the sections were mounted with Vectashield Vibrance (Vector Laboratories, H-1700).

For staining paraffinized sections, the sections were incubated in a 56 ˚C oven for 30 minutes. Afterward, deparaffinization and rehydration were performed as follows: two xylene washes, the first one for 15 minutes and the second one quickly; then two washes in 100% ethanol, then once in 96% ethanol, and then another two washes in 70% ethanol. This step was followed by a complete wash under running water for 5 minutes. At this point, the sections were ready for antigen retrieval. For all the antibodies in this work, head-induced epitope retrieval (HIER) at pH 6 using citrate buffer was utilized. The citrate solution was prepared in the following way: 2.5 mL of 0.1 M citric acid, 10.25 mL of sodium citrate, with deionized water added to the mix to bring the final amount to 125 mL. To perform HIER, sections were immersed in the citrate buffer and placed in a plastic container and heated in a steam cooker for 30 minutes. Subsequently, the plastic container with the slides was taken out of the steam cooker and left to equilibrate to room temperature (20-30 minutes). The only exception in antigen retrieval was for APP staining, where the sections were incubated in 10% formic acid for 15-20 minutes. The sections were then washed under running water for 5 minutes, after which they were ready for next steps of staining, namely blocking and permeabilization. For DAB immunohistochemistry, there was an extra step of quenching endogenous peroxidase activity, which was done by BLOXALL blocking solution (Vector Laboratories, SP-6000), followed by a five-minute wash in PBS.

For staining frozen sections that were stored in a -20 ˚C freezer, the sections were allowed to incubate at room temperature, and were subsequently rehydrated in PBS. The sections were then ready for the next steps of staining, namely blocking and permeabilization. Staining of coverslips was implemented by fixing the cells on cold 4% PFA solution, followed by 3 PBS washes. The coverslips were then ready to be blocked and permeabilized, as described below.

Next, the samples were permeabilized and blocked. This was performed simultaneously using a buffer composed of 0.1% Triton-X-100 and 5% Fetal Bovine Serum (FBS) in PBS. All slides were covered in 200 μL of this combined blocking and permeabilization solution for 1 hour at room temperature. Meanwhile, primary antibodies were prepared in a separate blocking solution consisting of 2% FBS, 2% BSA, and 0.2% fish gelatin in PBS. Subsequently, excess solution was gently removed

from the slides, and 100 μL of the antibody solution was applied. The slides were then covered with HybriSlip™ Hybridization Covers (Grace BioLabs, 714022) and incubated in a humid chamber overnight at 4 ˚C. The blocking solution on coverslips was simply aspirated and the antibody solution was applied without any covering.

For immunofluorescence staining, the process continued the following day with two washes in PBST (0.05% Tween-20 in PBS) and a final wash in PBS, each lasting five minutes. Secondary antibodies were prepared in the same blocking solution that was used for the primary antibody. After the washes, add 100 μL of the secondary antibody solution was applied to the sections, which were covered with the other side of the HybriSlip and incubated at room temperature for a minimum of 1 hour. Afterward, the slides were washed in the same manner as for the primary antibody. Subsequently, the sections were incubated in the working DAPI (4',6-Diamidino-2-Phenylindole, Dihydrochloride) solution for 20 minutes. DAPI working solution was prepared as follows: 1:5000 in PBS from a 5 mg/mL stock solution of DAPI (Invitrogen, D1306). This was followed by two to three PBS washes, each lasting five minutes. Mouse tissue was then ready for coverslipping. For human tissue, 0.3% Sudan Black B (Sigma Aldrich, 199664) solution in 70% ethanol was applied to the sections for 20-30 seconds. This step was also followed by three washes in PBS, each lasting five minutes. Sections were then coverslipped (No. 1.5H, 170±5 μm) with Vectashield Vibrance (Vector Laboratories, H-1700) or ProLong Diamond Antifade Mountant (Invitrogen, P36970).

For DAB immunohistochemistry, VECTASTAIN Elite ABC-HRP Kit for rabbit (Vector Laboratories, PK-6101) was used according to the manufacturer's protocol. Essentially, the first day of the staining is very similar to immunofluorescence, other than the application of BLOXALL solution which was already discussed. On the second day, however, the sections were incubated with the kit's biotinylated secondary antibody, followed by incubating with the kit's ABC reagent, as detailed in the manufacturer's protocol. Subsequently, a working DAB solution (1 drop of reagent 1 in 1 mL of the provided diluent) from the ImmPACT DAB kit (Vector Laboratories, SK-4105) was applied to the sections. The incubation time needs to be determined for every antigen, antibody, and type of tissue separately. After washing under running

water for five minutes, the sections were counterstained with hematoxylin QS counterstain (H-3404-100) for 45 seconds. This step was followed by another 5 minutes of washing under running tap water. Lastly, the sections were rapidly dehydrated with two washes in 99% isopropanol for at least one minute per wash and coverslipped with VectaMount Express Mounting Medium (H-5700-60).

Table 5 shows the primary and secondary antibodies used in this dissertation for immunostaining.

For Luxol Fast Blue staining, NovaUltra Luxol FastBlue Stain Kit (IHCWorld, IW-3005) was used according to the manufacturer's protocol for our paraffinized tissue to visualize white matter. Briefly, sections were deparaffinized in two changes of xylene for 10 minutes each. They were then rehydrated with two changes of 100% ethanol (five minutes each), followed by three minutes in 95% ethanol. Next, they were immersed and incubated in the provided Luxol Fast Blue solution in 56 ˚C oven overnight. On the next day, the excess stain was washed away with 95% ethanol and then rinsed in distilled water. Differentiation was accomplished by submersion in lithium carbonate solution (provided in the kit) for a few dips up to 30 seconds and then continued with submersion in 70% ethanol for 30 seconds. Subsequently, sections were rinsed in distilled water and checked microscopically to determine whether the white matter is sharply defined (blue white matter, clear gray matter). If the differentiation was not satisfactory, the differentiation steps would be repeated. Counterstaining was achieved by immersion in Cresyl Violet solution (staining neuronal cell bodies, provided in the kit) for 1-2 minutes followed by rinsing in distilled water. Sections were then differentiated with 95% ethanol for five minutes. For dehydration, two changes of 100% ethanol for 5 minutes each were performed. Lastly, sections were cleared with two changes of xylene, each lasting five minutes, and then coverslipped with VectaMount Express Mounting Medium (H-5700-60).

For Oil Red O (Sigma Aldrich, 1024190250) staining, the ready-to-use solution was used according to the manufacturer's protocol. Essentially, cryosections were incubated and moved about for 20 seconds in 60% isopropanol followed by 10 minutes in the provided Oil Red O solution. The sections were then incubated for 30 seconds

in 60% isopropanol followed by 20 seconds in distilled water. Next, they were counterstained with the hematoxylin QS counterstain (H-3404-100) for 45 seconds and washed for 3 minutes under running tap water. The sections were then coverslipped with an aqueous mounting medium, such as Vectashield Vibrance (Vector Laboratories, H-1700).

Antibody Name	Host	Manufacturer	Cat. No.	Dilution
PLIN4	Rabbit	NovusBio	NBP2-13776	1:200
GFAP	Chicken	Synaptic Systems	173 006	1:500
C-Terminal APP	Rabbit	Sigma-Aldrich	A8717	1:500
Serpin A3N	Goat	R&D Systems	AF4709	1:200
IBA1	Rat	Abcam	ab283346	1:400
CA2	Rat	R&D Systems	MAB2184	1:200
PLIN2	Rabbit	NovusBio	NB110-40877	1:200
S100B	Rabbit	NovusBio	NB110-57478	1:200
anti-rabbit Alexa Fluor 488	Goat	Invitrogen	A-11008	1:250
anti-rabbit Alexa Fluor 555	Goat	Invitrogen	A-21428	1:250
anti-rat Alexa Fluor 488	Goat	Invitrogen	A-11006	1:250
anti-rat Alexa Fluor 647	Goat	Invitrogen	A-21247	1:250
anti-chicken Alexa Fluor 647	Goat	Invitrogen	A-21449	1:250
anti-goat Alexa Fluor 555	Donkey	Invitrogen	A-21432	1:250

Table 5: primary and secondary antibodies used for immunostaining in this dissertation.

3.4 Microscopy and Image Analysis

All fluorescence microscopy images in this dissertation were acquired using Zeiss LSM710 confocal laser scanning microscope with ZEN 2010 software. All images are 1024 x 1024 pixels and obtained with 8-bit depth and a pixel dwell time of 3 μs. For all acquisitions, the pinhole was to 1 Airy unit. Where beneficial, images were acquired with 2-4 averaging to reduce noise to signal ratio. Brightfield images were obtained with Leica DMi8 inverted microscope. Settings were adjusted for each antibody and staining separately, the same settings were used across the conditions for the sake of comparability and fairness.

For live cell imaging in the study of Peredox and PercevalHR, glass bottom μ-Dishes (Ibidi, 81158) were used. HEK293FT and primary neurons were imaged 72-96 hours post transfection. For live cell imaging, phenol red-containing media had to be

taken out, as phenol red would interfere with the fluorescence of the channels that I was using. In this regard, 20 mM HEPES (Gibco, 15630080) in HBSS (Gibco, 14025092) with 4.5 g/L D-glucose (Sigma Aldrich, G7021) was prepared and filtered under sterile conditions. This solution replaced the culture media that is described in the tissue culture section of materials and methods (section 3.8). Cells were allowed to equilibrate in the live cell chamber of LSM710 microscope in this solution. The live cell chamber was maintained at ~37 ˚C with ~5% CO2 content. Imaging was commenced when no variations in fluorescent signal were observed, which indicated that the cells had reached equilibrium with the live cell imaging chamber.

To analyze images, Python 3.8 (Python-Software-Foundation, 2022) with the following packages was used: aicsimageio version 4.9.4 (Eva Maxfield Brown, 2021), numpy version 1.23.5 (Harris et al., 2020), opencv-python version 4.6.0 (Bradski, 2000), scikit-image version 0.19.3 (van der Walt et al., 2014), and pandas version 2.0.3 (McKinney, 2010; The-pandas-development-team, 2020). The code snippet below shows the main functions that I created with and implemented from the aforementioned libraries for analyzing the imaging data.

```
import cv2
import numpy as np
import pandas as pd
from aicsimageio import AICSImage
from skimage.filters import threshold_li
from skimage.morphology import remove_small_holes, remove_small_objects,
label
from skimage.measure import regionprops, regionprops_table


def remove_background(img, background_thresh):
    ''' takes an image and a backgeound threshold, and removes the
background only '''
    xdim = np.shape(img)[0]
    ydim = np.shape(img)[1]
    img2 = np.copy(img)
    img_ravel = np.ravel(img2)
    img_ravel[img_ravel < background_thresh] = 0
    img2 = np.reshape(img_ravel, (xdim, ydim))
    return img2

def label_img(img, min_obj_size, remove_holes=False):
    ''' takes an image and object size to remove to make masks from images,
and returns the mask image, count and area'''
    img_thresh = img>threshold_li(img)
    if remove_holes == True:
```

```
        img_thresh = remove_small_holes(img_thresh)
    img_thresh = remove_small_objects(img_thresh, min_size=min_obj_size)
    # here one can try watershedding to see how it looks
    img_labelled = label(img_thresh)
    img_count = np.max(img_labelled)
    img_df = pd.DataFrame.from_dict(regionprops_table(img_labelled, img,
properties=['area']))
    img_area = img_df['area'].sum()
    return img_thresh, img_count, img_area

img = AICSImage('czi filepath')
NumCh = img.data.shape[1]

''' Make a maximum intensity projection image if a Z-stack exists'''

#Z_index = img.dims.order.find('Z') # commented out because it is always
'2' in my setting
if img.data.shape[2] > 1:
    max_projection =
np.zeros((img.data.shape[1],img.data.shape[3],img.data.shape[4]))
    for kk in range(img.data.shape[1]):
        max_projection[kk,:,:]= np.max(img.data[0,kk,:,:,:], axis=0)
else:
    try:
        del max_projection
    except:
        pass


if 'max_projection' not in globals():
    dapi = img.data[0, 0, 0, :, :]
    fitc = img.data[0, 1, 0, :, :]
    tritc = img.data[0, 2, 0, :, :]
    cy5 = img.data[0, 3, 0, :, :]

    dapi = remove_background(dapi, 0)
    fitc = remove_background(fitc, 0)
    tritc = remove_background(tritc, 0)
    cy5 = remove_background(cy5, 0)

else:
    max_projection = max_projection.astype('int')
    dapi = max_projection[0,:,:]
    fitc = max_projection[1,:,:]
    tritc = max_projection[2,:,:]
    cy5 = max_projection[3,:,:]

    dapi = remove_background(dapi, 0)
    fitc = remove_background(fitc, 0)
    tritc = remove_background(tritc, 0)
    cy5 = remove_background(cy5, 0)


# Rest of image processing using defined functions; results handled with
python
```

From this code, cell count, staining area, intensity, and image masks are easily calculated and can be visualized by further processing of data. For consistency, pandas DataFrame results were exported to a CSV file. The CSV files were read with R version 4.3 (R-Core-Team, 2023), and the results of the analysis were plotted with ggplot2 (Wickham, 2016).

3.5 Electron Microscopy

To perform electron microscopy, the harvesting of the animals was modified. The experiment involved two transgenic and two wildtype control animals. All animals, being littermates and female, were housed in the same cage, a scheme adopted to minimize variability. Selecting only female mice was intended to further explore the effects of cyclodextrin in females, as justified in the relevant Results section.

Mice were harvested on the eve of P40 by ketamine injection, as previously described. Throughout the entire procedure, extreme care was taken to not squeeze, stretch, distort, or dry the tissue. Initially, approximately 8 mL of HBSS without calcium and magnesium (Gibco, 14170112) was used for perfusion. The animals were further perfused with 20 mL of PFA/GA fixative cocktail, consisting of 2% PFA (Electron Microscopy Sciences, 15710), 2.5% Gluteraldehyde (Electron Microscopy Sciences, 16220), 2 mM calcium chloride (Electron Microscopy Sciences, 12340), and 0.1 M cacodylate buffer (Science Services).

Following perfusions, the brain was dissected and bisected into two hemispheres. Each hemisphere was fixed in the aforementioned PFA/GA fixative at 4 ˚C for 12 hours. The brain hemispheres were subsequently sectioned coronally at 200 μm using a vibratome. Following sectioning, the tissues were incubated in the fixative solution at 4 ˚C for 12h. Finally, the solution was changed to 0.1 M cacodylate buffer, all the while ensuring meticulous care prevent tissue from drying out.

After perfusion and immersion fixation in a 4 % PFA, 2.5 % GA, and 2 mM $CaCl_2$ solution buffered in 0.1 M sodium cacodylate at pH 7.4, samples were kept for up to 3 days in sodium cacodylate buffer. Before subsequent processing, using fine

scalpels under a binocular microscope, 1x1 mm² pieces of the hippocampus were dissected from the already prepared coronal sections.

Heavy metal staining, dehydration, and resin infiltration were done according to the standard “reduced osmium-thiocarbohydrazide-osmium (rOTO) en bloc staining” protocol (Kislinger et al., 2020) with reduced osmium tetroxide concentrations.

In summary, samples were postfixed in 1% osmium tetroxide (EMS), buffered in 0.1 M sodium cacodylate (Science Services) at pH 7.4, followed by 2.5% potassium ferrocyanide in the same buffer. Samples were rinsed with buffer once and twice with water. Next, samples were treated with 1% aqueous thiocarbohydrazide (Sigma) for 45 min at 40 °C. After another wash in water, samples were treated with 1% aqueous osmium tetroxide, washed again and further contrasted by overnight incubation in 1% aqueous uranyl acetate at 4° C and 2h at 50° C. Samples were dehydrated in a graded series of ethanol and infiltrated with LX112 (LADD) in rising concentrations using acetone as an intermedium. The resin was polymerized at 60°C for 48 hours.

After polymerization, samples were sectioned on a Leica UC7 ultramicrotome (Leica Microsystems). For scanning electron microscopy (SEM), 100 nm thick sections were cut with a 35° ultra-diamond knife (Diatome) and collected onto plasma-treated, carbon-coated Kapton tape (provided by Jeff Lichtman, Harvard University).

SEM images were taken with a Zeiss Crossbeam Gemini 340 SEM with a four-quadrant backscattered electron detector at 8kV and a working distance of 7.5 mm. Following low-resolution imaging for locating the sections, regions of interest were located at intermediate resolutions between 200 nm and 50 nm/pixel, with the final high-resolution images of the regions of interest being imaged at 4 nm/pixel.

The width of the corpus callosum in each sample was analyzed using FIJI/ImageJ2 version 2.14.0/1.54f (Rueden et al., 2017; Schindelin et al., 2012). Myelinated axons in the corpus callosum area were counted using Python, incorporating the previously cited packages as well as Cellpose 2.0 (Stringer et al., 2021) to reliably segment the myelinated axons. Results were further analyzed and visualized as previously described.

3.6 Immunoblotting

To isolate protein from hindbrains, the tissues were first pulverized with a pestle and mortar. RIPA buffer (Serva, 39244.01), supplemented with 2% sodium dodecyl sulfate (SDS) and Halt protease inhibitor cocktail (Thermo Scientific, 78429), was added to the tissue to facilitate homogenization. The homogenization of the tissues was performed using Percellys 2mL soft tissue tubes (Bertin Cop., P000912-LYSK0-A) in the Percellys homogenizer, set to the hard tissue program, at 4 ˚C.

BCA assay (Thermo Scientific, 23225) was used to measure protein content following the manufacturer's protocol. The results were analyzed with R version 4.3 (R-Core-Team, 2023) to calculate the concentration of each sample. For immunoblotting, the samples were diluted to a concentration of 1 mg/mL with the supplemented RIPA buffer. Final preparation of samples for immunoblotting involved the use of 4x Laemmli protein sample buffer (Bio-Rad, 1610747) which necessitates the addition of 2-mercaptoethanol as a reducing agent. Then, the samples were incubated at 95 ˚C for 10 minutes, and subsequently stored at -20 ˚C for further experiments.

To perform immunoblotting, Novex 10-20% Tricine gels (Invitrogen, EC66252BOX) with SeeBlue™ Plus2 Pre-stained Protein Standard (Invitrogen, LC5925) were employed. The gels were run in 1x tricine cathode buffer (0.01 M Tris, 0.01 M Tricine, 0.0035 M SDS) at 80 volts for 20 minutes, followed by 120 volts for 1 hour. iBlot2® PVDF mini stacks (Invitrogen, IB24002) were used with the transfer performed on the iBlot2 gel transfer device (Invitrogen, IB21001) using the default P0 program.

For pStat3 immunoblotting, the blocking buffer consisted of 5% BSA in TBSTx (1x TBS with 0.2% Triton-X-100). For all other antibodies, 0.2% iBlock (Invitrogen, T2015) in TBSTx served as the blocking buffer. Membranes were blocked with the appropriate blocking buffer for 1-2 hours at room temperature, shaking at ~150 rpm. All antibodies were diluted in their respective blocking buffer. After the blocking step, the membranes were incubated in the primary antibody solution overnight at 4 ˚C on

a shaker. Subsequently, the membranes were washed a minimum of three times with TBSTx for 10 minutes per wash. Next, the HRP-conjugated secondary antibody was applied to the membranes and incubated at room temperature for 2 hours with shaking. Upon conclusion of this step, three more 10-minute washes were performed. Finally, each membrane was treated with 1 mL of Immobilon Forte Western HRP substrate (Millipore, WBLUF0500) for development. The membranes were then imaged with Cytiva's Amersham ImageQuant 800. For reblotting the same membrane to assess loading control proteins, the membranes were incubated with 200 mM NaOH for 3 minutes at room temperature while shaking. The membranes were then washed and re-blocked with the same blotting procedure ensued. Table 6 details the primary and secondary antibodies used for immunoblotting.

Antibody Name	Host	Manufacturer	Cat. No.	Dilution
STAT3	Rabbit	Cell Signaling Technologies	4904S	1:1000
pSTAT3	Rabbit	Cell Signaling Technologies	9145S	1:1000
Serpin A3N	Goat	R&D Systems	AF4709	1:2000
Calnexin	Rabbit	Enzo	ADI-SPA-860-F	1:7000
beta-Actin	Mouse	Sigma-Aldrich	A5316	1:2500
anti-rabbit HRP	Goat	Promega	W401B	1:5000
anti-mouse HRP	Goat	Promega	W402B	1:5000
anti-goat HRP	Donkey	Santa Cruz	sc-2020	1:5000

Table 6: primary and secondary antibodies used for immunoblotting in this dissertation.

3.7 MSD Immunoassay

In this study, two MSD Immunoassays were conducted: the V-PLEX Proinflammatory Panel 1 Mouse kit (MSD, K15048D-2) and the V-PLEX Cytokine Panel 1 Mouse kit (MSD, K15245D-2). The samples were prepared as described in the previous section on immunoblotting – the same hindbrain samples that were taken for the BCA assay. For the proinflammatory panel, 13 mg/mL of protein per well was used, whereas for the cytokine panel, the concentration was 5 mg/mL of protein per well. The assays were performed following the manufacturer's protocol, and the plates were read with MSD's MESO QuickFlex SQ 120MM plate reader. Concentrations of

the biomarkers were calculated in the MSD's software. Concentration values within the detection range were exported to R for visualization and statistical analysis, as previously described.

3.8 Tissue Culture

HEK293FT cells were cultured in high glucose DMEM (Gibco, 11965092) supplemented with 10% FBS and 1% non-essential amino acids (Gibco, 11140050). The culture was maintained in a 37 ˚C incubator with 5% CO_2. Upon reaching ~80% confluency, the culture was split 1:10 in a new 10 cm dish, assisted by 0.05% Trypsin-EDTA (Gibco, 25300054) to loosen the cells' attachment to the plate.

Primary rat neurons, hippocampal for imaging and cortical for the mass-spectrometry experiment, were cultured from embryonic day 19 Sprague-Dawley rats. Prior to dissection, culture dishes were coated with 1.5% PDL (Sigma-Aldrich, P7280) in 0.1 M borate buffer (40 mM boric acid, 10 mM sodium tetraborate, pH 8.5) for 4 hours, followed by thorough washing. The rat dam was euthanized by CO_2 and all the pups were removed from the uterus. The brains of the pups were placed and dissected in HBSS. Hippocampi and cortices were placed in HBSS and kept on ice. In 5 mL of HBSS, 300 μL of 2.5% trypsin was added to the hippocampal tubes while 500 μL of 2.5% trypsin (Life Technologies, 15090046) and 350 μL of DNase I (Sigma, D-25; 100mg in 10ml HBSS stock, pH 7-8) were added to cortical tubes. This solution was then incubated for 15 minutes at 37 ˚C. The tissue was washed and then dissociated by trituration. After the debris is settled, cells were counted and plated. The seeding density for hippocampal neurons was approximately 25,000 cells/cm², while for cortical neurons, it was approximately 100,000 cells/cm². The culture media was based on neurobasal medium (Gibco, 21103049) and supplemented with 2% B-27 (Gibco, 17504044), 1% Pen/Strep (Gibco, 15070063), and 0.25% L-Glutamine (Gibco, A2916801). Hippocampal neurons were supplemented with an additional 0.125% L-Glutamate (Sigma-Aldrich, 1.06445).

3.8.1 Transfection and Transduction

The transfection protocol for HEK293FT cells began one day post-splitting. Initially, the medium was completely aspirated and replaced with pre-warmed Opti-MEM (Gibco, 31985070) at 50% of the original volume. Next, the transfection mixture was prepared: per 1 cm^2 of surface area, 0.4 μg of construct DNA was combined with 25 μL of OptiMEM. In parallel, 0.75 μL of Lipofectamine 2000 (Invitrogen, 11668019) was gently mixed with 25 μL of OptiMEM. The solutions were incubated at room temperature for 5 minutes. Subsequently, the two mixtures were added together, and mixed gently by inversion. The mixture was allowed to incubate for 20 minutes at room temperature. After the 20-minute incubation, the transfection mixture was gently added to the cells. 4-6 hours later, the transfection medium was replaced with a fresh maintenance medium.

Transfection of primary neurons began with preheating 50 mL neurobasal medium to which 125 μL of L-Glutamine (200 mM) was added. For each 35 mm μ-Dish that was used for live cell imaging, 4.5 μg of construct DNA was combined with 250 μL of L-Glutamine supplemented Neurobasal medium, while also mixing 6.25 μL of Lipofectamine 2000 with 250 μL of the Neurobasal medium. After 5 minutes of incubation, the two solutions were mixed with each other gently. The mixture was incubated at room temperature for 20 minutes. Upon the conclusion of the incubation time, the medium of neurons was collected and saved. The transfection medium was then applied to neurons (500 μL for a 35 mm dish) and incubated for 45 minutes in an incubator at 37 $^{\circ}$C and supplied with 5% CO_2. Following the incubation, the transfection medium was aspirated and washed twice with warm Neurobasal medium (~2 mL for 35 mm dish). The originally saved medium was reintroduced to the neurons.

The poly(GA) constructs utilized for transfection were cloned in-house by the Edbauer lab. These constructs contain 149 repeats of poly(GA) and result in aggregate formation in both HEK293FT cells and primary rat neurons. Peredox-mCherry (GW1-Peredox-mCherry was a gift from Gary Yellen (Addgene plasmid # 32380; http://n2t.net/addgene:32380; RRID:Addgene_32380)) and PercevalHR (GW1-PercevalHR was a gift from Gary Yellen (Addgene plasmid # 49082;

http://n2t.net/addgene:49082; RRID:Addgene_49082)) were obtained from Addgene and replicated with a Midi prep (Macherey-Nagel, 740410.50) according to the manufacturer's protocol. It is important to note that the repeat-containing constructs were exclusively transformed into NEB Stable (NEB, C3040H) or Stbl3 (Invitrogen, C737303) competent bacteria and grown at 30 ˚C.

To transduce neurons, lentiviral constructs were initially packaged as detailed in section 3.9 on lentiviral packaging. Determining the titer of each lentiviral batch was not necessary as our protocol consistently maintains the titer within an acceptable range. For a 10 cm dish, about 10 μL of virus (double for TDP-25) was sufficient to transduce all the neurons while avoiding overt toxicity from the viral treatment itself. Treatment was administered on DIV 6 (with the date of plating being DIV 0). Neurons were subsequently harvested 7 days later (DIV 6+7).

3.9 Lentiviral Packaging

To ensure sufficient transduction of neurons for subsequent mass spectrometry analysis, an adequate quantity of lentiviral constructs was prepared. Importantly, constructs containing repeats were exclusively transformed into NEB Stable (NEB, C3040H) or Stbl3 (Invitrogen, C737303) competent bacteria, and cultured at 30 ˚C. These constructs all had a synapsin promoter, which facilitates specific expression in neurons (Schoch et al., 1996). The constructs also contained a Woodchuck Hepatitis Virus (WHV) Posttranscriptional Regulatory Element (WPRE) sequence to increase the expression of the transgene (Lee et al., 2005). One construct contained only GFP which served as a control. Other constructs contained poly(GA)$_{149}$-GFP, poly(GR)$_{149}$-GFP, and TDP-25-GFP (wildtype TDP-25). In these plasmids, the transgene sequence was flanked by long terminal repeat (LTR) sequences. All constructs are available upon request from the Edbauer lab.

Other than the lentiviral vector, two other constructs were required to package the lentivirus, namely pVSV-G (pMD2.G was a gift from Didier Trono (Addgene plasmid # 12259; http://n2t.net/addgene:12259; RRID:Addgene_12259)) which codes for the envelope protein and psPAX2 (psPAX2 was a gift from Didier Trono (Addgene

plasmid # 12260; http://n2t.net/addgene:12260; RRID:Addgene_12260)) which contains the gag gene encoding for structural proteins and the pol gene encoding for enzymes required for reverse transcription and integration into the host cell genome (Milone & O'Doherty, 2018).

To commence packaging the virus, a fresh batch of HEK293FT cells was thawed. The standard medium was prepared as previously described. The cells were maintained, split, and proliferated until reaching 15 million cells to plate per each lentiviral construct that was to be packaged. 5 million cells per 10 cm dish were plated, with three dishes per construct. The next day, the cells were co-transfected as follows: the medium was replaced with 5 mL of warm OptiMEM supplied with 10% FBS. For each construct (i.e., per three 10 cm dishes), 18.6 μg of lentiviral vector of choice, 11 μg of psPAX2, and 6.4 μg of pVSV-G plasmids were combined with 4500 μL of OptiMEM. For the same number of plates, 108 μL of Lipofectamine 2000 was mixed in 4500 μL of OptiMEM. After 5 minutes, the plasmids were combined with the lipofectamine 2000 solution, mixed, and incubated at room temperature for 20 minutes. 3 mL of this mixture was added to a 10 cm dish.

After 24 hours, media was exchanged with 10 mL high packaging media (DMEM Glutamax supplemented with 10% FBS and 1.2% BSA). On the third day, the presence of fluorescence in the cells was checked. A weak signal is expected due to the synapsin promoter. The supernatant (media) of the cells was then harvested and centrifuged for 5 minutes at room temperature to remove debris. The supernatant was filtered with 45 μm PES filter, loaded into Sw28 (Beckman, 342204) tubes, and centrifuged at 22,000 rpm for 2 hours at 4 ˚C. Subsequently, the supernatant was aspirated thoroughly but carefully and 120 μL of Neurobasal medium was added to the invisible pellet. This was incubated at 4 ˚C overnight. The next day, the virus was resuspended and aliquoted as required for downstream application.

3.10 snRNAseq Nuclei Isolation and Library Preparation

Single nucleus RNA sequencing (snRNAseq) was selected over single-cell RNA sequencing (scRNAseq) because our collaborators at the Liebscher lab

processed a significant amount of human post-mortem tissue using this method. Employing snRNAseq facilitated a more effective comparison of data between mice and human samples. Additionally, snRNAseq permits the snap-freezing of samples, providing the opportunity to harvest multiple samples within a single day, unlike scRNAseq which necessitates immediate sample processing. Further, some cell types, e.g., microglia, could change their activation states during this processing.

As the hippocampus is not a homogenous tissue, the entire hippocampus was processed for single nucleus RNA sequencing. To ensure RNA quality, some other brain regions that were simultaneously harvested were sampled. RNA was isolated from a small part of these samples with the RNeasy micro kit (Qiagen 74004). RNA Integrity Number (RIN) was measured for these samples by Agilent RNA 6000 Nano kit (Agilent, 50671511) and run an Agilent 2100 Bioanalyzer instrument according to the manufacturer's instructions. RIN of 7 or above was deemed acceptable, and the selected samples met this criterion.

Upon confirming RNA quality, nuclei were isolated from the hippocampi of female P40 mice using a modified version of the "Frankenstein protocol for nuclei isolation from fresh and frozen tissue" (G Martelotto, 2020), as adapted by our collaborator. Next, the nuclei were sorted via fluorescence-activated nuclei sorting (FANS). A total of 20,000 nuclei per sample were sorted through a DAPI+ gate, employing a 70 μm nozzle for single-cell precision of sorting in an Aria III Cell Sorter (BD Biosciences). The estimated recovery was approximately 10,000 nuclei. Subsequently, two additional gates, NeuN+ and NeuN-, were established using an Alexa Fluor 488 conjugated anti-NeuN antibody (Abcam, ab190195) to yield 5000 neurons and 5000 glial cells per sample. An example of the FANS process for one of the samples is illustrated in Figure 8.

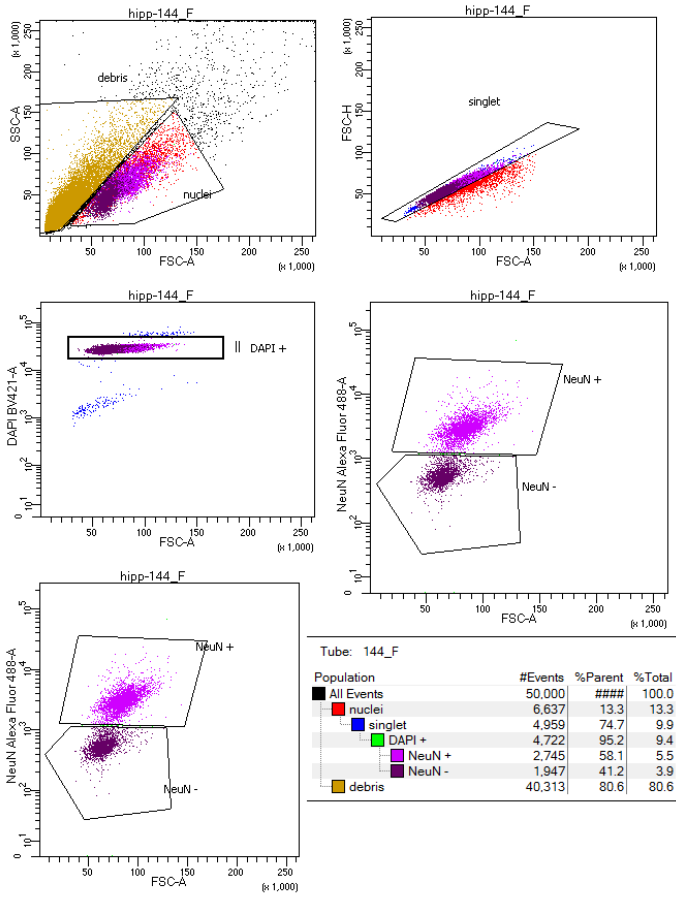

Figure 8: DAPI+ nuclei are selected in FANS and divided 1:1 into NeuN+ and NeuN- nuclei.

The sorted nuclei were deposited into a 96-well plate, each well pre-filled with RT Reagent B (18.8 μl), Template Switch Oligo (2.4 μl), and Reducing Agent (2.0 μl) from the Chromium Next GEM Single Cell 3' Kit v3.1 (10x Genomics, 1000268). This reagent setup, provided by the Chromium Next GEM Single Cell 3' Kit v3.1, was employed for the generation of cDNA libraries. Gel Bead-in-Emulsions (GEMs) were generated with chip G (10x Genomics, 1000120) on the microfluidic platform 10x Genomics Chromium Single Cell Controller. Next, the samples were barcoded, enabling the mRNA (each having a unique molecular identifier (UMI)) from each nucleus to have a unique barcode. This step is crucial for subsequent analyses to determine the origin of each mRNA molecule from the respective nuclei.

The cDNA was extracted with Dynabeads MyOne SILANE beads (Invitrogen, 370-12D) and amplified by PCR. The PCR product was purified with SPRIselect reagent (Beckman Coulter, Cat #B23318). Subsequently, the 3' gene expression

library was constructed with primers for the Illumina NGS platform and Dual Index Kit TT set A (10x Genomics, 1000215) which enabled individual sample identification.

Finally, the pooled libraries were sent to the Institute of Clinical Molecular Biology (IKMB) of the University of Kiel, where they were sequenced by Illumina's NovaSeq6000 system using S4 flow cell type (500M reads/sample) with a 2 x 150 bp paired-end read length.

3.11 snRNAseq Data Analysis

Sequencing results were initially processed using Cell Ranger version 6.1.2 from 10x Genomics to align reads to the mouse reference genome (mm10-2020-A) and import to a Seurat (Hao et al., 2021) object. A series of quality control measures were applied to the data including the calculation of doublet score at the sample level. A doublet score was assigned using DoubletFinder (McGinnis et al., 2019). Subsequently, high-resolution clustering was performed. Clusters exhibiting more than 20% doublets were entirely removed. As this procedure did not appear to remove all doublet clusters, the remaining clusters with co-expression of neuronal as well as glial markers were manually removed. Next, clusters with low-quality cells, as identified by low numbers of distinct UMIs per cell, were also fully removed. Lastly, all individual cells that received a true value from DoubletFinder were eliminated from the analysis using Seurat version 4.3.0 (Hao et al., 2021) in R 4.2.0 (R-Core-Team, 2022).

Using Seurat's built-in functions, the Seurat object was normalized by a scale factor of 10000 and variable features were found using 3000 features with the 'vst' selection method. The data was then scaled and principal component analysis (PCA) was run on it with 25 dimensions (minimum 15 necessary as per elbow plot).

Following this, the data was integrated using Harmony version 0.1.1 (Korsunsky et al., 2019). Dimensionality reduction was then conducted through UMAP with 45 dimensions, as informed by the elbow plot, and the reduction parameter was set to 'harmony'. 'FindNeighbors' function was subsequently used to prepare the data for clustering, with 45 dimensions. To achieve optimal clustering, various resolutions

in the function 'FindClusters' were tested. These clusters were then fed to clustree version 0.5.0 (Zappia & Oshlack, 2018), which is a package that enables choosing an optimal clustering resolution. The resolution which produces the most 'stable' clusters should be chosen. Figure 9 shows the clusters that were made with different resolutions. Here, the 0.45 resolution was chosen. This choice was not only made by looking at clustree outputs, but also by manually checking the UMAPs from the dimensional plots and selecting for the resolution that made the best compromise. There are of course further subclusters present in some clusters, but our research focus was satisfied by this clustering. The main workflow used to cluster the cells is illustrated in the code provided snippet:

```
# Assuming a Seurat object called "obj" and loaded libraries are loaded
obj <- NormalizeData(obj, normalization.method = "LogNormalize", scale.factor = 10000, verbose=FALSE)
obj <- FindVariableFeatures(obj, selection.method = "vst", nfeatures = 3000, verbose=FALSE)
obj <- ScaleData(obj, features = VariableFeatures(obj), vars.to.regress = NULL, verbose=FALSE)
obj <- RunPCA(obj, features = VariableFeatures(obj), assay = 'RNA', verbose = FALSE)

# obj <- SCTransform(obj, ncells = 10000, assay = "RNA", vst.flavor = 'v2', variable.features.n = NULL,
#variable.features.rv.th = 1.4, return.only.var.genes = F, vars.to.regress = '
#percent.mito', do.scale = FALSE, seed.use = 42)
# obj <- RunPCA(obj, assay = "SCT", dims = 1:30)
# The two functions above (commented out) are an alternative to the lines above Both approaches had similar results


obj <- FindNeighbors(obj, dims = 1:25, verbose=F) # dims from elbow plot (not shown here)
obj <- RunUMAP(obj, dims = 1:dims,verbose=FALSE)

set.seed(1)       #Harmony uses the seed for randomization and it is modified by many functions, for example RunUMAP.
obj <- RunHarmony(obj, "sample", plot_convergence = T, verbose=T, kmeans_init_nstart=20, kmeans_init_iter_max=100)

obj <- RunUMAP(obj, dims = 1:45, reduction = 'harmony', verbose=F, seed.use=42) # now 45 dimensions because of the elbow plot
obj <- FindNeighbors(obj, dims = 1:45, reduction = 'harmony', verbose=F)

res <- c(0.2, 0.25, 0.3, 0.35, 0.4, 0.45, 0.5, 0.6, 0.7, 0.8, 0.9, 1)
for (ii in res){
  obj <- FindClusters(obj, resolution = ii, verbose=F)
}


clustree(obj, prefix = "RNA_snn_res.")
```

To annotate clusters, 'FindAllMarkers' function from Seurat was employed, and its output was sorted to ease accessing the top markers of each cluster. Some clusters were identified through known markers, such as GFAP marker for astrocytes. For additional cluster identification, the top markers of these clusters were input into PanglaoDB (Franzén et al., 2019) for a more informative and unbiased clustering. Identification of clusters that are labeled as dentate gyrus (DG) neurons was aided with Janelia's Hipposeq (Cembrowski et al., 2016) based on their top markers.

To perform pseudobulk analysis, the data was converted to the SinglgeCellExperiment class using SingleCellExperiment package version 1.20.0 (Amezquita et al., 2020). Aggregated count data was then analyzed using the DESeq2 package version 1.36.0 (Love et al., 2014) to identify differentially expressed genes. The PCA plot shown in the results was also generated through the DESeq2 package.

Cell-cell communication analysis was conducted using CellChat version 1.6.1(Jin et al., 2021) following the standard vignette. All FeaturePlots and DotPlots were generated using Seurat's built-in functions. All single cell analyses were performed on an x86_64-conda-linux-gnu (64-bit) platform running under Linux Ubuntu 22.04.3.

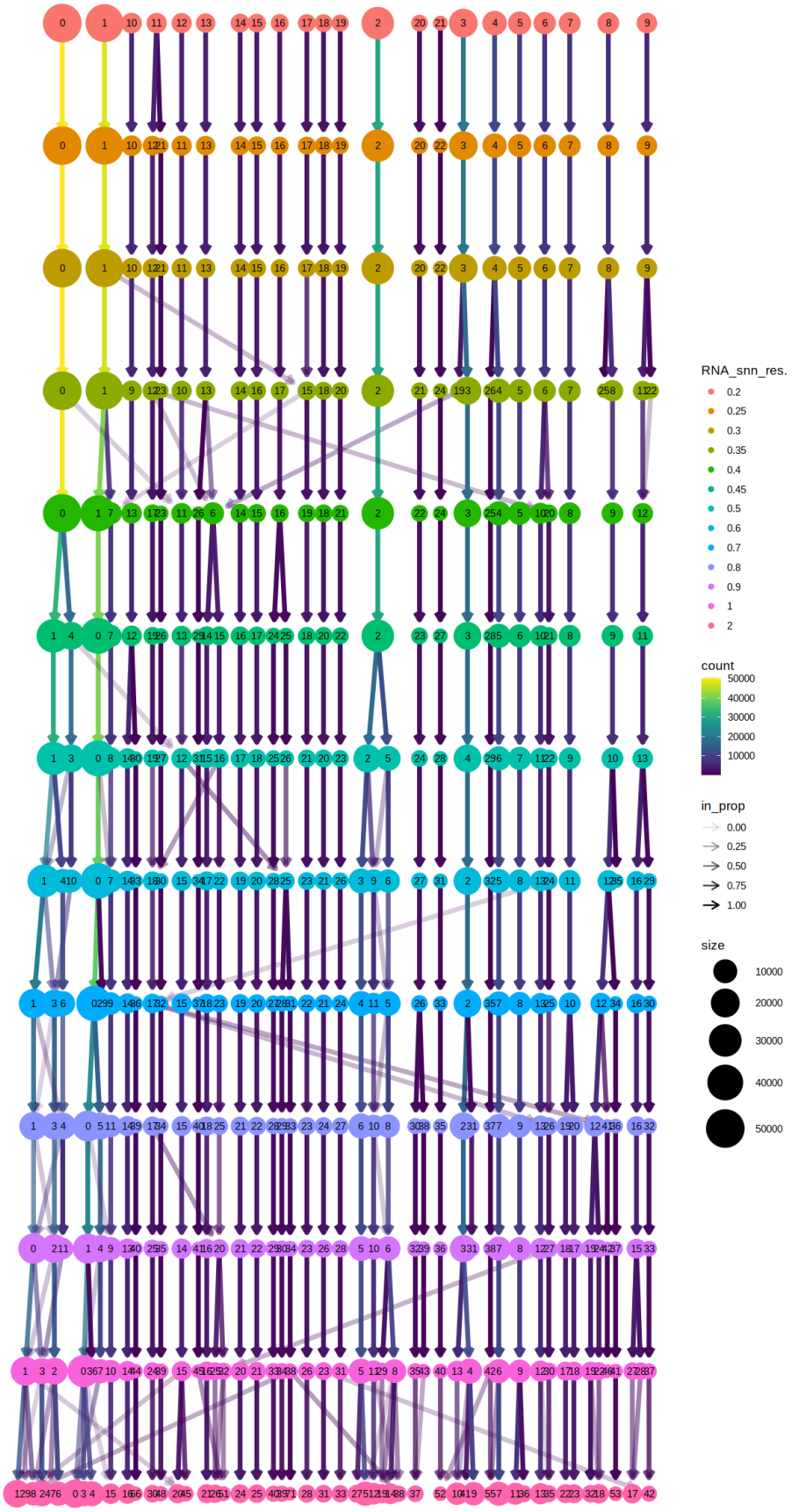

Figure 9: Clustree visualizes different resolutions in clustering. Resolution 0.45 was chosen.

4. Results

4.1 Baricitinib Does Not Modulate the Survival of GA-Nes Mice

Rational

Given the strong neuroinflammation observed in the GA-Nes mouse model (LaClair et al., 2020), an exploration of the JAK-STAT pathway inhibition was pursued as a potential therapeutic avenue. As detailed in the introduction section of this dissertation, this mouse model demonstrates upregulation of Stat1 and Stat3, along with phosphorylated Stat1 and Stat3 (LaClair et al., 2020), signifying the activation of JAK-STAT pathway. To inhibit this pathway, Janus kinase (JAK) inhibitors are widely used in both therapeutic and research settings. While other inhibitors, such as ruxolitinib and tofacitinib, are also prevalent in research, they possess a relatively short elimination half-life of approximately 3 hours (Appeldoorn et al., 2023; Krishnaswami et al., 2015). Therefore, a third JAK inhibitor, baricitinib, was selected due to its proven efficacy in inhibiting JAK1/2 and its substantially longer elimination half-life of up to 12.9 hours, as observed in patients with atopic dermatitis (WHO-Prequalification-Team, 2021).

Study Design

The elimination half-life of the drug was a critical factor in the selection of the drug, as administering the drug more than once per day would not have been practical due to the large number of animals. Furthermore, given the young age and the small size of these mice – often weighing less than 10 grams – conducting surgery to insert an osmotic pump would be infeasible. Therefore, baricitinib was administered at 10 mg/kg daily via subcutaneous injection starting at P28 (Figure 10), until the mice reached their humane endpoint, as determined by a scoring system approved by the Bavarian government. An initial dose of 50 mg/kg starting at P21 was tested, but the mice were unable to tolerate such a dose at such an early age and all injected animals expired.

Consequently, the dosage and starting age were adjusted to inhibit the JAK-STAT pathway without compromising the homeostatic functions of the mice.

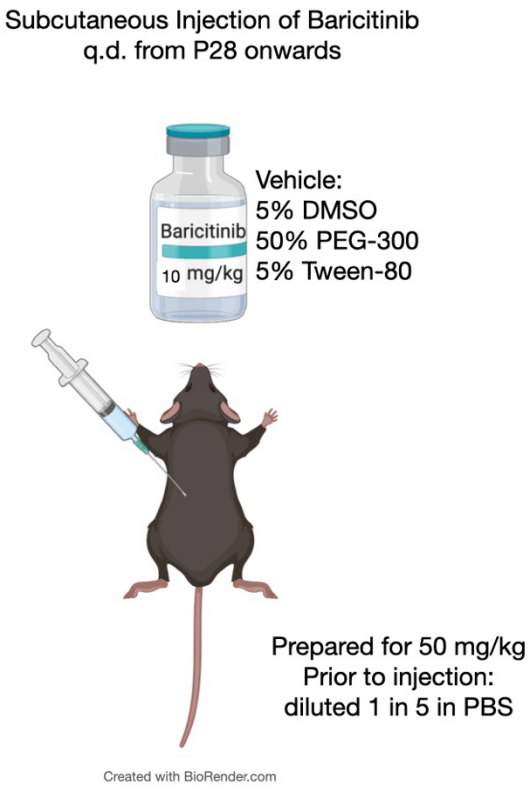

Figure 10: Baricitinib treatment scheme for mice. This figure was created with BioRender.com; and a publication license was obtained from BioRender for the purpose of this dissertation.

Confirmation of Drug's Efficacy *in vitro*

Prior to the animal study, the efficacy of the baricitinib batch was assessed in HEK293FT cells to ensure the intended functionality, especially since it was purchased in bulk from a lesser-known vendor. To induce inflammatory conditions, poly(I:C) at 10 μg/mL was employed, as recommended by the manufacturer. Poly(I:C), a dsRNA mimic, elicits an inflammatory response by binding to various sensors, notably RIG-I, MDA5, and TLR3. These receptors subsequently trigger cellular responses that activate JAK, leading to phosphorylated Stat and resulting in altered gene expression (Dai et al., 2006). Although pStat1 is closely associated with the dsRNA response, pStat3 is also found to be upregulated (Melkamu et al., 2013). Given the elevated levels of pStat3 in the cell model following poly(I:C) treatment, pStat3 was selected as a proxy for the drug's efficacy and target engagement.

The IC50 of baricitinib, as determined in cell-free assays by the manufacturer, was reported to be 6 nM. Consequently, doses of 60 nM, 600 nM, and 6 μM of baricitinib were tested in the cell assays, alongside the respective vehicle. In cell culture, poly(I:C) induced upregulation of phosphorylated Stat3, which was inhibited by the 60 nM and 600 nM doses of baricitinib, while the 6 μM dose proved toxic to the cells. In summary, the efficacy of the drug in engaging the target was successfully confirmed within a cellular model (data not shown).

Treatment Neither Modulates Survival nor Sufficiently Engages Target

Upon confirming the efficacy of the drug in cell culture and establishing the appropriate drug dosage regimen for the mice, the in vivo experiment was initiated in the GA-Nes mice. Starting from the first dose (P28), mice's weight was closely monitored and recorded, as weight loss is a primary criterion for euthanasia. However, the primary measure for the success of the therapy was considered to be survival. The Kaplan-Meier estimator, employing the log-rank test to evaluate significant differences in survival, indicated no significant extension of survival for transgenic mice treated with baricitinib compared to those receiving the vehicle. Figure 11 presents the survival curve of the mice, with a p-value of 0.11, failing to reject the null hypothesis.

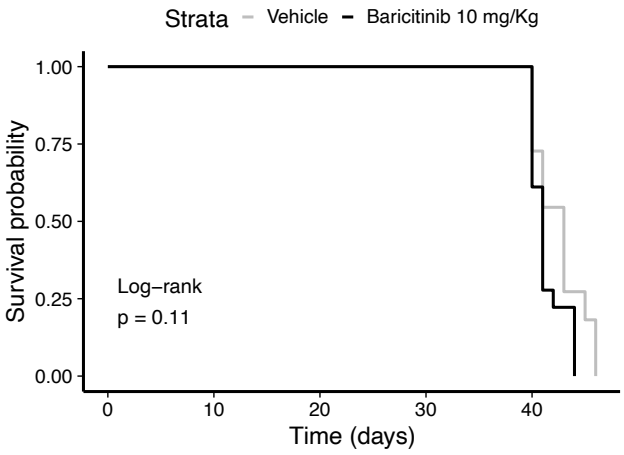

Figure 11: Survival curve of transgenic mice treated by baricitinib or vehicle shows no significant difference between treatments (p=0.11, log-rank non-parametric test). n = 11 vehicle (7 males, 4 females), 18 baricitinib (10 males, 8 females), with no appreciable difference with the treatment that can be attributed to gender.

Given the lack of efficacy of the drug in significantly modulating survival, target engagement was evaluated by measuring pSTAT3, replicating the methodology applied previously in cells. Figure 12 shows a western blot of pooled cortices from a subset of these mice (n=3). It indicates that pStat3, though marginally elevated in transgenic mice, did not show a significant reduction at a dosage of 10 mg/kg of baricitinib. This observation suggests insufficient target engagement.

Figure 12: Western blot of pStat3 shows the phosphorylation of STAT3 in transgenic mice (Tg), but there is no rescue observed by treatment with baricitinib, indicating a probable insufficient target engagement. Wildtype (WT) mice do not exhibit any detectable pStat3 with either treatment. Positive and negative controls originate from unperfused mice with previously confirmed pStat3 expression.

In addition, the potential impact on neuromuscular junctions (NMJs) was assessed. For this purpose, anti-β-Tubulin III and Bungarotoxin were employed to label axons and acetylcholine receptors on skeletal muscle fibers, respectively. Figure 13 displays representative examples from each condition. The analysis revealed minimal NMJ loss in transgenic mice at this age, indicating that a rescue effect was not observed. Given the absence of any discernible beneficial effects from this drug, the decision was made to shift focus to other projects, utilizing the insights gained from this endeavor for future research.

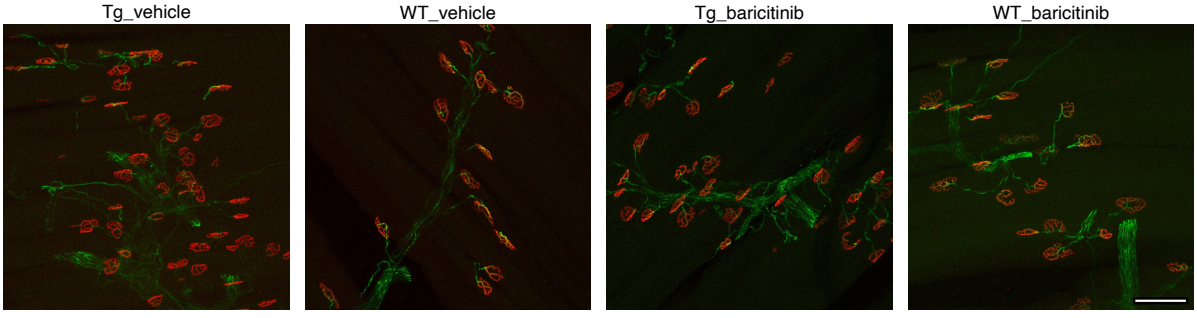

Figure 13: There is no appreciable loss of NMJs at the humane endpoint. Images are enhanced for better visibility. Bungarotoxin is in red and anti-β-Tubulin III is in green. Scale bar = 75 μm.

4.2 Metabolomics Studies: DietGel and Energy Sensors

As highlighted in the introduction, metabolism is significantly impacted in both ALS patients and the GA-Nes mouse model, with the latter requiring euthanasia around 6 weeks of age primarily due to steep weight loss (LaClair et al., 2020). Thus, investigating the impact of poly(GA) on metabolism was a critical step. This research utilized two approaches: *in vitro* and *in vivo*. The objective of the *in vivo* study was to explore the therapeutic effects of a modified diet for transgenic mice. Since weight loss is the principal reason for euthanasia, mitigating weight loss through dietary improvements could enable further investigation into more advanced neuropathological features in the GA-Nes, such as NMJ loss. Conversely, in the *in vitro* study, the focus was on quantifying gross metabolic changes in poly-GA expressing cells by monitoring energy carriers like ATP and NADH through live cell trackers and metabolomics analysis.

4.2.1 Dietary Modification with DietGels Does Not Modulate Survival

In this experiment, GA-Nes transgenic mice and their wildtype controls were provided with DietGel 76A, DietGel Recovery, and Hydrogel in addition to regular food pellets. The components of these gels are detailed in the materials and methods section in Table 4. A key characteristic of these diets is that DietGel 76A is high in protein content, while DietGel Recovery is characterized by a high caloric content, particularly rich in carbohydrates. Hydrogel, on the other hand, served as a control food, being a non-wetting water gel utilized in this context.

The primary aim of this pilot study was to monitor both the survival and weight of the mice. The gel administration began at P2 and was subsequently changed three times per week. Starting from P35, due to increased consumption, the gels were replaced daily. The mice underwent occasional monitoring, with the frequency of such monitoring intensifying as the mice aged. For this pilot, two mice were allocated to each gel under the transgenic condition, while two to four mice were allocated to each gel under the wildtype condition. No significant weight changes were noted in the wildtype control mice (see Figure 14a). However, in the transgenic mice, both DietGels

appeared to marginally alleviate the low-weight phenotype. Nonetheless, the pattern of weight loss was comparable to that observed with Hydrogel, displaying a similar slope when weight decline commenced after the age of 5 weeks (see Figure 14b). Subsequent analysis revealed no significant survival benefits associated with such diets (see Figure 15). Therefore, it was concluded that continuing with this treatment approach was not warranted.

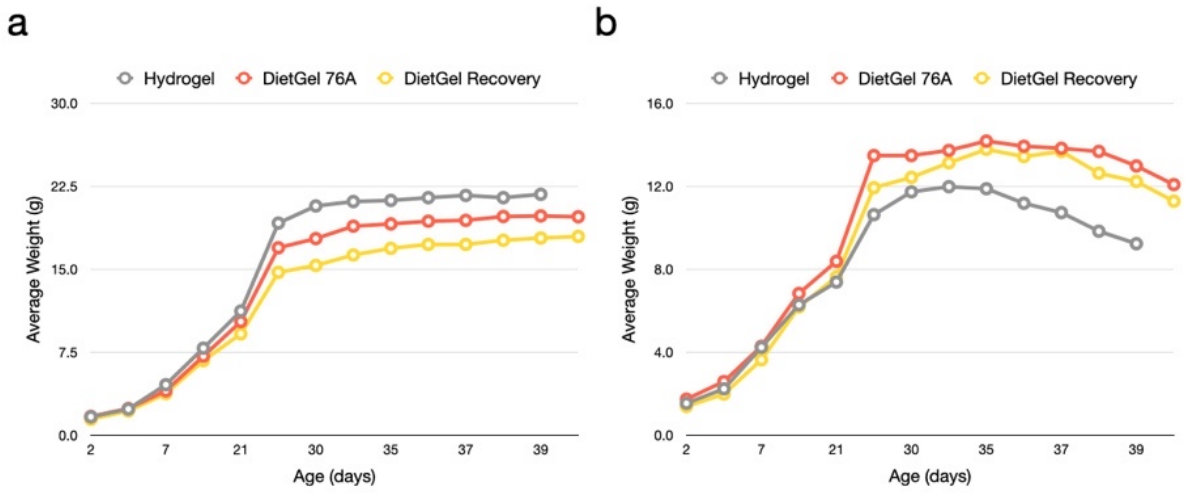

Figure 14: DietGels marginally improve the weight of GA-Nes transgenic mice. a) Wildtype controls demonstrate a noticeable difference in weight gain pattern. b) Transgenic GA-Nes mice exhibit an initial weight gain with either of the DietGels compared to Hydrogel. Nevertheless, the weight loss pattern is similar across all treatments, resulting in euthanasia at around the same age. n = 6 total (2 in each group). All animals in this pilot were males.

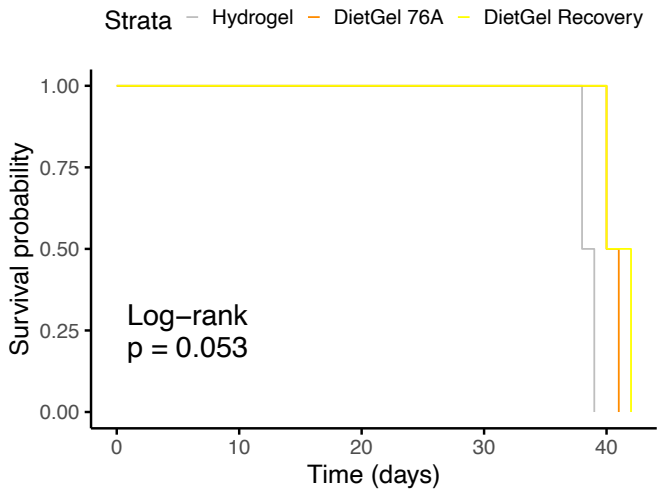

Figure 15: DietGels do not significantly extend survival of the GA-Nes mice in this pilot. n = 6 total (2 in each group). All animals in this pilot were males.

4.2.2 Energy Carriers in Neurons Do Not Show Any Difference

Rational and Study Design

Given the metabolic changes observed in ALS, the decision was made to employ fluorescent sensors to monitor energy carriers in cells. Two sensors were initially selected: PercevalHR for sensing the ATP:ADP ratio (Tantama et al., 2013), and Peredox for the NADH: NAD+ ratio (Hung et al., 2011; Hung & Yellen, 2014). Both sensors operate in live cell environments, fluorescing at two distinct wavelengths depending on the abundance of the ATP/ADP and NADH/NAD^+, respectively. An increase in either wavelength signals a rise in the corresponding species. The primary goal was to assess the suitability of each sensor in a live cell context. For this purpose, HEK293FT cells were transfected with a poly(GA) construct (hereafter referred to simply as GA for brevity), which includes an iRFP670 tag. This tag allows for visualization without interfering with the sensor channels. Following confirmation of their suitability, the plan was to use primary rat neurons transduced with GA constructs, aiming for a more relevant and accurate assessment by these sensors.

PercevalHR, as an ATP/ADP Sensor, Does Not Function

Firstly, PercevalHR was employed to measure ATP to ADP ratios, with an excitation wavelength of ~500 nm indicating increased ATP levels, and ~420 nm for increased ADP levels. The emission peak occurs at ~530 nm (Tantama et al., 2013). It is crucial to acknowledge that PercevalHR's efficacy is significantly influenced by the pH of the cell culture solution. pH fluctuations were monitored using another live cell sensor, pHRed, which emits maximally at 578 nm at pH 5.5 and at 445 nm at pH 9.0 (Tantama et al., 2011). Regrettably, PercevalHR did not yield consistent or reliable data in our experimental setup. The primary issue was the live cell setting's susceptibility to external air exposure, leading to occasional pH instability (as indicated by shifting of the sensor’s intensities), despite the presence of adequate buffers in the solution. The variability between replicates was too great to justify further experiments with PercevalHR. Further, the application of inhibitors such as Iodoacetamide (IAA, inhibitor of glycolysis), Oligomycin A(inhibitor of ATP synthase), or Rotenone (inhibits

mitochondrial electron transport) failed to elicit the expected effects. Consequently, the decision was made to discontinue further experiments with this sensor. Figure 16 illustrates an example of PercevalHR recorded intensities in the GA-transfected and control-transfected conditions.

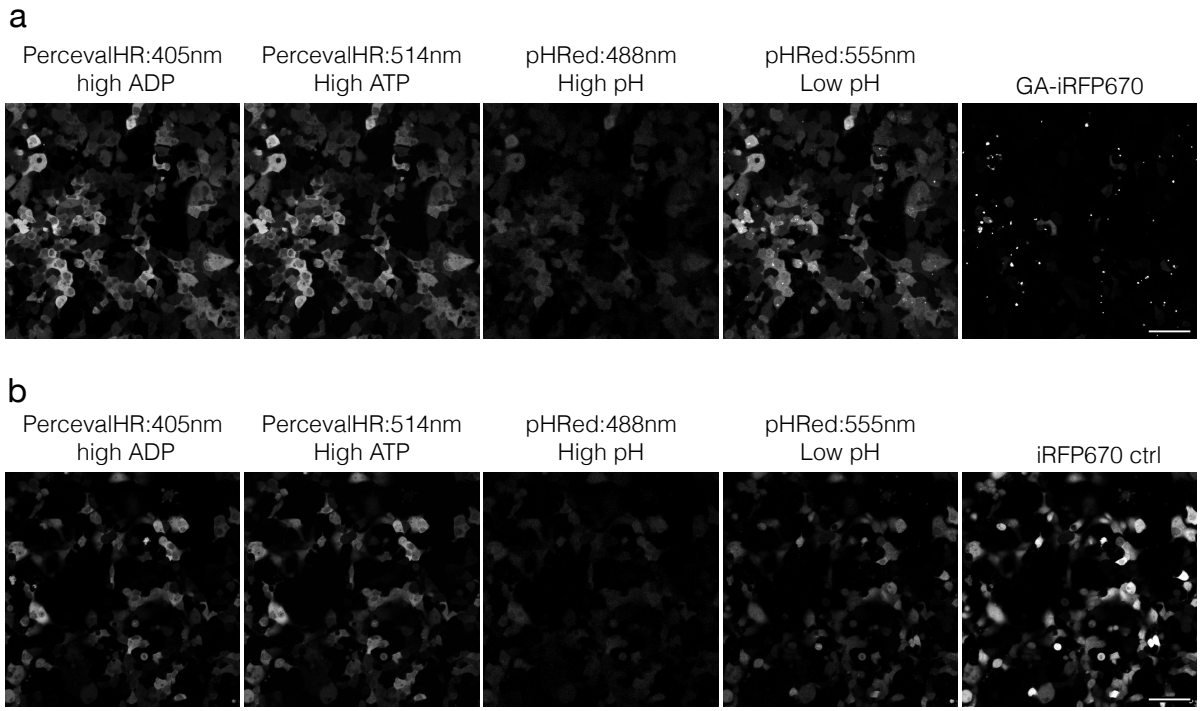

Figure 16: PercevalHR is not a suitable sensor in our setting. a) GA-iRFP670 transfected HEK293FT cells showing similar intensities for ADP and ATP, while pH might be out of the valid range of PercevalHR. b) iRFP670-control transfected HEK293FT cells showing similar intensities for ADP and APT, while pH might be out the valid range of PercevalHR. Images are enhanced. Scale bars = 75 μm.

Peredox, an NADH /NAD$^+$ sensor, Is Functional, But Shows No Difference

Secondly, Peredox (measuring the NADH/NAD+ ratio) was evaluated. This sensor appeared more promising due to its pH resistance. Peredox-mCherry comprises two fluorescent subunits: The first, containing T-sapphire, excites at 405 nm and emits at 525 nm, indicative of higher NADH levels. The second, containing mCherry, excites at 575 nm and emits at 640 nm, indicative of higher NAD+ levels (Hung et al., 2011; Hung & Yellen, 2014). Consistent NADH/NAD+ ratios were observed, and Iodoacetamide (IAA), Oligomycin A, and Rotenone were tested as positive controls. IAA elicited a clear response, establishing it as the positive control for subsequent experiments. However, in HEK293FT cells, no significant difference was noted between conditions with and without GA, suggesting that these cells may not be ideal

for detecting such changes, or that no change in the NADH/NAD+ ratio occurs under these conditions. Figure 17 displays the Peredox sensor activity in transfected HEK293FT cells.

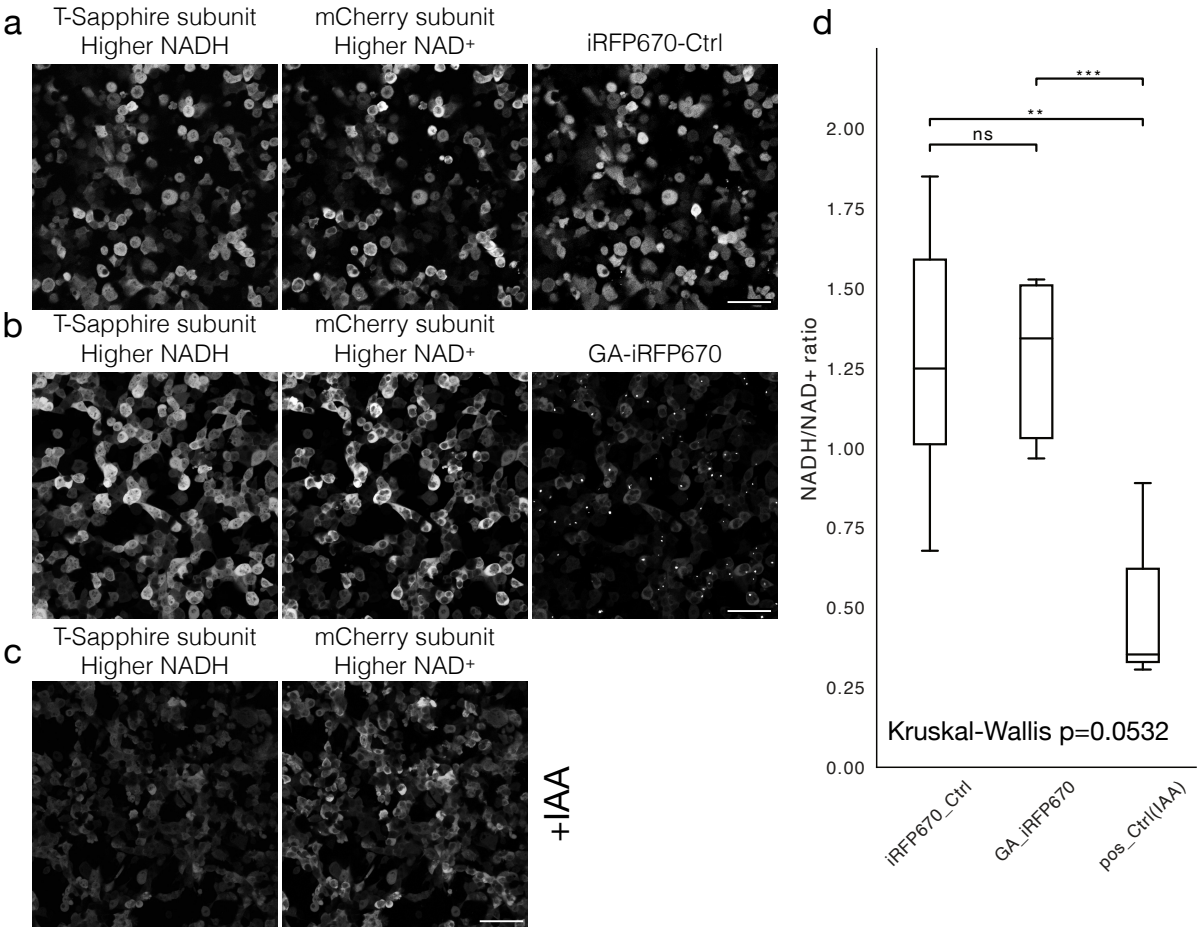

Figure 17: Peredox, which measures the NADH/NAD+ ratio, shows no difference in HEK293FT cells transfected with GA compared to a control construct. a,b) An example images of control and GA-transfected cells show successful transfection of Peredox and GA/Ctrl constructs. Scale bars = 75 μm. c) Example image of positive control (IAA) shows a reduced NADH signal and thus suggests a reduced NADH/NAD+ ratio. Scale bars = 75 μm. d) Quantification of each condition with the Kruskal-Wallis test gave a p-value of approximately 0.0532 (near significance). Post hoc analysis revealed that IAA positive control is significantly different from either treatment (Ctrl vs IAA p = 0.0083; GA vs IAA p = 0.001) while Ctrl and GA do not significantly differ (p = 0.4627). Images are enhanced for better visibility, but unmodified images are used for quantification.

Even though no differences were observed between cells transfected with GA or control constructs, it is possible that HEK293FT cells may not be the most suitable model for studying neurodegeneration. A second possibility is that any differences are too subtle to be detected by this sensor. A third explanation, of course, could be the absence of actual differences. To explore the first and second scenarios further, primary rat neurons were employed. These neurons were co-transfected with GA and

control constructs to specifically address the potential model suitability issue. In these experiments, no significant differences were noted between the GA-transfected neurons and the control group. Additionally, the primary rat neuron cultures exhibited greater variability, which also rendered the response to the positive control, Iodoacetamide (IAA), not significantly different between groups, despite a clearly discernible trend. Figure 18 illustrates the activity of the Peredox sensor in transfected primary rat neurons.

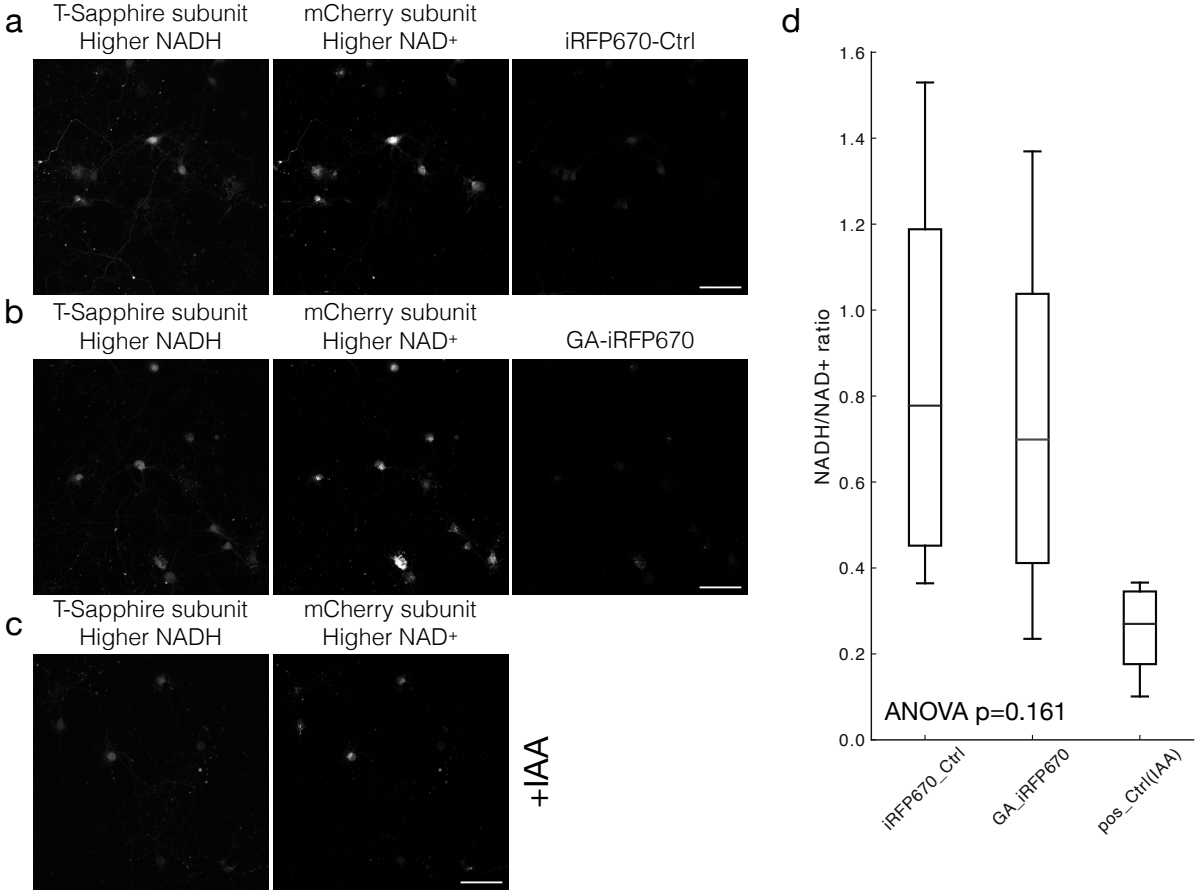

Figure 18: Peredox, which measures the NADH/NAD+ ratio, shows no difference in primary rat neurons (hippocampal) transfected with GA compared to a control construct. a,b) Example images of control and GA-transfected cells show successful transfection of Peredox and GA/Ctrl constructs. Scale bars = 75 μm. c) Example image of positive control (IAA) indicates reduced NADH signal and thus suggests a reduced NADH/NAD+ ratio. Scale bars = 75 μm. d) Quantification of each condition with ANOVA gave a non-significant p-value due to high variability. The trend clearly shows that IAA, but not GA, results in a lowered NADH/NAD+ ratio. Images are enhanced for better visibility, but unmodified for quantification.

Mass Spectrometry at Creative Proteomics Does Not Show Any Difference

Given the absence of any significant or noticeable differences between the experimental conditions using Peredox, our objective shifted towards investigating the

potential for subtle differences that the sensor might not detect. To this end, mass spectrometry, renowned for its accuracy in measuring molecular compositions, was selected as the method of choice. Consequently, lentiviral constructs were prepared, encompassing poly(GA)149-GFP, poly(GR)149-GFP, TDP-25-GFP, or simply GFP. Twelve 10 cm dishes of primary rat cortical neurons for each construct underwent transduction, with successful expression subsequently confirmed. Figure 19 illustrates the verified expression of these constructs.

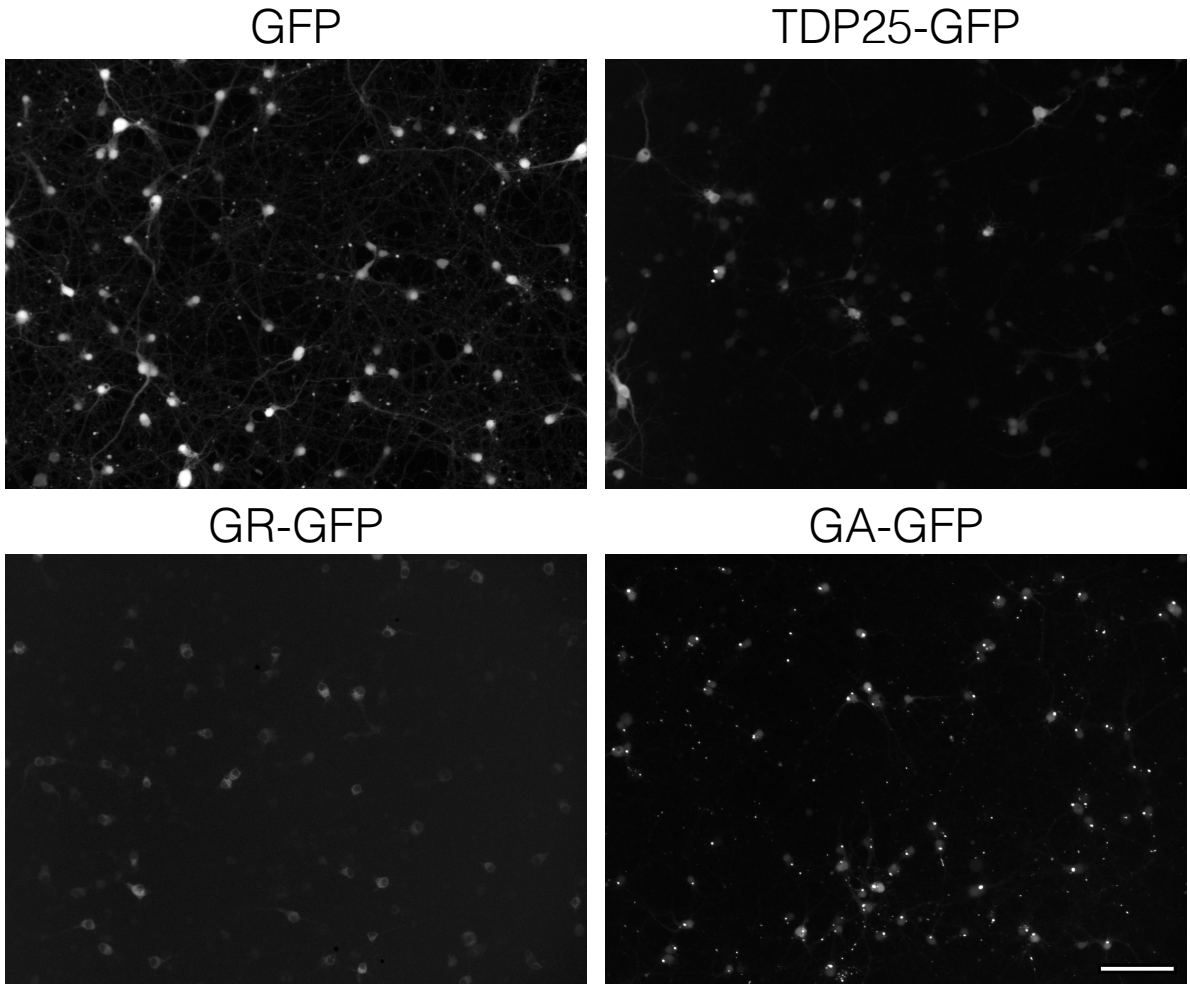

Figure 19: Expression of four lentiviral constructs is confirmed in rat cortical neurons. Images are taken from the GFP channel. The presence of aggregates is confirmed in GA condition in every cell and in a few cells in the TDP25 condition. Images are enhanced for better visibility. Scale bars = 75 μm.

Primary neuronal cell pellets were harvested into four biological replicates (based on the rat they originate from) for each construct, resulting in a total of 16 samples, and submitted to Creative Proteomics for a comprehensive analysis of 9 metabolites relevant to ATP/NAD dynamics. The metabolites analyzed included AMP, ADP, ATP,

GDP, GTP, NAD, NADH, NADP, and NADPH. From these, six meaningful ratios were derived for further analysis: ATP/ADP, ATP/AMP, ADP/AMP, GTP/GDP, NADH/NAD, and NADPH/NADP. Figure 20 presents a summary of these findings, indicating no significant differences across the analyzed ratios.

While the absence of significant findings initially puzzled us, insights from a recent conference presentation by Dr. Robert Kalb's research group offered a potential explanation for our results. This perspective is elaborated upon in the discussion section of this dissertation. Following these revelations, the focus of my doctoral research shifted towards another project, which is detailed in the subsequent section of results.

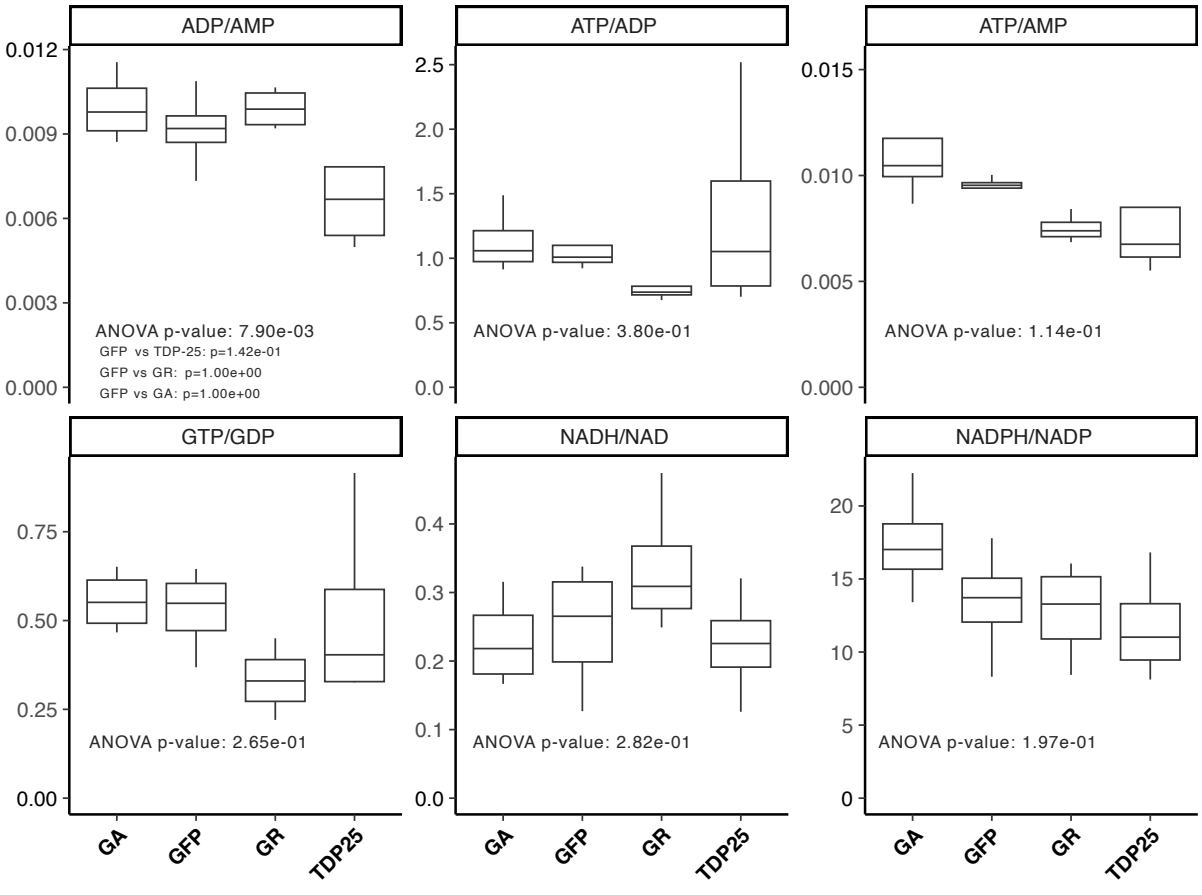

Figure 20: Metabolite ratios from LC-MS analysis show no significant differences among any of the groups. ADP/AMP initially had a significant p-value from ANOVA, but none of the comparisons are significant in t-tests with Bonferroni correction, as indicated directly in the figure.

4.3 Cyclodextrin Study

Important Notice: Please note that some of the data, figures, and text from this section will appear in a peer-reviewed publication – At the time of the final submission of this dissertation, the manuscript is under revision at Nature Communications, titled "Correction of dysregulated lipid metabolism normalizes gene expression in oligodendrocytes and prolongs lifespan of a poly-GA C9orf72 mouse model". The sole first author of this manuscript is myself, and the corresponding author would be Prof. Dr. Dieter Edbauer. This notice serves to obviate any allegations of plagiarism. A blocking note due to publishing in a journal is requested.

This section presents parts of results from the dissertation that highlights the therapeutic potential of 2-hydroxypropyl-β-cyclodextrin (commonly known as HP-β-CD, HPβCD, or HPbCD, hereafter referred to as CD) in the GA-Nes ALS mouse model. This was a serendipitous discovery, because we initially used 2-HP-β-cyclodextrin as a solvent for another anti-inflammatory compound (a low-dose CSF1R inhibitor, which is not discussed here), and noticed that even mice in the vehicle group lived longer than historical data, while the compound had no added benefit. Given that CD is not only a commonly used vehicle, but also under clinical investigation for NPC and AD, I systematically tested the therapeutic effect of CD in GA-Nes mice.

4.3.1 CD Extends Survival in Females GA-Nes Mice

To analyze the effects of CD, I initially conducted a survival study in the GA-Nes mouse model, as this is clinically the most relevant readout. Following national animal welfare laws, mice were euthanized upon reaching a humane endpoint based on a predefined scoring system, primarily attributed to significant weight loss. Starting from postnatal day 21 (P21), mice received daily subcutaneous injections of 2000 mg/Kg CD solution (as previously described) or an equivalent volume of the vehicle (30 mM citric buffer at pH 5.0). Both CD and its vehicle were well-tolerated, exhibiting no signs of toxicity. However, it was noted that a single injection of the same dose of CD dissolved in PBS, a neutral buffer, resulted in acute toxicity, necessitating euthanasia due to symptoms such as cold body, rapid breathing, and the mouse lying

on its side. We can only speculate that the formulation of CD in PBS and citric acid affects the solubility of CD or its interaction with cellular components.

This study comprised four treatment groups: wildtype mice treated with vehicle (WT_Vehicle), wildtype mice treated with CD (WT_CD), transgenic mice treated with vehicle (Tg_Vehicle), and transgenic mice treated with CD (Tg_CD). The cohort, including both male and female mice, showed an extension of survival due to CD treatment in approximately half of the female mice, while males exhibited no significant difference in lifespan. Figure 21 displays the Kaplan-Meier survival plot, separately illustrating the survival statistics for males and females.

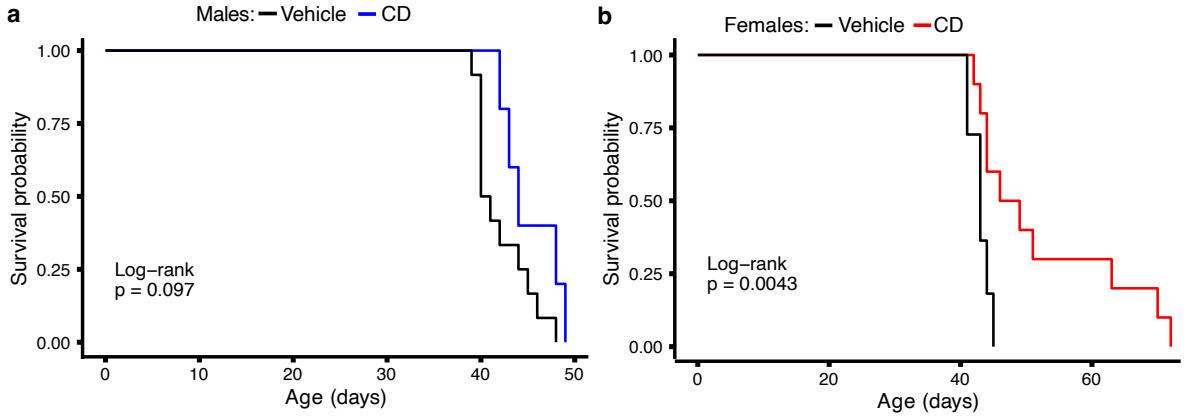

Figure 21: Daily CD treatment improves survival of female but not male mice. a) Survival analysis by Kaplan-Meier plot shows that CD administered at 2000 mg/kg q.d. does not affect the survival of male transgenic mice significantly (p=0.097, n = 12 vehicle vs 5 CD). b) Survival analysis by Kaplan-Meier curve shows that CD administered at 2g/kg q.d. significantly improves the survival of female mice (p=0.0043, n = 11 vehicle vs 10 CD)

4.3.2 P40 Cohort Allows Comparable Analyses

To investigate how CD extends survival, the treatment protocol was replicated, with termination at a fixed endpoint at postnatal day 40 (P40) to facilitate comparative biological analyses, because even after significant life extension end stage pathology may look similar in all mice. We chose P40 for analysis, because it is the earliest time point female mice required termination in the survival study (Figure 21). Given the observed extension of survival predominantly in female mice, the cohort for this subsequent study was specifically limited to females, thereby excluding males. The findings from this female-only cohort at P40 are discussed next.

Poly(GA) Levels Are Unaffected by CD Treatment

This cohort, comprising exclusively female mice harvested on P40, facilitated direct comparisons as all mice were age-matched. The initial investigation focused on determining whether CD influences poly(GA) levels in tissue. Given that the transgene encoding poly(GA) also encompasses GFP, frozen sections could be directly visualized for GFP fluorescence under a microscope, obviating the need for immunostaining. Consequently, GFP signals across all four conditions were compared, with Figure 22 displaying representative examples from each condition. As anticipated, no fluorescent signal was detected in wildtype mice. No discernible difference in signal intensity was observed in transgenic mice due to CD treatment. Therefore, it was concluded that CD exerts therapeutic benefits in GA-Nes mice without altering poly(GA) levels. It was also noted that poly(GA) is expressed across many cell types, including glial cells such as astrocytes and oligodendrocytes.

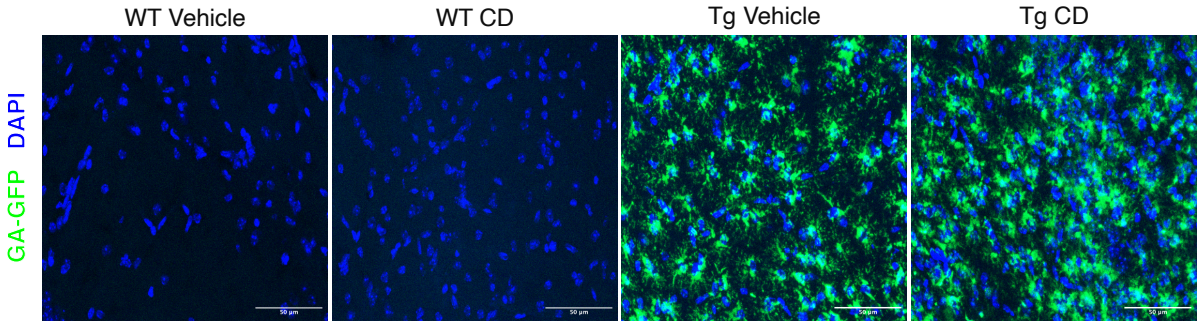

Figure 22: Fluorescence microscopy of endogenous GA-GFP in frozen tissue confirms its expression in transgenic mice, the lack of expression in wild-type mice, while also highlighting no appreciable reduction upon CD treatment. scale bars = 50 μm.

CD Significantly Lowers NfL

Neurofilament light chain (NfL), recognized as a marker of neuronal damage and death, was evaluated in sera collected from this cohort. Given that all mice in this study share the same gender, genotype, and time point, the NfL measurements provide a sensitive assessment quantitative of the extent of neuronal damage and death. Figure 23 illustrates that NfL levels are significantly elevated in female mice at

P40 due to the expression of poly(GA). Importantly, CD treatment appears to partially, yet significantly, mitigate NfL levels in transgenic mice.

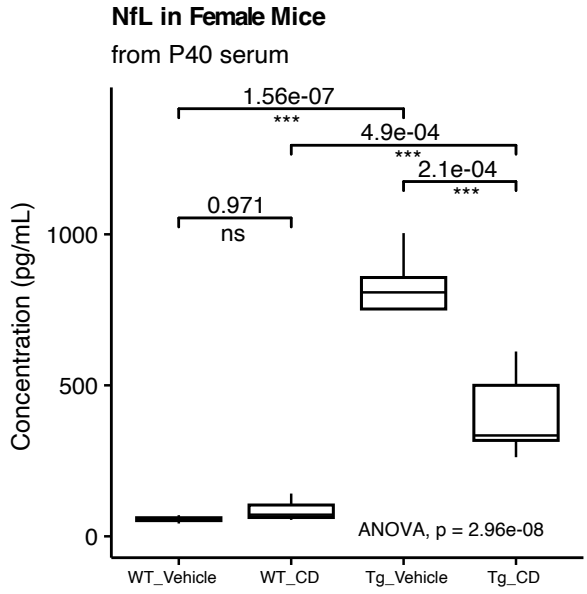

Figure 23: Serum NfL from a cohort of mice sacrificed at postnatal day 40 (P40) shows an increase in transgenic mice (p= 1.56e-07), which is partially but significantly rescued by CD treatment (p= 2.1e-04, n = 4 vehicle vs 5 CD). p-values are obtained from Tukey's HSD post-hoc.

4.3.2.1 snRNAseq Provides a Plethora of Data, Highlighting Oligodendrocytes

To elucidate CD's therapeutic mechanisms, single-nucleus RNA sequencing (snRNAseq) was conducted on hippocampal tissue from female mice, with the findings detailed in the sections that follow.

4.3.2.1.1 Clustering and Annotation

To elucidate the target of therapy, assess both cell autonomous and non-cell autonomous effects, and facilitate a comprehensive comparative analysis of treatment groups, I used single nucleus sequencing. snRNAseq was chosen over single-cell RNA sequencing (scRNAseq) to enable direct comparison with human datasets and to allow the processing of frozen samples. Utilizing the 10x Genomics platform, snRNAseq analysis of P40 female hippocampi was conducted. The hippocampus was selected due to its pronounced pathology in GA-Nes mice, as previously reported (LaClair et al., 2020). For each sample, 10,000 nuclei, comprising an equal distribution

of 5,000 NeuN-positive and 5,000 NeuN-negative nuclei (isolated via Fluorescence-Activated Nuclei Sorting - FANS), were sequenced.

Following alignment and quality control procedures, the data were clustered into 30 distinct groups using Seurat version 4.3.0 (Hao et al., 2021), as detailed in the Materials and Methods section regarding clustering and annotation methodologies. This analysis identified 17 neuronal clusters, one neuroblast cluster, 11 glial cell clusters, and one cluster of unknown classification (which could represent a mixed cell population or cells undergoing reprogramming). All clusters are illustrated in Figure 24a, which includes two separate Uniform Manifold Approximation and Projection (UMAP) visualizations to highlight the transgene's substantial impact on the clusters. Figure 24b presents quality control metrics for all clusters, confirming that each cluster met the QC standards.

For each animal in the study (n: WT_vehicle=4, Tg_Vehicle=3, WT_CD=4, Tg_CD=4), 10,000 cells were sequenced. Following QC procedures, a total of 90,772 cells were obtained from 8 animals under the WT conditions, and 66,263 cells from 7 animals in the Tg conditions. Table 7 details the absolute number of cells identified in each cluster for each of the 4 experimental conditions.

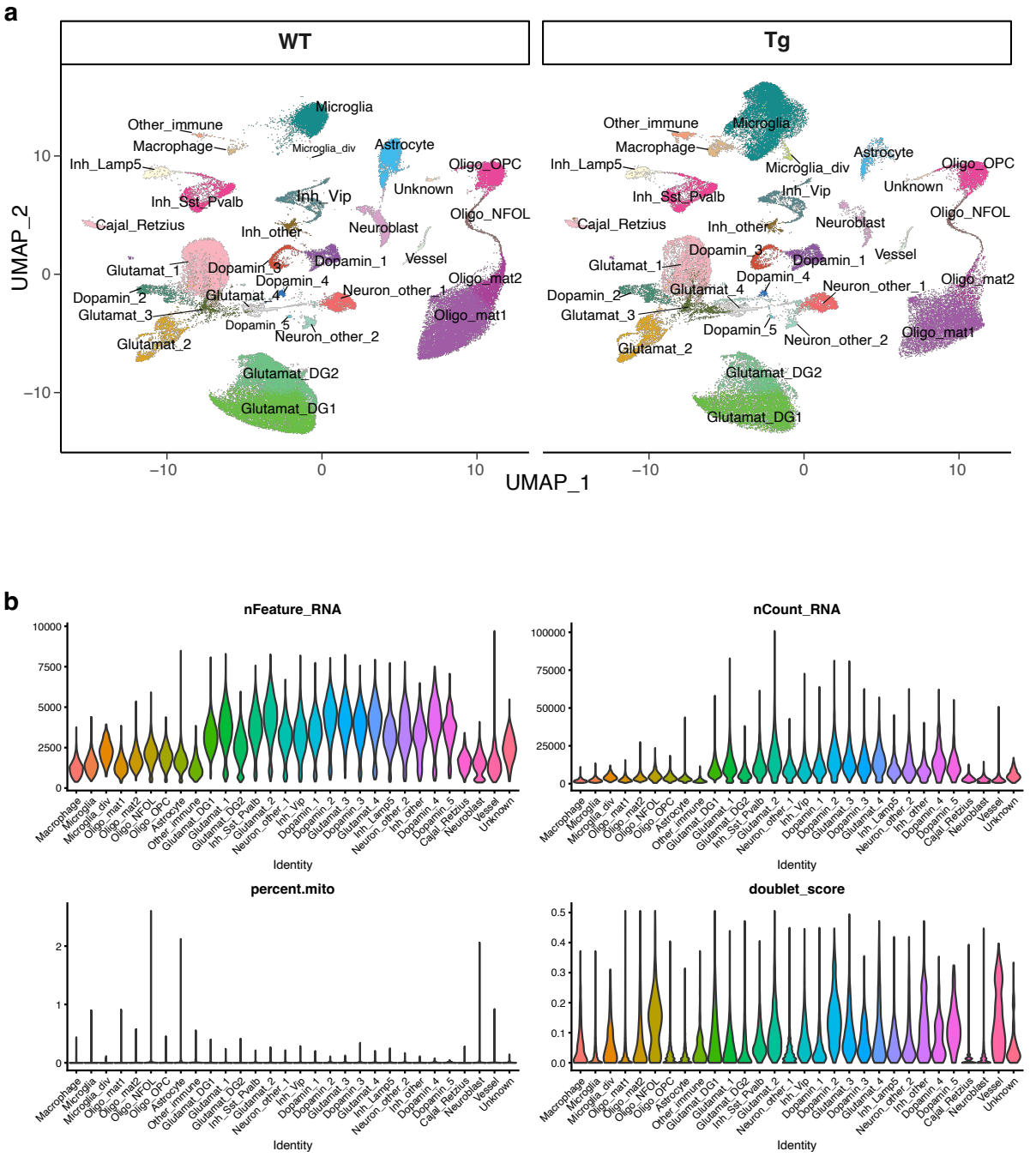

Figure 24: snRNAseq results cluster into 30 distinct entities. a) UMAP dimensional plot of clusters in transgenic and wildtype conditions highlight modulation of glia, especially microglia and oligodendrocytes. b) All clusters satisfy quality control measures of number of detected genes (nFeature_RNA), total RNA content (nCount_RNA), percentage of mitochondrial gene expression, and doublet score.

Cluster Name	WT_Vehicle	WT_CD	Tg_Vehicle	Tg_CD	Total
Astrocyte	979	3512	287	367	**5145**
Cajal_Retzius	681	475	520	460	**2136**
Dopamin_1	765	961	1080	788	**3594**
Dopamin_2	358	694	585	721	**2358**
Dopamin_3	431	573	660	528	**2192**
Dopamin_4	117	202	117	128	**564**
Dopamin_5	38	45	49	34	**166**
Glutamat_1	3286	4416	1872	2351	**11925**
Glutamat_2	403	1372	969	1473	**4217**
Glutamat_3	341	747	875	582	**2545**
Glutamat_4	242	481	312	614	**1649**
Glutamat_DG1	7481	6411	4422	4335	**22649**
Glutamat_DG2	4701	4450	1408	1796	**12355**
Inh_Lamp5	438	443	410	339	**1630**
Inh_other	138	605	216	251	**1210**
Inh_Sst_Pvalb	1013	1369	1475	1144	**5001**
Neuron_other_1	1026	1179	775	965	**3945**
Neuron_other_2	349	373	280	504	**1506**
Neuroblast	1010	1407	233	428	**3078**
Inh_Vip	878	941	1046	834	**3699**
Macrophage	104	100	392	379	**975**
Microglia	3776	2804	8104	5910	**20594**
Microglia_div	1	4	87	201	**293**
Other_immune	34	66	322	373	**795**
Oligo_mat1	10667	8218	3914	5086	**27885**
Oligo_mat2	2072	1850	302	668	**4892**
Oligo_NFOL	382	576	279	339	**1576**
Oligo_OPC	1702	2394	1382	1667	**7145**
Unknown	27	51	71	119	**268**
Vessel	170	443	132	303	**1048**
Total	**43610**	**47162**	**32576**	**33687**	**157035**

Table 7: Absolute number of cells per cluster per condition.

I identified six distinct clusters of glutamatergic neurons, two of which were attributed to the dentate gyrus. Additionally, four clusters of inhibitory neurons were identified, including three clusters characterized as somatostatin-, parvalbumin-, Vip-, and Lamp5-expressing inhibitory neurons. Five other neuronal clusters were identified as dopaminergic neurons, while the remaining two neuron clusters could not be further specified.

Glial clusters exhibited more pronounced effects from transgene expression, as illustrated in the UMAP dimensional plot in Figure 24. The proliferation of immune-related cells in transgenic mice was notably evident. For instance, the dividing

microglia cluster, labeled ‘Microglia_div’, was virtually absent in wildtype mice, with some mice lacking any cells in this cluster, whereas all transgenic mice showed a significant presence of cells within this cluster. The ‘Other_immune’ cluster predominantly comprises T cells, but also includes B cells and other immune cells such as natural killer cells. This cluster was significantly expanded in the transgenic condition. Unexpectedly, the astrocyte cluster appeared depleted in the transgenic condition. However, consistent with previous data (LaClair et al., 2020), this observation was not corroborated by immunofluorescence staining of astrocytes, as demonstrated in Figure 34 in the validation section. This discrepancy could arise from biases in nuclei isolation or possibly from an upregulation of microglia, which might artificially reduce the astrocyte nuclei count during sorting. Other glial clusters showing a noticeable difference in their UMAP representation between wildtype (WT) and transgenic (Tg) conditions include the two mature oligodendrocyte clusters, ‘Oligo_mat1’ and ‘Oligo_mat2’. Figure 25 displays the normalized number of cells in each cluster, with each data point normalized by the total number of cells from the respective animal.

While some clusters exhibit significant changes in normalized cell counts following CD administration, it is imperative to exercise caution to avoid overinterpretation of such results. Thus, changes in cell numbers attributed to transgene expression were only considered when supported by a well-established biological rationale. For instance, the upregulation of immune cells is a documented phenomenon in GA-Nes mice (LaClair et al., 2020), underscoring the necessity of understanding each cluster’s biological significance before interpreting cell count variations. To facilitate the interpretation of biological roles, an examination of markers for each cluster is recommended. Figure 26 displays dot plots highlighting the top five markers for each cluster. It is important to note that further analysis of cell/nuclei numbers was not the primary focus of this study, as the investigation of differentially expressed genes (DEGs) offers a more objective and quantitative method for elucidating the therapeutic targets of CD.

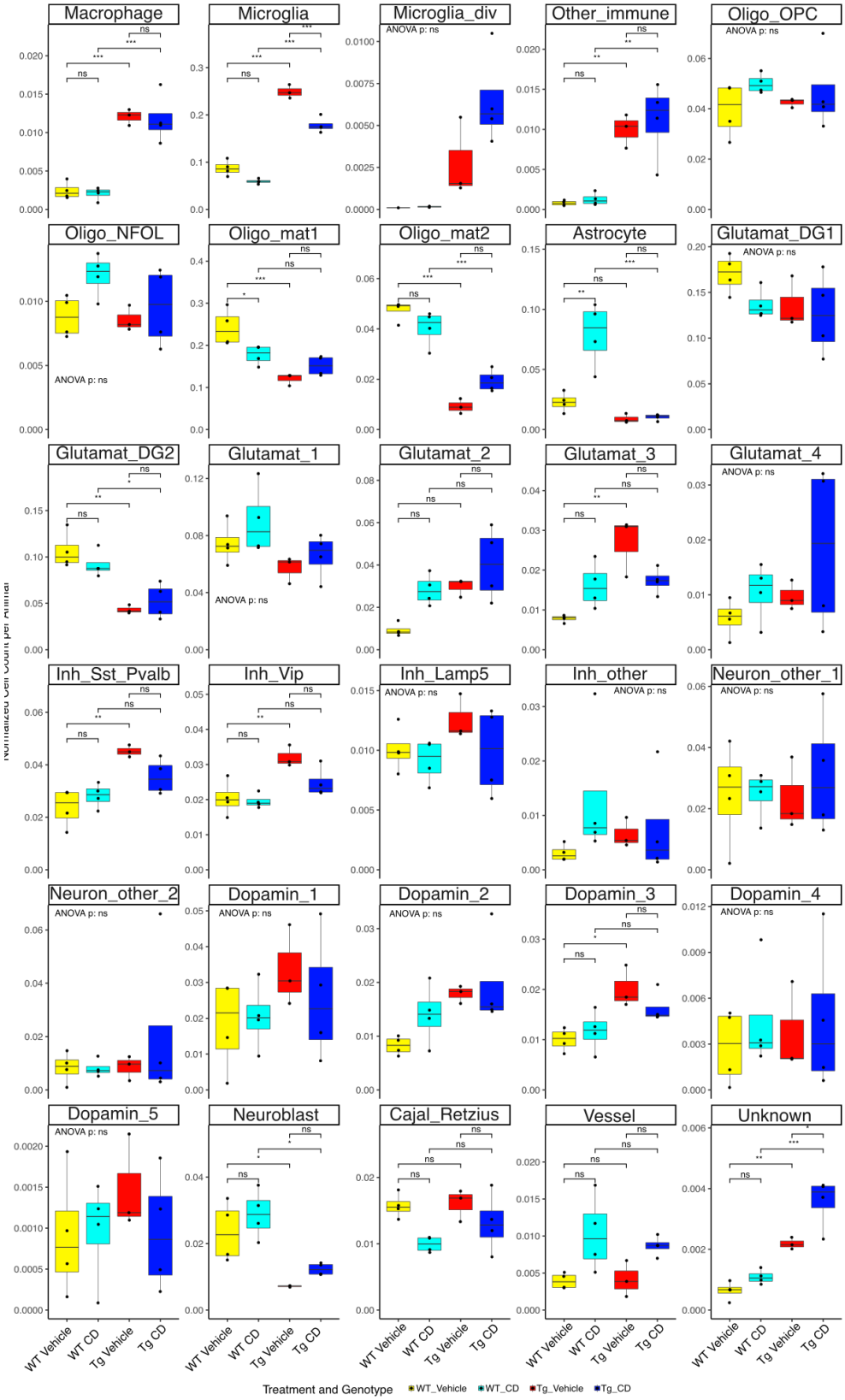

Figure 25: Normalized number of cells to total number of cells per animal shows dramatic changes in glial cells mainly due to the transgene expression. Although not all changes are confirmed (e.g., astrocytes or oligodendrocytes), the changes in immune cells appear biologically meaningful.

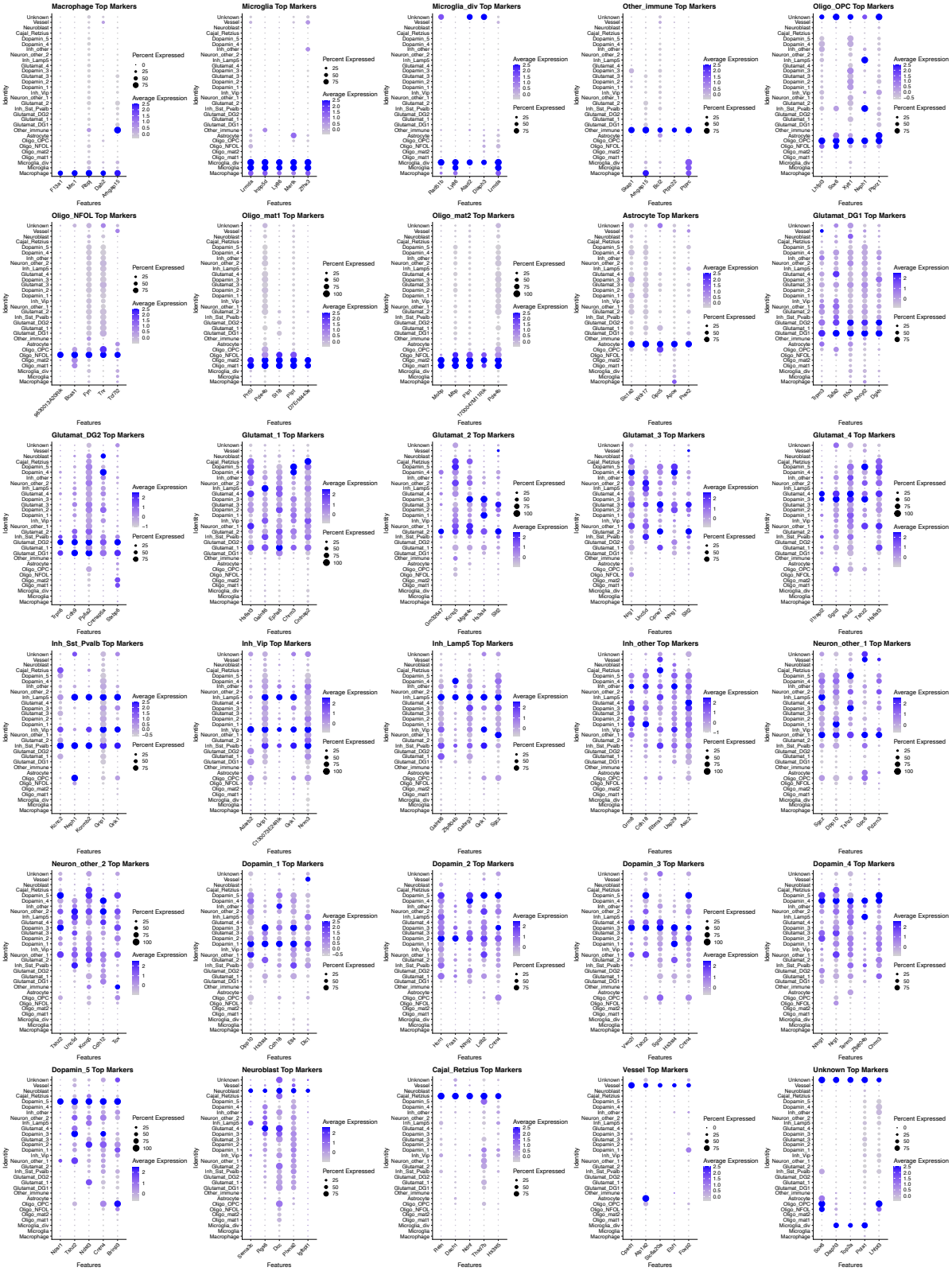

Figure 26: Dot plots show the expression of the top 5 differentially expressed genes for a given cluster across all clusters. The size of a circle encodes the percentage of cells within a cluster that express the respective gene, while the color intensity encodes the expression level of the respective gene.

4.3.2.1.2 Pseudobulk Analysis Reveals Oligodendrocytes and Neuroblasts as Primary Targets of CD

To elucidate the genes differentially expressed across each condition, pseudobulk analysis was conducted on all clusters for all conditions. This approach enabled a comparative analysis of the effects of transgene expression by contrasting the Tg_Vehicle condition with the WT_Vehicle condition, as well as the impact of CD administration by comparing the Tg_CD condition to the Tg_Vehicle condition. A stringent threshold was set for log fold changes (|LFC| > 1) to identify significant expression changes. By averaging the expression of all genes with LFC > 1 and visualizing them in UMAPs for all conditions using the AddModuleScore function, it was observed that genes upregulated as a result of CD administration were predominantly associated with neuroblasts, as illustrated in Figure 27a. Similarly, analysis of genes with LFC < -1 revealed that genes downregulated due to CD therapy were primarily found in oligodendrocytes, as depicted in Figure 27b.

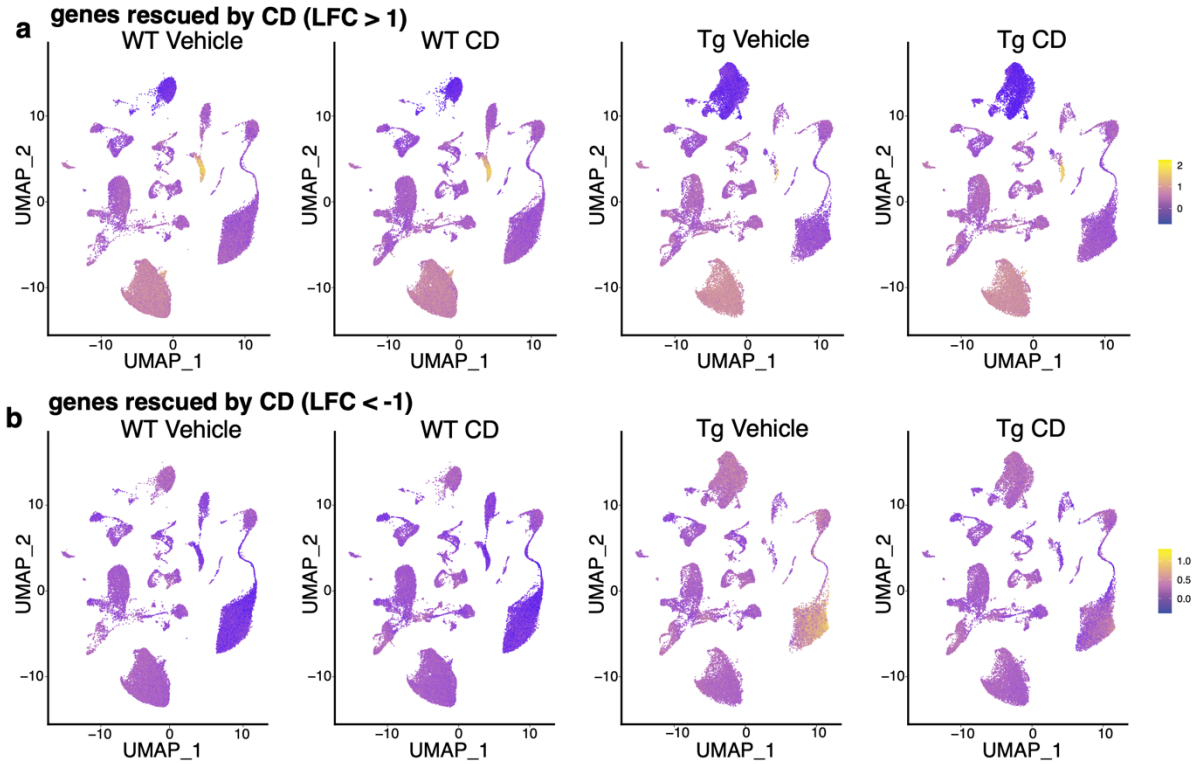

Figure 27: AddModulScore FeaturePlots to show average expression of all genes with |LFC|>1 reveal neuroblast and oligodendrocyte clusters are highly modulated by CD administration. a) UMAPs of upregulated (LFC > 1) genes by CD treatment highlight neuroblasts. b) UMAPs of downregulated (LFC < -1) genes by CD treatment highlight enrichment in oligodendrocytes.

Subsequent to the pseudobulk analysis, Principal Component Analysis (PCA) was conducted on the top 500 DEGs for each cluster. Figure 28 illustrates the PCA outcomes for all clusters, with each data point representing an individual sequenced animal. It was observed that poly(GA) expression impacts nearly all cell clusters apart from some dopaminergic neuron clusters. CD administration also influenced numerous clusters, yet the majority of neuronal clusters remained largely unaffected. Upon examining the variance explained by each principal component, it becomes clear that CD administration predominantly impacts oligodendrocytes and neuroblasts. The impact of CD treatment, as observed in principal component analysis (PCA), is interpreted as more substantial when the cells from a given transgenic animal (all cells in a given cluster for each animal are represented by a single dot in the PCA plot) treated with CD shift further away from those in transgenic animals treated with vehicle and move closer towards the wildtype animals. This spatial displacement in the PCA plots underscores the modulatory effect of CD on these specific cell types, aligning treated transgenic animals more closely with the wildtype phenotype in oligodendrocyte and neuroblast clusters, as this shift covers the highest amount of variance explained by the PCA. Notably, two out of the four animals subjected to CD therapy exhibited a more pronounced treatment effect on neuroblasts and mature oligodendrocytes at P40, as depicted in Figure 28. This observation of a 50% treatment success rate is consistent with the survival study findings, which demonstrated that approximately 50% of the female transgenic mice treated with CD experienced improved survival rates.

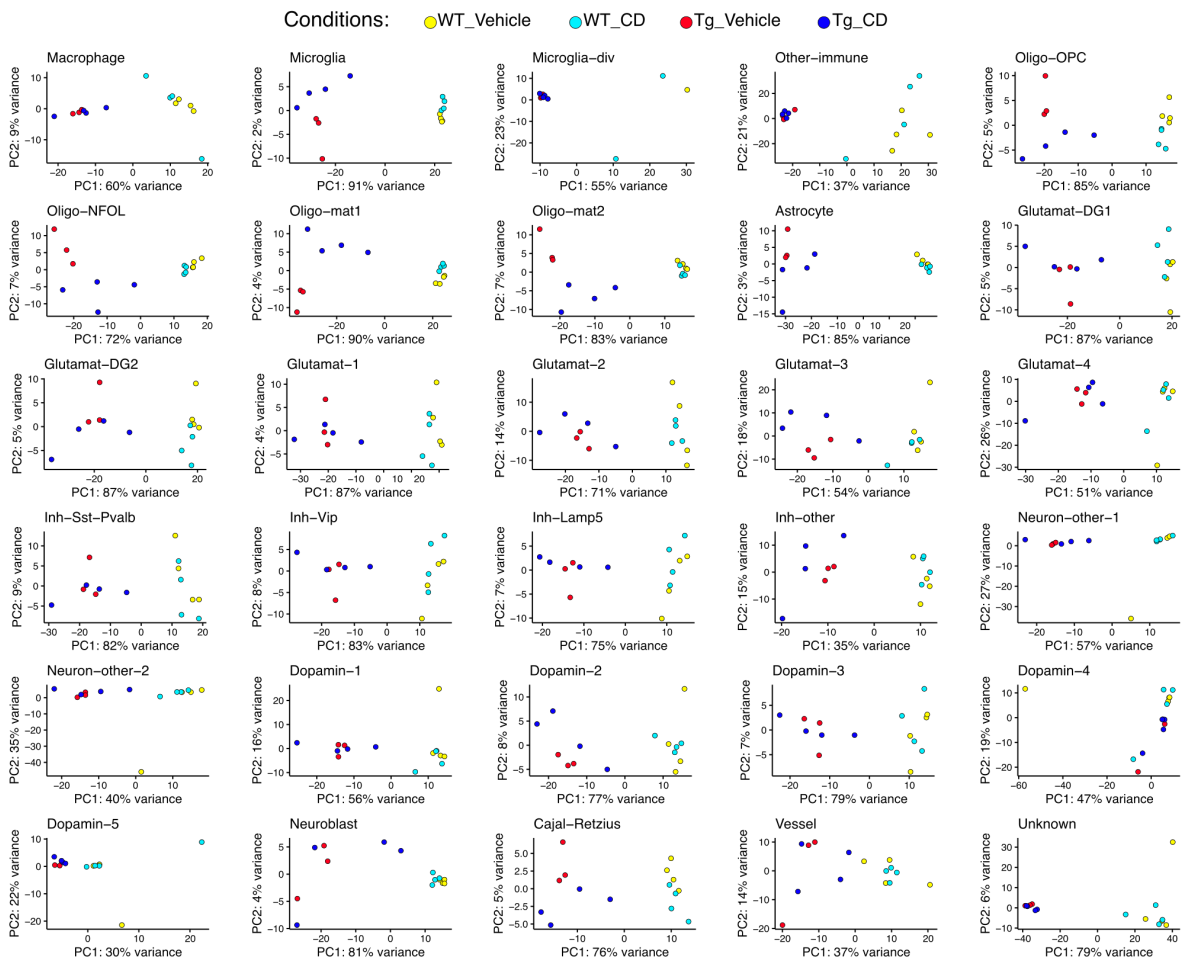

Figure 28: PCA plots of the top 500 DEGs for every cluster highlight mature oligodendrocytes and neuroblasts as targets of CD therapy.

In summary, the analysis of PCA plots and AddModuleScore FeaturePlot UMAPs collectively indicates that oligodendrocytes and neuroblasts are significant targets of CD therapy in the GA-Nes mouse model at P40. The decision to prioritize oligodendrocytes over neuroblasts for further investigation stems from their greater relevance in the context of ALS patients. Given that neurogenesis diminishes and holds less biological significance in aged individuals (Kempermann, 2015), oligodendrocytes present a more pertinent therapeutic target.

4.3.2.1.3 Disease-Associated Oligodendrocytes (DAO) Are Rescued by CD

Consequently, the two mature oligodendrocyte clusters were analyzed in detail to assess the significance and function of DEGs resulting from transgene expression and CD administration. Recent research has identified a specific oligodendrocyte state linked to neurodegenerative diseases, known as disease-associated oligodendrocyte

(DAO or DOL) (Kenigsbuch et al., 2022; Pandey et al., 2022). While the involvement of oligodendrocytes in ALS has been less extensively explored, abnormalities in these cells have been noted in the disease (Gong et al., 2022; Valori & Neumann, 2021). Notably, genes such as Serpina3n, C4b, and Il33 are associated with a common disease signature across oligodendrocytes in Alzheimer's disease and Multiple Sclerosis (Kenigsbuch et al., 2022). Among these, Serpina3n is highlighted as a primary marker of DAOs, based on studies conducted across various mouse models (Kenigsbuch et al., 2022; Pandey et al., 2022).

Our oligodendrocyte clusters were found to express key DAO markers, notably including the Serpina3n, Il33, and C4b. Importantly, there is a partial but significant rescue effect due to CD administration. Figure 29a displays a heatmap of genes identified as DAO markers in Kenigsbuch et al., with the left panel illustrating the transgene effect and the right panel depicting the CD administration's rescue effect. Additionally, Figure 29b presents volcano plots for our mature oligodendrocyte clusters along with the CD rescue effect. Beyond the recognized markers such as Serpina3n, C4b, and Il33, our oligodendrocyte gene signature also encompasses upregulation of Kcnma1, Rhoj, Fmn1, and Apod, which are similarly reverted by CD administration.

Figure 29c features a Seurat FeaturePlot of Serpina3n expression across the four experimental conditions. Serpina3n, predominantly expressed by oligodendrocytes, is virtually absent in wildtype conditions but upregulated in the Tg_Vehicle condition and notably reduced in the Tg_CD condition. Figures 29b and 29c corroborate that the DAO population primarily resides within the Oligo_mat1 cluster, although the Oligo_mat2 cluster also exhibits some DAO gene expression, albeit to a lesser degree. Consequently, it is demonstrated that a subset of GA-Nes oligodendrocytes transitions to a disease-associated state, which can be ameliorated through CD administration.

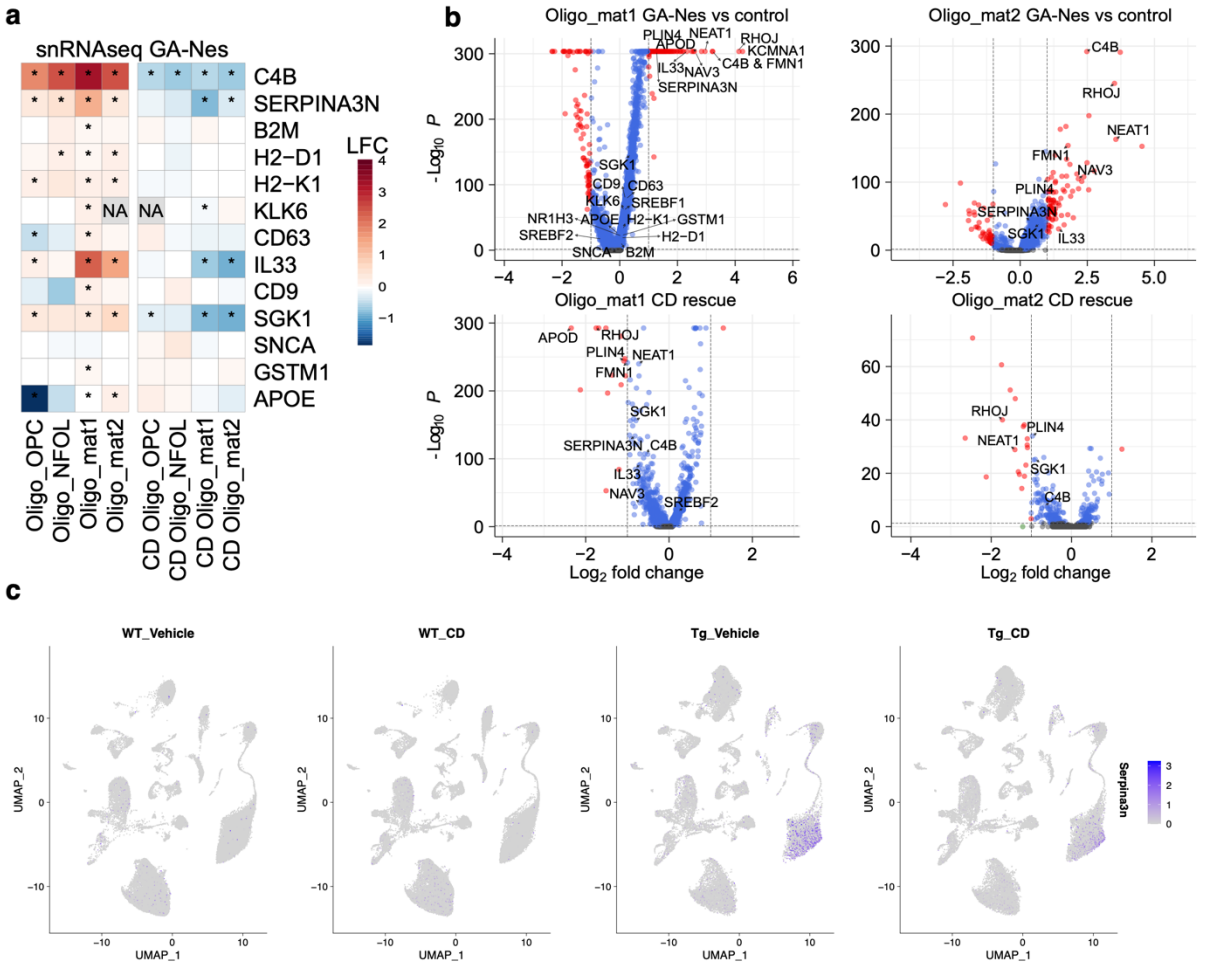

Figure 29: Disease-associated oligodendrocyte phenotype in GA-Nes mice is rescued by CD injection. a) Heatmap of previously published (Kenigsbuch et al., 2022) DOA genes in transgenic mice compared to wild type mice injected with vehicle (left pane) and transgenic mice injected with CD compared to those injected with vehicle (right pane) shows significant rescue of some DAO genes. Stars indicate a statistically significant modulation. b) Volcano plots of Oligo_mat1 and Oligo_mat2 clusters show upregulated DAO markers (known genes as well as candidate genes for ALS-DAO) due to transgene expression and their rescue by CD. c) FeaturePlot of Serpina3n highlights its expression in transgenic mice and its partial rescue by CD administration.

4.3.2.1.4 CellChat Analysis Highlights Myelination

To understand the signaling changes due to transgene expression as well as CD therapy better, I performed cell-cell communication analysis using CellChat version 1.6.1 (Jin et al., 2021), leveraging single-nuclei expression data. The initial focus was on assessing information flow across all clusters under two distinct conditions. “Information flow” quantifies the intensity or volume of signaling transpiring through specific pathways or interactions. Figure 30a illustrates both the relative and absolute information flow comparisons between transgenic and wildtype conditions, whereas Figure 30b contrasts the information flow in transgenic mice treated with

vehicle versus CD. Pathways annotated in black font signify the absence of statistically significant changes.

Considering all clusters, the analysis revealed numerous signaling alterations between transgenic and wildtype comparisons. Notable significant information flow increases were observed in pathways such as CLDN, VISFATIN, COLLAGEN, SEMA4, MPZ, AGRN, and GRN within the transgenic condition, alongside a downregulation in the ACTIVIN pathway. Conversely, the most pronounced changes in pathways among transgenic mice due to CD treatment involved the downregulation of APP and CLDN pathways.

To further elucidate the effect of treatment on oligodendrocyte clusters, previously identified as therapeutic targets, a detailed analysis of incoming and outgoing signals within each cluster for Tg_Vehicle and Tg_CD conditions was performed. This analysis, presented in Figure 31, encompasses all four oligodendrocyte-related clusters. Across the oligodendrocyte clusters, the LAMININ pathway emerges as specifically and significantly modulated in the Tg_CD condition compared to Tg_Vehicle. Additionally, the impact of poly(GA) expression on this pathway, as demonstrated in Figure 30, suggests a potential rescue effect in the Tg_CD condition, underscoring the therapeutic significance of CD treatment on oligodendrocyte signaling dynamic.

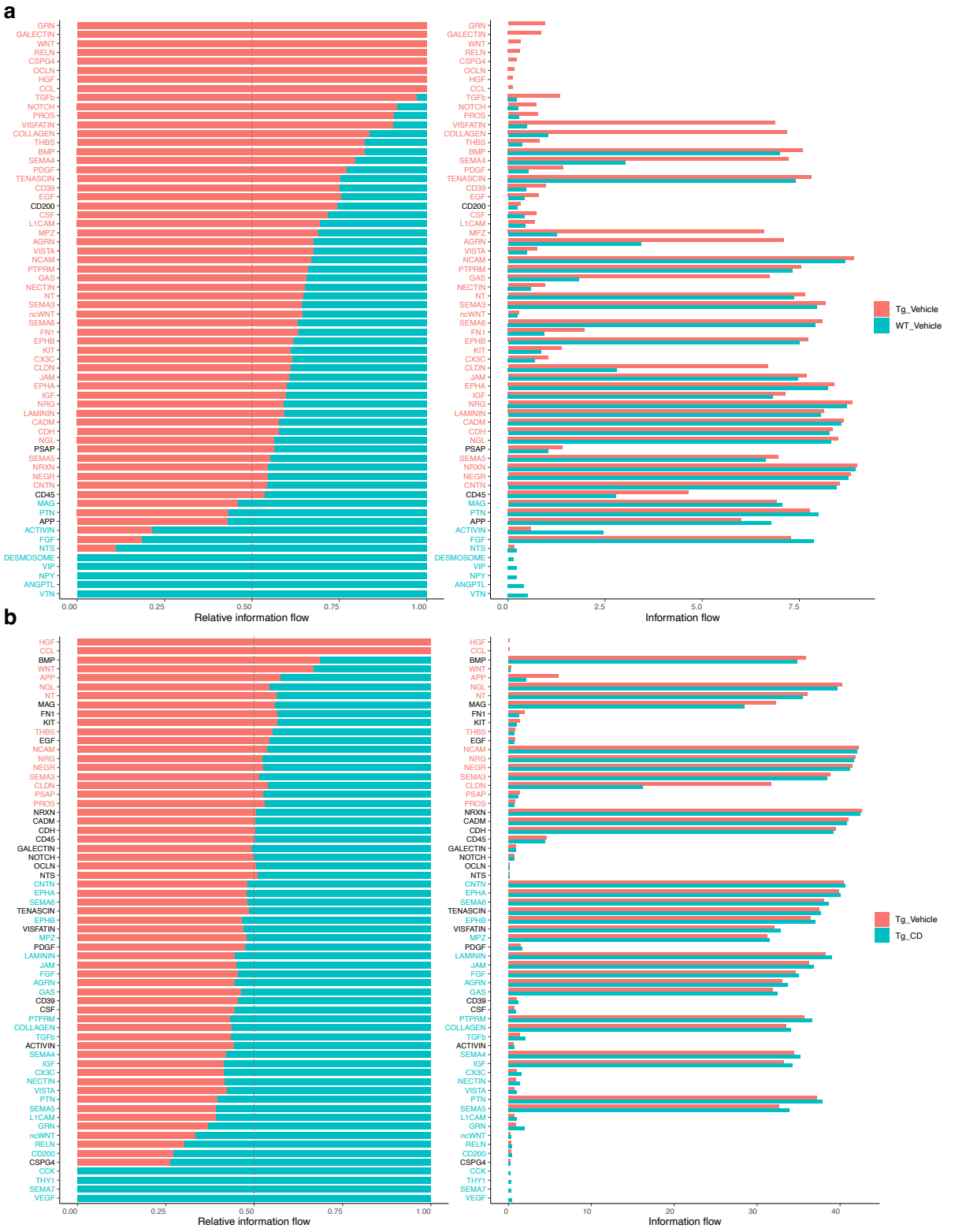

Figure 30: Information flow from CellChat analysis on all cell types show various significant changes. Detected pathways that are not significant are in black font. a) Transgene expression mainly affects CLDN, VISFATIN, COLLAGEN, SEMA4, MPZ, AGRN, GAS, GRN, and ACTIVIN pathways. b) CD therapy mainly affects APP and CLDN pathways.

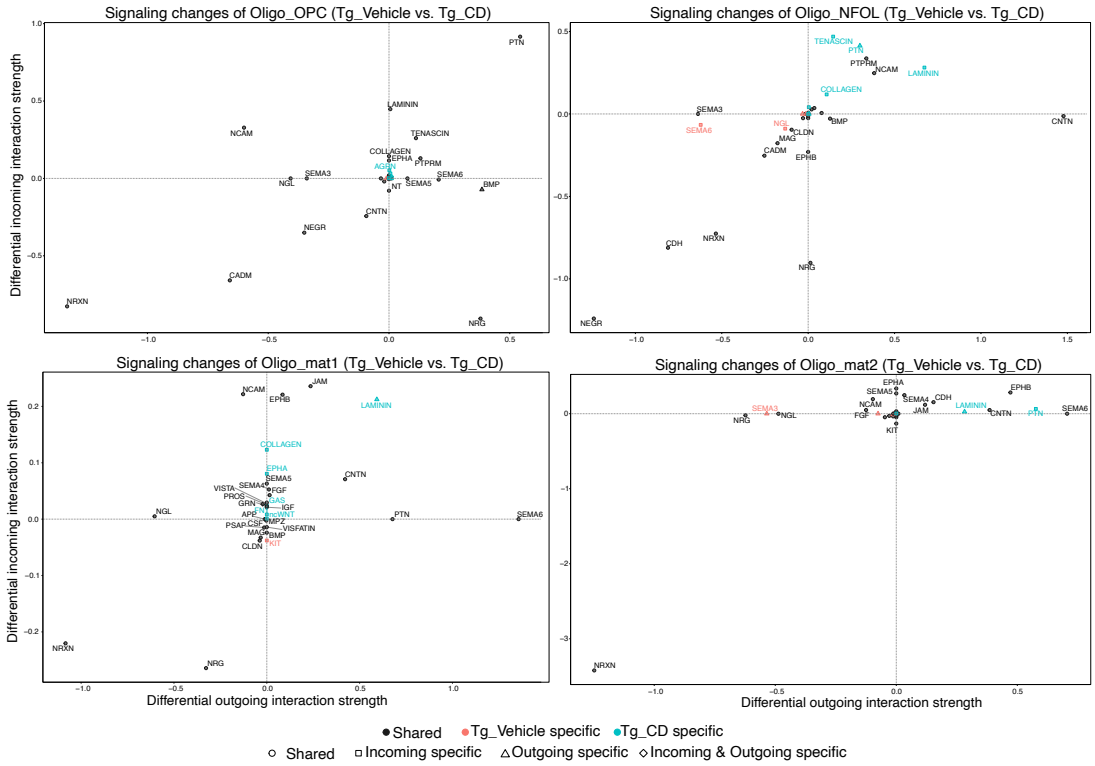

Figure 31: Differential incoming and outgoing interaction strength of all four oligodendrocyte clusters highlights the LAMININ pathway in the context of CD therapy.

To more effectively illustrate the modulations within the LAMININ pathway, circle plots depicting this pathway's interactions in the two transgenic conditions were created using CellChat, as displayed in Figure 32a. In this visualization, the Tg_CD condition reveals a denser network of connections compared to the Tg_Vehicle condition. To delve deeper into the intricacies of these connections, heatmaps of the LAMININ pathway for both Tg_Vehicle and Tg_CD conditions are presented in Figure 32b and 32c, respectively. The heatmaps elucidate the involvement of the LAMININ pathway in mature oligodendrocytes, as the pathways seems obliterated in Tg_Vehicle condition and restored in Tg_CD condition. Although the communication probability within the LAMININ pathway is low in wildtype conditions, where oligodendrocytes are somewhat involved (data not shown, but bearing resemblance to the Tg_CD condition), it suggests that CD administration effectively restores LAMININ signaling in oligodendrocytes.

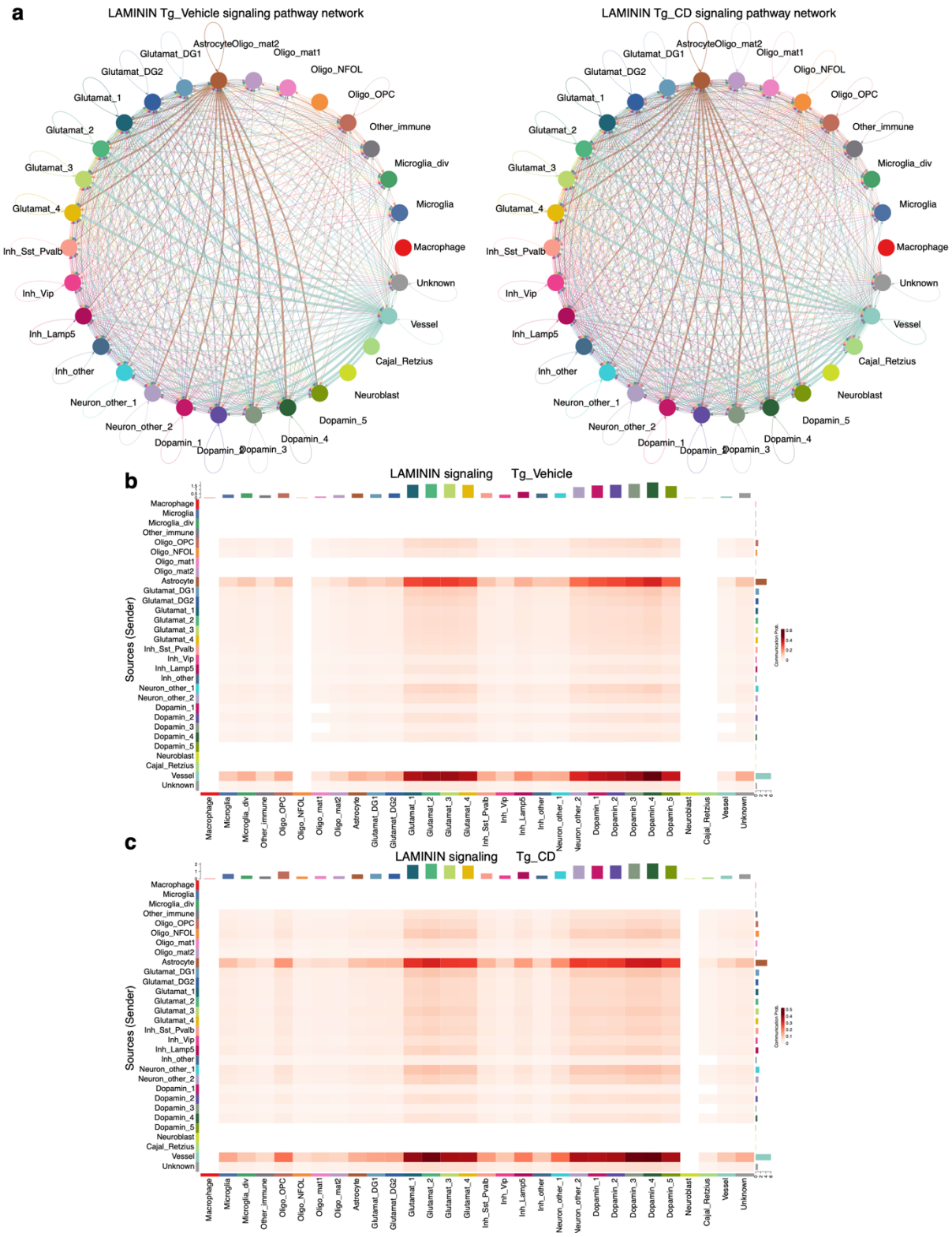

Figure 32: CD therapy restores the LAMININ signaling pathway in mature oligodendrocytes. a) Circle plot of the LAMININ signaling pathway indicates that in the Tg_CD condition, autocrine laminin is restored in the oligodendrocyte clusters, while the entire network is slightly denser compared to the Tg_Vehicle condition. b,c) Heatmap of LAMININ signaling indicates the restoration of signaling that originates from mature oligodendrocyte clusters that are completely absent in Tg_Vehicle condition.

To investigate the LAMININ signaling pathway in more detail, we examined the ligand-receptors pairs of laminins and integrins (Figure 33). Intriguingly, Lama2, a gene encoding for Laminin α2, shows significant downregulation as a result of poly(GA) expression, as depicted in the left panel of the figure. This downregulation is notably counteracted by a relative upregulation following CD administration, highlighted in the right panel. Similarly, Itgb4, the gene coding for Integrin β4 which binds to Laminin α2 (Rambukkana et al., 1997), is downregulated upon poly(GA) expression, with subsequent rescue observed following CD treatment.

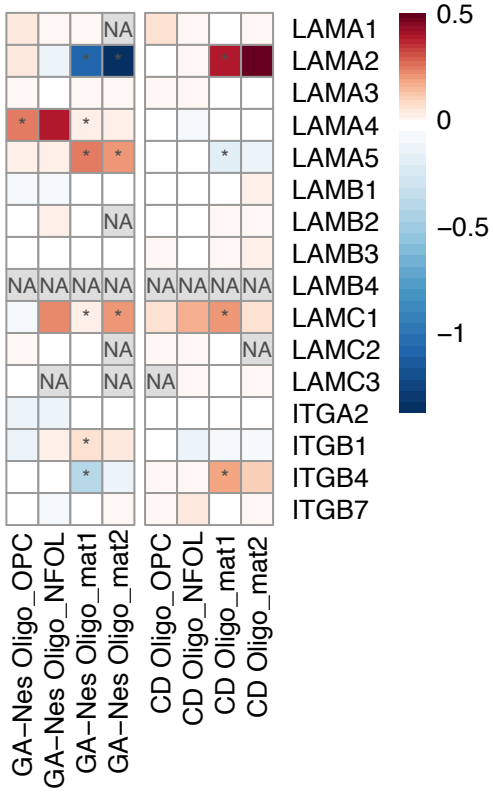

Figure 33: CD administration restores Lama2 expression, which is downregulated in vehicle-treated transgenic mice. Integrin β4, which binds to Laminin α2, is also rescued. NA values indicate no detectable expression of the gene, while stars indicate a significant modulation.

4.3.2.2 snRNAseq Validation and Further Interpretation

While snRNAseq yields insightful data, it is crucial to validate these findings to mitigate the risk of reporting inaccurate information. Validation can be conducted

through qPCR or bulk RNAseq for RNA-level confirmation, or through immunostaining, western blotting, or other immunoassays for protein-level validation. In this dissertation, I validated snRNAseq results at the protein level to remain closer to cellular processes and mechanisms.

4.3.2.2.1 Astrocytes are Not Reduced in Transgenic Mice

snRNAseq analysis revealed an upregulation of astrocytes in the WT_CD condition. Figure 34 clarifies that there is no actual upregulation of astrocytes in the WT_CD condition, challenging the snRNAseq result, indicating a probable sampling bias. Consequently, there is no reduction of astrocytes in transgenic conditions.

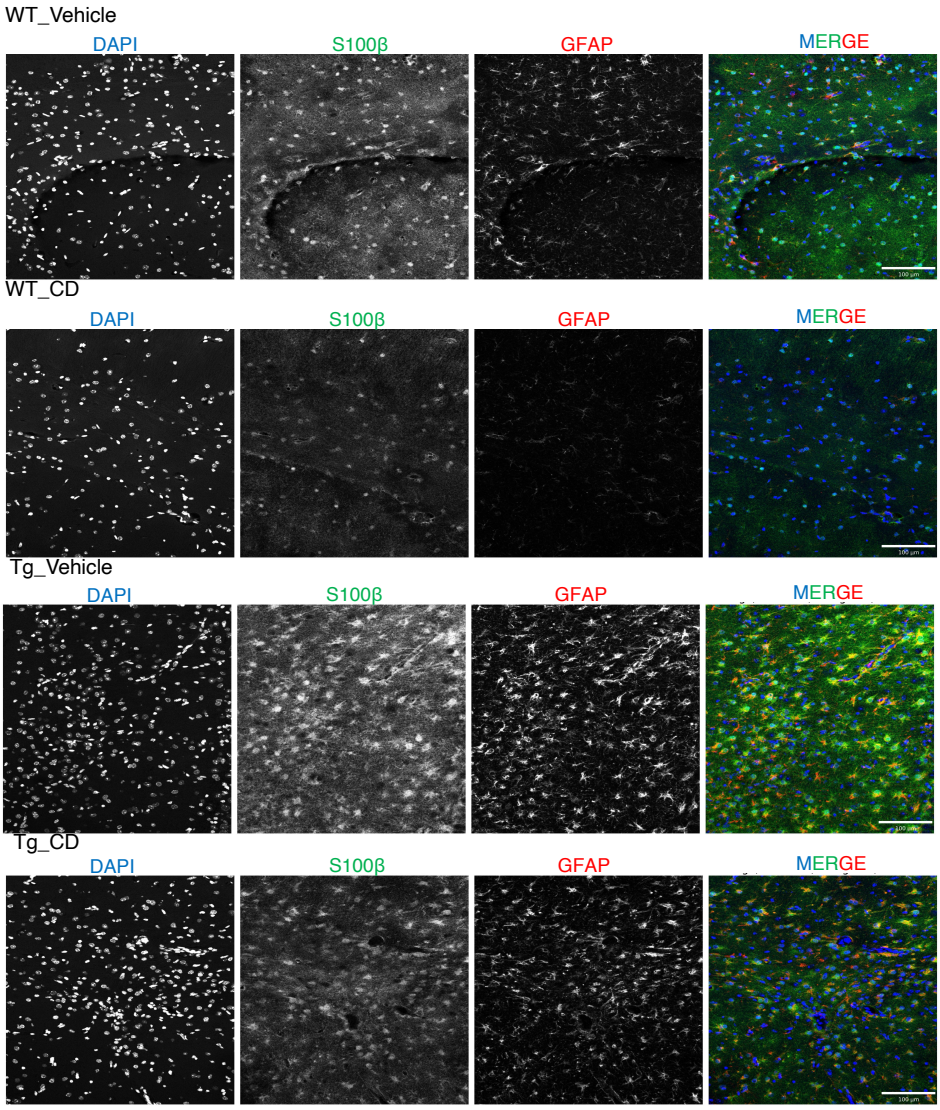

Figure 34: Astrocyte markers S100β and GFAP do not confirm the upregulation of astrocytes seen in the snRNAseq data in WT_CD condition. Scale bars = 100 μm.

In transgenic mice, there is a strong proliferation of microglia (LaClair et al., 2020), which is accurately reflected in our sequencing data (Figure 24a). Given this proliferation and the methodological approach of sorting 5000 NeuN- nuclei, it is plausible that counts of other cell types, including oligodendrocytes, appear relatively depleted. This apparent depletion could be attributed to the expansion of the microglial population rather than a true decrease in other glial nuclei. Consequently, this study focuses on differentially expressed genes (DEGs), which offer a more precise understanding of the genetic landscape underpinning these observations.

4.3.2.2.2 DAO Markers Are Validated by Staining, WB, and ELISA

As previously mentioned, Serpina3n in mice and its human counterpart SERPINA3 (coding for AACT) are crucial markers of DAOs (Kenigsbuch et al., 2022). The expression of Serpina3n and its rescue by CD in our transgenic mouse model was validated using immunofluorescence and immunoblotting techniques, as depicted in Figure 35.

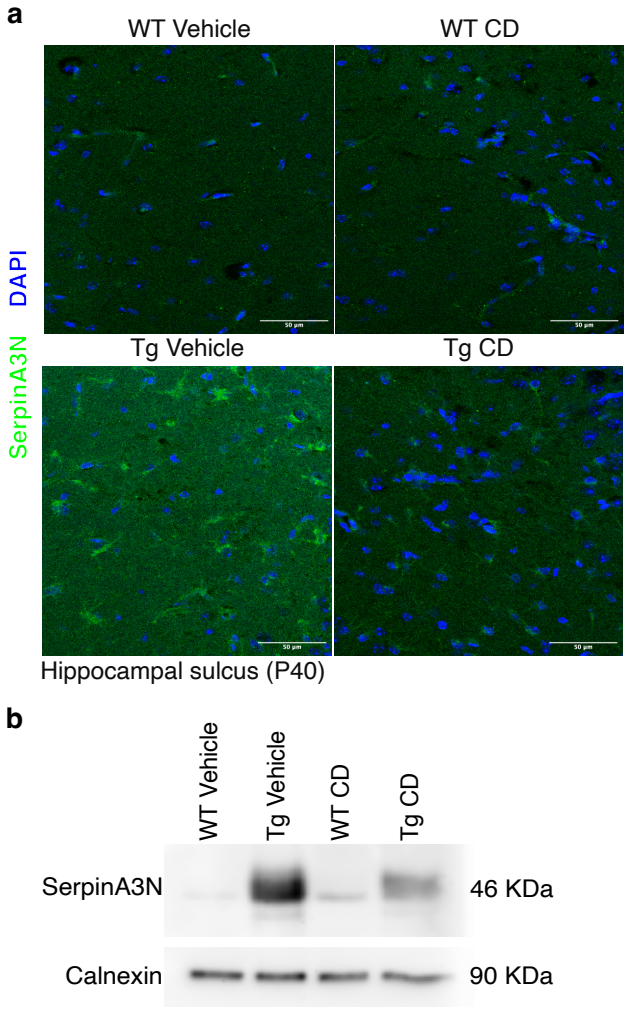

Figure 35: Serpina3n overexpression and its rescue are validated. a) Serpin A3N immunofluorescence from fixed-frozen tissue demonstrates that increased expression of this key DAO marker in transgenic GA-Nes mice is curtailed by CD treatment, confirming the snRNAseq results. Scale bars = 50 μm. b) Western blot of pooled hindbrains (n: WT_vehicle=4, Tg_Vehicle=3, WT_CD=4, Tg_CD=4) confirms the reduction of Serpin A3N expression upon CD treatment.

An MSD immunoassay was used to measure IL33 levels in hindbrain lysates, alongside the examination of other potential immune modulations. Figures 36 and 37 demonstrate MSD's commercial cytokine panel and proinflammatory panel, respectively.

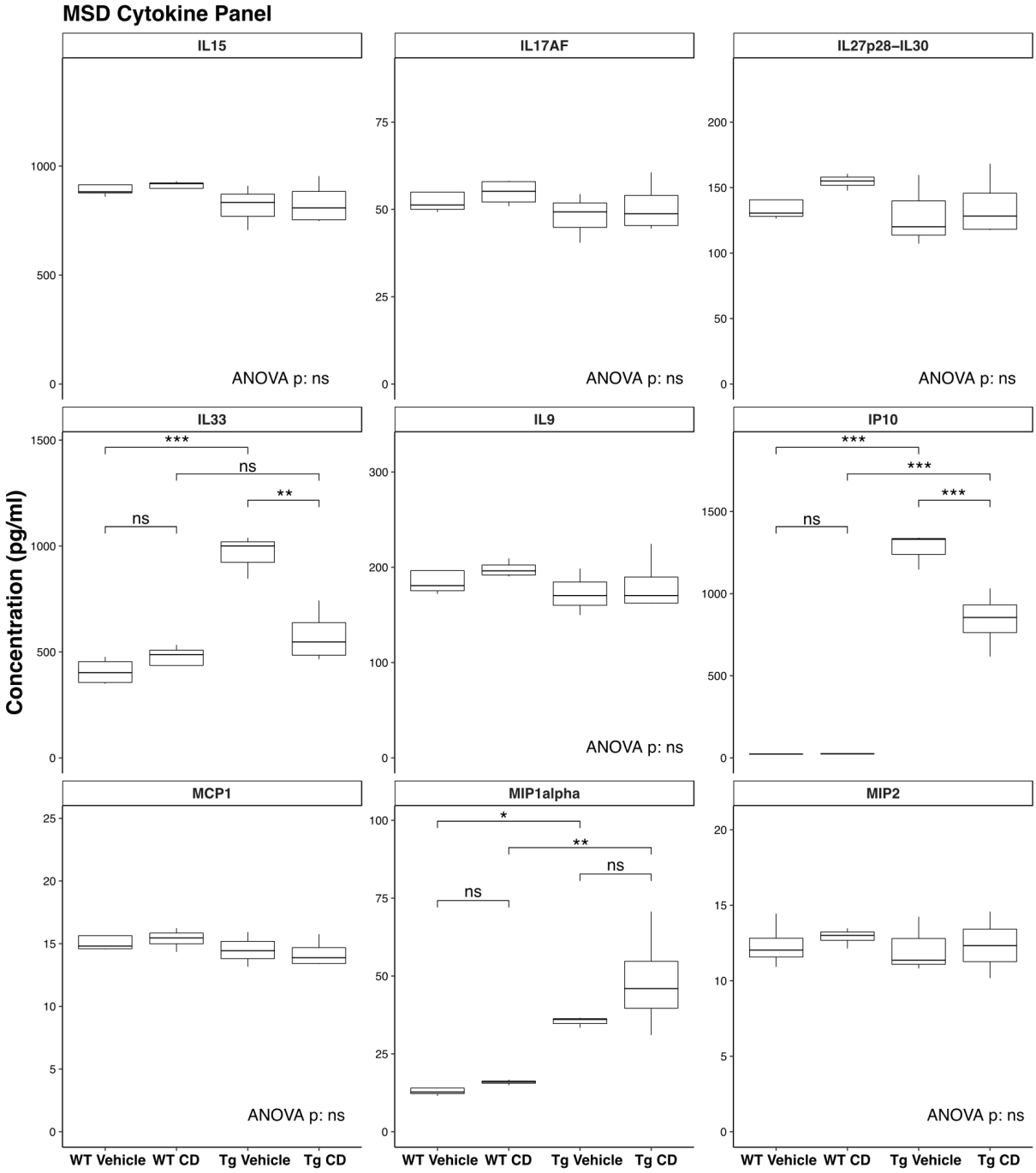

Figure 36: MSD Cytokine Panel from hindbrain samples confirms full IL33 rescue back to wildtype levels. Moreover, IP10 is also partially rescued by CD. p-values are obtained from Tukey's HSD post-hoc (n: WT_vehicle=4, Tg_Vehicle=3, WT_CD=4, Tg_CD=4).

These analyses confirmed the significant upregulation of IL33 in transgenic conditions and its comprehensive rescue by CD administration. IL33 levels seem to be fully rescued by CD treatment. Moreover, interferon-induced IP10/CXCL10 shows a significant rescue effect with CD. The lack of change or rescue in other cytokines underscores that CD therapy predominantly impacts oligodendrocytes, with lesser effects on immune cells.

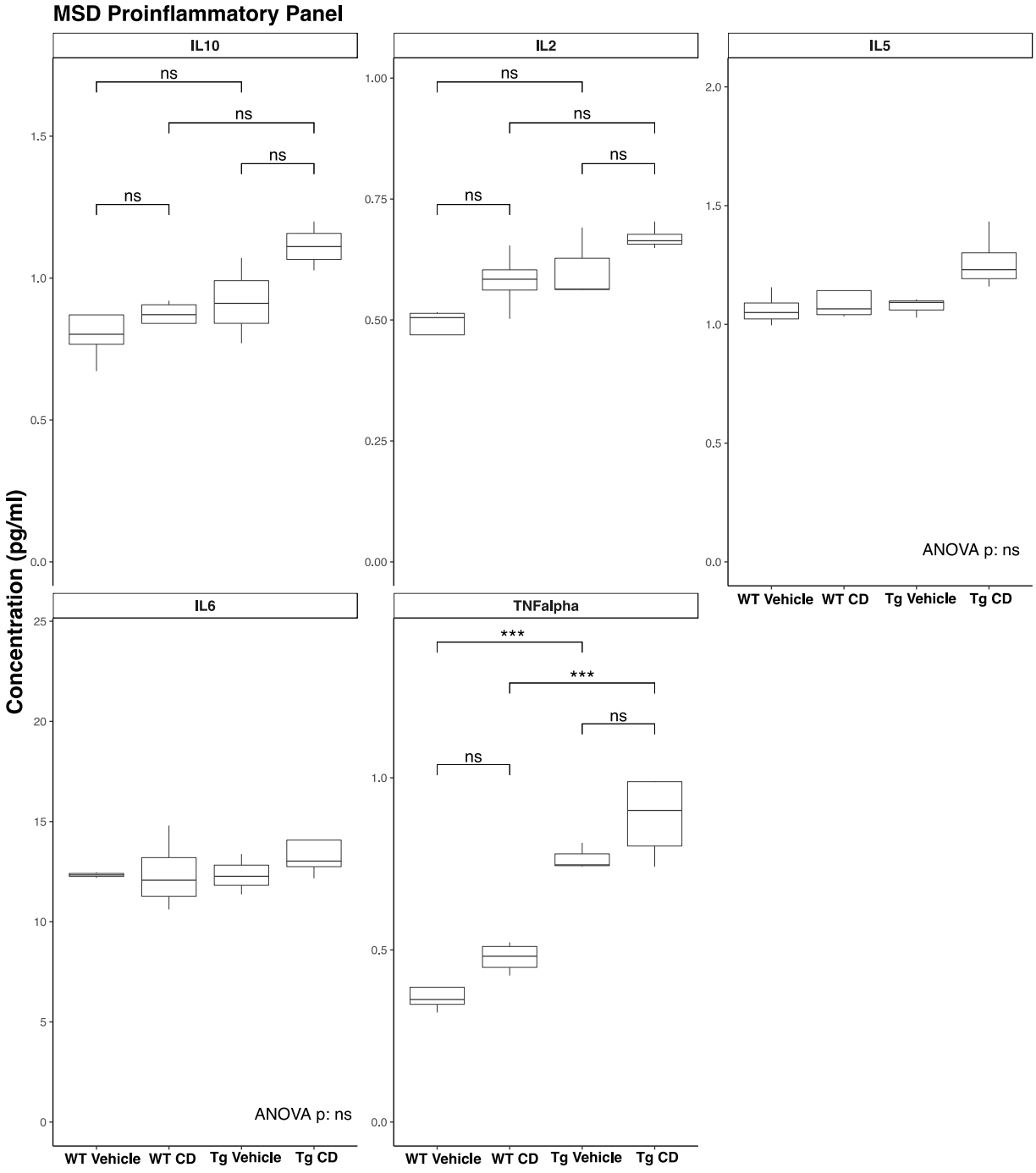

Figure 37: The detected species of the MSD Proinflammatory Panel from hindbrain samples do not show any rescue effect. The highest modulated protein is TNFalpha, for which no rescue is observed. p-values are obtained from Tukey's HSD post-hoc (n: WT_vehicle=4, Tg_Vehicle=3, WT_CD=4, Tg_CD=4).

In summary, the induction of DAOs in poly-GA mice and their rescue following CD administration have been conclusively confirmed at the protein level through three distinct methodologies. Consequently, the findings related to DAOs from snRNAseq analyses are now robustly validated.

4.3.2.2.3 Cholesterol Dysmetabolism Is Rescued by CD

Given the established role of CD in sequestering cholesterol (Walenbergh et al., 2015), cholesterol metabolism was examined in bulk RNAseq data from previous research on GA-Nes (LaClair et al., 2020), GA-CFP (Schludi et al., 2017), and rNLS8 (Riemenschneider et al., 2023) mouse models, alongside TargetALS data on ALS patients as accessed on February 2020 (TargetALS-Postmortem-Tissue-Core, 2020). The heatmap in Figure 38a reveals a consistent downregulation of cholesterol biosynthesis genes across all three mouse models and in spinal cord tissues from ALS patients. Conversely, key cholesterol export genes, Abca1 and Abcg1, are markedly upregulated, along with storage genes, notably Plin2 and Plin4. This pattern indicates a potential cholesterol overload in ALS, prompting cellular responses to mitigate this by decreasing synthesis and enhancing export and storage mechanisms. The categorization of genes into respective pathways was informed by the KEGG database (Kanehisa, 2019; Kanehisa et al., 2023; Kanehisa & Goto, 2000).

To further elucidate the impact of CD administration on cholesterol dysmetabolism, analysis was extended to the current snRNAseq data from GA-Nes mouse hippocampi, focusing on the same gene set across all cell types (illustrated in Figure 38b) and specifically within the two mature oligodendrocyte clusters (shown in Figure 38c). This analysis revealed a consistent pattern of decreased cholesterol biosynthesis alongside enhanced export and storage in response to transgene expression, suggesting a cholesterol overload scenario. Notably, CD administration appeared to mitigate these effects, with the most pronounced rescue observed for Apod, a lipid transport protein, and Plin4, a protein associated with lipid storage and considered a marker for lipid droplets (Itabe et al., 2017; Wolins et al., 2003). Plin4 emerged as a particularly compelling candidate for further investigation due to its consistent response across all examined mouse models (marked by a significant log-fold change in GA-Nes) and in the spinal cord tissues of ALS patients, coupled with a notable rescue effect following CD treatment.

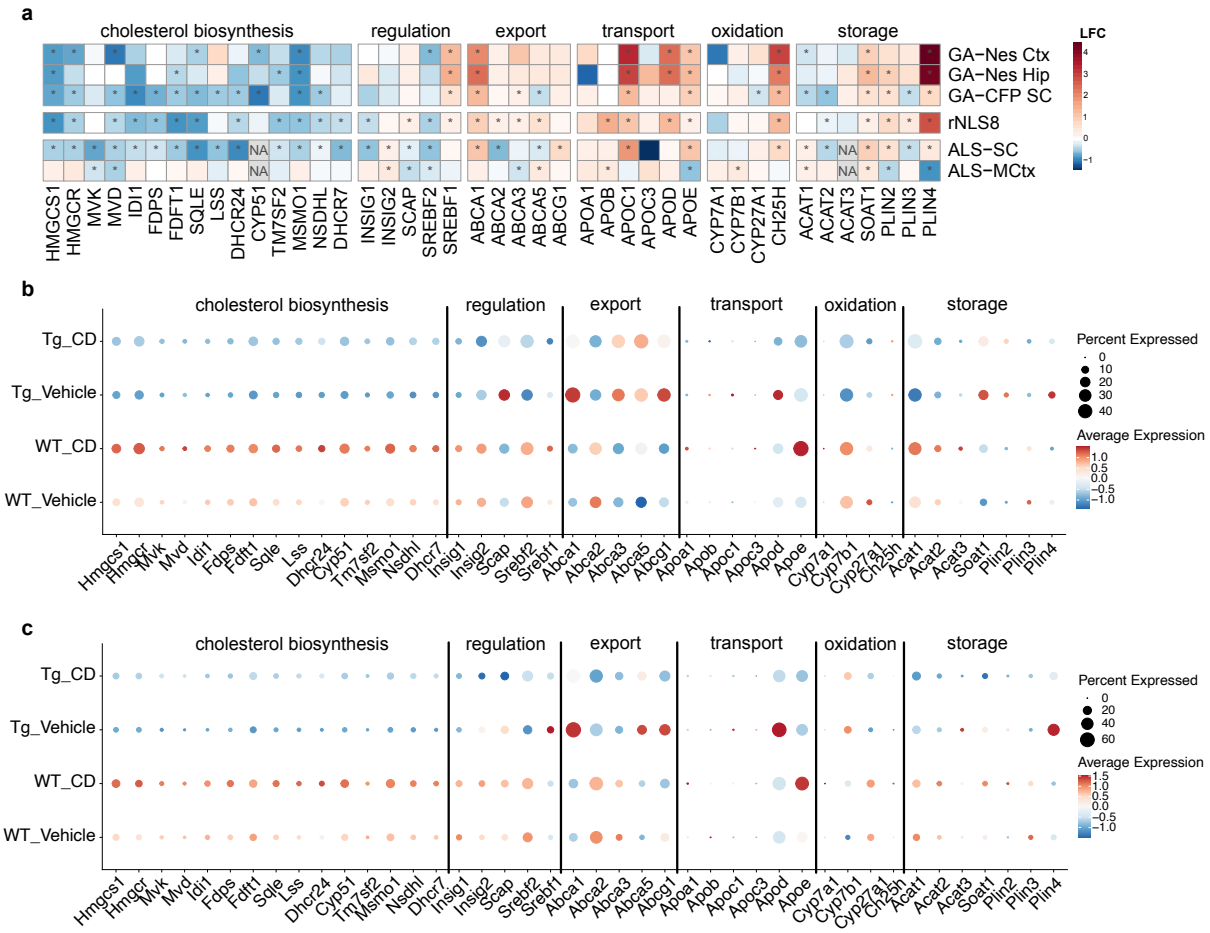

Figure 38: Cholesterol metabolism in ALS is disturbed. a) Heatmap of cholesterol metabolism genes taken from bulk RNAseq data in mouse models and patients indicates downregulation of cholesterol biosynthesis and upregulation of export and storage. b,c) DotPlot of all cell types (b) and mature oligodendrocyte clusters (c), confirm the downregulation of cholesterol biosynthesis and upregulation of export and storage in our dataset.

Given the observed cholesterol dysmetabolism in GANes mice, as evidenced by gene expression data in Figure 38, further investigation focused on the lipid droplet marker PLIN4, a protein whose expression in the brain remains largely understudied due to its minimal presence in wildtype conditions (Itabe et al., 2017). In ALS models, particularly in GA-Nes mice, significant overexpression of PLIN4 is observed, suggesting its upregulation as a disease-related phenomenon. Oligodendrocytes were identified as the primary cell type responsible for increased production of PLIN4, as illustrated in Figure 39. This figure provides confirmation of PLIN4's upregulation and its partial rescue following CD administration at the single-nucleus level. Figures 39c-d show confirmation of expression of PLIN4 in oligodendrocytes and no other glia by immunostaining, highlighting the specificity of this marker's expression within these cells.

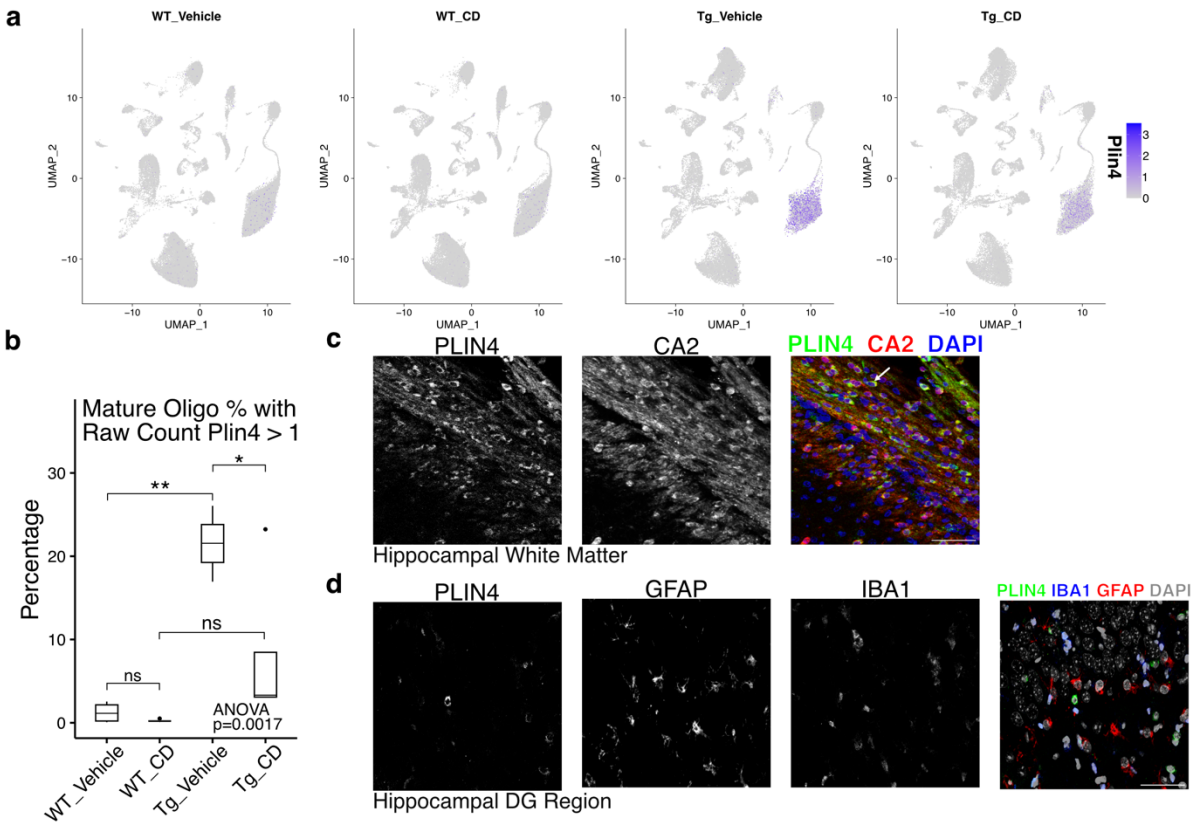

Figure 39: Plin4 production is upregulated in oligodendrocytes of GA-Nes mic e, and rescued by CD treatment. a) FeaturePlot of PLIN4 shows upregulation of its expression in transgenic mice and rescue by CD treatment. b) The percentage of mature oligodendrocytes with more than one read of PLIN4 (raw count) is dramatically increased with the expression of the GA transgene and partially rescued by CD treatment. c,d) PLIN4 colocalizes with CA2+ oligodendrocytes but not Iba1+ microglia or GFAP+ astrocytes. Images are adjusted for brightness and contrast for better visibility. Scale bars = 50 μm.

To further validate the snRNAseq findings regarding PLIN4 expression across different conditions in GA-Nes mice, immunostaining techniques were employed. The results showed minimal PLIN4 staining under wildtype conditions, with only background signal levels detected. As depicted in Figure 40a, oligodendrocytes in transgenic mice express PLIN4, however, this expression is notably lower in Tg_CD condition compared to Tg_Vehicle condition. Quantitative analysis of PLIN4-positive oligodendrocytes is presented in Figure 40b.

To corroborate the upregulation of PLIN4 as a marker of disease, spinal cord sections from ALS patients were immunostained. This staining revealed increased PLIN4 expression across various anatomical areas of the spinal cord in disease conditions, with the most significant differences observed in the anterior white matter, shown in Figure 40c. Notably, PLIN4 expression was detected in non-C9ORF72 ALS patients, suggesting potential relevance to sALS. However, it was not possible to

reliably colocalize the PLIN4 signal with CNP⁺ oligodendrocytes or GFAP⁺ astrocytes in patients, indicating the need for further investigation to fully understand PLIN4's cellular distribution and its implications in ALS pathology. Better marker antibodies and optimized staining methods are needed to clarify this in the future.

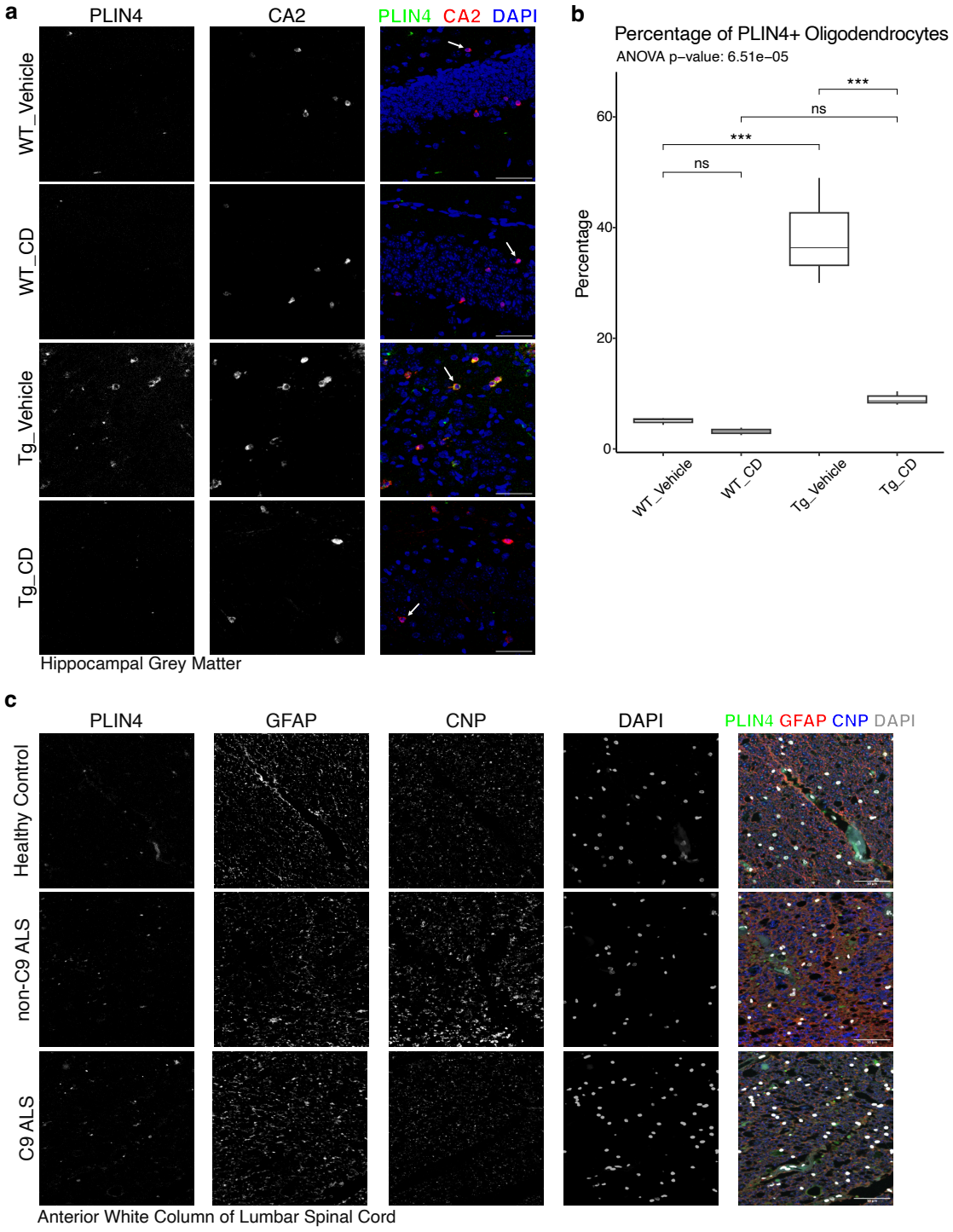

Figure 40: PLIN4 upregulation in patients and mice as well as its rescue in CD-treated animals is validated. a) PLIN4 (green) immunofluorescence costained with DAPI and CA2 (red) confirm the transgenic upregulation and CD-mediated rescue that was observed in snRNAseq analysis. Red arrows

indicate CA2+ oligodendrocytes. images are enhanced for viewing, but unmodified for quantification; Scale bars = 50 μm. b) Quantification of the percentage of PLIN4+ oligodendrocytes (CA2+) from immunostaining highlights a dramatic increase of PLIN4+ oligodendrocytes with the expression of the transgene (~30-40% of all CA2+ oligodendrocytes), and a dramatic rescue by CD treatment (~5% of all CA2+ oligodendrocytes). c) PLIN4 immunofluorescence shows an upregulation of PLIN4 in the anterior white matter of the lumbar spinal cord in C9 ALS and non-C9 ALS patients compared to healthy controls. Images are adjusted for brightness and contrast for better viewing. Scale bars = 50 μm.

4.3.2.2.4 Electron Microscopy Showcases Disturbances in Myelination

In light of the observed upregulation of PLIN4, the investigation sought to directly identify lipid droplets. However, Oil Red O staining did not reveal any lipid droplets in P40 mice, as evidenced in Figure 41. This led to the hypothesis that the droplets might be too small for detection by Oil Red O staining. Consequently, electron microscopy was chosen for subsequent analysis, with its results to be detailed in the following section. This approach was also motivated by the suspicion that cholesterol dysmetabolism could stem from disturbances in myelination, as myelin is cholesterol-rich (Saher et al., 2005). Thus, electron microscopy was selected to provide insights into both lipid droplets and potential myelin disturbances.

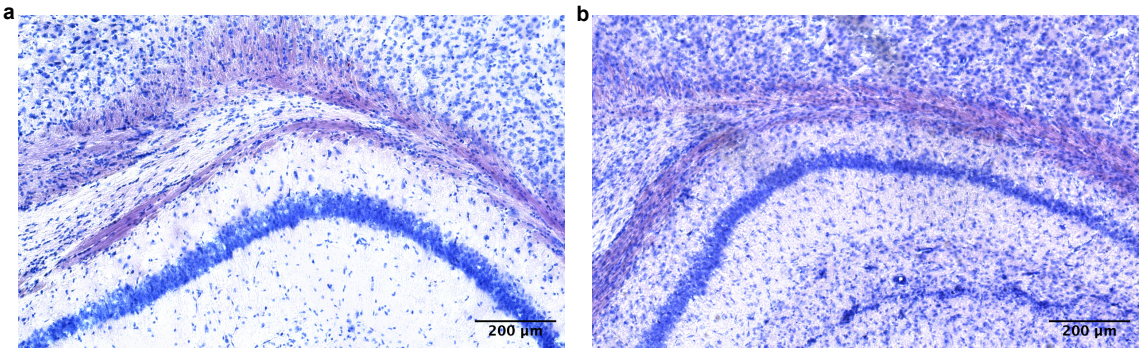

Figure 41: Oil Red O staining of neutral lipids does not show obvious lipid droplets in wildtype (a, left image) or transgenic (b, right image) conditions. Counterstain: Hematoxylin QS; scale bars = 200 μm.

To investigate the presence of lipid droplets, electron microscopy was conducted on P40 transgenic and wildtype mice without treatment. Contrary to expectations, scanning electron microscopy did not provide clear evidence of increased lipid droplets. Amorphous electron-dense materials were observed, potentially indicative of poly(GA) expression or small lipid droplets, although these findings were inconclusive (data not shown). The absence of definitive proof of lipid droplets in our mouse model prompted a deeper analysis of the snRNAseq results to elucidate the CD rescue effect further.

Gene ontology (GO) analysis was carried out on genes from each cluster with a log fold change (LFC) greater than 0.5 or less than -0.5, excluding GO terms represented by fewer than four genes. Notably, myelination emerged as a significant GO hit, particularly within the Oligo_mat1 cluster, as illustrated in Figure 42a. A heatmap depicting the expression of myelin components in oligodendrocytes (Figure 42b) highlighted the downregulation of myelin genes due to poly(GA) expression, with CD administration facilitating their rescue.

Additionally, examination of the corpus callosum revealed substantial white matter shrinkage and a reduced number of myelinated axons in transgenic animals, as shown in Figure 42c-d. Luxol Fast Blue (LFB) staining confirmed the reduction in white matter adjacent to the CA2 region of the hippocampus, with the effect being statistically significant, albeit less pronounced than seen with scanning electron microscopy (Figure 42e-f). Further disturbances in myelination were documented with scanning electron microscopy, as depicted in Figure 42g. Qualitative disruptions in myelin and neurites were labeled with APP in GANes mice and were partially (and qualitatively) rescued by CD treatment (Figure 42h), aligning with the observed rescue effect in NfL levels (Figure 23). APP was used here as a marker of neurite health and dystrophic neurites (Billnitzer et al., 2013).

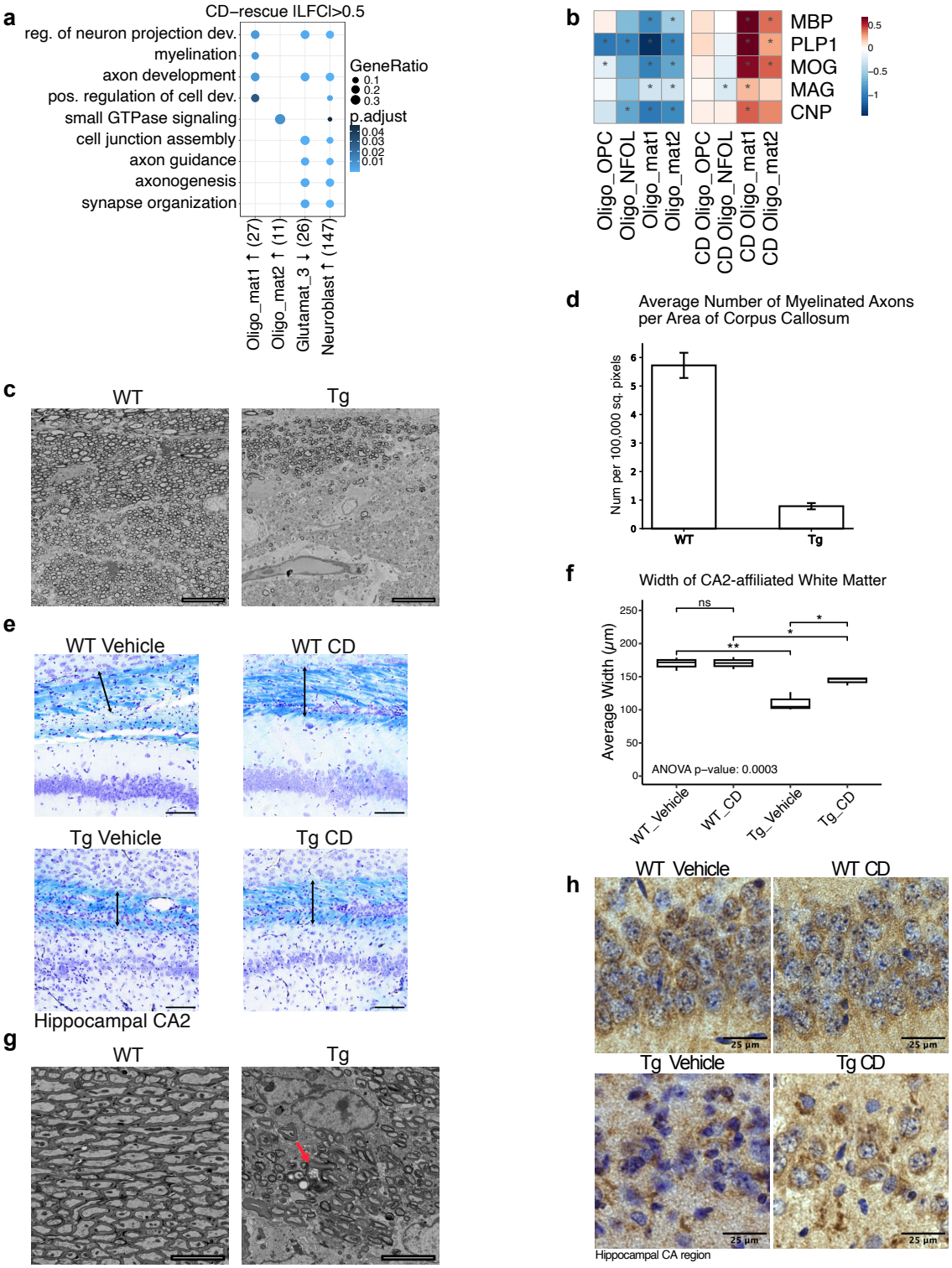

Figure 42: Myelination is impaired by poly(GA) transgene, contributing to lipid pathology that is rescued by CD. a,b) GO analysis and myelin gene heatmap reveal improved myelination as a primary effect of CD therapy. c,d) transgene causes the shrinkage of corpus callosum (SEM scalebar = 10 μm) and a reduction in the number of myelinated axons per area (n=2 in each group). e,f) LFB staining confirms shrinkage of white matter, with CD partially rescuing the phenotype (scale bars = 100 μm). g,h) Myelin (red arrow) and axons are disturbed by transgene expression (SEM scalebar = 5 μm), which is confirmed in APP staining. CD-injected transgenic mice show a qualitative degree of improvement in APP staining (scale bars = 25 μm).

4.3.2.2.5 Measurement of Cholesterol and Cholesteryl Esters

Given the observed disturbances in myelination and cholesterol metabolism, the need to measure cholesterol and cholesteryl esters (CEs) became evident. Our collaborators in Sanofi conducted mass spectrometry analyses using midbrain tissue from our mice. Figure 43 presents the measurements for various cholesterol esters, the cumulative sum of all cholesterol esters, and cholesterol itself.

Interestingly, cholesterol levels were significantly reduced in GA-Nes mice, and CD treatment did not markedly reverse this trend. On the other hand, cholesteryl esters were notably elevated in the Tg_Vehicle condition, with CD treatment effectively restoring their levels to near wildtype values. Specifically, CE 16:1 (a cholesteryl ester with 16 carbon atoms and 1 double bond, indicating mono-unsaturation), CE 18:1, and CE 22:4 showed significant changes, whereas CE 18:2 levels varied too much to yield statistical significance.

The increase in CEs, crucial components of lipid droplets, aligns with the upregulation of PLIN4 expression. The decrease in cholesterol levels may contribute to reduced developmental myelination or secondary myelination loss noted in Figure 42. Consequently, CD's mechanism of action appears to involve the sequestration of cholesterol or the facilitation of its further metabolism and clearance, leading to several positive outcomes, including enhanced survival rates and reduced NfL levels.

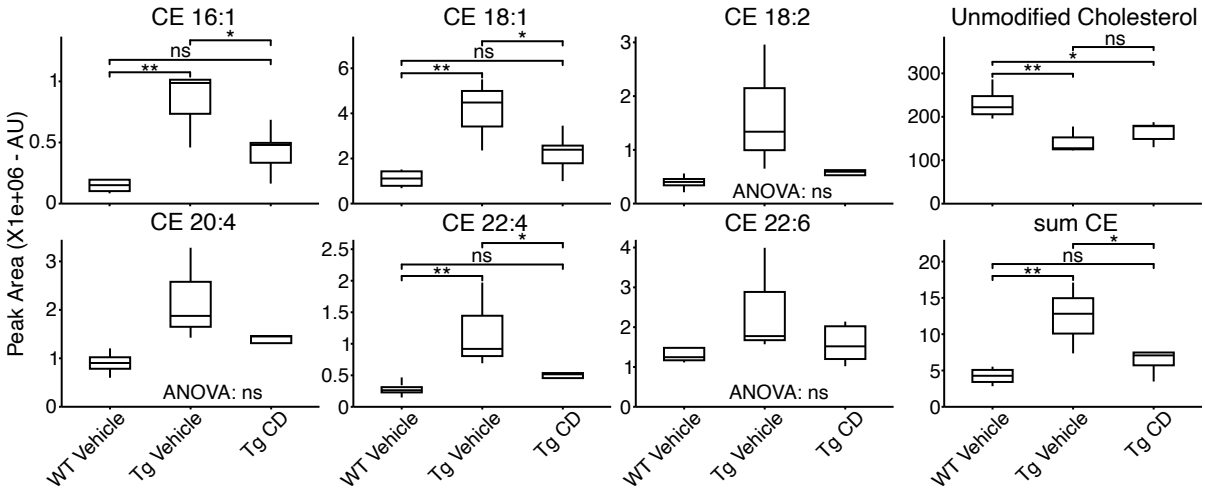

Figure 43: Cholesterol esters are upregulated in transgenic mice and rescued back to near wildtype level with CD administration, while cholesterol is downregulated and is not rescued (n: WT_Vehicle=4, Tg_Vehicle=3, Tg_CD=5; ANOVA with Fisher's LSD for posthoc comparison).

5. Discussion

5.1 JAK inhibitors As a Potential Therapeutic Agent in ALS

Neuroinflammation is a common characteristic of many neurodegenerative diseases, including ALS, where it likely exhibits both protective and detrimental effects (Kwon & Koh, 2020). Initially, neuroinflammation may serve a protective role, for instance, by shielding against damage-associated molecular patterns (DAMPs) (Kwon & Koh, 2020). However, persistent neuroinflammation can lead to a harmful cycle, exacerbating neurodegeneration (Hickman et al., 2018). It has been observed that the transition of microglia from a protective to a pro-inflammatory/toxic phenotype impedes remyelination, thereby aggravating disease progression and facilitating further neuronal loss (Stephenson et al., 2018).

Various studies using single cell RNA sequencing technology have contributed immensely to the understanding of microglia states, as microglia are quite sensitive to their environment (McCauley & Baloh, 2019). A landmark study by the Amit lab in 2017 identified a novel microglial phenotype in an Alzheimer's disease model, termed disease-associated microglia (DAM), which appears to limit neurodegeneration (H. Keren-Shaul et al., 2017). Concurrently, research by the Tsai lab elucidated the dynamic states of microglia across early and late disease phases in the hippocampi of Alzheimer's disease mice (Mathys et al., 2017). Moreover, an earlier study in 2007 using $SOD1^{G93A}$ mice revealed that the microglia expressing mutant SOD1 are more neurotoxic than wildtype microglia (Xiao et al., 2007). Beyond microglia, other immune cells within the CNS, including CNS-resident macrophages (e.g., perivascular, meningeal, and choroid plexus macrophages) and T cells (McCauley & Baloh, 2019), as well as astrocytes (Giovannoni & Quintana, 2020), also play crucial roles in neurodegenerative processes.

Given the pivotal role of neuroinflammation in ALS, numerous drug trials aim to mitigate its effects (Mead et al., 2023). However, these trials are often hindered by high costs and lengthy timelines, as introducing a new compound to the market typically takes 10-15 years (Nosengo, 2016). In this context, drug repurposing

emerges as a compelling strategy, leveraging existing drugs for new therapeutic applications. The urgency induced by the COVID-19 pandemic, coupled with advancements in AI technology, has notably accelerated drug repurposing efforts through the analysis of protein–protein interaction networks pertinent to disease states, such as those described in BenevolentAI Knowledge Graph (Zeng et al., 2020; Zhou et al., 2020).

Utilizing the BenevolentAI Knowledge Graph, researchers have pinpointed ALS-associated genes, with subsequent pathway enrichment analyses illuminating the significance of neuroinflammatory pathways (Richardson et al., 2023). Among these, STAT3—alongside its counterparts STAT1 and STAT2, primarily activated by Janus Kinases (JAKs)—emerges as a critical pathway in both ALS and muscle atrophy (Richardson et al., 2023). JAKs phosphorylate STATs, thereby triggering a cascade of signaling (see introduction section for more details). Figure 44, taken from (Richardson et al., 2023), depicts how STAT3 signaling potentially contributes to non-cell autonomous neuron death, underscoring the rationale for a closer examination of JAK inhibitors. These inhibitors, particularly those already approved for use, are postulated to enhance mitochondrial function, promote autophagy, alleviate neuroinflammation and glial toxicity, mitigate muscle denervation and atrophy, diminish excitotoxicity, and reduce ER stress (Richardson et al., 2023). Thus, the potential of JAK inhibitors in neurodegenerative diseases deserves a more thorough investigation. The utility of JAK inhibitors (jakinibs) in other neurodegenerative disorders is slowly being more recognized, such as AD (Rusek et al., 2023).

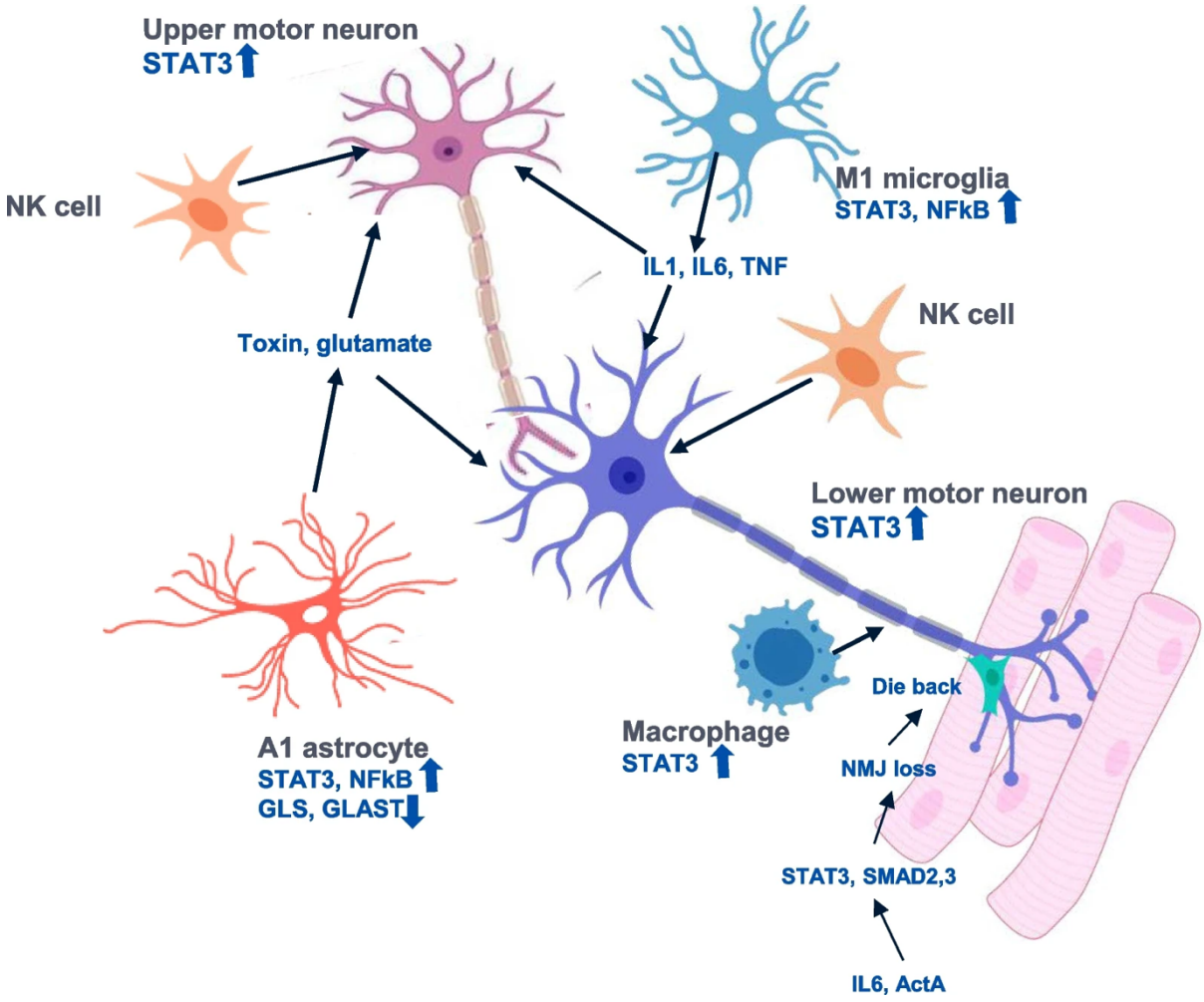

Figure 44: STAT3 signaling is thought to contribute to a non-cell autonomous death of motor neurons. Microglia, astrocytes, macrophages, and natural killer cells all contribute to this cell death. This figure is taken directly from (Richardson et al., 2023) under CC BY 4.0 DEED license, which permits free and full use when credit is attributed.

Research on jakinibs in ALS, though limited, has yielded promising results. A 2022 research from Feldman lab demonstrated the efficacy of tofacitinib, a JAK inhibitor approved in the United States in 2012, within an ALS context (Figueroa-Romero et al., 2022). The investigation involved administering tofacitinib to an NK cell line and subsequently to $SOD1^{G93A}$ mice. Findings revealed that tofacitinib attenuated natural killer cell activity in $SOD1^{G93A}$ mice, leading to reduced cytotoxicity, pro-inflammatory gene expression, and pro-inflammatory cytokine secretion (Figueroa-Romero et al., 2022). However, a notable limitation of this study was its focus on peripheral NK cells rather than those capable of brain penetration. Despite this, the modulation of peripheral immunity may still offer therapeutic benefits.

GA-Nes mice exhibit signs of excessive neuroinflammation and STAT3 phosphorylation (LaClair et al., 2020), as described in detail in the introduction section. To inhibit neuroinflammation, we used baricitinib as a therapeutic measure, which did not yield beneficial results in survival. We selected baricitinib for intervention based on its prolonged half-life and demonstrated BBB penetration capabilities (Gavegnano et al., 2019). Tofacitinib and ruxolitinib were deemed unsuitable due to their shorter half-lives and the challenges in administering them to the small-sized GA-Nes mice via osmotic pumps. Our investigation focused exclusively on the central nervous system (CNS), diverging from previous studies that concentrated on peripheral effects (Dang et al., 2021; Sui & Lv, 2022). Unfortunately, the analysis of STAT phosphorylation brain lysates (Figure 12), revealed no noticeable target engagement, and survival, our primary endpoint, remained unaffected (Figure 10). The lack of target engagement might be attributed to the overpowering immune response or low drug dose, alternative pathways activating STAT3, or simply alternative pathways not targeted by baricitinib.

There remains a possibility that baricitinib exerted effects in the peripheral systems of the GA-Nes mice, but not in the CNS. Given the severe neuroinflammation in these mice, the dosage of 10 mg/kg may have been insufficient. A higher dose of 50 mg/kg induced severe acute side effects requiring termination, necessitating the adoption of the lower dosage. This dosing strategy was informed by prior research demonstrating that baricitinib could mitigate neurocognitive impairments in SCID mice at both 10 mg/kg and 50 mg/kg doses, with BBB penetration confirmed at these doses (Gavegnano et al., 2019). Although not shown in the results section, a pilot study exploring a 25 mg/kg dose failed to influence survival outcomes, indicating a complex interplay between dosage, efficacy, and safety in the GA-Nes model.

In the realm of other neurodegenerative diseases, jakinibs have shown efficacy. For instance, tofacitinib was therapeutically employed in an Alzheimer's Disease (AD) model, where mice subjected to Aβ1–42 intracerebroventricular injections exhibited decreased levels of pro-inflammatory cytokines, such as TNF-α and IL-6, and significant improvements in learning and memory capabilities, as assessed by the Morris water maze (Sui & Lv, 2022). Additionally, baricitinib, a JAK1/2 inhibitor known for its extended half-life, has been effectively utilized to curb pro-inflammatory cytokine

production and lymphocyte proliferation in an experimental autoimmune encephalomyelitis (EAE) mouse model, which models multiple sclerosis (MS) (Dang et al., 2021). Nevertheless, it is noteworthy that these studies predominantly focused on the spleen rather than the brain (Dang et al., 2021).

In light of evidence indicating that cytoplasmic dsRNA found in C9ORF72 ALS/FTD brains triggers an antiviral response (Rodriguez et al., 2021), a phase I/II clinical trial employing baricitinib for both AD and ALS patients commenced in 2022. The outcomes of this trial are eagerly anticipated in the second half of 2024 (Massachusetts-General-Hospital, 2022).

However, previous studies involving jakinibs in models of neurodegeneration, as reviewed earlier in this discussion, did not demonstrate modulation of survival. This suggests that achieving a survival modulation in such an aggressive ALS mouse model might have been overly ambitious, regardless of potential peripheral target engagement. GA-Nes mice typically reach a humane endpoint at approximately 6-7 weeks of age (LaClair et al., 2020), a timeframe that was established in earlier findings. The discussion on neuroinflammation's dual role—providing benefit early in the disease progression while becoming neurotoxic later—reveals a complex interplay of effects. Considering the shortened lifespan of these mice and the severity of the disease model, the window for therapeutic intervention may be exceedingly narrow, and we might have missed it. Another important factor to consider is that at such a young age, microglia are crucial for the development of the brain (Mehl et al., 2022), therefore any aggressive anti-inflammatory therapy can exert deleterious effects on brain development. Consequently, even if peripheral target engagement had been demonstrated, the inherent constraints of our chosen disease model could significantly limit the feasibility of our treatment approach.

For future anti-inflammatory therapies in the GA-Nes mice, a more global inhibition, such as inhibiting microglia or infiltration of T cells with drugs like natalizumab, tested at varying time points, might be more conclusive in deciphering whether neuroinflammation is exerting a protective or a toxic effect in this model.

5.2 Analysis of Dysmetabolism in ALS Mouse and Cell Models

Dietary Adjustments Did Not Extend the Lifespan of GA-Nes Mice

In a 2004 study published in PNAS, researchers demonstrated that dietary adjustments in SOD1^{G93A} mice significantly enhanced their well-being, evidenced by reduced adipose tissue accumulation and a 20% extension in mean survival (Dupuis et al., 2004). Considering weight loss as the primary criterion for euthanasia in GA-Nes mice (LaClair et al., 2020), we embarked on a pilot study aimed at dietary modulations with two supplements (rich in carbohydrates and proteins) to assess potential improvements in survival among GA-Nes mice. Despite observing moderate weight gains, the primary endpoint of our study—survival—remained unaffected, with the rate of weight loss at 6-7 weeks of age unchanged. The dietary supplements employed, DietGel 76A and DietGel Recovery, were not high in lipid content. Previous research has indicated that a high-caloric diet rich in lipids, particularly cholesterol, can enhance the general well-being of both ALS patients (Park et al., 2021; Prado et al., 2023) and mouse models (Dupuis et al., 2004). However, DietGel 76A and DietGel Recovery contain only 1.5 grams and 1.9 grams of fat per 100 grams of supplement, respectively (detailed nutritional information can be found in the Materials and Methods section). Given the rapid progression of the disease in this model and the supplements' relatively low lipid content, it is plausible that the GA-Nes mice did not derive significant benefits from these dietary adjustments. Moreover, setting survival as a readout may have been overly optimistic, given the aggressive nature of the disease in this model (LaClair et al., 2020).

As mentioned in the introduction, body mass index (BMI) is a significant prognostic factor in amyotrophic lateral sclerosis (ALS), with patients presenting a BMI less than 18 facing significantly poorer outcomes compared to those with a higher BMI (Desport et al., 1999). Conversely, a BMI exceeding 30-35 is also associated with an adverse prognosis (Moglia et al., 2019). Hypermetabolism, a characteristic feature of ALS that manifests prior to the onset of disease symptoms, coupled with issues such as muscle weakness, contributes to the decline in BMI observed in ALS patients (Bouteloup et al., 2009). This reduction in BMI correlates with alterations in three

metabolite clusters: sphingolipids and/or ceramides, bile acid metabolites, and fatty acids (Dupuis & Chio, 2023), implications of which in disease are discussed below (although they are currently unknown in GA-Nes mice). The consequences of hypermetabolism and lowered BMI are quite relevant in the GA-Nes mice, as the primary reason for euthanasia in these mice is weight loss at 6-7 weeks of age.

Significant correlations between changes in sphingolipid and/or ceramide levels in both the periphery and the central nervous system (CNS) of patients and disease progression have been documented (Goutman et al., 2022). Notably, substantial sphingolipid metabolism disruptions were identified in the $SOD1^{G93A}$ mouse model as early as 2002 (Cutler et al., 2002). Pharmacological targeting of serine palmitoyltransferase to reduce sphingolipid synthesis led to decreased accumulation of ceramides, sphingomyelin, and cholesterol esters, concurrently offering protection to motor neurons against excitotoxic and oxidative stress (Cutler et al., 2002). Moreover, the application of tauroursodeoxycholic acid (TUDCA), a bile acid derivative, to stem cell-derived motor neurons harboring the $hSOD1^{A4V}$ mutation exhibited neuroprotective effects, and its administration in $SOD1^{G93A}$ mice ameliorated muscle denervation (Thams et al., 2019). Additionally, fatty acid oxidation presents another pertinent mechanism in ALS, where the inhibition of fatty acid β-oxidation using Ranolazine improved the pathological phenotype in $SOD1^{G93A}$ mice and reduced their energy expenditure (Scaricamazza et al., 2020).

Given the information discussed here, future dietary and pharmacological interventions could be more specifically targeting the implicated molecules, such as modulating disturbed sphingolipid or cholesterol phenotype. A metabolomics study alongside the introduction of a high-fat diet, while continuing to monitor survival, may offer more comprehensive insights. DietGel Boost might be a promising starting point for future research as it is a high-calorie gel with a high-fat content and therefore might not only more effectively recover BMI in the GA-Nes mice, but also alleviate the lipid phenotype of these mice. Employing fixed-timepoint analyses could illuminate additional potential benefits of dietary adjustments, such as improved myelination and reduced neurofilament light chain (NfL) levels, providing a more nuanced understanding of the dietary intervention's impact.

ALS-related Inclusion Bodies Had No Detectable Effect on Basic Metabolic Parameters in Primary Neurons

Our investigation extended to analyzing metabolic alterations in transduced primary rat neurons, employing live cell reporters and mass spectrometry for this purpose. Despite the anticipation of distinctive metabolic shifts, no significant differences were detected in hippocampal neurons transduced with poly(GA) by Peredox, a fluorescence reporter of NADH:NAD^+ ratio. Similarly, we could not detect any differences in cortical neurons transduced with poly(GA), poly(GR), or TDP-25 by mass spectrometry. This finding stands in contrast to several studies that have reported a variety of metabolic changes in ALS-afflicted neurons.

A notable study differentiated induced pluripotent stem cells (iPSCs) into spinal motor neurons, cardiomyocytes, and cortical neurons to assess metabolic discrepancies (Hor et al., 2021). This research uncovered motor neuron-specific metabolic deficiencies in mutants via metabolic flux analysis utilizing the MitoStress assay. Additionally, it revealed hyper-acetylation of mitochondrial proteins, a phenomenon linked to diminished activity of Sirtuin-3 (SIRT3). Remarkably, the activation of SIRT3 not only mitigated these metabolic aberrations but also enhanced ATP production specifically in motor neurons, without affecting cardiomyocytes or cortical neurons (Hor et al., 2021).

Continuing our exploration into ALS-associated metabolic alterations, another study focusing on pre-symptomatic primary motor neurons from $SOD1^{G93A}$ mice identified a metabolic signature characterized by the upregulation of energy-transducing enzymes, notably HADHA (associated with fatty acid oxidation) and the ketogenic enzyme ACAT2 (Szelechowski et al., 2018a). Interestingly, modulating fatty acid oxidation impacted cell viability, whereas inhibiting uncoupling protein 2 (UCP2) ameliorated the ATP deficits observed in ALS motor neurons, both mitochondrially and cytoplasmically (Szelechowski et al., 2018a). This study, along with the study from the previous paragraph, highlight the importance of employing motor neurons for metabolic studies, which explains our negative results with hippocampal and cortical neurons.

In contrast to our study, the Kalb lab's investigations into cortical neurons harboring ALS-related mutations (mutant SOD1 and TDP43) unveiled a metabolic rewiring. Despite normal ATP levels and redox status (as in our study), these neurons exhibited altered concentrations of tricarboxylic acid (TCA) cycle metabolites, including lactate, fumarate, and malate (Riechers et al., 2022).

In our study, we employed hippocampal neurons for metabolic reporting with a fluorescence sensor and cortical neurons for mass spectrometry analyses. Consequently, our negative results with these parameters corroborate those reported in the literature; highlighting that the use of specific neuronal types, particularly motor neurons, is critical in discerning the metabolic differences in ALS research. Further investigations could probe the TCA cycle metabolites to elucidate the impact of poly(GA) expression on metabolism in cortical neurons, or directly investigate the more relevant motoneurons for dysregulation of energy carrier levels.

5.3 Cholesterol Accumulation and Clearance in Neurodegeneration

Lipid Dysregulation in Neurodegenerative Diseases

The role of lipid accumulation and lipid clearance in neurodegenerative diseases has been gaining increasing amounts of attention. Recent studies have underscored the connection between the dynamics of lipid turnover and the progression and severity of these diseases.

In our mouse model, we noted an increase in cholesterol esters and a decrease in cholesterol levels, with the latter also evidenced by the downregulation of biosynthesis pathways. The concurrent upregulation of cholesterol export pathways in our findings suggests that the reduction in cholesterol synthesis might be a response to the accumulation of cholesterol esters, potentially due to inadequate transportation mechanisms. Furthermore, demyelination could be another factor contributing to the cholesterol ester overload (Amaducci et al., 1978). It remains unclear whether impaired cholesterol transport leads to insufficient myelination in our model or if myelin loss itself results in cholesterol accumulation. To unravel these complexities, future investigations should incorporate electron microscopy at various fixed time points to

elucidate the specific relationship between cholesterol dynamics and myelination or demyelination processes.

Although the association between cholesterol and Alzheimer's disease (AD) pathogenesis has been extensively studied, other lipids, including phosphoinositides and phosphatidic acid, also play crucial roles in neurodegenerative processes (Di Paolo & Kim, 2011). Intriguingly, Alois Alzheimer himself identified a third pathological hallmark of AD, referred to as ‘adipose inclusions’ or ‘lipid granules,’ highlighting the historical recognition of lipids in AD pathology (Foley, 2010). Nevertheless, the link between lipids and AD was more concretely established by the discovery of APOE type 4 allele as the “strongest genetic risk factor for AD” (Corder et al., 1993). The APOE ε4 variant is implicated in the metabolism of cholesterol and triglycerides, with its protein product having an affinity for amyloid-β (Aβ). This interaction is pivotal in modulating the clearance and aggregation of Aβ, suggesting a key mechanism by which lipid metabolism influences AD progression (Kim et al., 2009).

More specifically, cholesterol's involvement in amyloidogenesis is well-documented (Di Paolo & Kim, 2011). The process involves the esterification of excess free cholesterol by ACAT1, leading to the formation of cholesterol esters. These esters accumulate in intracellular lipid droplets or are effluxed through the plasma membrane into the extracellular space (Chang et al., 2006). In cell culture models, inhibition of ACAT1 with CP-113,818 has been shown to reduce levels of both Aβ and cholesterol esters. Conversely, an increase in cholesterol esters correlates with elevated secretion of Aβ from cells (Puglielli et al., 2001). Additionally, upregulation of ABCA1, a transporter facilitating cholesterol efflux to extracellular lipid acceptors including APOE, is associated with decreased Aβ levels (Sun et al., 2003). *In vivo* studies further support this, showing that ABCA1 deletion leads to diminished APOE lipidation and enhanced amyloidogenesis (Hirsch-Reinshagen et al., 2009). However, application of CD did not change the amount of poly(GA) aggregates, as evidenced by fluorescent images of frozen sections shown in Figure 22. Therefore, it is unlikely that cholesterol and cholesterol esters play a similar role in the poly(GA) mouse model.

Cholesterol also intersects with the processing of amyloid precursor protein (APP) by BACE1, which occurs within lipid rafts. Specifically, reducing cholesterol levels diminishes the interaction between lipid rafts and BACE1, thereby decreasing amyloidogenic APP processing (Vetrivel & Thinakaran, 2010). Complementary to its influence on APP processing, cholesterol augments Aβ aggregation. Although gangliosides such as GM1 primarily modulate Aβ aggregation, the seeding capacity of GM1 is notably enhanced in cholesterol-rich environments (Matsuzaki et al., 2010). An important mechanism of free cholesterol (FC) toxicity involves the FC/phospholipid ratio in lipid rafts that has to be maintained within a homeostatic range (Tabas, 2002). Therefore, it is a likely scenario that low phospholipid levels lower the production of cholesterol in poly(GA) mice in order to maintain the homeostatic ratio, leading to undermyelination of axons. However, such lipid raft disturbances do not seem to greatly affect the aggregation levels as administration of CD did not seem to greatly change the aggregation levels. Future experiments should measure phospholipid levels in GA-Nes mice to get a clearer picture of the disease mechanism.

The implications of cholesterol dysregulation in the realm of neurodegenerative conditions extend beyond Alzheimer's disease (AD). Notably, Niemann-Pick type C (NPC) disease, which results from mutations in the cholesterol transporters NPC1 and NPC2, leads to the lysosomal accumulation of cholesterol (Pfeffer, 2019). Beyond NPC, cholesterol dysmetabolism has been observed in a wide array of disorders, including amyotrophic lateral sclerosis (ALS), Parkinson's disease (PD), Huntington’s Disease (HD), depression, stroke, traumatic brain injury, and normal aging (Martin et al., 2014). Nevertheless, delineating whether cholesterol plays a causative role or is merely a consequence of these conditions remains elusive. In our study, we detected lower amounts of cholesterol in transgenic conditions, while cholesterol esters were increased. However, the mice in this study were perfused, therefore blood cholesterol levels were not taken into account. Downregulation of cholesterol biosynthesis genes and upregulation of genes for storage and export of cholesterol in our data aligns with the observations of cholesterol overload seen in NPC, while low intracellular cholesterol levels could possibly suggest increased cholesterol in the periphery. Future research should pinpoint the origin of such cholesterol overload.

Cholesterol Metabolism and Clearance as Promising Therapeutic Targets

The dysregulation of cholesterol ester (CE) clearance plays an important role in the pathology of neurodegenerative diseases. The toxicity associated with free cholesterol necessitates its esterification into cholesterol esters, which are then sequestered in lipid droplets. Free cholesterol (FC) can cause toxicity by disturbing the lipid balance within the cell. When the FC:phospholipid ratio surpasses what is considered a homeostatic range, lipid rafts turn too rigid and lose their fluidity, resulting in a slew of problems, especially for integral membrane proteins (Tabas, 2002).

The storage mechanism of converting free cholesterol into cholesteryl esters, while vital, has limited capacity, prompting a reduction in cholesterol biosynthesis as a measure to mitigate cholesterol-mediated toxicity (Song et al., 2021). However, this adaptive response, by lowering cholesterol metabolism, may inadvertently impact crucial biological processes, including myelination and synaptic transmission, highlighting the delicate balance required to maintain cholesterol within a certain homeostatic range (Petrov et al., 2016). Figure 45 illustrates the cellular mechanisms employed to prevent excessive cholesterol accumulation, demonstrating the intricate balance between cholesterol esterification, storage, and the regulation of cholesterol biosynthesis (Song et al., 2021).

In GA-Nes mice, neuronal death and demyelination coincide and could mutually reinforce one another, potentially leading to the release and subsequent need for clearance of large amounts of cholesterol. Although we measured lower cholesterol amounts from perfused brain lysates, downregulation of cholesterol biosynthesis and upregulation of cholesterol export and storage indicate cholesterol overload, perhaps in the periphery. Concurrently, the cellular machinery in GA-Nes mice faces additional stress, such as proteasome stalling (Khosravi et al., 2020), potentially hindering the clearance of excess cholesterol from the brain and liver. Thus, facilitating the removal of surplus cholesterol or cholesterol esters could improve cellular survival. More investigations are needed to confirm this hypothesis. Additionally, systemic clearance of cholesterol-related lipids might restore cholesterol production in myelinating cells, offering a potential avenue for rescuing myelination. Further investigation is required

to elucidate and confirm these mechanisms in GA-Nes and other ALS mouse models. Three critical factors must be considered when interpreting data from this study in the context of other literature studies: the distribution of aggregates in GA-Nes mice, their age, and their gender. In our study, all mice are harvested at P40, informed by our previous studies as the earliest time point requiring euthanasia, which is before adulthood, while the studies discussed here are conducted on adult mice. Secondly, all the investigated mice are female, while the majority of studies in this discussion are in a mix of genders, which is notable because gender can influence lipid profile and metabolism (Ethun, 2016). Thirdly, the transgenic GA-Nes mice express poly(GA) in all CNS neurons and glial cells, which can cause a more widespread lipid disturbance that glia might have less capability to compensate for compared to the targeted expression of a transgene in a subset of cells.

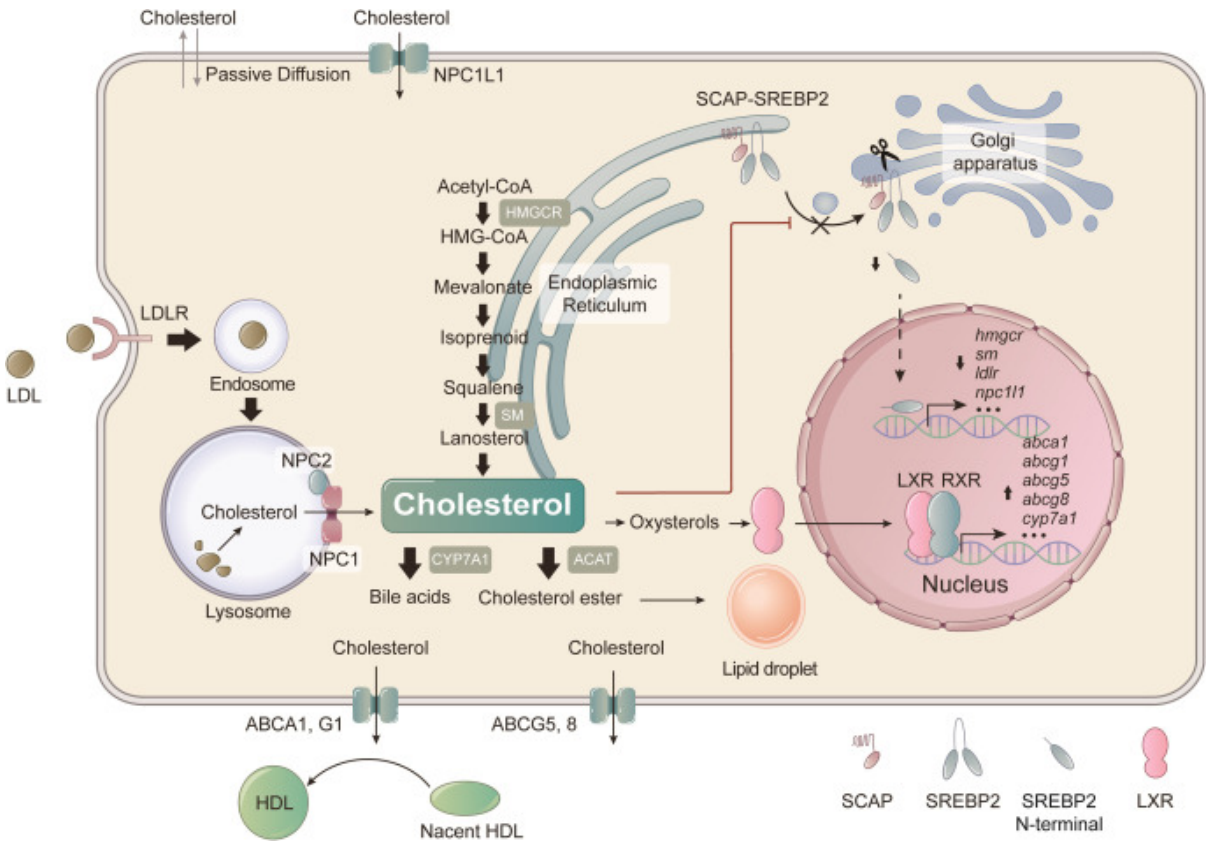

Figure 45: Cellular mechanism to metabolize cholesterol and combat excess cholesterol. This figure is licensed to be reused in this dissertation under license number 5721620639903 (Song et al., 2021).

The inert cholesterol esters can become biologically active following oxidative modification (Gonen & Miller, 2020). As discussed in the introduction section, cells

undergo oxidative stress in the context of ALS (Smith et al., 2019). Cholesterol esters undergo oxidation to form oxidized cholesterol esters (OxCEs) via free radical mechanisms. These OxCEs can be ingested by macrophages, leading to profound alterations in macrophage structure and function, including the formation of foam cells—a process implicated in various pathological states (Gonen & Miller, 2020). While we have not measured OxCEs in our dataset, CE levels are significantly higher in poly(GA) mice. Future studies should measure OxCE levels and investigate macrophages inside the brain and in the periphery in order to determine whether such a mechanism occurs in poly(GA) expressing mice.

Interestingly, oxysterols, oxidized derivatives of cholesterol, are also subject to esterification. The esterification of 24(S)-hydroxycholesterol by ACAT in neurons, for instance, can trigger cell death through the formation of atypical lipid droplets (LD-like structures) associated with the enlarged endoplasmic reticulum (ER) lumina (Takabe et al., 2016). This phenomenon underscores the potential cytotoxic effects of altered cholesterol metabolism within the nervous system. Although we do not have any data on oxysterol levels in poly(GA) mice, investigating the toxic oxysterol species can provide valuable insights into the mechanism of the disease as well as possible therapeutic avenues. This is relevant in GA-Nes mice given the evident disturbances in cholesterol metabolism.

Moreover, cholesteryl ester storage disease (CESD), which primarily affects the liver due to deficient lysosomal acid lipase (LAL) activity, results in the accumulation of cholesterol esters. This condition exemplifies the severe consequences of disrupted cholesterol ester metabolism, including premature death (Bernstein et al., 2013). Although CESD predominantly impacts hepatic function, the mechanisms of cholesterol ester accumulation and oxidative modification have broader implications for understanding and treating neurodegenerative diseases. In GA-Nes mice, we observe increased CE levels in the brain. The periphery, however, was not examined. Future studies can investigate the liver more carefully to determine this.

Lipid rafts, composed of cholesterol and sphingolipids among other lipids, facilitate the aggregation of pathogenic proteins such as Aβ, α-synuclein, and prion

proteins. These proteins, in turn, can deplete membrane cholesterol, further disrupting cellular homeostasis (Petrov et al., 2016). Myelin, which contains the largest amount of cholesterol, is particularly vulnerable to disruptions in lipid metabolism, as evidenced in frontotemporal dementia (FTD) associated with GRN or C9ORF72 mutations (Marian et al., 2023). Both FTD-GRN and FTD-C9ORF72 seem to have disrupted lysosomal homeostasis and show white matter lipid loss, but lipid metabolism pertinent to myelination (especially sphingolipid levels) is more severely affected in FTD-GRN (Marian et al., 2023). In our dataset, we observed a lower number of myelinated axons and shrinkage of white matter in transgenic mice compared to wild types. The cholesterol disturbances seen in poly(GA) mice can perhaps be complementary to sphingolipid metabolism disturbances. Future studies should also measure sphingolipid levels in order to determine the exact pathological mechanism.

The clearance of excess cholesterol, a potentially toxic species, and cholesterol esters, inert molecules susceptible to conversion into toxic entities, is crucial for cellular health. Remarkably, the brain constitutes 23-25% of the total body cholesterol in humans and about 15% in mice, emphasizing the significance of cholesterol in neural function (Dietschy, 2009). Nevertheless, the cholesterol ester amount is maintained at a relatively low level in the brain. Upon upregulation of CEs, lipid droplets appear in neuronal cytoplasm (Petrov et al., 2016). In GA-Nes mice, we observe a significant upregulation of CE levels, but we do not observe any large lipid droplets with Oil Red O staining or SEM. More data from lipidomic and proteomic investigations is needed to paint a complete picture of the lipid pathology in the disease. Speculation from the data available could suggest that cholesterol esters cannot reach the other components of lipid droplets in order to successfully make a lipid droplet. This could further expose the CEs to various metabolic processes, such as oxidation with free radicals. While without more data this remains a hypothesis, there is a clear therapeutic potential in clearing toxic cholesterol species, as their accumulation can cause toxicity.

5.4 Cyclodextrin as a Therapeutic Agent in Neurodegeneration

2-hydroxypropyl-β-cyclodextrin (HP-β-CD, here also simply referred to as CD), recognized for its cholesterol-sequestering properties, has traditionally been utilized as an excipient in drug formulations (Neufeld et al., 1996). The unique cholesterol-binding capacity of CD has led researchers to explore its therapeutic potential in Niemann-Pick disease type C (NPC), a disorder characterized by lysosomal cholesterol accumulation (Berry-Kravis, 2021). Early interventions using CD in NPC treatment demonstrated considerable success, even though CD's ability to cross the blood-brain barrier (BBB) is limited (Camargo et al., 2001). Despite its promising health outcomes in mice, CD has not been universally adopted as standard care for NPC, partly due to its association with ototoxicity—specifically, the rapid loss of cochlear outer hair cells (OHCs) and resultant permanent hearing loss following administration (Crumling et al., 2017).

In our study, 2000 mg/kg of CD administered subcutaneously daily starting from P21 resulted in survival extension in some of the female but not male mice. The observed gender-specific response to CD treatment in GA-Nes mice aligns with some previous findings and remains an area for further exploration. Holzman et al. (2021) reported gender-specific benefits of treatment in an NPC1 mouse model, also predominantly favoring females. This further supports the notion that gender may play a significant role in the therapeutic outcomes of neurodegenerative disease treatments (Holzmann et al., 2021). Moreover, the disease progression in male GA-Nes mice was marginally more rapid, with males reaching humane endpoints approximately 1-2 days earlier than females, as depicted in Kaplan-Meier survival curves in Figure 21. This observation suggests a potential differential severity of the disease by gender in this model, which may influence treatment efficacy. ALS occurs more in males compared to females, with a ratio of 1.6:1 (Chio et al., 2013). Moreover, $SOD1^{G93A}$ male mice also show an earlier age of onset (McCombe & Henderson, 2010). Therefore, it is possible that the disease is stronger in male poly(GA) mice or that the therapeutic window is shorter, thus resulting in the sex difference. Nevertheless, the exact reason for this effect is unknown and requires more research.

CD's application extends to Alzheimer's disease models, where it has shown significant neuroprotective effects. Research by Yao et al. in 2012 reported a marked reduction in Aβ42 levels in N2a cells harboring the APP Swedish mutation upon CD treatment. In Tg19959 mice, which express two APP mutations, CD treatment resulted in reduced Aβ42 plaque deposition, enhanced spatial learning and memory, and a decrease in tau-immunoreactive dystrophic neurites. These findings underscore CD's potential not only to facilitate cellular clearance mechanisms but also to diminish Aβ42 production (Yao et al., 2012). Nevertheless, these modulations might not be relevant in ALS, as the observed improvements are probably due to altered APP processing.

A 2022 study by Blanchard et al. from the Tsai lab employed an APOE4 mouse model of AD to investigate APOE4-related cholesterol dysregulation and its impact on myelination. The study showed aberrant cholesterol deposition in oligodendrocytes which is coincidental with reduced myelination (Blanchard et al., 2022). This study illustrated CD's efficacy in ameliorating myelination deficits and improving cognitive functions, reinforcing the compound's therapeutic promise in addressing cholesterol dysregulation and enhancing neural integrity in neurodegenerative conditions (Blanchard et al., 2022). While we do not have clear data showing selective cholesterol deposition in oligodendrocytes, our data clearly indicates cholesterol dysmetabolism and myelin disturbances, as previously discussed. Moreover, administration of CD ameliorated the myelin phenotype, which corroborates the findings of this study. Another study also showed improved remyelination upon CD administration in a defective cholesterol clearance model, further aligning with our data (Cantuti-Castelvetri et al., 2018).

Cyclodextrin (CD) has also demonstrated promising therapeutic benefits for Parkinson’s Disease (PD). Jarazo et al. (2021) explored CD's efficacy across cellular, organoid, and mouse models, revealing that CD enhances autophagy and mitophagy in neuronal cultures, reduces neurotoxicity in PD mouse models, and promotes dopaminergic differentiation in organoids. These findings underscore CD’s potential to mitigate PD pathology by supporting neuronal health and function (Jarazo et al., 2021).

CD has been shown to have anti-inflammatory effects (Becktel et al., 2022; Zimmer et al., 2016). However, our data showed limited anti-inflammatory effects upon CD administration. IL-33 and IP10 were reduced in GA-Nes mice upon CD administration. IL-33 rescue effect was most likely in the context of disease-associated oligodendrocytes, which leaves IP10 downregulation as a notable anti-inflammatory effect observed in our study. While immune cells were also affected by CD administration, the most notable modulations are in oligodendrocytes and neuroblasts.

In the context of stroke, Becktel et al. in 2022 reported that CD therapy modulates lipid metabolism genes, reduces immune cell expression, and diminishes lipid droplet accumulation along with T cell and B cell counts in stroke lesions. This evidence suggests CD's beneficial effects extend to modulating inflammatory responses and lipid metabolism in stroke, highlighting its broad therapeutic applications (Becktel et al., 2022). Outside of CNS, CD has been shown to treat atherosclerosis via macrophage reprogramming (Zimmer et al., 2016). However, in their study, Abca1 levels were increased upon CD treatment (Zimmer et al., 2016), while in our dataset Abca1 levels were lowered. This could possibly indicate that CD exerts its effect via a different mechanism in poly(GA) mice compared to the atherosclerosis model. The observed decrease in Abca1 levels could signify a shift towards a more homeostatic state, reflecting a reduced necessity for cholesterol export (Azizidoost et al., 2021). Similar observations regarding downregulation of Abca1 levels following CD therapy have been reported in other studies as well (Coisne et al., 2016), while a defective cholesterol clearance model showed upregulation of Abca1 upon CD administration (Cantuti-Castelvetri et al., 2018). These conflicting data underscore the variable impact of CD on lipid metabolism across different disease models.

The application of CD in Amyotrophic Lateral Sclerosis (ALS) remains relatively unexplored and thus is a major focus of this thesis. In the GA-Nes mice, CD administration notably decreased neurofilament light chain (NfL) levels, ameliorated disease-associated oligodendrocyte phenotypes, and extended lifespan in approximately half of the treated female mice. One study that used the widely-used 2-hydroxypropyl-β-cyclodextrins (CD), which is also used in this work, reported that

administration of CD does not have any effect on the progression of disease in SOD1^{G93A} mice (Greensmith & Bryson, 2023).

Comparing our successful CD application in ALS to other studies that reported no efficacy (Greensmith & Bryson, 2023), several key differences emerge. For instance, the administration frequency and dosing in our study—daily injections—contrasted with the failed SOD1^{G93A} study's once-weekly injection of a high dose of 4000 mg/kg. This difference in treatment regimen could significantly impact the therapeutic effectiveness of CD (Calias, 2017). Moreover, the myelin phenotype is perhaps stronger in poly(GA) model than in the SOD1^{G93A} model. While SOD1^{G93A} mice display aberrant myelination (Vinsant et al., 2013), poly(GA) mice probably have a much more aggressive myelination phenotype leading to a higher potential for effective therapy with CD. Nevertheless, without controlling for the CD regimen and the start of the intervention relative to disease onset it is difficult to compare the effectivity of CD in the aforementioned mouse models.

Furthermore, the specific characteristics of the CD used, particularly the degree of substitution (DS), which refers to the number of hydroxypropyl groups attached to each β-cyclodextrin in place of a hydroxyl group, are crucial for its therapeutic potential. Our CD compound had a DS of 5, while the production batches range from 4 to 9, denoting a high variability that can possibly alter results and cause inconsistencies between studies. Future studies should always report the DS of their CD compound. CDs with lower degrees of substitution are more susceptible to aggregation, which can influence their efficacy and bioavailability (Malanga et al., 2016). Another study demonstrated that CDs with higher DS show increased osmotic pressures, and that DS greatly affects the colligative properties of CD (Proniuk & Blanchard, 2001). A reaction scheme illustrating CD synthesis is shown in Figure 46, to clarify the distinction between compounds with high and low degrees of substitution (Malanga et al., 2016). This aspect is critical, as evidenced by Camargo et al. (2001), who tested three different CD variants in NPC1 therapy; only two of the compounds, which likely had the optimal degree of substitution, demonstrated therapeutic potential (Camargo et al., 2001).

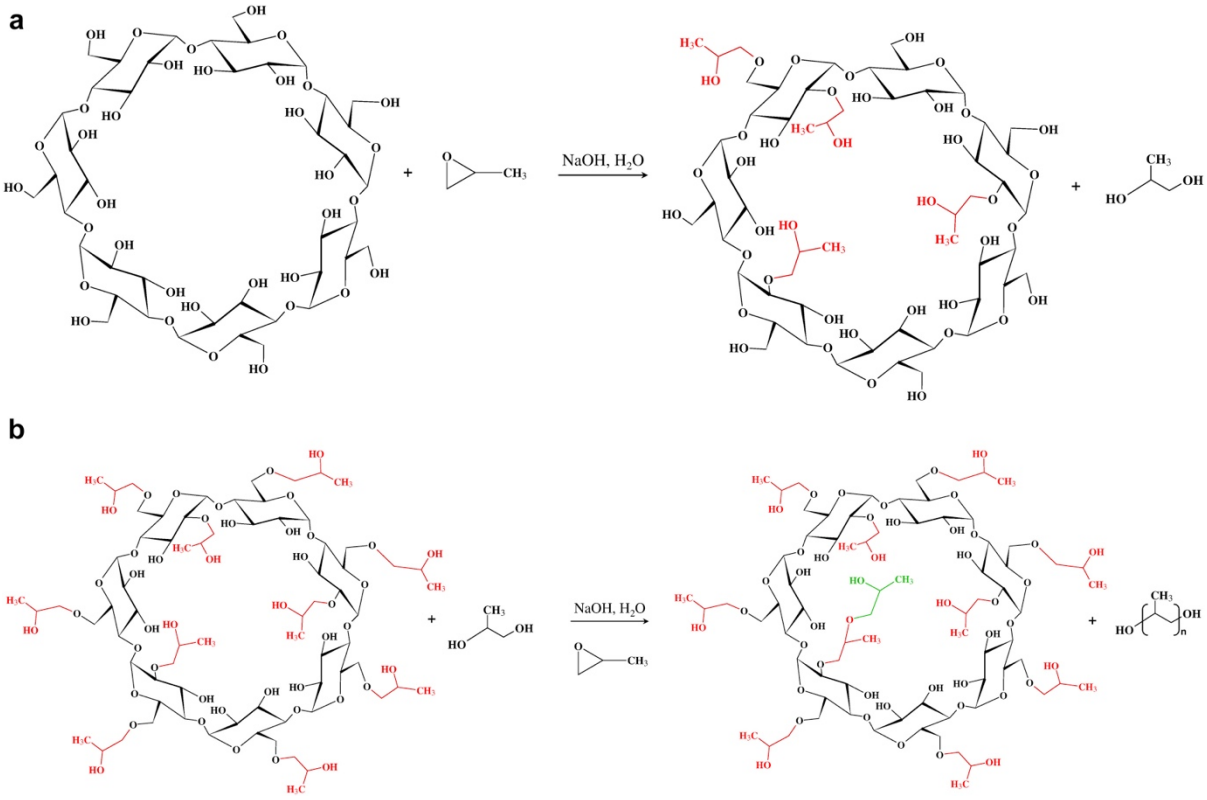

Figure 46: Synthesis scheme of CD with a) low and b) high degree of substitution. The figure is taken from (Malanga et al., 2016) with permission under license number 5717030464388.

The efficacy of CD therapy in neurodegenerative conditions is highly dependent on the specific disease context. One critical factor influencing CD's cholesterol-sequestering capability is the presence of sphingomyelin, which may act as a barrier or regulator of CD's access to membrane cholesterol (Neufeld et al., 1996). Notably, CD's ability to inhibit the esterification of lysosomally-derived cholesterol is evident in control cells but diminishes in NPC1 cells or wildtype cells treated with neutral sphingomyelinase, suggesting a complex interplay between sphingomyelin and CD's mechanism of action (Neufeld et al., 1996).

Neurodegenerative diseases are increasingly recognized to involve aspects of lipid metabolism and clearance dysfunction (Estes et al., 2021), presenting a unique opportunity for employing CD as a therapeutic intervention. Nevertheless, as delineated in this discussion, the efficacy of CD is profoundly influenced by the specific disease context and therapeutic approach employed. While promising, the development of CD-based treatments necessitates further, more detailed research to refine these compounds into more effective therapeutics.

A notable advancement in this field is the ongoing clinical trial of a modified CD, known as Trappsol Cyclo, aimed at treating NPC and AD patients. Preliminary phase I/II results appear encouraging (Sharma et al., 2023), signaling a significant step forward in the application of CD in neurodegenerative disease treatment. Nonetheless, a comprehensive understanding of the mechanism of action of this compound is essential, particularly to mitigate or entirely eliminate its ototoxic effects while preserving its cholesterol-sequestering capabilities.

The potential of CD to alter the course of disease progression in neurodegenerative disorders offers the hope to possibly alter the disease course in many patients. This underscores the need for continued research and clinical trials to fully explore and harness CD's therapeutic benefits.

5.5 Signaling Changes in GA-Nes Highlight Myelination and Neurite Outgrowth

Research into signaling changes in ALS has revealed significant insights, although further research is needed to better understand and apply such insights into the disease context. Initial studies highlighted alterations in interferon signaling among the first signaling-related changes identified in ALS (Wang et al., 2011). Subsequent research uncovered abnormalities in retinoid (Kolarcik & Bowser, 2012) and Wnt signaling (Yu et al., 2013). Further research has identified modifications in BDNF (Just-Borràs et al., 2019) and neuropeptide signaling (Kabiljo et al., 2023). Moreover, an analysis of post-mortem spinal cord samples from ALS patients indicated increased pathway activity of p53, TNFα, androgen, hypoxia, and NFκB, whereas EGFR and VEGF signaling pathways showed significant reduction (Ziff et al., 2023).

Our findings in GA-Nes from bulk RNAseq (LaClair et al., 2020) and through CellChat analysis of snRNAseq data similarly indicate an upregulation of immune and interferon pathways. Additionally, we identified a range of other signaling pathways in the GA-Nes snRNAseq dataset via CellChat that are significantly modulated by transgene expression across all cell clusters, depicted in Figure 30. Notably, the CLDN, VISFATIN, COLLAGEN, SEMA4, MPZ, AGRN, GAS, GRN, and ACTIVIN

pathways were the most altered due to transgene expression. CD administration predominantly modulated the APP and CLDN pathways when considering all cell types in the analysis. The ligand-receptor pairs are not always the same across all clusters and cell types. Some pathways like the APP pathway have more limited LR pairs. For example, App – Cd74 interaction exists in all cell types except for the "other_immune" cluster where it is not detected as a modulated pathway. While we later focus on the specific signaling changes in oligodendrocyte clusters, a brief description and potential connection to GA-Nes mice is discussed below for some of the aforementioned changes when considering all cell types.

It is important to not overinterpret such results as we performed snRNAseq and not scRNAseq, meaning that cytoplasmic RNA is lost in our studies. snRNAseq was chosen over single-cell RNA sequencing (scRNAseq) to enable direct comparison with human datasets and to allow the processing of frozen samples. Furthermore, relative cell numbers can affect the signaling strength being reported here. An unbiased sampling would be indicative of the degree of signaling changes, but our somewhat biased sampling is less quantitative. Biased sampling is apparent by comparing Figure 25 and Figure 34. The discrepancy in these two figures can be due to biases in nuclei isolation or due to the massive upregulation of microglia artificially reducing the astrocyte and oligodendrocyte nuclei count during sorting. Thus, changes in cell number should be interpreted only within a biological context to avoid overinterpretation. Yet another important factor to consider is that snRNAseq was solely performed on female mice at P40, therefore sex-specific signaling pathways as well as pathways required for development might confound this data. Furthermore, the only tissue analyzed here is the hippocampus, which means that many important signaling pathways from other parts of the brain are not included in this dataset.

The Claudin (CLDN) pathway is crucial for tight junction integrity (Zhao et al., 2018) and blood-brain barrier function (Hashimoto et al., 2023; Sladojevic et al., 2019). For example, claudin-5 is the most enriched tight junction protein in the BBB and has been implicated in MS and AD (Greene et al., 2019). In CellChat, CLDN pathway only includes Cldn11 (coding for OSP, or oligodendrocyte specific protein) autocrine signaling, which appears to be upregulated in GA-Nes mice. This pathway's main

annotation in CellChat is listed as cell-cell adhesion (Jin et al., 2021). Data from the literature indicates that Cldn11 is indeed a tight junction protein that plays a role in cell motility regulation, as well as influencing cell barrier, cell polarity, and paracellular transport (Li et al., 2018). In the CNS, Cldn11 is involved in myelination in oligodendrocytes (Bronstein et al., 2000; Maheras et al., 2018) and the BBB in the context of MS (Uchida et al., 2019). Upregulation of this gene in oligodendrocytes possibly indicates a compensatory mechanism to the myelin phenotype and to strengthen the blood-brain barrier. CD administration seems to further increase the expression of Cldn11 in both our wildtype and transgenic mice (data not shown).

The VISFATIN (NAMPT/PBEF1) pathway, integral to NAD+ biosynthesis, plays an important role in neuroprotection, neuroinflammation, and energy metabolism. This pathway was shown to be modulated in aging (Garten et al., 2015). The CellChat LR pairs, namely NAMPT-INSR and NAMPT-ITGA5_ITGB1, are identified as secreted signaling (Jin et al., 2021). GA-Nes mice show disturbances in metabolism, with weight loss being the primary reason for euthanasia; thus, modulation of this pathway does have a biological basis and may perhaps be useful in future metabolic interventions.

Collagen, as the predominant protein in the extracellular matrix (ECM), contributes to the structural integrity of the brain. This pathway contains 198 LR pairs in CellChat, with many integrin receptors. Its influence on cell adhesion, neurite growth, and potential involvement in neurodegenerative diseases emphasizes the importance of ECM components in maintaining neural health and function (Frantz et al., 2010). GO analysis (data not shown, except for CD rescue in Figure 42a) highlights axon development and cell junction assembly in GA-Nes mice, while extracellular matrix disruptions have also been reported in ALS (Maguire, 2017). Similarly, semaphorins, particularly Sema4, are key players in axonal guidance, neuronal growth, and the establishment of neural networks (Yazdani & Terman, 2006). In CellChat, all 14 LR pairs of Sema4 pathway (with many plexin receptors) are annotated as responsible for cell-cell adhesion (Jin et al., 2021). Sema4 involvement in neural development and regeneration points to the critical role of signaling molecules in guiding neural connectivity and plasticity (Yazdani & Terman, 2006).

AGRN (Agrin) serves as a fundamental component in the maintenance of neuromuscular junctions (NMJs) (Bezakova & Ruegg, 2003). However, it should be stressed that we only sequenced hippocampal tissue, so no conclusion regarding NMJ function can be made from this dataset. Furthermore, CellChat lists Agrn – Dag1 as the sole LR pair (Jin et al., 2021). Agrn maintains similar expression levels in all four conditions of our data, but modulations in Dag1 suggest a role of this pathway in neuronal migration, axon guidance, synapse formation and maintenance (Jahncke & Wright, 2022). While unrelated to the signaling observed here, Agrn – Lrp4 signaling might affect lipid metabolism given that LRP4/MEGF7 can bind ApoE (Hayashi, 2011), but more research is needed for concrete conclusions. Agrn – Lrp4 – Musk signaling is however well-documented in NMJ postsynaptic differentiation, with Musk being specific to muscle tissue, which is not included in our dataset (Zong & Jin, 2013).

GRN (progranulin), known for its association with frontotemporal dementia (FTD), implicates signaling pathways in neuronal growth, survival, and inflammation. (Bateman & Bennett, 2009). Grn – Sort1 signaling might also have implications for lipid metabolism, given the role in sortilins in for lipid metabolism, where sortilin-induced lipid accumulation has been reported in the literature (Liu et al., 2023).

The ACTIVIN pathway's role in neuroprotection, neurogenesis, and inflammatory responses aligns well with observed phenotypes and DEGs of GA-Nes mouse model likely as compensatory mechanisms, emphasizing the relevance of this pathway in responses to neural injury and degeneration (Werner & Alzheimer, 2006). Of the ligands within this pathway in CellChat, only Inhba is notably expressed (limited to neuron clusters), while its receptors Acvr1b, Acvr2a, and Acvr2b show sporadic but widespread expression in all clusters.

Similarly, the APP pathway's connection to neural growth and survival, as well as its notorious role in the aberrant production of Aβ aggregates in neurodegeneration, illustrate the multifaceted impact of signaling pathways on disease pathology (Müller et al., 2017). App – Cd74 signaling is better described in the context of AD, where Cd74 has been shown to interact with App in order to suppress Aβ production (Matsuda et al., 2009). Another research using an AD mouse model and postmortem

human tissue identified Mbp+Cd74+ oligodendrocytes and linked them to AD progression (Park et al., 2023). While interesting, the significance of this pathway in ALS is not well-understood and requires further research. Cd74+ oligodendrocytes, however, were not observed in our dataset.

The GAS (Growth-Arrest Specific) family's contribution to cell growth, proliferation, and apoptosis, with implications in neurodevelopment and degeneration, further exemplifies the complexity of cellular responses to neural challenges. For instance, the possibility of GAS1 (LR pair: Shh-Gas1) protecting against neurodegeneration by promoting neuronal differentiation provides a potential for modulating cell growth pathways (Bautista et al., 2018; Zarco et al., 2013). However, CellChat has listed Gas6 as the only ligand in this pathway, with the following receptor genes: Axl (present in our dataset in microglia), Mertk (in microglia and astrocyte), and Tyro3 (in oligodendrocyte). These interactions have been described in cancer and platelet considerations (Wu et al., 2018; Zhai et al., 2023), but not in ALS. More specific research is needed to prove exactly how relevant this pathway can be in ALS.

Lastly, the MPZ (Myelin Protein Zero) pathway, essential for myelin sheath formation and maintenance, highlights the critical role of myelination in neural function and the potential impact of myelin disruption in neurodegenerative diseases (Shy, 2006). MPZ is a major PNS myelination protein, accounting for more than 50% of all PNS proteins (Shy, 2006). Further investigation into our data indicates that very few cells express the Mpz gene (less than 0.03% of cells), with very little overall expression amounts. Given the low expression, the modulation of this pathway could be an artifact due to low expression, however, more careful research is needed to draw firm conclusions.

Determining the precise role of signaling modulations in the progression of neurodegenerative diseases—whether they exacerbate or counteract disease mechanisms—necessitates focused and targeted research. Such investigations go beyond the scope of our current study, yet it is essential to acknowledge the complexity and nuanced impact of these signaling changes. One observation here was the lower number of inflammatory pathways in CellChat analysis compared to

other pathways. For example, we see phosphorylation of STAT3 with WB (from a previous study), but this is not a major pathway described in CellChat. Moreover, recent research claims that snRNAseq is not suitable for the description of activation states of microglia, at least in humans (Thrupp et al., 2020). This is an important point that could also have implications for signaling pathways.

Our findings illuminate that the pathways most significantly affected by transgene expression across all cell types are intricately linked with crucial physiological and pathological processes. These include myelination, which is fundamental for the efficient transmission of neural signals; the organization of the extracellular matrix (ECM) and the blood-brain barrier (BBB), both critical for maintaining neural tissue structure and protecting the neural environment; inflammation, which can both support and hinder neural function depending on the context; and neuronal growth, protection, and degeneration, which are directly involved in progression as well as onset of neurodegenerative diseases.

Our research has led to the identification of oligodendrocytes as the primary targets of CD therapy in the context of neurodegenerative diseases. The analysis of signaling pathways within oligodendrocytes has brought the LAMININ pathway into focus as a critical target of CD therapy. Laminins, integral glycoproteins of the ECM, play pivotal roles in a myriad of cellular processes, including cell adhesion, differentiation, migration, neurite outgrowth, and the maintenance of the BBB (Colognato & Yurchenco, 2000). Their significance extends to the development of oligodendrocytes and the process of myelination, underscoring their essential contribution to central nervous system (CNS) integrity and functionality (Kang & Yao, 2022). Over 143 LR pairs in the LAMININ pathway are listed in the CellChat database (Jin et al., 2021), with many of those interactions also observed in our dataset. Figure 33 visualizes gene expression changes in some of the major components of this pathway, namely laminins and integrins.

Our investigation into ligand-receptor pairs has spotlighted the interaction between Laminin α2 (encoded by the Lama2 gene) and integrin β4, with Laminin α2 implicated in CNS myelination processes (Relucio, 2011). Notably, we observed

downregulation of the Lama2 gene in both spinal cord tissue of patients, based on data from TargetALS patient RNA sequencing ((TargetALS-Postmortem-Tissue-Core, 2020), analysis courtesy of Dieter Edbauer) and mature oligodendrocytes in the Tg_Vehicle condition. This downregulation appears to be ameliorated following CD treatment, suggesting a therapeutic effect of CD on the LAMININ pathway and, by extension, oligodendrocyte function and myelination.

The relevance of Lama2 extends to clinical observations, as mutations in this gene are associated with a form of congenital muscular dystrophy characterized by aberrant CNS white matter signals on MRI, further indicating the critical role of Laminin α2 in neural health (Arreguin & Colognato, 2020). The evidence points to Lama2 as a promising therapeutic target warranting further detailed investigation, however, more research is needed to confirm this.

These findings not only highlight the potential for targeted therapies aimed at restoring myelination and oligodendrocyte function but also underscore the necessity for continued research into the mechanisms by which CD therapy influences neurodegenerative disease pathways. The identification of Lama2 and the LAMININ pathway as key components in this therapeutic context could provide new avenues for research, aiming to unravel the complex interplay between ECM components, oligodendrocyte development, and myelination in the pursuit of symptomatic or curative treatments for neurodegenerative diseases. Nevertheless, these results should not be overinterpreted and any subsequent experiment should require extensive validation.

5.6 Oligodendrocyte PLIN4 As a Possible Marker of Disease and DAOs

One of the most prominent features of the GA-Nes mice in this dissertation was the discovery of disease-associated oligodendrocyte (DAO) signature. While the DAO signature in our dataset shares some key genes with published datasets (e.g., Serpina3n, Il33, and C4b), there are several unique markers, such as ApoD and Plin4; although Plin4 was described as a disease-specific oligodendrocyte marker by one study in MS (Falcão et al., 2018). While ApoD as a lipocalin might play a significant

role in cholesterol management, the absence of a reliable antibody against this protein complicates research efforts.

PLIN4, the least studied member of the perilipin family, differs markedly from its counterparts (Brasaemle, 2007). It is the most prevalent perilipin in muscle tissue, where its subsarcolemmal accumulation can lead to a distinct condition known as PLIN4-mediated myopathy, where PLIN4 accumulates in the subsarcolemmal regions within muscle fibers (Maggi et al., 2023). Although the full range of PLIN4 functions remains unclear, it is recognized as a marker of lipid droplets (Han et al., 2018). However, its role likely extends beyond merely encasing lipid droplets as we observed Plin4 upregulation but no major lipid droplet pathology in GA-Nes hippocampi. On the other hand, its role could simply be limited to encasing lipid droplets but clearance and transport issues in our model might have prevented the formation of lipid droplets.

In a 2018 Nature Medicine study, Falcão et al. discovered that PLIN4 is also expressed by oligodendrocytes in an EAE model, particularly by those exhibiting the disease signature (e.g., Serpina3n, C4b), which they termed disease-specific oligodendrocytes. Intriguingly, this study also observed a staining pattern identical to ours, underscoring the potential of PLIN4 as a marker for disease-specific oligodendrocytes (Falcão et al., 2018).

Another study by Zhu et al. uncovered the direct relevance of PLIN4 in ALS, demonstrating widespread expression of Plin4 in the spinal cord of $SOD1^{G93A}$ mice. This expression notably increased from pre-onset through onset to progression stages, correlating with neuronal death (Zhu et al., 2021). Contrary to our findings, which highlighted PLIN4 immunostaining predominantly in oligodendrocytes (although sometimes in other cells), Zhu et al. reported primarily neuronal expression. They proposed that alterations in Plin4 expression and distribution might play a role in neuron death (Zhu et al., 2021). Our gene expression data, however, indicates that only oligodendrocytes express Plin4. The detection of PLIN4 in other cell types might involve intercellular transport but should be further investigated. However, we could not colocalize the PLIN4 signal with CNP^{+} oligodendrocytes or $GFAP^{+}$ astrocytes in patient immunostainings. This indicates the need for further studies on the cellular

distribution of PLIN4 and its role in ALS pathology. More optimized antibodies might pave the way for such studies.

The question of whether PLIN4 contributes to neuronal death directly or as a consequence of lipid metabolism issues remains unresolved. Oil Red O staining revealed no large lipid droplets in the hippocampi of GA-Nes mice (Figure 41). Scanning electron microscopy detected some amorphous electron-dense material (data not shown) but did not reveal any significant accumulation of lipid droplets, suggesting the complexity of PLIN4's involvement in ALS pathology requires further investigation.

Nonetheless, the observed upregulation of PLIN4 in the spinal cords of ALS patients (TargetALS-Postmortem-Tissue-Core, 2020), together with its expression in $SOD1^{G93A}$ spinal cords (Zhu et al., 2021), and its oligodendrocyte-specific expression in the EAE mouse model of MS (Falcão et al., 2018), supports a significant role for Plin4 in disease mechanisms. Plin4 thus emerges not only as a potential marker of disease progression but also as a candidate for therapeutic targeting, especially in the context of demyelination, as the studies reporting Plin4 upregulation have also coincided with myelin damage. Cholesterol can be released from degraded myelin, leading to cholesterol overload, which necessitates esterification and subsequently storage, where PLIN4 plays a role.

6. Concluding Remarks and Future Directions

In this dissertation, I have detailed the strategies deployed during my doctoral research to address the poly(GA)-related pathology of ALS in a fast-progressing mouse model. Despite high anticipation, an anti-inflammatory treatment using a JAK inhibitor (baricitinib) did not significantly alter the survival outcomes of GA-Nes mice, likely attributed to the extreme level of neuroinflammation and, potentially, the delayed initiation of treatment. This suggests that for anti-inflammatory therapy to be effective in ALS, the therapeutic approach should clearly define the optimal therapeutic window and dosage. A possible strategy might involve administering the drug through chow, including to the dams, to ensure exposure before weaning, as neuroinflammation is already present at 3 weeks of age. However, the potential adverse effects of broadly inhibiting the immune system in developing mice must be cautiously considered, given the critical role of the immune system in development (Mehl et al., 2022). Nevertheless, this would not be an issue when treating ALS patients.

Additionally, dietary modification in GA-Nes mice, aimed at influencing survival, yielded neither positive nor negative outcomes. Insights from our subsequent snRNAseq study and CD treatment indicate that future dietary interventions should specifically target the inclusion of various lipids in high concentrations. Metabolic monitoring could be effectively conducted using metabolic cages, providing a direct measure of the intervention's impact and nominating specific lipid classes for dietary supplementation in mice and potentially patients. For cellular metabolic studies, explicit use of motoneurons is needed to highlight differences in ATP or NADH levels.

CD treatment, conversely, showed promising effects on survival in a subset of female GA-Nes mice (but not male). Our investigations revealed a disorder in cholesterol metabolism within these mice, thereby laying a stronger foundation for the application of CD therapy. Notably, while cholesterol esters experienced an upregulation, cholesterol levels themselves were found to be downregulated, and remained unchanged upon CD treatment. While it is possible that not all cells experience cholesterol overload, this discrepancy may be attributed to perfusion in case most of the cholesterol is deposited peripherally. Future research should

investigate the blood cholesterol levels as well as brain levels. Measurement of cholesterol metabolites can provide more information on the mechanism and guide research to discover a more effective therapy.

Intriguingly, large lipid droplets were not observed in the SEM analysis of untreated transgenic animals, despite significant upregulation of cholesterol esters and Plin4 expression in transgenic mice. This may suggest a potential disruption in lipid droplet formation in GA-Nes, possibly indicative of underlying issues in lipid clearance and transport mechanisms. Additionally, we observed a distinct myelination phenotype; SEM revealed a notably thinner corpus callosum in untreated transgenic mice, a finding corroborated by LFB staining, which showed reduced white matter width. CD treatment of transgenic mice resulted in a partial mitigation of these effects. Further investigation through CellChat signaling analysis also pointed to notable alterations in myelination processes. However, it remains unclear whether CD therapy primarily inhibits demyelination or fosters remyelination, necessitating additional experiments across various time points to elucidate this mechanism.

Looking ahead, exploring varying dosages and treatment regimens of CD, not only in the GA-Nes mouse model but also in other ALS models, will be instrumental in assessing the broader applicability of CD therapy for ALS. This expanded research scope will enable a more comprehensive understanding of CD's therapeutic potential across different ALS pathologies. Moreover, the pursuit of cyclodextrin trials is essential for identifying a non-ototoxic formulation that can serve as a viable complementary therapy for ALS patients. Investigation of DAOs and lipid metabolism, especially a potential gender effect, in the context of ALS, can provide specific therapeutic targets that can potentially alleviate the disease, possibly with fewer side effects.

Bibliography

Abdel-Khalik, J., Yutuc, E., Crick, P. J., Gustafsson, J. A., Warner, M., Roman, G., Talbot, K., Gray, E., Griffiths, W. J., Turner, M. R., & Wang, Y. (2017). Defective cholesterol metabolism in amyotrophic lateral sclerosis. *J Lipid Res*, *58*(1), 267-278. https://doi.org/10.1194/jlr.P071639

Abo-Rady, M., Kalmbach, N., Pal, A., Schludi, C., Janosch, A., Richter, T., Freitag, P., Bickle, M., Kahlert, A. K., Petri, S., Stefanov, S., Glass, H., Staege, S., Just, W., Bhatnagar, R., Edbauer, D., Hermann, A., Wegner, F., & Sterneckert, J. L. (2020). Knocking out C9ORF72 Exacerbates Axonal Trafficking Defects Associated with Hexanucleotide Repeat Expansion and Reduces Levels of Heat Shock Proteins. *Stem Cell Reports*, *14*(3), 390-405. https://doi.org/10.1016/j.stemcr.2020.01.010

Agrawal, N., Farhat, N. Y., Sinaii, N., Do, A. D., Xiao, C., Berry-Kravis, E., Bianconi, S., Masvekar, R., Bielekova, B., Solomon, B., & Porter, F. D. (2023). Neurofilament light chain in cerebrospinal fluid as a novel biomarker in evaluating both clinical severity and therapeutic response in Niemann-Pick disease type C1. *Genetics in Medicine*, *25*(3). https://doi.org/10.1016/j.gim.2022.11.017

Alboukadel Kassambara, M. K., Przemyslaw Biecek, Scheipl Fabian. (2021). *survminer: Drawing Survival Curves using 'ggplot2'*. In (Version 0.4.9) https://CRAN.R-project.org/package=survminer

Allen, S. P., Hall, B., Woof, R., Francis, L., Gatto, N., Shaw, A. C., Myszczynska, M., Hemingway, J., Coldicott, I., Willcock, A., Job, L., Hughes, R. M., Boschian, C., Bayatti, N., Heath, P. R., Bandmann, O., Mortiboys, H., Ferraiuolo, L., & Shaw, P. J. (2019). C9orf72 expansion within astrocytes reduces metabolic flexibility in amyotrophic lateral sclerosis. *Brain*, *142*(12), 3771-3790. https://doi.org/10.1093/brain/awz302

Amaducci, L., Antuono, P., Bartolini, L., De Medio, G. E., Inzitari, D., & Porcellati, G. (1978). A possible mechanism for cholesteryl ester formation during demyelination. *Neurochemical Research*, *3*(6), 725-731. https://doi.org/10.1007/BF00965995

Amezquita, R. A., Lun, A. T. L., Becht, E., Carey, V. J., Carpp, L. N., Geistlinger, L., Marini, F., Rue-Albrecht, K., Risso, D., Soneson, C., Waldron, L., Pages, H., Smith, M. L., Huber, W., Morgan, M., Gottardo, R., & Hicks, S. C. (2020). Orchestrating single-cell analysis with Bioconductor. *Nat Methods*, *17*(2), 137-145. https://doi.org/10.1038/s41592-019-0654-x

Andersen, P. M., & Al-Chalabi, A. (2011). Clinical genetics of amyotrophic lateral sclerosis: what do we really know? *Nat Rev Neurol*, *7*(11), 603-615. https://doi.org/10.1038/nrneurol.2011.150

Antlsperger, G., & Schmid, G. (1996, 1996//). Toxicological Comparison of Cyclodextrins. Proceedings of the Eighth International Symposium on Cyclodextrins, Dordrecht.

Appel, S. H., Beers, D. R., & Zhao, W. (2021). Amyotrophic lateral sclerosis is a systemic disease: peripheral contributions to inflammation-mediated neurodegeneration. *Current Opinion in Neurology*, *34*(5), 765-772. https://doi.org/10.1097/wco.0000000000000983

Appeldoorn, T. Y. J., Munnink, T. H. O., Morsink, L. M., Hooge, M. N. L., & Touw, D. J. (2023). Pharmacokinetics and Pharmacodynamics of Ruxolitinib: A Review. *Clin Pharmacokinet*, *62*(4), 559-571. https://doi.org/10.1007/s40262-023-01225-7

Arreguin, A. J., & Colognato, H. (2020). Brain Dysfunction in LAMA2-Related Congenital Muscular Dystrophy: Lessons From Human Case Reports and Mouse Models. *Frontiers in Molecular Neuroscience*, *13*. https://doi.org/10.3389/fnmol.2020.00118

Ash, P. E., Bieniek, K. F., Gendron, T. F., Caulfield, T., Lin, W. L., Dejesus-Hernandez, M., van Blitterswijk, M. M., Jansen-West, K., Paul, J. W., 3rd, Rademakers, R., Boylan, K. B., Dickson, D. W., & Petrucelli, L. (2013). Unconventional translation of C9ORF72 GGGGCC expansion generates insoluble polypeptides specific to c9FTD/ALS. *Neuron*, *77*(4), 639-646. https://doi.org/10.1016/j.neuron.2013.02.004

Azizidoost, S. H., Babaahmadi-Rezaei, H., Nazeri, Z., Cheraghzadeh, M., & Kheirollah, A. (2021). Impact of Methyl-beta-Cyclodextrin and Apolipoprotein A-I on The Expression of ATP-Binding Cassette Transporter A1 and Cholesterol Depletion in C57BL/6 Mice Astrocytes. *Cell J*, *23*(1), 93-98. https://doi.org/10.22074/cellj.2021.7061

Balendra, R., & Isaacs, A. M. (2018). C9orf72-mediated ALS and FTD: multiple pathways to disease. *Nat Rev Neurol*, *14*(9), 544-558. https://doi.org/10.1038/s41582-018-0047-2

Bateman, A., & Bennett, H. P. (2009). The granulin gene family: from cancer to dementia. *Bioessays*, *31*(11), 1245-1254. https://doi.org/10.1002/bies.200900086

Bautista, E., Zarco, N., Aguirre-Pineda, N., Lara-Lozano, M., Vergara, P., Gonzalez-Barrios, J. A., Aguilar-Roblero, R., & Segovia, J. (2018). Expression of Gas1 in Mouse Brain: Release and Role in Neuronal Differentiation. *Cell Mol Neurobiol*, *38*(4), 841-859. https://doi.org/10.1007/s10571-017-0559-0

Baysoy, A., Bai, Z., Satija, R., & Fan, R. (2023). The technological landscape and applications of single-cell multi-omics. *Nature Reviews Molecular Cell Biology*, *24*(10), 695-713. https://doi.org/10.1038/s41580-023-00615-w

Beck, J., Poulter, M., Hensman, D., Rohrer, J. D., Mahoney, C. J., Adamson, G., Campbell, T., Uphill, J., Borg, A., Fratta, P., Orrell, R. W., Malaspina, A., Rowe, J., Brown, J., Hodges, J., Sidle, K., Polke, J. M., Houlden, H., Schott, J. M., . . . Mead, S. (2013). Large C9orf72 hexanucleotide repeat expansions are seen in multiple neurodegenerative syndromes and are more frequent than expected in the UK population. *Am J Hum Genet*, *92*(3), 345-353. https://doi.org/10.1016/j.ajhg.2013.01.011

Becktel, D. A., Zbesko, J. C., Frye, J. B., Chung, A. G., Hayes, M., Calderon, K., Grover, J. W., Li, A., Garcia, F. G., Tavera-Garcia, M. A., Schnellmann, R. G., Wu, H. J., Nguyen, T. V., & Doyle, K. P. (2022). Repeated Administration of 2-Hydroxypropyl-beta-Cyclodextrin (HPbetaCD) Attenuates the Chronic Inflammatory Response to Experimental Stroke. *J Neurosci*, *42*(2), 325-348. https://doi.org/10.1523/JNEUROSCI.0933-21.2021

Beers, D. R., & Appel, S. H. (2019). Immune dysregulation in amyotrophic lateral sclerosis: mechanisms and emerging therapies. *Lancet Neurol*, *18*(2), 211-220. https://doi.org/10.1016/S1474-4422(18)30394-6

Beland, L. C., Markovinovic, A., Jakovac, H., De Marchi, F., Bilic, E., Mazzini, L., Kriz, J., & Munitic, I. (2020). Immunity in amyotrophic lateral sclerosis: blurred lines between excessive inflammation and inefficient immune responses. *Brain Commun*, *2*(2), fcaa124. https://doi.org/10.1093/braincomms/fcaa124

Bernstein, D. L., Hulkova, H., Bialer, M. G., & Desnick, R. J. (2013). Cholesteryl ester storage disease: review of the findings in 135 reported patients with an underdiagnosed disease. *J Hepatol*, *58*(6), 1230-1243. https://doi.org/10.1016/j.jhep.2013.02.014

Berry-Kravis, E. (2021). Niemann-Pick Disease, Type C: Diagnosis, Management and Disease-Targeted Therapies in Development. *Semin Pediatr Neurol*, *37*, 100879. https://doi.org/10.1016/j.spen.2021.100879

Bezakova, G., & Ruegg, M. A. (2003). New insights into the roles of agrin. *Nature Reviews Molecular Cell Biology*, *4*(4), 295-309. https://doi.org/10.1038/nrm1074

Billnitzer, A. J., Barskaya, I., Yin, C., & Perez, R. G. (2013). APP independent and dependent effects on neurite outgrowth are modulated by the receptor associated protein (RAP). *J Neurochem*, *124*(1), 123-132. https://doi.org/10.1111/jnc.12051

Blanchard, J. W., Akay, L. A., Davila-Velderrain, J., von Maydell, D., Mathys, H., Davidson, S. M., Effenberger, A., Chen, C. Y., Maner-Smith, K., Hajjar, I., Ortlund, E. A., Bula, M., Agbas, E., Ng, A., Jiang, X., Kahn, M., Blanco-Duque, C., Lavoie, N., Liu, L., . . . Tsai, L. H. (2022). APOE4 impairs myelination via cholesterol dysregulation in oligodendrocytes. *Nature*, *611*(7937), 769-779. https://doi.org/10.1038/s41586-022-05439-w

Bousoik, E., & Montazeri Aliabadi, H. (2018). "Do We Know Jack" About JAK? A Closer Look at JAK/STAT Signaling Pathway. *Front Oncol*, *8*, 287. https://doi.org/10.3389/fonc.2018.00287

Bouteloup, C., Desport, J. C., Clavelou, P., Guy, N., Derumeaux-Burel, H., Ferrier, A., & Couratier, P. (2009). Hypermetabolism in ALS patients: an early and persistent phenomenon. *J Neurol*, *256*(8), 1236-1242. https://doi.org/10.1007/s00415-009-5100-z

Bradski, G. (2000). The OpenCV Library. *Dr. Dobb's Journal of Software Tools*.

Brasaemle, D. L. (2007). Thematic review series: Adipocyte Biology. The perilipin family of structural lipid droplet proteins: stabilization of lipid droplets and control of lipolysis. *Journal of Lipid Research*, *48*(12), 2547-2559. https://doi.org/10.1194/jlr.R700014-JLR200

Brasaemle, D. L., Barber, T., Wolins, N. E., Serrero, G., Blanchette-Mackie, E. J., & Londos, C. (1997). Adipose differentiation-related protein is an ubiquitously expressed lipid storage droplet-associated protein. *J Lipid Res*, *38*(11), 2249-2263. https://www.ncbi.nlm.nih.gov/pubmed/9392423

Bronstein, J. M., Tiwari-Woodruff, S., Buznikov, A. G., & Stevens, D. B. (2000). Involvement of OSP/claudin-11 in oligodendrocyte membrane interactions: role in biology and disease. *J Neurosci Res*, *59*(6), 706-711. https://doi.org/10.1002/(SICI)1097-4547(20000315)59:6<706::AID-JNR2>3.0.CO;2-D

Byrne, S., Elamin, M., Bede, P., Shatunov, A., Walsh, C., Corr, B., Heverin, M., Jordan, N., Kenna, K., Lynch, C., McLaughlin, R. L., Iyer, P. M., O'Brien, C., Phukan, J., Wynne, B., Bokde, A. L., Bradley, D. G., Pender, N., Al-Chalabi, A., & Hardiman, O. (2012). Cognitive and clinical characteristics of patients with amyotrophic lateral sclerosis carrying a C9orf72 repeat expansion: a population-based cohort study. *Lancet Neurol*, *11*(3), 232-240. https://doi.org/10.1016/S1474-4422(12)70014-5

Cai, Z., & Xiao, M. (2016). Oligodendrocytes and Alzheimer's disease. *International Journal of Neuroscience*, *126*(2), 97-104. https://doi.org/10.3109/00207454.2015.1025778

Calias, P. (2017). 2-Hydroxypropyl-beta-cyclodextrins and the Blood-Brain Barrier: Considerations for Niemann-Pick Disease Type C1. *Curr Pharm Des*, *23*(40), 6231-6238. https://doi.org/10.2174/1381612823666171019164220

Camargo, F., Erickson, R. P., Garver, W. S., Hossain, G. S., Carbone, P. N., Heidenreich, R. A., & Blanchard, J. (2001). Cyclodextrins in the treatment of a mouse model of Niemann-Pick C disease. *Life Sci*, *70*(2), 131-142. https://doi.org/10.1016/s0024-3205(01)01384-4

Cantuti-Castelvetri, L., Fitzner, D., Bosch-Queralt, M., Weil, M.-T., Su, M., Sen, P., Ruhwedel, T., Mitkovski, M., Trendelenburg, G., Lütjohann, D., Möbius, W., & Simons, M. (2018). Defective

cholesterol clearance limits remyelination in the aged central nervous system. *Science*, *359*(6376), 684-688. https://doi.org/10.1126/science.aan4183

Cembrowski, M. S., Wang, L., Sugino, K., Shields, B. C., & Spruston, N. (2016). Hipposeq: a comprehensive RNA-seq database of gene expression in hippocampal principal neurons. *eLife*, *5*. https://doi.org/10.7554/eLife.14997

Chang, T. Y., Chang, C. C., Ohgami, N., & Yamauchi, Y. (2006). Cholesterol sensing, trafficking, and esterification. *Annu Rev Cell Dev Biol*, *22*, 129-157. https://doi.org/10.1146/annurev.cellbio.22.010305.104656

Chen, X., Yazdani, S., Piehl, F., Magnusson, P. K. E., & Fang, F. (2018). Polygenic link between blood lipids and amyotrophic lateral sclerosis. *Neurobiol Aging*, *67*, 202 e201-202 e206. https://doi.org/10.1016/j.neurobiolaging.2018.03.022

Chen, Y., Quan, S., Patil, V., Kunjamma, R. B., Tokars, H. M., Leisten, E. D., Chan, J., Wong, Y., & Popko, B. (2023). Insights into the mechanism of oligodendrocyte protection and remyelination enhancement by the integrated stress response. *bioRxiv*. https://doi.org/10.1101/2023.01.23.525156

Chio, A., Logroscino, G., Hardiman, O., Swingler, R., Mitchell, D., Beghi, E., Traynor, B. G., & Eurals, C. (2009). Prognostic factors in ALS: A critical review. *Amyotroph Lateral Scler*, *10*(5-6), 310-323. https://doi.org/10.3109/17482960802566824

Chio, A., Logroscino, G., Traynor, B. J., Collins, J., Simeone, J. C., Goldstein, L. A., & White, L. A. (2013). Global epidemiology of amyotrophic lateral sclerosis: a systematic review of the published literature. *Neuroepidemiology*, *41*(2), 118-130. https://doi.org/10.1159/000351153

Cicardi, M. E., Cristofani, R., Rusmini, P., Meroni, M., Ferrari, V., Vezzoli, G., Tedesco, B., Piccolella, M., Messi, E., Galbiati, M., Boncoraglio, A., Carra, S., Crippa, V., & Poletti, A. (2018). Tdp-25 Routing to Autophagy and Proteasome Ameliorates its Aggregation in Amyotrophic Lateral Sclerosis Target Cells. *Sci Rep*, *8*(1), 12390. https://doi.org/10.1038/s41598-018-29658-2

Clayton, B. L. L., & Tesar, P. J. (2021). Oligodendrocyte progenitor cell fate and function in development and disease. *Curr Opin Cell Biol*, *73*, 35-40. https://doi.org/10.1016/j.ceb.2021.05.003

Coisne, C., Hallier-Vanuxeem, D., Boucau, M.-C., Hachani, J., Tilloy, S., Bricout, H., Monflier, E., Wils, D., Serpelloni, M., Parissaux, X., Fenart, L., & Gosselet, F. (2016). β-Cyclodextrins Decrease Cholesterol Release and ABC-Associated Transporter Expression in Smooth Muscle Cells and Aortic Endothelial Cells. *Frontiers in Physiology*, *7*. https://doi.org/10.3389/fphys.2016.00185

Colognato, H., & Yurchenco, P. D. (2000). Form and function: the laminin family of heterotrimers. *Dev Dyn*, *218*(2), 213-234. https://doi.org/10.1002/(SICI)1097-0177(200006)218:2<213::AID-DVDY1>3.0.CO;2-R

Corder, E. H., Saunders, A. M., Strittmatter, W. J., Schmechel, D. E., Gaskell, P. C., Small, G. W., Roses, A. D., Haines, J. L., & Pericak-Vance, M. A. (1993). Gene dose of apolipoprotein E type 4 allele and the risk of Alzheimer's disease in late onset families. *Science*, *261*(5123), 921-923. https://doi.org/10.1126/science.8346443

Crumling, M. A., King, K. A., & Duncan, R. K. (2017). Cyclodextrins and Iatrogenic Hearing Loss: New Drugs with Significant Risk. *Front Cell Neurosci*, *11*, 355. https://doi.org/10.3389/fncel.2017.00355

Cutler, R. G., Pedersen, W. A., Camandola, S., Rothstein, J. D., & Mattson, M. P. (2002). Evidence that accumulation of ceramides and cholesterol esters mediates oxidative stress-induced death of motor

neurons in amyotrophic lateral sclerosis. *Ann Neurol*, *52*(4), 448-457. https://doi.org/10.1002/ana.10312

Cykowski, M. D., Dickson, D. W., Powell, S. Z., Arumanayagam, A. S., Rivera, A. L., & Appel, S. H. (2019). Dipeptide repeat (DPR) pathology in the skeletal muscle of ALS patients with C9ORF72 repeat expansion. *Acta Neuropathol*, *138*(4), 667-670. https://doi.org/10.1007/s00401-019-02050-8

D'Amico, E., Grosso, G., Nieves, J. W., Zanghi, A., Factor-Litvak, P., & Mitsumoto, H. (2021). Metabolic Abnormalities, Dietary Risk Factors and Nutritional Management in Amyotrophic Lateral Sclerosis. *Nutrients*, *13*(7). https://doi.org/10.3390/nu13072273

Dai, X., Sayama, K., Yamasaki, K., Tohyama, M., Shirakata, Y., Hanakawa, Y., Tokumaru, S., Yahata, Y., Yang, L., Yoshimura, A., & Hashimoto, K. (2006). SOCS1-negative feedback of STAT1 activation is a key pathway in the dsRNA-induced innate immune response of human keratinocytes. *J Invest Dermatol*, *126*(7), 1574-1581. https://doi.org/10.1038/sj.jid.5700294

Dang, C., Lu, Y., Chen, X., & Li, Q. (2021). Baricitinib Ameliorates Experimental Autoimmune Encephalomyelitis by Modulating the Janus Kinase/Signal Transducer and Activator of Transcription Signaling Pathway. *Frontiers in Immunology*, *12*. https://doi.org/10.3389/fimmu.2021.650708

Davison, C. (1941). Amyotrophic Lateral Sclerosis. *Archives of Neurology & Psychiatry*, *46*(6). https://doi.org/10.1001/archneurpsyc.1941.02280240094006

De Marchi, F., Munitic, I., Amedei, A., Berry, J. D., Feldman, E. L., Aronica, E., Nardo, G., Van Weehaeghe, D., Niccolai, E., Prtenjaca, N., Sakowski, S. A., Bendotti, C., & Mazzini, L. (2021). Interplay between immunity and amyotrophic lateral sclerosis: Clinical impact. *Neurosci Biobehav Rev*, *127*, 958-978. https://doi.org/10.1016/j.neubiorev.2021.06.027

DeJesus-Hernandez, M., Mackenzie, I. R., Boeve, B. F., Boxer, A. L., Baker, M., Rutherford, N. J., Nicholson, A. M., Finch, N. A., Flynn, H., Adamson, J., Kouri, N., Wojtas, A., Sengdy, P., Hsiung, G. Y., Karydas, A., Seeley, W. W., Josephs, K. A., Coppola, G., Geschwind, D. H., . . . Rademakers, R. (2011). Expanded GGGGCC hexanucleotide repeat in noncoding region of C9ORF72 causes chromosome 9p-linked FTD and ALS. *Neuron*, *72*(2), 245-256. https://doi.org/10.1016/j.neuron.2011.09.011

Desport, J. C., Preux, P. M., Truong, T. C., Vallat, J. M., Sautereau, D., & Couratier, P. (1999). Nutritional status is a prognostic factor for survival in ALS patients. *Neurology*, *53*(5), 1059-1063. https://doi.org/10.1212/wnl.53.5.1059

Di Paolo, G., & Kim, T.-W. (2011). Linking lipids to Alzheimer's disease: cholesterol and beyond. *Nature Reviews Neuroscience*, *12*(5), 284-296. https://doi.org/10.1038/nrn3012

Diagnosis, E. T. F. o., Management of Amyotrophic Lateral, S., Andersen, P. M., Abrahams, S., Borasio, G. D., de Carvalho, M., Chio, A., Van Damme, P., Hardiman, O., Kollewe, K., Morrison, K. E., Petri, S., Pradat, P. F., Silani, V., Tomik, B., Wasner, M., & Weber, M. (2012). EFNS guidelines on the clinical management of amyotrophic lateral sclerosis (MALS)--revised report of an EFNS task force. *Eur J Neurol*, *19*(3), 360-375. https://doi.org/10.1111/j.1468-1331.2011.03501.x

Dietschy, J. M. (2009). Central nervous system: cholesterol turnover, brain development and neurodegeneration. *Biol Chem*, *390*(4), 287-293. https://doi.org/10.1515/BC.2009.035

Dodge, J. C., Jensen, E. H., Yu, J., Sardi, S. P., Bialas, A. R., Taksir, T. V., Bangari, D. S., & Shihabuddin, L. S. (2020). Neutral Lipid Cacostasis Contributes to Disease Pathogenesis in Amyotrophic Lateral Sclerosis. *J Neurosci*, *40*(47), 9137-9147. https://doi.org/10.1523/JNEUROSCI.1388-20.2020

Dodge, J. C., Treleaven, C. M., Pacheco, J., Cooper, S., Bao, C., Abraham, M., Cromwell, M., Sardi, S. P., Chuang, W.-L., Sidman, R. L., Cheng, S. H., & Shihabuddin, L. S. (2015). Glycosphingolipids are modulators of disease pathogenesis in amyotrophic lateral sclerosis. *Proceedings of the National Academy of Sciences*, *112*(26), 8100-8105. https://doi.org/10.1073/pnas.1508767112

Donnelly, C. J., Zhang, P. W., Pham, J. T., Haeusler, A. R., Mistry, N. A., Vidensky, S., Daley, E. L., Poth, E. M., Hoover, B., Fines, D. M., Maragakis, N., Tienari, P. J., Petrucelli, L., Traynor, B. J., Wang, J., Rigo, F., Bennett, C. F., Blackshaw, S., Sattler, R., & Rothstein, J. D. (2013). RNA toxicity from the ALS/FTD C9ORF72 expansion is mitigated by antisense intervention. *Neuron*, *80*(2), 415-428. https://doi.org/10.1016/j.neuron.2013.10.015

Dupuis, L., & Chio, A. (2023). The “metabolic axis” of ALS: The role of body weight in disease pathogenesis. *Muscle & Nerve*, *67*(3), 191-192. https://doi.org/10.1002/mus.27784

Dupuis, L., Corcia, P., Fergani, A., Gonzalez De Aguilar, J. L., Bonnefont-Rousselot, D., Bittar, R., Seilhean, D., Hauw, J. J., Lacomblez, L., Loeffler, J. P., & Meininger, V. (2008). Dyslipidemia is a protective factor in amyotrophic lateral sclerosis. *Neurology*, *70*(13), 1004-1009. https://doi.org/10.1212/01.wnl.0000285080.70324.27

Dupuis, L., Oudart, H., Rene, F., Gonzalez de Aguilar, J. L., & Loeffler, J. P. (2004). Evidence for defective energy homeostasis in amyotrophic lateral sclerosis: benefit of a high-energy diet in a transgenic mouse model. *Proc Natl Acad Sci U S A*, *101*(30), 11159-11164. https://doi.org/10.1073/pnas.0402026101

Dupuis, L., Pradat, P. F., Ludolph, A. C., & Loeffler, J. P. (2011). Energy metabolism in amyotrophic lateral sclerosis. *Lancet Neurol*, *10*(1), 75-82. https://doi.org/10.1016/S1474-4422(10)70224-6

Estes, R. E., Lin, B., Khera, A., & Davis, M. Y. (2021). Lipid Metabolism Influence on Neurodegenerative Disease Progression: Is the Vehicle as Important as the Cargo? *Front Mol Neurosci*, *14*, 788695. https://doi.org/10.3389/fnmol.2021.788695

Ethun, K. (2016). Chapter 9 - Sex and Gender Differences in Body Composition, Lipid Metabolism, and Glucose Regulation. In G. N. Neigh & M. M. Mitzelfelt (Eds.), *Sex Differences in Physiology* (pp. 145-165). Academic Press. https://doi.org/https://doi.org/10.1016/B978-0-12-802388-4.00009-4

Eva Maxfield Brown, D. T., Jamie Sherman, Madison Swain-Bowden, Talley Lambert, and AICSImageIO Contributors. (2021). *AICSImageIO: Image Reading, Metadata Conversion, and Image Writing for Microscopy Images in Pure Python*. In GitHub. https://github.com/AllenCellModeling/aicsimageio

Falcão, A. M., van Bruggen, D., Marques, S., Meijer, M., Jäkel, S., Agirre, E., Samudyata, Floriddia, E. M., Vanichkina, D. P., ffrench-Constant, C., Williams, A., Guerreiro-Cacais, A. O., & Castelo-Branco, G. (2018). Disease-specific oligodendrocyte lineage cells arise in multiple sclerosis. *Nature Medicine*, *24*(12), 1837-1844. https://doi.org/10.1038/s41591-018-0236-y

Fang, T., Jozsa, F., & Al-Chalabi, A. (2017). Nonmotor Symptoms in Amyotrophic Lateral Sclerosis: A Systematic Review. *Int Rev Neurobiol*, *134*, 1409-1441. https://doi.org/10.1016/bs.irn.2017.04.009

Farg, M. A., Sundaramoorthy, V., Sultana, J. M., Yang, S., Atkinson, R. A., Levina, V., Halloran, M. A., Gleeson, P. A., Blair, I. P., Soo, K. Y., King, A. E., & Atkin, J. D. (2014). C9ORF72, implicated in amytrophic lateral sclerosis and frontotemporal dementia, regulates endosomal trafficking. *Hum Mol Genet*, *23*(13), 3579-3595. https://doi.org/10.1093/hmg/ddu068

Figueroa-Romero, C., Monteagudo, A., Murdock, B. J., Famie, J. P., Webber-Davis, I. F., Piecuch, C. E., Teener, S. J., Pacut, C., Goutman, S. A., & Feldman, E. L. (2022). Tofacitinib Suppresses Natural

Killer Cells In Vitro and In Vivo: Implications for Amyotrophic Lateral Sclerosis. *Frontiers in Immunology*, *13*. https://doi.org/10.3389/fimmu.2022.773288

Foley, P. (2010). Lipids in Alzheimer's disease: A century-old story. *Biochim Biophys Acta*, *1801*(8), 750-753. https://doi.org/10.1016/j.bbalip.2010.05.004

Fossgreen, A. (2023, 4.12.2023). Anna kann wieder Treppen steigen und etwas durch die Nase atmen. *Tages-Anzeiger*. https://www.tagesanzeiger.ch/medizinisches-wunder-anna-kann-wieder-treppen-steigen-und-etwas-durch-die-nase-atmen-295585217116

Frantz, C., Stewart, K. M., & Weaver, V. M. (2010). The extracellular matrix at a glance. *J Cell Sci*, *123*(Pt 24), 4195-4200. https://doi.org/10.1242/jcs.023820

Franzén, O., Gan, L.-M., & Björkegren, J. L. M. (2019). PanglaoDB: a web server for exploration of mouse and human single-cell RNA sequencing data. *Database*, *2019*. https://doi.org/10.1093/database/baz046

Frömming, K.-H., & Szejtli, J. (1994). Pharmacokinetics and Toxicology of Cyclodextrins. In K.-H. Frömming & J. Szejtli (Eds.), *Cyclodextrins in Pharmacy* (pp. 33-44). Springer Netherlands. https://doi.org/10.1007/978-94-015-8277-3_3

G Martelotto, L. (2020). Frankenstein' protocol for nuclei isolation from fresh and frozen tissue for snRNAseq V.2. *protocols.io*. https://doi.org/10.17504/protocols.io.3fkgjkw

Garofalo, S., Cocozza, G., Bernardini, G., Savage, J., Raspa, M., Aronica, E., Tremblay, M. E., Ransohoff, R. M., Santoni, A., & Limatola, C. (2022). Blocking immune cell infiltration of the central nervous system to tame Neuroinflammation in Amyotrophic lateral sclerosis. *Brain Behav Immun*, *105*, 1-14. https://doi.org/10.1016/j.bbi.2022.06.004

Garten, A., Schuster, S., Penke, M., Gorski, T., de Giorgis, T., & Kiess, W. (2015). Physiological and pathophysiological roles of NAMPT and NAD metabolism. *Nature Reviews Endocrinology*, *11*(9), 535-546. https://doi.org/10.1038/nrendo.2015.117

Gavegnano, C., Haile, W. B., Hurwitz, S., Tao, S., Jiang, Y., Schinazi, R. F., & Tyor, W. R. (2019). Baricitinib reverses HIV-associated neurocognitive disorders in a SCID mouse model and reservoir seeding in vitro. *J Neuroinflammation*, *16*(1), 182. https://doi.org/10.1186/s12974-019-1565-6

Ghasemi, M., & Brown, R. H., Jr. (2018). Genetics of Amyotrophic Lateral Sclerosis. *Cold Spring Harb Perspect Med*, *8*(5). https://doi.org/10.1101/cshperspect.a024125

Giovannoni, F., & Quintana, F. J. (2020). The Role of Astrocytes in CNS Inflammation. *Trends Immunol*, *41*(9), 805-819. https://doi.org/10.1016/j.it.2020.07.007

Gonen, A., & Miller, Y. I. (2020). From Inert Storage to Biological Activity—In Search of Identity for Oxidized Cholesteryl Esters. *Frontiers in Endocrinology*, *11*. https://doi.org/10.3389/fendo.2020.602252

Gong, Z., Ba, L., & Zhang, M. (2022). Dysfunction of the oligodendrocytes in amyotrophic lateral sclerosis. *J Biomed Res*, *36*(5), 336-342. https://doi.org/10.7555/JBR.36.20220009

González De Aguilar, J.-L. (2019). Lipid Biomarkers for Amyotrophic Lateral Sclerosis. *Frontiers in Neurology*, *10*. https://doi.org/10.3389/fneur.2019.00284

Gould, S., & Scott, R. C. (2005). 2-Hydroxypropyl-β-cyclodextrin (HP-β-CD): A toxicology review. *Food and Chemical Toxicology*, *43*(10), 1451-1459. https://doi.org/10.1016/j.fct.2005.03.007

Goutman, S. A., Guo, K., Savelieff, M. G., Patterson, A., Sakowski, S. A., Habra, H., Karnovsky, A., Hur, J., & Feldman, E. L. (2022). Metabolomics identifies shared lipid pathways in independent amyotrophic lateral sclerosis cohorts. *Brain*, *145*(12), 4425-4439. https://doi.org/10.1093/brain/awac025

Greenberg, A. S., Coleman, R. A., Kraemer, F. B., McManaman, J. L., Obin, M. S., Puri, V., Yan, Q. W., Miyoshi, H., & Mashek, D. G. (2011). The role of lipid droplets in metabolic disease in rodents and humans. *J Clin Invest*, *121*(6), 2102-2110. https://doi.org/10.1172/JCI46069

Greenberg, A. S., Egan, J. J., Wek, S. A., Garty, N. B., Blanchette-Mackie, E. J., & Londos, C. (1991). Perilipin, a major hormonally regulated adipocyte-specific phosphoprotein associated with the periphery of lipid storage droplets. *J Biol Chem*, *266*(17), 11341-11346. https://www.ncbi.nlm.nih.gov/pubmed/2040638

Greene, C., Hanley, N., & Campbell, M. (2019). Claudin-5: gatekeeper of neurological function. *Fluids and Barriers of the CNS*, *16*(1), 3. https://doi.org/10.1186/s12987-019-0123-z

Greensmith, L., & Bryson, J. B. (2023). The cholesterol depleting agent, (2-Hydroxypropyl)-ss-cyclodextrin, does not affect disease progression in SOD1(G93A) mice. *Amyotroph Lateral Scler Frontotemporal Degener*, 1-7. https://doi.org/10.1080/21678421.2023.2239867

Guzel, M., Naziroglu, M., Akpinar, O., & Cinar, R. (2021). Interferon Gamma-Mediated Oxidative Stress Induces Apoptosis, Neuroinflammation, Zinc Ion Influx, and TRPM2 Channel Activation in Neuronal Cell Line: Modulator Role of Curcumin. *Inflammation*, *44*(5), 1878-1894. https://doi.org/10.1007/s10753-021-01465-4

Han, S., Gim, Y., Jang, E.-H., & Hur, E.-M. (2022). Functions and dysfunctions of oligodendrocytes in neurodegenerative diseases. *Frontiers in Cellular Neuroscience*, *16*. https://doi.org/10.3389/fncel.2022.1083159

Han, X., Liu, Y., Dai, Y., Xu, T., Hu, Q., Yi, X., Rui, L., Hu, G., & Hu, J. (2022). Neuronal SH2B1 attenuates apoptosis in an MPTP mouse model of Parkinson's disease via promoting PLIN4 degradation. *Redox Biology*, *52*, 102308. https://doi.org/https://doi.org/10.1016/j.redox.2022.102308

Han, X., Zhu, J., Zhang, X., Song, Q., Ding, J., Lu, M., Sun, S., & Hu, G. (2018). Plin4-Dependent Lipid Droplets Hamper Neuronal Mitophagy in the MPTP/p-Induced Mouse Model of Parkinson's Disease. *Front Neurosci*, *12*, 397. https://doi.org/10.3389/fnins.2018.00397

Hao, Y., Hao, S., Andersen-Nissen, E., Mauck, W. M., 3rd, Zheng, S., Butler, A., Lee, M. J., Wilk, A. J., Darby, C., Zager, M., Hoffman, P., Stoeckius, M., Papalexi, E., Mimitou, E. P., Jain, J., Srivastava, A., Stuart, T., Fleming, L. M., Yeung, B., . . . Satija, R. (2021). Integrated analysis of multimodal single-cell data. *Cell*, *184*(13), 3573-3587 e3529. https://doi.org/10.1016/j.cell.2021.04.048

Harris, C. R., Millman, K. J., van der Walt, S. J., Gommers, R., Virtanen, P., Cournapeau, D., Wieser, E., Taylor, J., Berg, S., Smith, N. J., Kern, R., Picus, M., Hoyer, S., van Kerkwijk, M. H., Brett, M., Haldane, A., Del Rio, J. F., Wiebe, M., Peterson, P., . . . Oliphant, T. E. (2020). Array programming with NumPy. *Nature*, *585*(7825), 357-362. https://doi.org/10.1038/s41586-020-2649-2

Hashimoto, Y., Greene, C., Munnich, A., & Campbell, M. (2023). The CLDN5 gene at the blood-brain barrier in health and disease. *Fluids and Barriers of the CNS*, *20*(1). https://doi.org/10.1186/s12987-023-00424-5

Hayashi, H. (2011). Lipid metabolism and glial lipoproteins in the central nervous system. *Biol Pharm Bull*, *34*(4), 453-461. https://doi.org/10.1248/bpb.34.453

helpful.dev. (2024). *Diagrams: Show Me*. In OpenAI. https://openai.com/

Hickman, S., Izzy, S., Sen, P., Morsett, L., & El Khoury, J. (2018). Microglia in neurodegeneration. *Nature Neuroscience*, *21*(10), 1359-1369. https://doi.org/10.1038/s41593-018-0242-x

Hirsch-Reinshagen, V., Burgess, B. L., & Wellington, C. L. (2009). Why lipids are important for Alzheimer disease? *Mol Cell Biochem*, *326*(1-2), 121-129. https://doi.org/10.1007/s11010-008-0012-2

Hoang, T. N., Pino, M., Boddapati, A. K., Viox, E. G., Starke, C. E., Upadhyay, A. A., Gumber, S., Nekorchuk, M., Busman-Sahay, K., Strongin, Z., Harper, J. L., Tharp, G. K., Pellegrini, K. L., Kirejczyk, S., Zandi, K., Tao, S., Horton, T. R., Beagle, E. N., Mahar, E. A., . . . Paiardini, M. (2021). Baricitinib treatment resolves lower-airway macrophage inflammation and neutrophil recruitment in SARS-CoV-2-infected rhesus macaques. *Cell*, *184*(2), 460-475 e421. https://doi.org/10.1016/j.cell.2020.11.007

Holzmann, C., Witt, M., Rolfs, A., Antipova, V., & Wree, A. (2021). Gender-Specific Effects of Two Treatment Strategies in a Mouse Model of Niemann-Pick Disease Type C1. *Int J Mol Sci*, *22*(5). https://doi.org/10.3390/ijms22052539

Hoque, S., Kondo, Y., Sakata, N., Yamada, Y., Fukaura, M., Higashi, T., Motoyama, K., Arima, H., Higaki, K., Hayashi, A., Komiya, T., Ishitsuka, Y., & Irie, T. (2020). Differential Effects of 2-Hydroxypropyl-Cyclodextrins on Lipid Accumulation in Npc1-Null Cells. *Int J Mol Sci*, *21*(3). https://doi.org/10.3390/ijms21030898

Hor, J.-H., Santosa, M. M., Lim, V. J. W., Ho, B. X., Taylor, A., Khong, Z. J., Ravits, J., Fan, Y., Liou, Y.-C., Soh, B.-S., & Ng, S.-Y. (2021). ALS motor neurons exhibit hallmark metabolic defects that are rescued by SIRT3 activation. *Cell Death & Differentiation*, *28*(4), 1379-1397. https://doi.org/10.1038/s41418-020-00664-0

Horvath, C. M. (2004). The Jak-STAT pathway stimulated by interferon gamma. *Sci STKE*, *2004*(260), tr8. https://doi.org/10.1126/stke.2602004tr8

Hung, Y. P., Albeck, J. G., Tantama, M., & Yellen, G. (2011). Imaging cytosolic NADH-NAD(+) redox state with a genetically encoded fluorescent biosensor. *Cell Metab*, *14*(4), 545-554. https://doi.org/10.1016/j.cmet.2011.08.012

Hung, Y. P., & Yellen, G. (2014). Live-cell imaging of cytosolic NADH-NAD+ redox state using a genetically encoded fluorescent biosensor. *Methods Mol Biol*, *1071*, 83-95. https://doi.org/10.1007/978-1-62703-622-1_7

Ilieva, H., Vullaganti, M., & Kwan, J. (2023). Advances in molecular pathology, diagnosis, and treatment of amyotrophic lateral sclerosis. *BMJ*, *383*, e075037. https://doi.org/10.1136/bmj-2023-075037

Itabe, H., Yamaguchi, T., Nimura, S., & Sasabe, N. (2017). Perilipins: a diversity of intracellular lipid droplet proteins. *Lipids Health Dis*, *16*(1), 83. https://doi.org/10.1186/s12944-017-0473-y

Jafarinia, H., van der Giessen, E., & Onck, P. R. (2020). Phase Separation of Toxic Dipeptide Repeat Proteins Related to C9orf72 ALS/FTD. *Biophys J*, *119*(4), 843-851. https://doi.org/10.1016/j.bpj.2020.07.005

Jahncke, J. N., & Wright, K. M. (2022). The many roles of dystroglycan in nervous system development and function. *Developmental Dynamics*, *252*(1), 61-80. https://doi.org/10.1002/dvdy.516

Jarazo, J., Barmpa, K., Modamio, J., Saraiva, C., Sabaté-Soler, S., Rosety, I., Griesbeck, A., Skwirblies, F., Zaffaroni, G., Smits, L. M., Su, J., Arias-Fuenzalida, J., Walter, J., Gomez-Giro, G., Monzel, A. S.,

Qing, X., Vitali, A., Cruciani, G., Boussaad, I., . . . Schwamborn, J. C. (2021). Parkinson's Disease Phenotypes in Patient Neuronal Cultures and Brain Organoids Improved by 2-Hydroxypropyl-β-Cyclodextrin Treatment. *Movement Disorders*, *37*(1), 80-94. https://doi.org/10.1002/mds.28810

Jin, S., Guerrero-Juarez, C. F., Zhang, L., Chang, I., Ramos, R., Kuan, C. H., Myung, P., Plikus, M. V., & Nie, Q. (2021). Inference and analysis of cell-cell communication using CellChat. *Nat Commun*, *12*(1), 1088. https://doi.org/10.1038/s41467-021-21246-9

Johnson, S. A., Fang, T., De Marchi, F., Neel, D., Van Weehaeghe, D., Berry, J. D., & Paganoni, S. (2022). Pharmacotherapy for Amyotrophic Lateral Sclerosis: A Review of Approved and Upcoming Agents. *Drugs*, *82*(13), 1367-1388. https://doi.org/10.1007/s40265-022-01769-1

Joyce, A. R., & Palsson, B. Ø. (2006). The model organism as a system: integrating 'omics' data sets. *Nature Reviews Molecular Cell Biology*, *7*(3), 198-210. https://doi.org/10.1038/nrm1857

Just-Borràs, L., Hurtado, E., Cilleros-Mañé, V., Biondi, O., Charbonnier, F., Tomàs, M., Garcia, N., Lanuza, M. A., & Tomàs, J. (2019). Overview of Impaired BDNF Signaling, Their Coupled Downstream Serine-Threonine Kinases and SNARE/SM Complex in the Neuromuscular Junction of the Amyotrophic Lateral Sclerosis Model SOD1-G93A Mice. *Molecular Neurobiology*, *56*(10), 6856-6872. https://doi.org/10.1007/s12035-019-1550-1

Kabashi, E., Lin, L., Tradewell, M. L., Dion, P. A., Bercier, V., Bourgouin, P., Rochefort, D., Bel Hadj, S., Durham, H. D., Velde, C. V., Rouleau, G. A., & Drapeau, P. (2010). Gain and loss of function of ALS-related mutations of TARDBP (TDP-43) cause motor deficits in vivo. *Human Molecular Genetics*, *19*(4), 671-683. https://doi.org/10.1093/hmg/ddp534

Kabiljo, R., Marriott, H., Hunt, G. P., Pfaff, A. L., Al Khleifat, A., Adey, B., Jones, A., Troakes, C., Quinn, J. P., Dobson, R. J. B., Koks, S., Al-Chalabi, A., & Iacoangeli, A. (2023). Transcriptomics Analyses of ALS Post-mortem Motor Cortex highlight alteration and potential biomarkers in the Neuropeptide Signalling pathway. *medRxiv*. https://doi.org/10.1101/2023.05.05.23289551

Kanehisa, M. (2019). Toward understanding the origin and evolution of cellular organisms. *Protein Sci*, *28*(11), 1947-1951. https://doi.org/10.1002/pro.3715

Kanehisa, M., Furumichi, M., Sato, Y., Kawashima, M., & Ishiguro-Watanabe, M. (2023). KEGG for taxonomy-based analysis of pathways and genomes. *Nucleic Acids Res*, *51*(D1), D587-D592. https://doi.org/10.1093/nar/gkac963

Kanehisa, M., & Goto, S. (2000). KEGG: kyoto encyclopedia of genes and genomes. *Nucleic Acids Res*, *28*(1), 27-30. https://doi.org/10.1093/nar/28.1.27

Kang, M., & Yao, Y. (2022). Laminin regulates oligodendrocyte development and myelination. *Glia*, *70*(3), 414-429. https://doi.org/10.1002/glia.24117

Kantner, I., & Erben, R. G. (2012). Long-Term Parenteral Administration of 2-Hydroxypropyl-β-Cyclodextrin Causes Bone Loss. *Toxicologic Pathology*, *40*(5), 742-750. https://doi.org/10.1177/0192623312441405

Kempermann, G. (2015). Activity Dependency and Aging in the Regulation of Adult Neurogenesis. *Cold Spring Harb Perspect Biol*, *7*(11). https://doi.org/10.1101/cshperspect.a018929

Kenigsbuch, M., Bost, P., Halevi, S., Chang, Y., Chen, S., Ma, Q., Hajbi, R., Schwikowski, B., Bodenmiller, B., Fu, H., Schwartz, M., & Amit, I. (2022). A shared disease-associated oligodendrocyte signature among multiple CNS pathologies. *Nat Neurosci*, *25*(7), 876-886. https://doi.org/10.1038/s41593-022-01104-7

Keren-Shaul, H., Spinrad, A., Weiner, A., Matcovitch-Natan, O., Dvir-Szternfeld, R., Ulland, T. K., David, E., Baruch, K., Lara-Astaiso, D., Toth, B., Itzkovitz, S., Colonna, M., Schwartz, M., & Amit, I. (2017). A Unique Microglia Type Associated with Restricting Development of Alzheimer's Disease. *Cell*, *169*(7), 1276-1290 e1217. https://doi.org/10.1016/j.cell.2017.05.018

Keren-Shaul, H., Spinrad, A., Weiner, A., Matcovitch-Natan, O., Dvir-Szternfeld, R., Ulland, T. K., David, E., Baruch, K., Lara-Astaiso, D., Toth, B., Itzkovitz, S., Colonna, M., Schwartz, M., & Amit, I. (2017). A Unique Microglia Type Associated with Restricting Development of Alzheimer's Disease. *Cell*, *169*(7), 1276-1290.e1217. https://doi.org/10.1016/j.cell.2017.05.018

Khosravi, B., LaClair, K. D., Riemenschneider, H., Zhou, Q., Frottin, F., Mareljic, N., Czuppa, M., Farny, D., Hartmann, H., Michaelsen, M., Arzberger, T., Hartl, F. U., Hipp, M. S., & Edbauer, D. (2020). Cell-to-cell transmission of C9orf72 poly-(Gly-Ala) triggers key features of ALS/FTD. *EMBO J*, *39*(8), e102811. https://doi.org/10.15252/embj.2019102811

Kilsdonk, E. P., Yancey, P. G., Stoudt, G. W., Bangerter, F. W., Johnson, W. J., Phillips, M. C., & Rothblat, G. H. (1995). Cellular cholesterol efflux mediated by cyclodextrins. *J Biol Chem*, *270*(29), 17250-17256. https://doi.org/10.1074/jbc.270.29.17250

Kim, J., Basak, J. M., & Holtzman, D. M. (2009). The role of apolipoprotein E in Alzheimer's disease. *Neuron*, *63*(3), 287-303. https://doi.org/10.1016/j.neuron.2009.06.026

Kim, S. M., Noh, M. Y., Kim, H., Cheon, S. Y., Lee, K. M., Lee, J., Cha, E., Park, K. S., Lee, K. W., Sung, J. J., & Kim, S. H. (2017). 25-Hydroxycholesterol is involved in the pathogenesis of amyotrophic lateral sclerosis. *Oncotarget*, *8*(7), 11855-11867. https://doi.org/10.18632/oncotarget.14416

Kislinger, G., Gnagi, H., Kerschensteiner, M., Simons, M., Misgeld, T., & Schifferer, M. (2020). ATUM-FIB microscopy for targeting and multiscale imaging of rare events in mouse cortex. *STAR Protoc*, *1*(3), 100232. https://doi.org/10.1016/j.xpro.2020.100232

Kolarcik, C. L., & Bowser, R. (2012). Retinoid signaling alterations in amyotrophic lateral sclerosis. *Am J Neurodegener Dis*, *1*(2), 130-145. https://www.ncbi.nlm.nih.gov/pubmed/23383387

Korobeynikov, V. A., Lyashchenko, A. K., Blanco-Redondo, B., Jafar-Nejad, P., & Shneider, N. A. (2022). Antisense oligonucleotide silencing of FUS expression as a therapeutic approach in amyotrophic lateral sclerosis. *Nature Medicine*, *28*(1), 104-116. https://doi.org/10.1038/s41591-021-01615-z

Korsunsky, I., Millard, N., Fan, J., Slowikowski, K., Zhang, F., Wei, K., Baglaenko, Y., Brenner, M., Loh, P. R., & Raychaudhuri, S. (2019). Fast, sensitive and accurate integration of single-cell data with Harmony. *Nat Methods*, *16*(12), 1289-1296. https://doi.org/10.1038/s41592-019-0619-0

Krishnaswami, S., Wang, T., Yuan, Y., Alvey, C. W., Checchio, T., Peterson, M., Shi, H., & Riese, R. (2015). Single- and multiple-dose pharmacokinetics of tofacitinib in healthy Chinese volunteers. *Clin Pharmacol Drug Dev*, *4*(5), 395-399. https://doi.org/10.1002/cpdd.202

Kumar, V., Hasan, G. M., & Hassan, M. I. (2017). Unraveling the Role of RNA Mediated Toxicity of C9orf72 Repeats in C9-FTD/ALS. *Front Neurosci*, *11*, 711. https://doi.org/10.3389/fnins.2017.00711

Kuzel, A. R., Lodhi, M. U., Syed, I. A., & Rahim, M. (2017). Atypical Initial Presentation of Painful Muscle Cramps in a Patient with Amyotrophic Lateral Sclerosis: A Case Report and Brief Review of the Literature. *Cureus*. https://doi.org/10.7759/cureus.1837

Kwiatkowski, T. J., Jr., Bosco, D. A., Leclerc, A. L., Tamrazian, E., Vanderburg, C. R., Russ, C., Davis, A., Gilchrist, J., Kasarskis, E. J., Munsat, T., Valdmanis, P., Rouleau, G. A., Hosler, B. A., Cortelli, P.,

de Jong, P. J., Yoshinaga, Y., Haines, J. L., Pericak-Vance, M. A., Yan, J., . . . Brown, R. H., Jr. (2009). Mutations in the FUS/TLS gene on chromosome 16 cause familial amyotrophic lateral sclerosis. *Science*, *323*(5918), 1205-1208. https://doi.org/10.1126/science.1166066

Kwon, H. S., & Koh, S.-H. (2020). Neuroinflammation in neurodegenerative disorders: the roles of microglia and astrocytes. *Translational Neurodegeneration*, *9*(1). https://doi.org/10.1186/s40035-020-00221-2

Kwon, I., Xiang, S., Kato, M., Wu, L., Theodoropoulos, P., Wang, T., Kim, J., Yun, J., Xie, Y., & McKnight, S. L. (2014). Poly-dipeptides encoded by the C9orf72 repeats bind nucleoli, impede RNA biogenesis, and kill cells. *Science*, *345*(6201), 1139-1145. https://doi.org/10.1126/science.1254917

LaClair, K. D., Zhou, Q., Michaelsen, M., Wefers, B., Brill, M. S., Janjic, A., Rathkolb, B., Farny, D., Cygan, M., de Angelis, M. H., Wurst, W., Neumann, M., Enard, W., Misgeld, T., Arzberger, T., & Edbauer, D. (2020). Congenic expression of poly-GA but not poly-PR in mice triggers selective neuron loss and interferon responses found in C9orf72 ALS. *Acta Neuropathol*, *140*(2), 121-142. https://doi.org/10.1007/s00401-020-02176-0

Lai, J. D., & Ichida, J. K. (2019). C9ORF72 protein function and immune dysregulation in amyotrophic lateral sclerosis. *Neurosci Lett*, *713*, 134523. https://doi.org/10.1016/j.neulet.2019.134523

Langhans, W., Berthoud, H. R., & Westerterp-Plantenga, M. (2016). Introduction to 'All roads take to the brain: neural control of energy homeostasis in health and disease'. *Int J Obes (Lond)*, *40*(2), 191-192. https://doi.org/10.1038/ijo.2015.245

Lee, Y. B., Glover, C. P., Cosgrave, A. S., Bienemann, A., & Uney, J. B. (2005). Optimizing regulatable gene expression using adenoviral vectors. *Exp Physiol*, *90*(1), 33-37. https://doi.org/10.1113/expphysiol.2004.028209

Li, C., Wei, Q., Gu, X., Chen, Y., Chen, X., Cao, B., Ou, R., & Shang, H. (2019). Decreased Glycogenolysis by miR-338-3p Promotes Regional Glycogen Accumulation Within the Spinal Cord of Amyotrophic Lateral Sclerosis Mice. *Front Mol Neurosci*, *12*, 114. https://doi.org/10.3389/fnmol.2019.00114

Li, H.-P., Peng, C.-C., Wu, C.-C., Chen, C.-H., Shih, M.-J., Huang, M.-Y., Lai, Y.-R., Chen, Y.-L., Chen, T.-W., Tang, P., Chang, Y.-S., Chang, K.-P., & Hsu, C.-L. (2018). Inactivation of the tight junction gene CLDN11 by aberrant hypermethylation modulates tubulins polymerization and promotes cell migration in nasopharyngeal carcinoma. *Journal of Experimental & Clinical Cancer Research*, *37*(1), 102. https://doi.org/10.1186/s13046-018-0754-y

Liu, B., Li, H., Repa, J. J., Turley, S. D., & Dietschy, J. M. (2008). Genetic variations and treatments that affect the lifespan of the NPC1 mouse. *J Lipid Res*, *49*(3), 663-669. https://doi.org/10.1194/jlr.M700525-JLR200

Liu, F., Chen, S., Ming, X., Li, H., Zeng, Z., & Lv, Y. (2023). Sortilin-induced lipid accumulation and atherogenesis are suppressed by HNF1b SUMOylation promoted by flavone of Polygonatum odoratum. *J Zhejiang Univ Sci B*, *24*(11), 998-1013. https://doi.org/10.1631/jzus.B2200682 (玉竹黄酮通过促进HNF1b蛋白的SUMO化修饰抑制sortilin介导的脂质积累及动脉粥样硬化.)

Liu, X., Ding, D., Chen, G. D., Li, L., Jiang, H., & Salvi, R. (2020). 2-Hydroxypropyl-beta-cyclodextrin Ototoxicity in Adult Rats: Rapid Onset and Massive Destruction of Both Inner and Outer Hair Cells Above a Critical Dose. *Neurotox Res*, *38*(3), 808-823. https://doi.org/10.1007/s12640-020-00252-7

Liu, Y., Wang, T., Ji, Y. J., Johnson, K., Liu, H., Johnson, K., Bailey, S., Suk, Y., Lu, Y. N., Liu, M., & Wang, J. (2018). A C9orf72-CARM1 axis regulates lipid metabolism under glucose starvation-induced nutrient stress. *Genes Dev*, *32*(21-22), 1380-1397. https://doi.org/10.1101/gad.315564.118

Ll Wilkinson, M. G., Deakin, C. T., Papadopoulou, C., Eleftheriou, D., & Wedderburn, L. R. (2021). JAK inhibitors: a potential treatment for JDM in the context of the role of interferon-driven pathology. *Pediatr Rheumatol Online J*, *19*(1), 146. https://doi.org/10.1186/s12969-021-00637-8

Love, M. I., Huber, W., & Anders, S. (2014). Moderated estimation of fold change and dispersion for RNA-seq data with DESeq2. *Genome Biol*, *15*(12), 550. https://doi.org/10.1186/s13059-014-0550-8

Lucia Appleton, S., Navarro-Orcajada, S., Martinez-Navarro, F. J., Caldera, F., Lopez-Nicolas, J. M., Trotta, F., & Matencio, A. (2021). Cyclodextrins as Anti-inflammatory Agents: Basis, Drugs and Perspectives. *Biomolecules*, *11*(9). https://doi.org/10.3390/biom11091384

Ludolph, A. C., Dorst, J., Dreyhaupt, J., Weishaupt, J. H., Kassubek, J., Weiland, U., Meyer, T., Petri, S., Hermann, A., Emmer, A., Grosskreutz, J., Grehl, T., Zeller, D., Boentert, M., Schrank, B., Prudlo, J., Winkler, A. S., Gorbulev, S., Roselli, F., . . . Group, L.-A. S. (2020). Effect of High-Caloric Nutrition on Survival in Amyotrophic Lateral Sclerosis. *Ann Neurol*, *87*(2), 206-216. https://doi.org/10.1002/ana.25661

Lynch, K. (2023). Pathogenesis and presentation of ALS: examining reasons for delayed diagnosis and identifying opportunities for improvement. *Am J Manag Care*, *29*(7 Suppl), S104-S111. https://doi.org/10.37765/ajmc.2023.89390

Mackenzie, I. R., Bigio, E. H., Ince, P. G., Geser, F., Neumann, M., Cairns, N. J., Kwong, L. K., Forman, M. S., Ravits, J., Stewart, H., Eisen, A., McClusky, L., Kretzschmar, H. A., Monoranu, C. M., Highley, J. R., Kirby, J., Siddique, T., Shaw, P. J., Lee, V. M., & Trojanowski, J. Q. (2007). Pathological TDP-43 distinguishes sporadic amyotrophic lateral sclerosis from amyotrophic lateral sclerosis with SOD1 mutations. *Ann Neurol*, *61*(5), 427-434. https://doi.org/10.1002/ana.21147

Macosko, E. Z., Basu, A., Satija, R., Nemesh, J., Shekhar, K., Goldman, M., Tirosh, I., Bialas, A. R., Kamitaki, N., Martersteck, E. M., Trombetta, J. J., Weitz, D. A., Sanes, J. R., Shalek, A. K., Regev, A., & McCarroll, S. A. (2015). Highly Parallel Genome-wide Expression Profiling of Individual Cells Using Nanoliter Droplets. *Cell*, *161*(5), 1202-1214. https://doi.org/10.1016/j.cell.2015.05.002

Maggi, L., Gibertini, S., Iannibelli, E., Gallone, A., Bonanno, S., Cazzato, D., Gerevini, S., Moscatelli, M., Blasevich, F., Riolo, G., Mantegazza, R., & Ruggieri, A. (2023). PLIN4-related myopathy: clinical, histological and imaging data in a large cohort of patients. *Journal of Neurology*, *270*(9), 4538-4543. https://doi.org/10.1007/s00415-023-11729-8

Maguire, G. (2017). Amyotrophic lateral sclerosis as a protein level, non-genomic disease: Therapy with S2RM exosome released molecules. *World J Stem Cells*, *9*(11), 187-202. https://doi.org/10.4252/wjsc.v9.i11.187

Maheras, K. J., Peppi, M., Ghoddoussi, F., Galloway, M. P., Perrine, S. A., & Gow, A. (2018). Absence of Claudin 11 in CNS Myelin Perturbs Behavior and Neurotransmitter Levels in Mice. *Scientific Reports*, *8*(1), 3798. https://doi.org/10.1038/s41598-018-22047-9

Malanga, M., Szemán, J., Fenyvesi, É., Puskás, I., Csabai, K., Gyémánt, G., Fenyvesi, F., & Szente, L. (2016). "Back to the Future": A New Look at Hydroxypropyl Beta-Cyclodextrins. *Journal of Pharmaceutical Sciences*, *105*(9), 2921-2931. https://doi.org/https://doi.org/10.1016/j.xphs.2016.04.034

Marian, O. C., Teo, J. D., Lee, J. Y., Song, H., Kwok, J. B., Landin-Romero, R., Halliday, G., & Don, A. S. (2023). Disrupted myelin lipid metabolism differentiates frontotemporal dementia caused by GRN and C9orf72 gene mutations. *Acta Neuropathologica Communications*, *11*(1), 52. https://doi.org/10.1186/s40478-023-01544-7

Marin, B., Desport, J. C., Kajeu, P., Jesus, P., Nicolaud, B., Nicol, M., Preux, P. M., & Couratier, P. (2011). Alteration of nutritional status at diagnosis is a prognostic factor for survival of amyotrophic lateral sclerosis patients. *J Neurol Neurosurg Psychiatry*, *82*(6), 628-634. https://doi.org/10.1136/jnnp.2010.211474

Martin, M. G., Pfrieger, F., & Dotti, C. G. (2014). Cholesterol in brain disease: sometimes determinant and frequently implicated. *EMBO Rep*, *15*(10), 1036-1052. https://doi.org/10.15252/embr.201439225

Martin, S., & Parton, R. G. (2006). Lipid droplets: a unified view of a dynamic organelle. *Nature Reviews Molecular Cell Biology*, *7*(5), 373-378. https://doi.org/10.1038/nrm1912

Massachusetts-General-Hospital. (2022). Neurodegenerative Alzheimer's Disease and Amyotrophic Lateral Sclerosis (NADALS) Basket Trial. In: https://classic.clinicaltrials.gov/show/NCT05189106.

Mathys, H., Adaikkan, C., Gao, F., Young, J. Z., Manet, E., Hemberg, M., De Jager, P. L., Ransohoff, R. M., Regev, A., & Tsai, L. H. (2017). Temporal Tracking of Microglia Activation in Neurodegeneration at Single-Cell Resolution. *Cell Rep*, *21*(2), 366-380. https://doi.org/10.1016/j.celrep.2017.09.039

Matsuda, S., Matsuda, Y., & D'Adamio, L. (2009). CD74 interacts with APP and suppresses the production of Abeta. *Mol Neurodegener*, *4*, 41. https://doi.org/10.1186/1750-1326-4-41

Matsuzaki, K., Kato, K., & Yanagisawa, K. (2010). Aβ polymerization through interaction with membrane gangliosides. *Biochimica et Biophysica Acta (BBA) - Molecular and Cell Biology of Lipids*, *1801*(8), 868-877. https://doi.org/https://doi.org/10.1016/j.bbalip.2010.01.008

McCauley, M. E., & Baloh, R. H. (2019). Inflammation in ALS/FTD pathogenesis. *Acta Neuropathol*, *137*(5), 715-730. https://doi.org/10.1007/s00401-018-1933-9

McCombe, P. A., & Henderson, R. D. (2010). Effects of gender in amyotrophic lateral sclerosis. *Gend Med*, *7*(6), 557-570. https://doi.org/10.1016/j.genm.2010.11.010

McGinnis, C. S., Murrow, L. M., & Gartner, Z. J. (2019). DoubletFinder: Doublet Detection in Single-Cell RNA Sequencing Data Using Artificial Nearest Neighbors. *Cell Syst*, *8*(4), 329-337 e324. https://doi.org/10.1016/j.cels.2019.03.003

McKinney, W. (2010). *Data Structures for Statistical Computing in Python* (S. v. d. W. a. J. Millman, Ed.). https://doi.org/10.25080/Majora-92bf1922-00a

Mead, R. J., Shan, N., Reiser, H. J., Marshall, F., & Shaw, P. J. (2023). Amyotrophic lateral sclerosis: a neurodegenerative disorder poised for successful therapeutic translation. *Nature Reviews Drug Discovery*, *22*(3), 185-212. https://doi.org/10.1038/s41573-022-00612-2

Mehl, L. C., Manjally, A. V., Bouadi, O., Gibson, E. M., & Tay, T. L. (2022). Microglia in brain development and regeneration. *Development*, *149*(8). https://doi.org/10.1242/dev.200425

Mehta, A. R., Walters, R., Waldron, F. M., Pal, S., Selvaraj, B. T., Macleod, M. R., Hardingham, G. E., Chandran, S., & Gregory, J. M. (2019). Targeting mitochondrial dysfunction in amyotrophic lateral sclerosis: a systematic review and meta-analysis. *Brain Commun*, *1*(1), fcz009. https://doi.org/10.1093/braincomms/fcz009

Mehta, P., Raymond, J., Punjani, R., Larson, T., Han, M., Bove, F., & Horton, D. K. (2022). Incidence of amyotrophic lateral sclerosis in the United States, 2014–2016. *Amyotrophic Lateral Sclerosis and Frontotemporal Degeneration*, *23*(5-6), 378-382. https://doi.org/10.1080/21678421.2021.2023190

Melkamu, T., Kita, H., & O'Grady, S. M. (2013). TLR3 activation evokes IL-6 secretion, autocrine regulation of Stat3 signaling and TLR2 expression in human bronchial epithelial cells. *J Cell Commun Signal*, *7*(2), 109-118. https://doi.org/10.1007/s12079-012-0185-z

Miller, R. G., Mitchell, J. D., & Moore, D. H. (2012). Riluzole for amyotrophic lateral sclerosis (ALS)/motor neuron disease (MND). *Cochrane Database Syst Rev*, *2012*(3), CD001447. https://doi.org/10.1002/14651858.CD001447.pub3

Milone, M. C., & O'Doherty, U. (2018). Clinical use of lentiviral vectors. *Leukemia*, *32*(7), 1529-1541. https://doi.org/10.1038/s41375-018-0106-0

Mizielinska, S., Lashley, T., Norona, F. E., Clayton, E. L., Ridler, C. E., Fratta, P., & Isaacs, A. M. (2013). C9orf72 frontotemporal lobar degeneration is characterised by frequent neuronal sense and antisense RNA foci. *Acta Neuropathol*, *126*(6), 845-857. https://doi.org/10.1007/s00401-013-1200-z

Moglia, C., Calvo, A., Grassano, M., Canosa, A., Manera, U., D'Ovidio, F., Bombaci, A., Bersano, E., Mazzini, L., Mora, G., Chio, A., Piemonte, & Valle d'Aosta Register for, A. L. S. (2019). Early weight loss in amyotrophic lateral sclerosis: outcome relevance and clinical correlates in a population-based cohort. *J Neurol Neurosurg Psychiatry*, *90*(6), 666-673. https://doi.org/10.1136/jnnp-2018-319611

Mohassel, P., Donkervoort, S., Lone, M. A., Nalls, M., Gable, K., Gupta, S. D., Foley, A. R., Hu, Y., Saute, J. A. M., Moreira, A. L., Kok, F., Introna, A., Logroscino, G., Grunseich, C., Nickolls, A. R., Pourshafie, N., Neuhaus, S. B., Saade, D., Gangfuß, A., . . . Bönnemann, C. G. (2021). Childhood amyotrophic lateral sclerosis caused by excess sphingolipid synthesis. *Nature Medicine*, *27*(7), 1197-1204. https://doi.org/10.1038/s41591-021-01346-1

Moldavski, O., Amen, T., Levin-Zaidman, S., Eisenstein, M., Rogachev, I., Brandis, A., Kaganovich, D., & Schuldiner, M. (2015). Lipid Droplets Are Essential for Efficient Clearance of Cytosolic Inclusion Bodies. *Dev Cell*, *33*(5), 603-610. https://doi.org/10.1016/j.devcel.2015.04.015

Mori, K., Arzberger, T., Grasser, F. A., Gijselinck, I., May, S., Rentzsch, K., Weng, S. M., Schludi, M. H., van der Zee, J., Cruts, M., Van Broeckhoven, C., Kremmer, E., Kretzschmar, H. A., Haass, C., & Edbauer, D. (2013). Bidirectional transcripts of the expanded C9orf72 hexanucleotide repeat are translated into aggregating dipeptide repeat proteins. *Acta Neuropathol*, *126*(6), 881-893. https://doi.org/10.1007/s00401-013-1189-3

Mori, K., Weng, S. M., Arzberger, T., May, S., Rentzsch, K., Kremmer, E., Schmid, B., Kretzschmar, H. A., Cruts, M., Van Broeckhoven, C., Haass, C., & Edbauer, D. (2013). The C9orf72 GGGGCC repeat is translated into aggregating dipeptide-repeat proteins in FTLD/ALS. *Science*, *339*(6125), 1335-1338. https://doi.org/10.1126/science.1232927

Müller, U. C., Deller, T., & Korte, M. (2017). Not just amyloid: physiological functions of the amyloid precursor protein family. *Nature Reviews Neuroscience*, *18*(5), 281-298. https://doi.org/10.1038/nrn.2017.29

Najt, C. P., Devarajan, M., & Mashek, D. G. (2022). Perilipins at a glance. *J Cell Sci*, *135*(5). https://doi.org/10.1242/jcs.259501

Neufeld, E. B., Cooney, A. M., Pitha, J., Dawidowicz, E. A., Dwyer, N. K., Pentchev, P. G., & Blanchette-Mackie, E. J. (1996). Intracellular Trafficking of Cholesterol Monitored with a Cyclodextrin*. *Journal of Biological Chemistry*, *271*(35), 21604-21613. https://doi.org/https://doi.org/10.1074/jbc.271.35.21604

Neumann, M., Sampathu, D. M., Kwong, L. K., Truax, A. C., Micsenyi, M. C., Chou, T. T., Bruce, J., Schuck, T., Grossman, M., Clark, C. M., McCluskey, L. F., Miller, B. L., Masliah, E., Mackenzie, I. R., Feldman, H., Feiden, W., Kretzschmar, H. A., Trojanowski, J. Q., & Lee, V. M. (2006). Ubiquitinated TDP-43 in frontotemporal lobar degeneration and amyotrophic lateral sclerosis. *Science*, *314*(5796), 130-133. https://doi.org/10.1126/science.1134108

Niedermeyer, S., Murn, M., & Choi, P. J. (2019). Respiratory Failure in Amyotrophic Lateral Sclerosis. *Chest*, *155*(2), 401-408. https://doi.org/10.1016/j.chest.2018.06.035

Nosengo, N. (2016). Can you teach old drugs new tricks? *Nature*, *534*(7607), 314-316. https://doi.org/10.1038/534314a

O'Reilly, É. J., Wang, H., Weisskopf, M. G., Fitzgerald, K. C., Falcone, G., McCullough, M. L., Thun, M., Park, Y., Kolonel, L. N., & Ascherio, A. (2012). Premorbid body mass index and risk of amyotrophic lateral sclerosis. *Amyotrophic Lateral Sclerosis and Frontotemporal Degeneration*, *14*(3), 205-211. https://doi.org/10.3109/21678421.2012.735240

Olzmann, J. A., & Carvalho, P. (2019). Dynamics and functions of lipid droplets. *Nat Rev Mol Cell Biol*, *20*(3), 137-155. https://doi.org/10.1038/s41580-018-0085-z

Paganoni, S., Macklin, E. A., Hendrix, S., Berry, J. D., Elliott, M. A., Maiser, S., Karam, C., Caress, J. B., Owegi, M. A., Quick, A., Wymer, J., Goutman, S. A., Heitzman, D., Heiman-Patterson, T., Jackson, C. E., Quinn, C., Rothstein, J. D., Kasarskis, E. J., Katz, J., . . . Cudkowicz, M. E. (2020). Trial of Sodium Phenylbutyrate-Taurursodiol for Amyotrophic Lateral Sclerosis. *N Engl J Med*, *383*(10), 919-930. https://doi.org/10.1056/NEJMoa1916945

Pandey, S., Shen, K., Lee, S. H., Shen, Y. A., Wang, Y., Otero-Garcia, M., Kotova, N., Vito, S. T., Laufer, B. I., Newton, D. F., Rezzonico, M. G., Hanson, J. E., Kaminker, J. S., Bohlen, C. J., Yuen, T. J., & Friedman, B. A. (2022). Disease-associated oligodendrocyte responses across neurodegenerative diseases. *Cell Rep*, *40*(8), 111189. https://doi.org/10.1016/j.celrep.2022.111189

Park, H., Cho, B., Kim, H., Saito, T., Saido, T. C., Won, K.-J., & Kim, J. (2023). Single-cell RNA-sequencing identifies disease-associated oligodendrocytes in male APP NL-G-F and 5XFAD mice. *Nature Communications*, *14*(1), 802. https://doi.org/10.1038/s41467-023-36519-8

Park, J.-W., Kim, M., Baek, S.-H., Sung, J. H., Yu, J.-G., & Kim, B.-J. (2021). Body Fat Percentage and Availability of Oral Food Intake: Prognostic Factors and Implications for Nutrition in Amyotrophic Lateral Sclerosis. *Nutrients*, *13*(11). https://doi.org/10.3390/nu13113704

Pennetta, G., & Welte, M. A. (2018). Emerging Links between Lipid Droplets and Motor Neuron Diseases. *Dev Cell*, *45*(4), 427-432. https://doi.org/10.1016/j.devcel.2018.05.002

Peters, O. M., & Brown, R. H. (2023). Amyotrophic lateral sclerosis. In *Neurobiology of Brain Disorders* (pp. 233-251). https://doi.org/10.1016/b978-0-323-85654-6.00026-5

Petrov, A. M., Kasimov, M. R., & Zefirov, A. L. (2016). Brain Cholesterol Metabolism and Its Defects: Linkage to Neurodegenerative Diseases and Synaptic Dysfunction. *Acta Naturae*, *8*(1), 58-73. https://www.ncbi.nlm.nih.gov/pubmed/27099785

Pfeffer, S. R. (2019). NPC intracellular cholesterol transporter 1 (NPC1)-mediated cholesterol export from lysosomes. *J Biol Chem*, *294*(5), 1706-1709. https://doi.org/10.1074/jbc.TM118.004165

Picelli, S., Faridani, O. R., Björklund, Å. K., Winberg, G., Sagasser, S., & Sandberg, R. (2014). Full-length RNA-seq from single cells using Smart-seq2. *Nature Protocols*, *9*(1), 171-181. https://doi.org/10.1038/nprot.2014.006

Prado, M. B., Jr., Pedro, K. M., & Adiao, K. J. B. (2023). Efficacy, safety and tolerability of high caloric diet in amyotrophic lateral sclerosis patients: A systematic review and meta-analysis. *Rev Neurol (Paris)*, *179*(9), 1008-1019. https://doi.org/10.1016/j.neurol.2023.01.731

Proniuk, S., & Blanchard, J. (2001). Influence of degree of substitution of cyclodextrins on their colligative properties in solution. *J Pharm Sci*, *90*(8), 1086-1090. https://doi.org/10.1002/jps.1062

Puglielli, L., Konopka, G., Pack-Chung, E., Ingano, L. A., Berezovska, O., Hyman, B. T., Chang, T. Y., Tanzi, R. E., & Kovacs, D. M. (2001). Acyl-coenzyme A: cholesterol acyltransferase modulates the generation of the amyloid beta-peptide. *Nat Cell Biol*, *3*(10), 905-912. https://doi.org/10.1038/ncb1001-905

Python-Software-Foundation. (2022). *Python 3.8.15 Documentation*. In https://www.python.org/downloads/release/python-3815/

R-Core-Team. (2022). *R: A Language and Environment for Statistical Computing*. R Foundation for Statistical Computing. https://www.R-project.org/

R-Core-Team. (2023). *R: A Language and Environment for Statistical Computing*. R Foundation for Statistical Computing. https://www.R-project.org/

Rambukkana, A., Salzer, J. L., Yurchenco, P. D., & Tuomanen, E. I. (1997). Neural Targeting of Mycobacterium leprae Mediated by the G Domain of the Laminin-α2 Chain. *Cell*, *88*(6), 811-821. https://doi.org/10.1016/s0092-8674(00)81927-3

Relucio, J. L. V. (2011). *The Role of Laminin a2 in Oligodendrocyte Development and CNS Myelination* Stony Brook University]. Stony Brook Theses & Dissertations. http://hdl.handle.net/1951/56101

Renton, A. E., Chio, A., & Traynor, B. J. (2014). State of play in amyotrophic lateral sclerosis genetics. *Nat Neurosci*, *17*(1), 17-23. https://doi.org/10.1038/nn.3584

Renton, A. E., Majounie, E., Waite, A., Simon-Sanchez, J., Rollinson, S., Gibbs, J. R., Schymick, J. C., Laaksovirta, H., van Swieten, J. C., Myllykangas, L., Kalimo, H., Paetau, A., Abramzon, Y., Remes, A. M., Kaganovich, A., Scholz, S. W., Duckworth, J., Ding, J., Harmer, D. W., . . . Traynor, B. J. (2011). A hexanucleotide repeat expansion in C9ORF72 is the cause of chromosome 9p21-linked ALS-FTD. *Neuron*, *72*(2), 257-268. https://doi.org/10.1016/j.neuron.2011.09.010

Richardson, P. J., Smith, D. P., de Giorgio, A., Snetkov, X., Almond-Thynne, J., Cronin, S., Mead, R. J., McDermott, C. J., & Shaw, P. J. (2023). Janus kinase inhibitors are potential therapeutics for amyotrophic lateral sclerosis. *Translational Neurodegeneration*, *12*(1), 47. https://doi.org/10.1186/s40035-023-00380-y

Riechers, S. P., Mojsilovic-Petrovic, J., Belton, T. B., Chakrabarty, R. P., Garjani, M., Medvedeva, V., Dalton, C., Wong, Y. C., Chandel, N. S., Dienel, G., & Kalb, R. G. (2022). Neurons undergo pathogenic metabolic reprogramming in models of familial ALS. *Mol Metab*, *60*, 101468. https://doi.org/10.1016/j.molmet.2022.101468

Riemenschneider, H., Simonetti, F., Sheth, U., Katona, E., Roth, S., Hutten, S., Farny, D., Michaelsen, M., Nuscher, B., Schmidt, M. K., Flatley, A., Schepers, A., Gruijs da Silva, L. A., Zhou, Q., Klopstock, T., Liesz, A., Arzberger, T., Herms, J., Feederle, R., . . . Edbauer, D. (2023). Targeting the glycine-rich domain of TDP-43 with antibodies prevents its aggregation in vitro and reduces neurofilament levels in vivo. *Acta Neuropathol Commun*, *11*(1), 112. https://doi.org/10.1186/s40478-023-01592-z

Rodriguez, S., Sahin, A., Schrank, B. R., Al-Lawati, H., Costantino, I., Benz, E., Fard, D., Albers, A. D., Cao, L., Gomez, A. C., Evans, K., Ratti, E., Cudkowicz, M., Frosch, M. P., Talkowski, M., Sorger, P.

K., Hyman, B. T., & Albers, M. W. (2021). Genome-encoded cytoplasmic double-stranded RNAs, found in C9ORF72 ALS-FTD brain, propagate neuronal loss. *Sci Transl Med*, *13*(601). https://doi.org/10.1126/scitranslmed.aaz4699

Rosen, D. R., Siddique, T., Patterson, D., Figlewicz, D. A., Sapp, P., Hentati, A., Donaldson, D., Goto, J., O'Regan, J. P., Deng, H. X., & et al. (1993). Mutations in Cu/Zn superoxide dismutase gene are associated with familial amyotrophic lateral sclerosis. *Nature*, *362*(6415), 59-62. https://doi.org/10.1038/362059a0

Rueden, C. T., Schindelin, J., Hiner, M. C., DeZonia, B. E., Walter, A. E., Arena, E. T., & Eliceiri, K. W. (2017). ImageJ2: ImageJ for the next generation of scientific image data. *BMC Bioinformatics*, *18*(1), 529. https://doi.org/10.1186/s12859-017-1934-z

Rusek, M., Smith, J., El-Khatib, K., Aikins, K., Czuczwar, S. J., & Pluta, R. (2023). The Role of the JAK/STAT Signaling Pathway in the Pathogenesis of Alzheimer's Disease: New Potential Treatment Target. *Int J Mol Sci*, *24*(1). https://doi.org/10.3390/ijms24010864

Saher, G., Brügger, B., Lappe-Siefke, C., Möbius, W., Tozawa, R.-i., Wehr, M. C., Wieland, F., Ishibashi, S., & Nave, K.-A. (2005). High cholesterol level is essential for myelin membrane growth. *Nature Neuroscience*, *8*(4), 468-475. https://doi.org/10.1038/nn1426

Scaricamazza, S., Salvatori, I., Giacovazzo, G., Loeffler, J. P., Rene, F., Rosina, M., Quessada, C., Proietti, D., Heil, C., Rossi, S., Battistini, S., Giannini, F., Volpi, N., Steyn, F. J., Ngo, S. T., Ferraro, E., Madaro, L., Coccurello, R., Valle, C., & Ferri, A. (2020). Skeletal-Muscle Metabolic Reprogramming in ALS-SOD1(G93A) Mice Predates Disease Onset and Is A Promising Therapeutic Target. *iScience*, *23*(5), 101087. https://doi.org/10.1016/j.isci.2020.101087

Scekic-Zahirovic, J., Sendscheid, O., El Oussini, H., Jambeau, M., Sun, Y., Mersmann, S., Wagner, M., Dieterle, S., Sinniger, J., Dirrig-Grosch, S., Drenner, K., Birling, M. C., Qiu, J., Zhou, Y., Li, H., Fu, X. D., Rouaux, C., Shelkovnikova, T., Witting, A., . . . Dupuis, L. (2016). Toxic gain of function from mutant FUS protein is crucial to trigger cell autonomous motor neuron loss. *EMBO J*, *35*(10), 1077-1097. https://doi.org/10.15252/embj.201592559

Schindelin, J., Arganda-Carreras, I., Frise, E., Kaynig, V., Longair, M., Pietzsch, T., Preibisch, S., Rueden, C., Saalfeld, S., Schmid, B., Tinevez, J. Y., White, D. J., Hartenstein, V., Eliceiri, K., Tomancak, P., & Cardona, A. (2012). Fiji: an open-source platform for biological-image analysis. *Nat Methods*, *9*(7), 676-682. https://doi.org/10.1038/nmeth.2019

Schludi, M. H., Becker, L., Garrett, L., Gendron, T. F., Zhou, Q., Schreiber, F., Popper, B., Dimou, L., Strom, T. M., Winkelmann, J., von Thaden, A., Rentzsch, K., May, S., Michaelsen, M., Schwenk, B. M., Tan, J., Schoser, B., Dieterich, M., Petrucelli, L., . . . Edbauer, D. (2017). Spinal poly-GA inclusions in a C9orf72 mouse model trigger motor deficits and inflammation without neuron loss. *Acta Neuropathol*, *134*(2), 241-254. https://doi.org/10.1007/s00401-017-1711-0

Schoch, S., Cibelli, G., & Thiel, G. (1996). Neuron-specific gene expression of synapsin I. Major role of a negative regulatory mechanism. *J Biol Chem*, *271*(6), 3317-3323. https://doi.org/10.1074/jbc.271.6.3317

Schoggins, J. W., & Rice, C. M. (2011). Interferon-stimulated genes and their antiviral effector functions. *Curr Opin Virol*, *1*(6), 519-525. https://doi.org/10.1016/j.coviro.2011.10.008

Sharma, R., Hastings, C., Staretz-Chacham, O., Raiman, J., Paucar, M., Spiegel, R., Murray, B., Hurst, B., Liu, B., Kjems, L., & Hrynkow, S. (2023). Long-term administration of intravenous Trappsol® Cyclo™ (HP-β-CD) results in clinical benefits and stabilization or slowing of disease progression in patients with Niemann-Pick disease type C1: Results of an international 48-week Phase I/II trial.

Molecular Genetics and Metabolism Reports, *36*, 100988. https://doi.org/https://doi.org/10.1016/j.ymgmr.2023.100988

Shy, M. E. (2006). Peripheral neuropathies caused by mutations in the myelin protein zero. *J Neurol Sci*, *242*(1-2), 55-66. https://doi.org/10.1016/j.jns.2005.11.015

Simpson, E. P., Henry, Y. K., Henkel, J. S., Smith, R. G., & Appel, S. H. (2004). Increased lipid peroxidation in sera of ALS patients: a potential biomarker of disease burden. *Neurology*, *62*(10), 1758-1765. https://doi.org/10.1212/wnl.62.10.1758

Sladojevic, N., Stamatovic, S. M., Johnson, A. M., Choi, J., Hu, A., Dithmer, S., Blasig, I. E., Keep, R. F., & Andjelkovic, A. V. (2019). Claudin-1-Dependent Destabilization of the Blood-Brain Barrier in Chronic Stroke. *J Neurosci*, *39*(4), 743-757. https://doi.org/10.1523/JNEUROSCI.1432-18.2018

Smith, E. F., Shaw, P. J., & De Vos, K. J. (2019). The role of mitochondria in amyotrophic lateral sclerosis. *Neuroscience Letters*, *710*. https://doi.org/10.1016/j.neulet.2017.06.052

Song, Y., Liu, J., Zhao, K., Gao, L., & Zhao, J. (2021). Cholesterol-induced toxicity: An integrated view of the role of cholesterol in multiple diseases. *Cell Metabolism*, *33*(10), 1911-1925. https://doi.org/10.1016/j.cmet.2021.09.001

Stephenson, J., Nutma, E., van der Valk, P., & Amor, S. (2018). Inflammation in CNS neurodegenerative diseases. *Immunology*, *154*(2), 204-219. https://doi.org/10.1111/imm.12922

Stewart, H., Rutherford, N. J., Briemberg, H., Krieger, C., Cashman, N., Fabros, M., Baker, M., Fok, A., DeJesus-Hernandez, M., Eisen, A., Rademakers, R., & Mackenzie, I. R. (2012). Clinical and pathological features of amyotrophic lateral sclerosis caused by mutation in the C9ORF72 gene on chromosome 9p. *Acta Neuropathol*, *123*(3), 409-417. https://doi.org/10.1007/s00401-011-0937-5

Stribl, C., Samara, A., Trumbach, D., Peis, R., Neumann, M., Fuchs, H., Gailus-Durner, V., Hrabe de Angelis, M., Rathkolb, B., Wolf, E., Beckers, J., Horsch, M., Neff, F., Kremmer, E., Koob, S., Reichert, A. S., Hans, W., Rozman, J., Klingenspor, M., . . . Floss, T. (2014). Mitochondrial dysfunction and decrease in body weight of a transgenic knock-in mouse model for TDP-43. *J Biol Chem*, *289*(15), 10769-10784. https://doi.org/10.1074/jbc.M113.515940

Stringer, C., Wang, T., Michaelos, M., & Pachitariu, M. (2021). Cellpose: a generalist algorithm for cellular segmentation. *Nat Methods*, *18*(1), 100-106. https://doi.org/10.1038/s41592-020-01018-x

Stuart, T., Butler, A., Hoffman, P., Hafemeister, C., Papalexi, E., Mauck, W. M., 3rd, Hao, Y., Stoeckius, M., Smibert, P., & Satija, R. (2019). Comprehensive Integration of Single-Cell Data. *Cell*, *177*(7), 1888-1902 e1821. https://doi.org/10.1016/j.cell.2019.05.031

Stuart, T., & Satija, R. (2019). Integrative single-cell analysis. *Nature Reviews Genetics*, *20*(5), 257-272. https://doi.org/10.1038/s41576-019-0093-7

Sui, S., & Lv, H. (2022). Cognitive improving actions of tofacitinib in a mouse model of Alzheimer disease involving TNF-α, IL-6, PI3K-Akt and GSK-3β signalling pathway. *International Journal of Neuroscience*, 1-9. https://doi.org/10.1080/00207454.2022.2151712

Sun, Y., Yao, J., Kim, T. W., & Tall, A. R. (2003). Expression of liver X receptor target genes decreases cellular amyloid beta peptide secretion. *J Biol Chem*, *278*(30), 27688-27694. https://doi.org/10.1074/jbc.M300760200

Svensson, V., Vento-Tormo, R., & Teichmann, S. A. (2018). Exponential scaling of single-cell RNA-seq in the past decade. *Nature Protocols*, *13*(4), 599-604. https://doi.org/10.1038/nprot.2017.149

Szelechowski, M., Amoedo, N., Obre, E., Léger, C., Allard, L., Bonneu, M., Claverol, S., Lacombe, D., Oliet, S., Chevallier, S., Le Masson, G., & Rossignol, R. (2018a). Metabolic Reprogramming in Amyotrophic Lateral Sclerosis. *Scientific Reports*, *8*(1), 3953. https://doi.org/10.1038/s41598-018-22318-5

Szelechowski, M., Amoedo, N., Obre, E., Léger, C., Allard, L., Bonneu, M., Claverol, S., Lacombe, D., Oliet, S., Chevallier, S., Le Masson, G., & Rossignol, R. (2018b). Metabolic Reprogramming in Amyotrophic Lateral Sclerosis. *Scientific Reports*, *8*(1). https://doi.org/10.1038/s41598-018-22318-5

Tabas, I. (2002). Consequences of cellular cholesterol accumulation: basic concepts and physiological implications. *J Clin Invest*, *110*(7), 905-911. https://doi.org/10.1172/JCI16452

Takabe, W., Urano, Y., Vo, D. H., Shibuya, K., Tanno, M., Kitagishi, H., Fujimoto, T., & Noguchi, N. (2016). Esterification of 24S-OHC induces formation of atypical lipid droplet-like structures, leading to neuronal cell death. *J Lipid Res*, *57*(11), 2005-2014. https://doi.org/10.1194/jlr.M068775

Tang, F., Barbacioru, C., Wang, Y., Nordman, E., Lee, C., Xu, N., Wang, X., Bodeau, J., Tuch, B. B., Siddiqui, A., Lao, K., & Surani, M. A. (2009). mRNA-Seq whole-transcriptome analysis of a single cell. *Nature Methods*, *6*(5), 377-382. https://doi.org/10.1038/nmeth.1315

Tantama, M., Hung, Y. P., & Yellen, G. (2011). Imaging intracellular pH in live cells with a genetically encoded red fluorescent protein sensor. *J Am Chem Soc*, *133*(26), 10034-10037. https://doi.org/10.1021/ja202902d

Tantama, M., Martinez-Francois, J. R., Mongeon, R., & Yellen, G. (2013). Imaging energy status in live cells with a fluorescent biosensor of the intracellular ATP-to-ADP ratio. *Nat Commun*, *4*, 2550. https://doi.org/10.1038/ncomms3550

TargetALS-Postmortem-Tissue-Core. (2020). *TargetALS RNAseq Raw Data*. https://www.targetals.org/resource/genomic-datasets/

Tefera, T. W., Steyn, F. J., Ngo, S. T., & Borges, K. (2021). CNS glucose metabolism in Amyotrophic Lateral Sclerosis: a therapeutic target? *Cell Biosci*, *11*(1), 14. https://doi.org/10.1186/s13578-020-00511-2

Thackaberry, E. A., Kopytek, S., Sherratt, P., Trouba, K., & McIntyre, B. (2010). Comprehensive Investigation of Hydroxypropyl Methylcellulose, Propylene Glycol, Polysorbate 80, and Hydroxypropyl-Beta-Cyclodextrin for use in General Toxicology Studies. *Toxicological Sciences*, *117*(2), 485-492. https://doi.org/10.1093/toxsci/kfq207

Thadeusz, F. (2022, 26.08.2022). Eingesperrt im eigenen Körper – und wieder befreit. *Der Spiegel*. https://www.spiegel.de/wissenschaft/medizin/als-heilung-eingesperrt-im-eigenen-koerper-und-wieder-befreit-a-add65e6f-6ac9-448d-8adb-2fe4be7e4099

Thams, S., Lowry, E. R., Larraufie, M. H., Spiller, K. J., Li, H., Williams, D. J., Hoang, P., Jiang, E., Williams, L. A., Sandoe, J., Eggan, K., Lieberam, I., Kanning, K. C., Stockwell, B. R., Henderson, C. E., & Wichterle, H. (2019). A Stem Cell-Based Screening Platform Identifies Compounds that Desensitize Motor Neurons to Endoplasmic Reticulum Stress. *Mol Ther*, *27*(1), 87-101. https://doi.org/10.1016/j.ymthe.2018.10.010

The-EndNote-Team. (2013). *EndNote*. In (Version EndNote 20) [54 bit]. Clarivate.

The-pandas-development-team. (2020). *pandas-dev/pandas: Pandas*. In (Version 2.0.3) Zenodo. https://doi.org/10.5281/zenodo.3509134

Thrupp, N., Sala Frigerio, C., Wolfs, L., Skene, N. G., Fattorelli, N., Poovathingal, S., Fourne, Y., Matthews, P. M., Theys, T., Mancuso, R., de Strooper, B., & Fiers, M. (2020). Single-Nucleus RNA-Seq Is Not Suitable for Detection of Microglial Activation Genes in Humans. *Cell Rep*, *32*(13), 108189. https://doi.org/10.1016/j.celrep.2020.108189

Tracey, T. J., Kirk, S. E., Steyn, F. J., & Ngo, S. T. (2021). The role of lipids in the central nervous system and their pathological implications in amyotrophic lateral sclerosis. *Semin Cell Dev Biol*, *112*, 69-81. https://doi.org/10.1016/j.semcdb.2020.08.012

Truett, G. E., Heeger, P., Mynatt, R. L., Truett, A. A., Walker, J. A., & Warman, M. L. (2000). Preparation of PCR-quality mouse genomic DNA with hot sodium hydroxide and tris (HotSHOT). *Biotechniques*, *29*(1), 52, 54. https://doi.org/10.2144/00291bm09

Tzeplaeff, L., Wilfling, S., Requardt, M. V., & Herdick, M. (2023). Current State and Future Directions in the Therapy of ALS. *Cells*, *12*(11). https://doi.org/10.3390/cells12111523

Uchida, Y., Sumiya, T., Tachikawa, M., Yamakawa, T., Murata, S., Yagi, Y., Sato, K., Stephan, A., Ito, K., Ohtsuki, S., Couraud, P. O., Suzuki, T., & Terasaki, T. (2019). Involvement of Claudin-11 in Disruption of Blood-Brain, -Spinal Cord, and -Arachnoid Barriers in Multiple Sclerosis. *Mol Neurobiol*, *56*(3), 2039-2056. https://doi.org/10.1007/s12035-018-1207-5

Valori, C. F., & Neumann, M. (2021). Contribution of RNA/DNA Binding Protein Dysfunction in Oligodendrocytes in the Pathogenesis of the Amyotrophic Lateral Sclerosis/Frontotemporal Lobar Degeneration Spectrum Diseases. *Front Neurosci*, *15*, 724891. https://doi.org/10.3389/fnins.2021.724891

van der Walt, S., Schonberger, J. L., Nunez-Iglesias, J., Boulogne, F., Warner, J. D., Yager, N., Gouillart, E., Yu, T., & scikit-image, c. (2014). scikit-image: image processing in Python. *PeerJ*, *2*, e453. https://doi.org/10.7717/peerj.453

Vance, C., Rogelj, B., Hortobagyi, T., De Vos, K. J., Nishimura, A. L., Sreedharan, J., Hu, X., Smith, B., Ruddy, D., Wright, P., Ganesalingam, J., Williams, K. L., Tripathi, V., Al-Saraj, S., Al-Chalabi, A., Leigh, P. N., Blair, I. P., Nicholson, G., de Belleroche, J., . . . Shaw, C. E. (2009). Mutations in FUS, an RNA processing protein, cause familial amyotrophic lateral sclerosis type 6. *Science*, *323*(5918), 1208-1211. https://doi.org/10.1126/science.1165942

Vandoorne, T., De Bock, K., & Van Den Bosch, L. (2018). Energy metabolism in ALS: an underappreciated opportunity? *Acta Neuropathol*, *135*(4), 489-509. https://doi.org/10.1007/s00401-018-1835-x

Vanier, M. T. (2010). Niemann-Pick disease type C. *Orphanet Journal of Rare Diseases*, *5*(1), 16. https://doi.org/10.1186/1750-1172-5-16

Vetrivel, K. S., & Thinakaran, G. (2010). Membrane rafts in Alzheimer's disease beta-amyloid production. *Biochim Biophys Acta*, *1801*(8), 860-867. https://doi.org/10.1016/j.bbalip.2010.03.007

Villarino, A. V., Kanno, Y., Ferdinand, J. R., & O'Shea, J. J. (2015). Mechanisms of Jak/STAT signaling in immunity and disease. *J Immunol*, *194*(1), 21-27. https://doi.org/10.4049/jimmunol.1401867

Vinsant, S., Mansfield, C., Jimenez-Moreno, R., Del Gaizo Moore, V., Yoshikawa, M., Hampton, T. G., Prevette, D., Caress, J., Oppenheim, R. W., & Milligan, C. (2013). Characterization of early pathogenesis in the SOD1(G93A) mouse model of ALS: part II, results and discussion. *Brain Behav*, *3*(4), 431-457. https://doi.org/10.1002/brb3.142

Walenbergh, S. M., Houben, T., Hendrikx, T., Jeurissen, M. L., van Gorp, P. J., Vaes, N., Olde Damink, S. W., Verheyen, F., Koek, G. H., Lutjohann, D., Grebe, A., Latz, E., & Shiri-Sverdlov, R. (2015). Weekly Treatment of 2-Hydroxypropyl-beta-cyclodextrin Improves Intracellular Cholesterol Levels in LDL Receptor Knockout Mice. *Int J Mol Sci*, *16*(9), 21056-21069. https://doi.org/10.3390/ijms160921056

Walther, T. C., & Farese, R. V., Jr. (2012). Lipid droplets and cellular lipid metabolism. *Annu Rev Biochem*, *81*, 687-714. https://doi.org/10.1146/annurev-biochem-061009-102430

Wang, H., Zhang, X., Yu, B., Peng, X., Liu, Y., Wang, A., Zhao, D., Pang, D., OuYang, H., & Tang, X. (2019). Cyclodextrin Ameliorates the Progression of Atherosclerosis via Increasing High-Density Lipoprotein Cholesterol Plasma Levels and Anti-inflammatory Effects in Rabbits. *J Cardiovasc Pharmacol*, *73*(5), 334-342. https://doi.org/10.1097/FJC.0000000000000660

Wang, R., Yang, B., & Zhang, D. (2011). Activation of interferon signaling pathways in spinal cord astrocytes from an ALS mouse model. *Glia*, *59*(6), 946-958. https://doi.org/10.1002/glia.21167

Wang, Z., Gerstein, M., & Snyder, M. (2009). RNA-Seq: a revolutionary tool for transcriptomics. *Nature Reviews Genetics*, *10*(1), 57-63. https://doi.org/10.1038/nrg2484

Weishaupt, J. H., Hyman, T., & Dikic, I. (2016). Common Molecular Pathways in Amyotrophic Lateral Sclerosis and Frontotemporal Dementia. *Trends in Molecular Medicine*, *22*(9), 769-783. https://doi.org/10.1016/j.molmed.2016.07.005

Werner, S., & Alzheimer, C. (2006). Roles of activin in tissue repair, fibrosis, and inflammatory disease. *Cytokine Growth Factor Rev*, *17*(3), 157-171. https://doi.org/10.1016/j.cytogfr.2006.01.001

Westergard, T., Jensen, B. K., Wen, X., Cai, J., Kropf, E., Iacovitti, L., Pasinelli, P., & Trotti, D. (2016). Cell-to-Cell Transmission of Dipeptide Repeat Proteins Linked to C9orf72-ALS/FTD. *Cell Rep*, *17*(3), 645-652. https://doi.org/10.1016/j.celrep.2016.09.032

WHO-Prequalification-Team. (2021). *Notes on the Design of Bioequivalence Study: Baricitinib*. World Health Organization. Retrieved 28.12.2023 from https://extranet.who.int/prequal/sites/default/files/document_files/BE_baricitinib_Nov2021.pdf

Wickham, H. (2016). *ggplot2: Elegant Graphics for Data Analysis*. Springer-Verlag New York. https://ggplot2.tidyverse.org

Wolins, N. E., Quaynor, B. K., Skinner, J. R., Tzekov, A., Croce, M. A., Gropler, M. C., Varma, V., Yao-Borengasser, A., Rasouli, N., Kern, P. A., Finck, B. N., & Bickel, P. E. (2006). OXPAT/PAT-1 is a PPAR-induced lipid droplet protein that promotes fatty acid utilization. *Diabetes*, *55*(12), 3418-3428. https://doi.org/10.2337/db06-0399

Wolins, N. E., Skinner, J. R., Schoenfish, M. J., Tzekov, A., Bensch, K. G., & Bickel, P. E. (2003). Adipocyte protein S3-12 coats nascent lipid droplets. *J Biol Chem*, *278*(39), 37713-37721. https://doi.org/10.1074/jbc.M304025200

Writing-Group-Edaravone, A. L. S. S. G. (2017). Safety and efficacy of edaravone in well defined patients with amyotrophic lateral sclerosis: a randomised, double-blind, placebo-controlled trial. *Lancet Neurol*, *16*(7), 505-512. https://doi.org/10.1016/S1474-4422(17)30115-1

Wu, G., Ma, Z., Cheng, Y., Hu, W., Deng, C., Jiang, S., Li, T., Chen, F., & Yang, Y. (2018). Targeting Gas6/TAM in cancer cells and tumor microenvironment. *Molecular Cancer*, *17*(1), 20. https://doi.org/10.1186/s12943-018-0769-1

Xiao, Q., Zhao, W., Beers, D. R., Yen, A. A., Xie, W., Henkel, J. S., & Appel, S. H. (2007). Mutant SOD1(G93A) microglia are more neurotoxic relative to wild-type microglia. *J Neurochem*, *102*(6), 2008-2019. https://doi.org/10.1111/j.1471-4159.2007.04677.x

Yao, J., Ho, D., Calingasan, N. Y., Pipalia, N. H., Lin, M. T., & Beal, M. F. (2012). Neuroprotection by cyclodextrin in cell and mouse models of Alzheimer disease. *J Exp Med*, *209*(13), 2501-2513. https://doi.org/10.1084/jem.20121239

Yazdani, U., & Terman, J. R. (2006). The semaphorins. *Genome Biology*, *7*(3), 211. https://doi.org/10.1186/gb-2006-7-3-211

Yoshida, A., Yamamoto, M., Hirayama, F., & Uekama, K. (1988). Improvement of Chemical Instability of Digitoxin in Aqueous Solution by Complexation with β-Cyclodextrin Derivatives. *CHEMICAL & PHARMACEUTICAL BULLETIN*, *36*(10), 4075-4080. https://doi.org/10.1248/cpb.36.4075

Yu, L., Guan, Y., Wu, X., Chen, Y., Liu, Z., Du, H., & Wang, X. (2013). Wnt Signaling is Altered by Spinal Cord Neuronal Dysfunction in Amyotrophic Lateral Sclerosis Transgenic Mice. *Neurochemical Research*, *38*(9), 1904-1913. https://doi.org/10.1007/s11064-013-1096-y

Zappia, L., & Oshlack, A. (2018). Clustering trees: a visualization for evaluating clusterings at multiple resolutions. *GigaScience*, *7*(7). https://doi.org/10.1093/gigascience/giy083

Zarco, N., Bautista, E., Cuellar, M., Vergara, P., Flores-Rodriguez, P., Aguilar-Roblero, R., & Segovia, J. (2013). Growth arrest specific 1 (GAS1) is abundantly expressed in the adult mouse central nervous system. *J Histochem Cytochem*, *61*(10), 731-748. https://doi.org/10.1369/0022155413498088

Zeng, P., & Zhou, X. (2019). Causal effects of blood lipids on amyotrophic lateral sclerosis: a Mendelian randomization study. *Hum Mol Genet*, *28*(4), 688-697. https://doi.org/10.1093/hmg/ddy384

Zeng, X., Song, X., Ma, T., Pan, X., Zhou, Y., Hou, Y., Zhang, Z., Li, K., Karypis, G., & Cheng, F. (2020). Repurpose Open Data to Discover Therapeutics for COVID-19 Using Deep Learning. *J Proteome Res*, *19*(11), 4624-4636. https://doi.org/10.1021/acs.jproteome.0c00316

Zhai, X., Pu, D., Wang, R., Zhang, J., Lin, Y., Wang, Y., Zhai, N., Peng, X., Zhou, Q., & Li, L. (2023). Gas6/AXL pathway: immunological landscape and therapeutic potential [Review]. *Frontiers in Oncology*, *13*. https://doi.org/10.3389/fonc.2023.1121130

Zhang, Y.-J., Jansen-West, K., Xu, Y.-F., Gendron, T. F., Bieniek, K. F., Lin, W.-L., Sasaguri, H., Caulfield, T., Hubbard, J., Daughrity, L., Chew, J., Belzil, V. V., Prudencio, M., Stankowski, J. N., Castanedes-Casey, M., Whitelaw, E., Ash, P. E. A., DeTure, M., Rademakers, R., . . . Petrucelli, L. (2014). Aggregation-prone c9FTD/ALS poly(GA) RAN-translated proteins cause neurotoxicity by inducing ER stress. *Acta Neuropathologica*, *128*(4), 505-524. https://doi.org/10.1007/s00401-014-1336-5

Zhao, J., Krystofiak, E. S., Ballesteros, A., Cui, R., Van Itallie, C. M., Anderson, J. M., Fenollar-Ferrer, C., & Kachar, B. (2018). Multiple claudin-claudin cis interfaces are required for tight junction strand formation and inherent flexibility. *Commun Biol*, *1*, 50. https://doi.org/10.1038/s42003-018-0051-5

Zheng, G. X., Terry, J. M., Belgrader, P., Ryvkin, P., Bent, Z. W., Wilson, R., Ziraldo, S. B., Wheeler, T. D., McDermott, G. P., Zhu, J., Gregory, M. T., Shuga, J., Montesclaros, L., Underwood, J. G., Masquelier, D. A., Nishimura, S. Y., Schnall-Levin, M., Wyatt, P. W., Hindson, C. M., . . . Bielas, J. H. (2017). Massively parallel digital transcriptional profiling of single cells. *Nat Commun*, *8*, 14049. https://doi.org/10.1038/ncomms14049

Zhou, B., Guo, Z., & Chen, P. (2023). Disease-Associated Oligodendrocyte: New Player in Alzheimer's Disease and CNS Pathologies. *Journal of Integrative Neuroscience*, *22*(4). https://doi.org/10.31083/j.jin2204090

Zhou, Y., Wang, F., Tang, J., Nussinov, R., & Cheng, F. (2020). Artificial intelligence in COVID-19 drug repurposing. *Lancet Digit Health*, *2*(12), e667-e676. https://doi.org/10.1016/S2589-7500(20)30192-8

Zhu, L., Hu, F., Li, C., Zhang, C., Hang, R., & Xu, R. (2021). Perilipin 4 Protein: an Impending Target for Amyotrophic Lateral Sclerosis. *Molecular Neurobiology*, *58*(4), 1723-1737. https://doi.org/10.1007/s12035-020-02217-5

Zhu, Q., Jiang, J., Gendron, T. F., McAlonis-Downes, M., Jiang, L., Taylor, A., Diaz Garcia, S., Ghosh Dastidar, S., Rodriguez, M. J., King, P., Zhang, Y., La Spada, A. R., Xu, H., Petrucelli, L., Ravits, J., Da Cruz, S., Lagier-Tourenne, C., & Cleveland, D. W. (2020). Reduced C9ORF72 function exacerbates gain of toxicity from ALS/FTD-causing repeat expansion in C9orf72. *Nat Neurosci*, *23*(5), 615-624. https://doi.org/10.1038/s41593-020-0619-5

Ziff, O. J., Neeves, J., Mitchell, J., Tyzack, G., Martinez-Ruiz, C., Luisier, R., Chakrabarti, A. M., McGranahan, N., Litchfield, K., Boulton, S. J., Al-Chalabi, A., Kelly, G., Humphrey, J., & Patani, R. (2023). Integrated transcriptome landscape of ALS identifies genome instability linked to TDP-43 pathology. *Nature Communications*, *14*(1), 2176. https://doi.org/10.1038/s41467-023-37630-6

Zimmer, S., Grebe, A., Bakke, S. S., Bode, N., Halvorsen, B., Ulas, T., Skjelland, M., De Nardo, D., Labzin, L. I., Kerksiek, A., Hempel, C., Heneka, M. T., Hawxhurst, V., Fitzgerald, M. L., Trebicka, J., Bjorkhem, I., Gustafsson, J. A., Westerterp, M., Tall, A. R., . . . Latz, E. (2016). Cyclodextrin promotes atherosclerosis regression via macrophage reprogramming. *Sci Transl Med*, *8*(333), 333ra350. https://doi.org/10.1126/scitranslmed.aad6100

Zong, Y., & Jin, R. (2013). Structural mechanisms of the agrin-LRP4-MuSK signaling pathway in neuromuscular junction differentiation. *Cell Mol Life Sci*, *70*(17), 3077-3088. https://doi.org/10.1007/s00018-012-1209-9

Zu, T., Gibbens, B., Doty, N. S., Gomes-Pereira, M., Huguet, A., Stone, M. D., Margolis, J., Peterson, M., Markowski, T. W., Ingram, M. A., Nan, Z., Forster, C., Low, W. C., Schoser, B., Somia, N. V., Clark, H. B., Schmechel, S., Bitterman, P. B., Gourdon, G., . . . Ranum, L. P. (2011). Non-ATG-initiated translation directed by microsatellite expansions. *Proc Natl Acad Sci U S A*, *108*(1), 260-265. https://doi.org/10.1073/pnas.1013343108

Declaration of Author Contribution

The author of this dissertation, namely Ali Rezaei, produced all the original data presented in this dissertation, except for the data by the collaborators below:

Zeynep Günes (AG Liebscher): preparation of snRNAseq library from tissue

Franz Bauernschmitt (AG Beltran): Initial analysis and QC of snRNAseq data

Georg Kislinger (AG Fetting): sample prep and SEM from fixed tissue

Dieter Edbauer: Analysis of TargetALS data (reuse from 2020 analysis) and GO analysis on current data – preparation of primary neuron culture

Daniel Farny and Virag Kocsis-Jutka (AG Edbauer): help with animal work on rare occasions

Brigitte Nuscher (AG Haass): NfL measurements from serum using the Simoa assay

Cholesterol and cholesteryl ester mass spectrometry was outsourced to Laura Parisi from Sanofi in Boston, MA, USA.

Mass Spectrometry of Metabolites was outsourced to Creative Proteomics. Sequencing of samples was outsourced to University of Kiel's sequencing facility.

Human tissue sections were provided by Dr. Thomas Arzberger (stained by me).

Eszter Katona (AG Edbauer) provided advice and training for MSD ELISA, while Garyfallia Gouna (AG Simons) provided advice with oligodendrocyte marker selection. Nellwyn Hagan (Sanofi) provided the formulation recipe of HP-β-CD in citrate buffer.

_____ _____

Ali Rezaei Prof. Dr. Dieter Edbauer

Acknowledgements

I believe that there is no such thing as a self-made man or true independence. Indeed, I worked very hard during my PhD, but my success in its completion depended on everyone around me, not just now but also from my past. We often only thank the people in our sight, as those are who we see, but if a warehouse worker in the supply chain did not work, I would not have had the reagents to do these experiments with. Nevertheless, I settle for thanking those in my sight as the least I can do.

Firstly, I thank my supervisor Prof. Dr. Dieter Edbauer who offered me a position in his lab and supported me through the thick and thin of various projects. Huge thanks go to my second TAC member Dr. Dudanova for all the help and support, if only there were more professors like you! All members of the Eddie lab deserve my thanks for not only their scientific support, but also for creating a great working environment. Above all, I must thank Dr. Katherine LaClair for her support and mentorship early in my PhD. Many thanks go to Henni for amazing discussions late nights in the lab, to Francesca for all the support, and to my friends and collaborators Virag and Zeynep for their help with the project and their friendship. I must also thank all administrative staff in the institute, especially Marcel and Sabine, without them, nothing gets done.

Above all, I feel gratitude towards my undergraduate mentors: Yiannis, Rob, and Asli. Without you guys, I would not have made it as a scientist. Thank you for taking my interest in science and growing it. You guys are amazing. In this light, I also thank all my teachers and mentors, from the first grade until now.

Without the support of my parents, I would not have been able to amount to anything. Thank you very much mom and dad for everything you sacrificed for me. Laura, my amazing girlfriend and partner in everything, thank you for all the support, especially for this thesis. Huge thanks go to all my friends in Munich and beyond; Agris, Farzad, Masood, Alex, Chris, and all the others, thank you guys for keeping me sane through this journey. I'll never forget how good times of unhealthy eating and gaming saved me from full burnout. And thanks to all the ones whose names I did not mention or did not know, but my work without them would not have been possible.

Eidesstattliche Versicherung/Affidavit

Ali Rezaei
(Studierende / Student)

Hiermit versichere ich an Eides statt, dass ich die vorliegende Dissertation "Therapeutic Potential of HP-β-CD in Ameliorating a poly(GA) Mouse Model of ALS" selbstständig angefertigt habe, mich außer der angegebenen keiner weiteren Hilfsmittel bedient und alle Erkenntnisse, die aus dem Schrifttum ganz oder annähernd übernommen sind, als solche kenntlich gemacht und nach ihrer Herkunft unter Bezeichnung der Fundstelle einzeln nachgewiesen habe.

I hereby confirm that the dissertation "Therapeutic Potential of HP-β-CD in Ameliorating a poly(GA) Mouse Model of ALS" is the result of my own work and that I have only used sources or materials listed and specified in the dissertation.

München / Munich

11.06.2024 Ali Rezaei

(Datum / Date) (Unterschrift / Signature)